Revised timing of Cenozoic Atlantic incursions and changing hinterland sediment sources during southern Patagonian orogenesis

Julie C. Fosdick[1], R.A. VanderLeest[1], J.E. Bostelmann T.[2,3,4,5], J.S. Leonard[6], R. Ugalde[7], J.L. Oyarzún[8], and Miguel Griffin[9]

[1]Department of Geosciences, University of Connecticut, 354 Mansfield Road, U-1045, Storrs, CT 06269, USA
[2]Instituto de Ciencias de la Tierra, Facultad de Ciencias, Universidad Austral de Chile, Los Laureles s/n, 5090000, Valdivia, Chile.
[3]Programa de Doctorado en Ciencias Mención Ecología y Evolución, Universidad Austral de Chile, Los Laureles s/n, 5090000, Valdivia, Chile.
[4]Red Paleontológica U-Chile, Laboratorio de Ontogenia y Filogenia, Departamento de Biología, Facultad de Ciencias, Universidad de Chile, Las Palmeras 3425, Santiago, Chile.
[5]Museo Regional de Aysén, kilómetro 3 camino a Coyhaique Alto, Coyhaique, Región de Aysén, Chile.
[6]School of Earth and Space Exploration, Arizona State University, AZ 85287 USA.
[7]Escuela de Geología, Facultad de Ciencias, Universidad Mayor, Manuel Montt 367, Providencia, Santiago, Chile.
[8]Parque Geo-Paleontológico La Cumbre-Baguales, Ruta 9 km 284, Magallanes, Chile
[9]CONICET—División Paleozoología Invertebrados, Museo de La Plata. Paseo del Bosque s/n, La Plata, Argentina.

ABSTRACT

New detrital zircon U-Pb geochronology data from the Cenozoic Magallanes-Austral Basin in Argentina and Chile ~51°S establish a revised chronostratigraphy of Paleocene – Miocene foreland synorogenic strata and document the rise and subsequent isolation of hinterland sources in the Patagonian Andes from the continental margin. The upsection loss of zircons derived from the hinterland Paleozoic and Late Jurassic sources between ca. 60-44 Ma documents a major shift in sediment routing due to Paleogene orogenesis in the greater Patagonian-Fuegian Andes. Changes in the proportion of grains from hinterland thrust sheets, comprised of Jurassic volcanics and Paleozoic metasedimentary rocks, provide a trackable signal of long-term shifts in orogenic drainage divide and topographic isolation due to widening of the retroarc fold-thrust belt. Youngest detrital zircon U-Pb ages confirm timing of Maastrichtian – Eocene strata, but require substantial age revisions for part of the overlying Cenozoic basinfill during the late Eocene and Oligocene. The upper Río Turbio Formation, previously mapped as

middle to late Eocene in the published record, records a newly recognized latest Eocene-Oligocene (37-27 Ma) marine incursion along the basin margin. We suggest that these deposits could be genetically linked to the distally placed units along the Atlantic coast, including the El Huemul Formation and the younger San Julián Formation, via an eastward deepening within the foreland basin system that culminated in a basin-wide Oligocene marine incursion in the Southern Andes. The overlying Río Guillermo Formation records onset of tectonically generated coarse-grained detritus ca. 24.3 Ma and a transition to the first fully nonmarine conditions on the proximal Patagonian platform since Late Cretaceous time, perhaps signaling a Cordilleran-scale upper plate response to increased plate convergence and tectonic plate reorganization.

INTRODUCTION

Tectonics, climate, and eustasy in convergent plate settings control first-order fluctuations between marine and terrestrial environments along continental margins and the transfer of sediment from orogens to basin depocenters. With the emergence of a new paradigm in the last three decades recognizing dynamic interactions and feedbacks between tectonics and climate (Heller et al., 1988; Beaumont et al., 1992; Willett, 1999), it is all the more essential to differentiate between their signals in the stratigraphic record. For instance, enhanced tectonism in foreland basin settings can cause crustal load-driven basin subsidence and deepening of marine environments (Flemings and Jordan, 1989; Simpson, 2006). Climate variations and orography influence precipitation and temperature gradients, which in turn effect erosion rates, vegetation cover, and even the location of deformation and drainage divides (Leeder, 1993; Bonnet and Crave, 2003; Rehak et al., 2010; Cruz et al., 2011). Globally, climate modulates the growth and ablation of continental ice sheets and sea level (Miller et al., 2005). Cenozoic marine transgressions are well-studied in terms of sequence stratigraphic models for global sea level change (e.g., Miocene US Atlantic history of Browning et al., 2006) and the dominant control of climatic optima are suitable for passive continental margins. However, in tectonically active, shallow-marine basins resolving the relative contributions of regional tectonics and eustasy,

driven by global mechanisms, must be carefully considered (Christie-Blick, 1991). For example, work in the Cretaceous interior seaway has demonstrated that tectonism is an important player in controlling parasequence progradation and subsidence (Painter and Carrapa, 2013), in addition to eustatic sea-level variations (Houston et al., 2000; Horton et al., 2004).

An improved understanding of the controls on subaerial emergence or subsidence of these landmasses is fundamental to evaluating potential linkages between mountain building and climate (e.g., Roe et al., 2008), eustatic sea level changes (Browning et al., 2006), sediment delivery to the oceans (Clift et al., 2001; Sommerfield and Wheatcroft, 2007; Romans and Graham, 2013), and biotic responses to changing ecosystems (Marshall et al., 1982; Sepkoski, 1996; Acosta et al., 2014; Palazzesi et al., 2014; Eronen et al., 2015). Moreover, better knowledge of the dynamic response of sedimentary and tectonic systems is critical to scientific issues of our time, including long-term climate change, biogeochemical fluxes to our lakes and oceans, and conservation of mineral and energy resources (Hodgson et al., 2018). A central requirement to unravel these competing processes is detailed chronology of sedimentation and changes in provenance preserved in the sedimentary basin fill. Lithologic variations and detrital geochronologic signals indicating the appearance of sediment that is associated with a diagnostic tectonic terrane or geologic unit are commonly used to infer timing of source area unroofing and to make paleogeographic, tectonic, or climatic interpretations (e.g., Jordan et al., 1993; Barbeau et al., 2009; Romans et al., 2010; Nie et al., 2012). However, the decline of a source as a prominent sediment contributor to basin infill – potentially through erosional removal, topographic blocking, or burial – is less commonly preserved in the depositional record. Sediment recycling and weathering of source areas can further complicate the cause of a waning

source signal (Johnsson and Basu, 1993; Cox et al., 1995; Fosdick et al., 2015; Limonta et al., 2015).

The Patagonian Andes, a high-latitude convergent orogen in South America, provides sediment to the genetically linked Magallanes-Austral Basin, which extends ~200 km from a retroarc thrust front to the southern Atlantic Ocean (Fig. 1). This relatively narrow distance results in the eastern Atlantic continental margin in Patagonia that is sensitive to sea level fluctuations driven by dynamic and tectonic loading of the flexural foredeep (Fosdick et al., 2014), variations in sediment flux across the coastal plain, eustasy, and global climate and far-field tectonics. The proximal Patagonian foredeep depocenter near 51°S remained predominantly deep marine from ca. 100-80 Ma (Natland et al., 1974; Biddle et al., 1986; Romans et al., 2011; Varela et al., 2019) followed by basin-filling and shoaling to shallow marine to marginal continental conditions ca. 78-60 Ma (Macellari et al., 1989; Malumián and Caramés, 1997; Schwartz and Graham, 2015; Moyano Paz et al., 2018, 2020; Tettamanti et al., 2018; Manríquez et al., 2019). This western part of the Magallanes-Austral Basin coevolved with the Cenozoic development of the southeastern Magallanes-Austral and Malvinas depocenters related to the Fuegian orocline (Ghiglione et al., 2010, 2016a, 2016b) and opening of the Drake Passage between Antarctica and South America (Scher and Martin, 2006; Lagabrielle et al., 2009). Following N-S early foreland development of basin subsidence and infilling, deformation across the Patagonian thrust-belt promoted a general eastward shift of deposition in Paleocene-Miocene time (Fosdick et al., 2011; Aramendía et al., 2019).

Near ~51°S, the proximal Cenozoic Magallanes-Austral Basin preserves shelfal facies overlain by near-shore and continental facies. Documented middle Cenozoic transgressions in Patagonia and Tierra del Fuego have been linked to Cenozoic global sea level rise due to climate

(Rodríguez Raising, 2010; Malumián and Náñez, 2011; Bechis et al., 2014) and phases of Andean orogenesis (Fosdick et al., 2011; Bostelmann et al., 2013; Gutiérrez et al., 2017). Most notably, stratigraphic units like the El Huemul Formation (late Eocene- early Oligocene), and the slightly younger San Julián Formation (late Oligocene), represent latest Paleogene shallow marine deposition along much of the Atlantic coast (Ameghino, 1906; Parras et al., 2012; Cuitiño et al., 2012, 2019; Parras and Cuitiño, 2018). These units mark the beginning of the '*Patagonian Sea*' incursion recorded as the *Juliense* (25–22 Ma) and *Leonense* (22–17.9 Ma) stages (Parras et al., 2012). Previous work has suggested that the *Patagonian Sea* was largely influenced by climate optima and eustatic transgressions (Parras et al., 2012) and/or tectonics (Dix and Parras, 2014; Parras et al., 2020). It is yet undetermined (1) if the inland sea reached the proximal part of the Magallanes-Austral Basin during the Oligocene, (2) how upland source areas changed during Cenozoic foreland sedimentation, and (3) to what extent these marine phases were driven by tectonic subsidence, changes in upland sediment routing/sediment flux, or eustasy. Differentiating among the relative impacts of these large-scale factors is important for recognizing the effects of external controls, such as global climate transitions, versus internal orogenic wedge dynamics (Dahlen et al., 1984; Willett, 1999) and source to sink connections in the transfer of sediment to the world's oceans.

We present new sediment provenance data and a new chronostratigraphy of Eocene – Miocene strata in the Magallanes-Austral Basin of southern Patagonia that (1) revise the age of marine incursions and changes in orogenic paleogeography during the transition to nonmarine conditions in southern Patagonia, (2) highlight the rise and subsequent isolation of a major hinterland source area due to basinward development of younger orogenic topography, and (3)

suggest recycling of Mesozoic grains from Upper Cretaceous sedimentary rocks, rather than direct sourcing from the Mesozoic batholith.

TECTONIC SETTING & BASIN STRATIGRAPHY

The Upper Cretaceous – Cenozoic Magallanes-Austral Basin (Fig. 1) records deposition during structural growth of the Patagonian-Fuegian Andes (Ramos and Ghiglione, 2008; Ghiglione et al., 2010, 2016a; Romans et al., 2011; Fosdick et al., 2011). Following marine conditions that have generally persisted since Late Jurassic time, the early foreland basin history was predominantly deep-marine, with southward deepening from a narrow continental shelf in the north (Macellari et al., 1989; Malkowski et al., 2013; Sickmann et al., 2018; Cuitiño et al., 2019) to bathyal conditions in the south (Biddle et al., 1986). Shoaling of the Upper Cretaceous marine depocenter led to dominantly shallow-marine, coastal, and deltaic sedimentation that persisted until Paleocene time (Macellari et al., 1989; Malumián and Caramés, 1997; Romans et al., 2011; González, 2015; Manríquez et al., 2019). Thrust front advancement of the Patagonian retroarc thrust belt promoted an eastward shift of the foreland deposition in Paleocene-Miocene time (Fosdick et al., 2011). The primary sediment sources to the Magallanes-Austral Basin include the Mesozoic-Cenozoic Southern Patagonian Batholith and related volcanics, Mesozoic basinal rocks of the Rocas Verdes Basin, and to a lesser extent, Paleozoic metamorphic rocks (Fig. 1). The proximity of the basin to an active magmatic arc throughout its history has resulted in intercalated volcanic ashes and abundant magmatically derived zircons proven useful for assessing controls on sedimentation, with prior focus on the Cretaceous strata (Fildani et al., 2003; Bernhardt et al., 2012; Varela et al., 2012; Malkowski et al., 2015, 2017b, 2017a; Schwartz et al., 2016; Sickmann et al., 2018).

During the Cenozoic, much of the South American extra-Andean regions north of Patagonia underwent predominately continental sedimentation, briefly punctuated by middle and late Miocene epicontinental marine incursions, and development of tidal-dominated wetland systems, like the *Paranean Sea* and the Pebbas lake (Martínez and del Río, 2002; Hoorn et al., 2010; Antoine et al., 2016; Ugalde, 2019). In contrast, most of the eastern Patagonian foreland south of the Deseado Massif seems to have been largely submerged in shelf to shallow marine and transitional depositional environments, during the structurally complicated development of the Magallanes-Austral and Malvinas foreland depocenters related to the oroclinal curved plate boundary with the Scotia plate (Ghiglione et al., 2010, 2016a) and tectonic separation of Antarctica from South America continents during opening of the Drake Passage (Ghiglione et al., 2008; Lagabrielle et al., 2009; Houben et al., 2013). In the Última Esperanza District of the Magallanes-Austral Basin, (Chile), Cenozoic strata are disconformable on Maastrichtian tide-influenced shelf-edge deltaic Dorotea Formation (Hünicken, 1955; Biddle et al., 1986; González, 2015; Schwartz and Graham, 2015; Manríquez et al., 2019; George et al., 2020). However, the timing and extent of this unconformity and its geologic significance is unresolved given limited chronology and stratigraphic correlation along the basin axis (Biddle et al., 1986; Fosdick et al., 2015; George et al., 2020). In our study area (Fig. 1), the Dorotea Formation is overlain by the laterally discontinuous Paleocene Cerro Dorotea Formation (Hünicken, 1955; Malumián and Caramés, 1997) and unconformably overlying Eocene shallow marine, estuarine, and deltaic Río Turbio Formation. (Hünicken, 1955; Ugalde, 2014; Otero and Soto-Acuña, 2015; Schwartz and Graham, 2015). Geological observations in Brunswick Peninsula, Isla Riesco, and Río Figueroa shows that this Paleogene stratigraphic separation decreases southward through Tierra del Fuego, where the Maastrichtian/Danian unconformity is restricted and more continuous sedimentation

occurred until Miocene time (Olivero and Malumián, 2008; Sánchez et al., 2010; Gallardo Jara et al., 2019; Torres Carbonell and Olivero, 2019).

A key stratigraphic unit within our study area is the Río Turbio Formation, which is characterized by glauconitic shallow-marine to lagoonal sandstone, siltstone, claystone, coquina, and interbedded minable coal seams (Malumián and Caramés, 1997; Rodríguez Raising, 2010; Nullo and Combina, 2011) and fossil assemblages of subtropical flora, palynomorphs, and marine invertebrates (Hünicken, 1955; Griffin, 1991; Schweitzer et al., 2012; Guerstein et al., 2014; Pujana and Ruiz, 2019; Panti, 2020). Debate persists on the depositional age of the Río Turbio Formation, with early biostratigraphic studies reporting Eocene through Miocene (Riccardi and Rolleri, 1980) or exclusively Eocene biozones (Malumián and Caramés, 1997; González Estebenet et al., 2015, 2017). This depositional unit records high-latitude organic-rich shallow marine and transitional deposition. Therefore, its age is highly relevant for understanding paleoenvironmental conditions and tectonic influences on sedimentation during past climate optima.

The Río Turbio Formation is unconformably overlain by the Río Guillermo Formation, a mostly fluvial sandstone, conglomerate, and coaly claystone with notable abundant silicified tree trunks preserved in life position (Hünicken, 1955; Malumián and Caramés, 1997; Rodríguez Raising, 2010; Leonard, 2017). Most previous workers have proposed an upper Eocene to early Oligocene age for the Río Guillermo Formation (Malumián et al., 2000; Ramos, 2005; Vento et al., 2017). Fluvial sedimentation in the Magallanes-Austral Basin was briefly interrupted by a shallow marine incursion, resulting in sandstone and mudstone deposits of the Estancia 25 de Mayo Formation (Cuitiño and Scasso, 2010; Cuitiño et al., 2012, 2019) and coeval informal units ("Estratos de Río del Oro"). This unit has been correlated to the distal Monte León Formation

along the Atlantic coast that, together, record the *Leonense* marine incursion of the *Patagonian Sea* at this latitude (Ameghino, 1906; Parras et al., 2012, 2020; Parras and Cuitiño, 2018). The overlying Santa Cruz Formation marks the last phase of major sedimentation and fluvial deposition in the Patagonian Andes ca. 19-16 Ma, prior to regional surface uplift and incision of the foreland basin (Furque and Camacho, 1972; Bostelmann et al., 2013; Cuitiño et al., 2016; Raigemborn et al., 2018). Multiple explanations have been postulated for this abrupt end to proximal foreland sedimentation along the Andean foothills and a shift to offshore deposition (Ghiglione et al., 2016b). Potential mechanisms include (1) reduced sediment supply caused by an orographic rain-shadow during topographic surface uplift (Blisniuk et al., 2005; 2006), (2) effects of flat slab subduction (Espinoza et al., 2010; Boutonnet et al., 2010; Ramírez de Arellano et al., 2012), and 3) regional surface uplift caused by migration of the Chile Ridge collision (Stevens Goddard and Fosdick, 2019) and dynamic response to opening of an asthenospheric slab window beneath Patagonia (Guillaume et al., 2009; Dávila et al., 2019), or some combination of these processes.

DETRITAL U-Pb GEOCHRONOLOGY

Sampling and Analytical Methods

We collected twelve sandstone samples from the Paleocene – Miocene outcrop belt exposed near Cerro Castillo township, Chile, and Estancia Cancha Carrera, Argentina, in Patagonia (Fig. 1) from previously studied stratigraphic sections (Hünicken, 1955; Malumián and Caramés, 1997; Rodríguez Raising, 2010; Leonard, 2017; Leonard et al., 2020). Sample information and locations are outlined in Table 1. Detrital zircons were extracted from ~5 kg medium-grained sandstone hand-samples using standard mineral separation techniques,

including crushing and grinding, fractionation of magnetic minerals with a Frantz isodynamic magnetic separator, and settling through heavy liquids to exclude phases with densities less than 3.3 g/cm^3. Final zircon separates were mounted in epoxy resin together with fragments of the Sri Lanka standard zircon. The mounts were polished to a depth of ~20 μm, CL and BSE imaged, and cleaned prior to isotopic analysis. U-Pb geochronology of zircons was conducted by laser ablation multicollector inductively coupled plasma mass spectrometry (LA-MC-ICPMS) using a Photon Machines Analyte G2 excimer laser using a spot diameter of 30 μm at the Arizona LaserChron Center (Gehrels et al., 2008; Gehrels, 2011). Analytical methods and data are available in the Data Repository.

Preferred calculated U-Pb ages use the ^{204}Pb corrected ^{206}Pb/^{238}U ratio for <900 Ma grains and the ^{204}Pb corrected ^{206}Pb/^{207}Pb ratio for >900 Ma grains. Uncertainties shown in these tables are at the 1σ level, and include only measurement errors. Analyses that are >20% discordant and 5% reverse discordant (by comparison of ^{206}Pb/^{238}U and ^{206}Pb/^{207}Pb ages) were excluded from provenance interpretations and maximum depositional age interpretations. Pb*/U concordia diagrams (Fig. A1) and probability density plots (Figs. A2 and A3) were generated using the routines in Isoplot (Ludwig, 2008). The age-probability diagrams show each age and its uncertainty (for measurement error only) as a normal distribution, and sum all ages from a sample into a single curve. Probability density plots for individual samples are presented in Figures A2 and A3, and compiled formation-level datasets are shown in Figure 2. For samples that yielded youngest age groups that could represent conceivable maximum depositional ages, we calculated error-weighted mean ages based on the following criteria: age clusters contained at least two overlapping concordant grains at 2σ uncertainty (Fig. 3; Table 1). For published samples from the Punta Barrosa, Cerro Toro, Tres Pasos, and Dorotea Formations (Figs. 2 and

4), we recalculated relative probability density curves from published U-Pb geochronological data (Fildani et al., 2003; Romans et al., 2010; Fosdick et al., 2011, 2015; Bernhardt et al., 2012).

Results and Interpretations

Detrital zircon U-Pb geochronology results (1,579 dated grains) from the Cerro Castillo – Cancha Carrera area reveal distinctive age groups in variable proportions up-section (Fig. 2): (1) Cenozoic age clusters that include early Miocene-Oligocene (20-30 Ma), Eocene (33-45 Ma), and Paleocene (60-65 Ma) ages; (2) a range of Cretaceous ages with clusters at ca. 66-80 Ma, and 80-136 Ma (3) a Late Jurassic – earliest Cretaceous age group (136-175 Ma), (4) smaller proportions of Devonian-Permian ages (250-420 Ma), (5) early Paleozoic and Mesoproterozoic ages (420-1600 Ma), and (6) few Mesoproterozoic and older grains. Cenozoic and Cretaceous zircon grains are mostly large (>100 μm), euhedral to subhedral, magmatically zoned zircons. In contrast, Jurassic zircons are mostly small (<60 μm in width), subangular or broken fragments of long and narrow volcanic crystals. Paleozoic and Proterozoic grains are mostly small (<50 μm) subrounded to rounded grains.

Dorotea and Cerro Dorotea formations

Detrital geochronology from four stratigraphic horizons (649 grains) within the mapped Cerro Dorotea Formation and its contact with the underlying Dorotea Formation yields major age groups between 60-66 Ma, 74-115 Ma, 123-160 Ma, 473-630 Ma, 960-1130 Ma, and fewer early Paleozoic and Proterozoic zircons. The lowest sample (15LDC05) collected from a horizon considered as part of the uppermost exposures of the Dorotea Formation yields an MDA of 65.8 ± 1.3 Ma. In the Cerro Dorotea Formation, two samples (14AVDZ1 and 14AVDZ1), collected from thick trough cross-bedded tan and orangish brown sandstone with interbedded siltstone and

coal-bearing mudstone, yield MDAs of 61.9 ± 0.3 Ma and 60.5 ± 0.8, respectively (Fig. 3). The stratigraphically highest level was sampled twice in the exact location (to overcome low zircon yield in the first sample), ~3 m below the top of the formation (14AVDZ3 + 15LDC02) and yields a MDA of 60.2 ± 1.3 Ma.

Lower member of the Río Turbio Formation

Three samples (413 grains) collected from the overlying greenish gray and brown glauconitic sandstone units, interpreted as subaqueous deltaic deposits, yield similar zircon U-Pb age distributions with a pronounced Eocene peak, two Late Cretaceous age clusters, and few Jurassic ages (Fig. 2). Estimation of MDAs from the youngest zircon population indicates sedimentation of the basal glauconitic sandstone by ca. 47.1 ± 2.7 Ma (14LDC-DZ4) and the overlying brown deltaic sandstone unit by 46.3 ± 1.3 Ma (14LDC-DZ2). The uppermost sample collected from a glauconitic sandstone at the top of the exposed unit yields a youngest age cluster with a MDA of 41.3 ± 0.3 Ma (17CCRT2-29).

Upper member of the Río Turbio Formation

We collected three detrital zircon U-Pb geochronology samples (312 grains) from fossiliferous and highly bioturbated marine strata of the upper member of the Río Turbio Formation. Using the stratigraphic subdivisions of Rodríguez Raising (2010) and the presence of a mappable and distinct coal seam as a reference, samples RT28DZ08 and RT28DZ07 were positioned in the upper half of Sequence VIII, and sample RT28DZ05 was collected from the top of Sequence IX (Rodríguez Raising, 2010) of the upper Río Turbio Formation. These samples yield robust age populations between 29-45 Ma, 63-109, 113-137 Ma, 218-288 Ma, and few Late Jurassic grains (Fig. 2). Proterozoic grains are noticeably lacking compared to underlying detrital

age distributions. Youngest age clusters from the upper half of the unit yield a MDA ca. 36.6 ± 0.3 Ma (RT28DZ08) and 35.4 ± 0.2 Ma (RT28DZ07). At the top of the ~506 m thick succession, organic-rich mudstones below the contact with the Río Guillermo Formation yield a MDA of ca. 26.6 ± 0.2 Ma (RT28DZ05).

Río Guillermo Formation

Two samples (205 grains) collected from the base of the Río Guillermo Formation yield U-Pb age peaks between 23-26 Ma, 33-36 Ma, a broad range of mid to late Cretaceous age between 72-128 Ma, 149-154 Ma, 275-304 Ma, and lesser numbers of Proterozoic grains (Fig. 2). The youngest zircon age peak from the bottom of the formation gives a MDA of ca. 24.3 ± 0.6 Ma (RT28DZ06). A second sample collected from the top of the Río Guillermo Formation, directly below a dated volcanic tuff (21.7 Ma zircon U-Pb SHRIMP-RG, Fosdick et al., 2011), yields a MDA of 22.8 ± 0.2 Ma (JCF09-237B).

The sampled section exhibits an upsection younging of zircons, increase in Cenozoic and Late Cretaceous zircons, and decrease in all zircon age groups older than ca. 135 Ma (Fig. 2). The most pronounced loss of Late Jurassic - Early Cretaceous (~20% to ~6%) and Paleozoic (40-17% to 7%), and Mesoproterozoic-Archean (20% to 8%) is observed across the Paleocene Cerro Dorotea Formation – middle Eocene Río Turbio Formation contact (Fig. 2 and Fig. 3). Only the Río Guillermo Formation exhibits a slight covarying increase in both the Late Jurassic - Early Cretaceous group and Paleozoic age group. These percentage trends persist, even when accounting for the large influx of Cenozoic grains, as shown by the normalized zircon age groups >66 Ma (Fig. 4).

DISCUSSION

Revised Timing of Foreland Sedimentation

New geochronological constraints on depositional ages in the Magallanes-Austral Basin suggest significantly younger timing for middle Cenozoic inland sea transgressions and onset of exclusively fluvial sedimentation in the study area (Fig. 5). These results redefine our understanding of the genetic relationship between sedimentation and changes in relative sea level, climate, and phases of deformation in the Andean orogenic belt (Fig. 6). Under the prevailing view, there are four major Cenozoic Atlantic transgressions in the Magallanes-Austral Basin of Patagonia and Tierra del Fuego: Maastrichtian-Danian, late Middle Eocene, late Oligocene – early Miocene (*Juliense*), and early Miocene (*Leonense*) (Malumián and Náñez, 2011; Parras et al., 2012; Perkins et al., 2012; Cuitiño et al., 2012). In the proximal Magallanes-Austral Basin near Cerro Castillo (Fig. 1), the Maastrichtian deltaic Dorotea Formation is overlain by the laterally discontinuous Paleocene Cerro Dorotea Formation and overlying Eocene estuarine and deltaic Río Turbio Formation (Fig. 5; Hünicken, 1955; Malumián and Caramés, 1997; Rodríguez Raising, 2010; Pearson et al., 2012; George et al., 2020). Debate persists on the age of the Río Turbio Formation (Malumián and Caramés, 1997; Rodríguez Raising, 2010; Schweitzer et al., 2012). Riccardi and Rolleri (1980) reported an Eocene through Miocene age, whereas more recent biostratigraphic work suggests exclusively Eocene biozones (Malumián and Caramés, 1997; Guerstein et al., 2014; González Estebenet et al., 2015, 2017). Based on such age assignments for these strata, many workers have interpreted the upper Cerro Dorotea through Río Turbio deposits within the paleoclimatic context of Paleogene climatic optima such as the Paleocene-Eocene Thermal Maximum and Early Eocene Climatic Optimum (Fig. 6; e.g., Nullo and Combina, 2011). Our data support this age (61-60 Ma) and paleoclimatic interpretation for the Cerro Dorotea Formation through only the basal portion of the lower Río

330 Turbio Formation, which is Lutetian (47-41 Ma) in age (Fig. 5). The Cerro Dorotea Formation is
331 recognized in Argentina and assigned to the Danian mostly based on the foraminiferal content
332 (Malumián and Náñez, 2011), but our radiometric age suggests a later, Selandian, maximum
333 depositional age, also giving the first formal confirmation of the occurrence of this Paleocene
334 lithostratigraphic unit in Chile.

335 The subaqueous deltaic lower Río Turbio Formation contains detrital zircons that indicate
336 Eocene sedimentation starting at ca. 47 Ma and continued through at least ca. 41 Ma (Fig. 5).
337 These depositional ages are compatible with middle Eocene age estimates from dinoflagellate
338 cyst biozonation, ranging from 46-39 Ma (Zone I of González Estebenet et al., 2015; and RTF 1
339 and 2 from González Estebenet et al., 2017), leaf impressions, shark teeth, and marine
340 invertebrate fossils recovered from these deposits (Griffin, 1991; Otero et al., 2013; Otero and
341 Soto-Acuña, 2015; Panti, 2019, 2020). Moreover, these strata show similar age, sedimentary
342 facies, fossil content, and mineral composition to those of its northern equivalent in the Man
343 Aike Formation near Lago Argentino (Marenssi et al., 2002; Casadío et al., 2009; Rodríguez
344 Raising, 2010; Cuitiño et al., 2019) and Sierra Baguales (Ugalde, 2014; Gutiérrez et al., 2017),
345 pointing to stratigraphic correlation of a regional, renewed depositional phase of foreland
346 sedimentation across the Paleocene unconformity surface (George et al., 2020).

347 In contrast, our findings from the upper Río Turbio Formation show substantially
348 younger ages ca. 37-27 Ma (Fig. 5), indicating that these deposits are not associated with
349 early/middle Eocene climatic events. Rather, they record late Eocene through Oligocene
350 paleoenvironmental and tectonic conditions (Fig. 6). The new depositional ages on the middle
351 and upper part of the upper Río Turbio Formation are compatible with the recently proposed
352 dinoflagellate cyst biozonation for this unit: samples RT28DZ08 and RT28DZ07 belong to

353 stratigraphic levels included within Zone III of González Estebenet et al. (2015), or RTF4 of
354 González Estebenet et al. (2017). These biostratigraphic levels were indirectly dated between
355 35.5 – 33.5 Ma (latest Eocene), making a good match with our observed U-Pb maximum
356 depositional ages. However, González Estebenet et al. (2015, 2017) note that preserved
357 palynomorphs were not recovered from the top of the Río Turbio Formation, and thus no
358 independent biostratigraphic age is presently available for the contact between the Río Turbio
359 and Río Guillermo formations. Our maximum depositional ages of ca. 27 Ma fill this important
360 gap in basin chronology.

361 We suggest a latest Eocene through Oligocene age (this work) for the upper Río Turbio
362 Formation. This interpretation is also more compatible with paleobotanical data that suggest
363 mesothermal conditions at high latitude, based on the abundance and diversity of fossilized
364 *Nothofagus* morphotype leaf impressions and wood fragments (Hünicken, 1955; Panti, 2019;
365 Pujana and Ruiz, 2019). Whereas the warm early to middle Eocene conditions in Patagonia
366 favored high tropical to subtropical (mega/mesothermal) plant diversity (Wilf et al., 2003; Panti,
367 2014, 2020), the late Eocene-Oligocene transition ushered forth increased diversification and
368 abundance of meso- and microthermal floral elements across southern Gondwana, including the
369 widespread dominion of genus *Nothofagus* (Acosta et al., 2014; Vento and Prámparo, 2018;
370 Panti, 2019; Pujana and Ruiz, 2019).

371 Our younger basin age model suggests that the deepening to offshore conditions in the
372 upper Río Turbio Formation ca. 37 Ma coincides with basin subsidence and deepening observed
373 in Tierra del Fuego during propagation of the Fuegian fold-thrust belt ensuing after the first
374 opening of the Drake Passage (Livermore et al., 2007; Ghiglione et al., 2008). This deepening
375 was also notably concurrent with a late Eocene marine transgression (Fig. 6) and the beginning

of the Antarctic ice sheet expansion (Zachos et al., 2001; Francis et al., 2008). Sustained shallow-marine conditions along the margin of the Magallanes Basin between ca. 37 and 27 Ma, despite Oligocene eustatic sea level fall suggests an additional tectonic mechanism for marine conditions. More broadly, we suggest that the upper Río Turbio Formation marks a phase of overall early Oligocene basin deepening, eastward loading of the foreland, and diachronous marine flooding driven by topographic loading from the fold-and-thrust belt (Fosdick et al., 2011) and coeval transpression across the North Scotia Ridge (Lagabrielle et al., 2009) (Fig. 6). It follows that the subsurface marine succession of the El Huemul Formation on the southern extreme of the Golfo de San Jorge Basin (Paredes et al., 2015) could represent the distal record of tectonically driven lithospheric flexure and basin deepening. Continued marine sedimentation evolved to a more extensive incursion along the Atlantic coast, represented by the San Julián Formation, during the beginning of the *Juliense* stage of the "*Patagonian Sea*" (Parras et al., 2012). Tectonic basin deepening in southern Patagonia may have followed deepening episodes in the Drake Passage, as suggested by changes in neodymium isotope ratios interpreted to record an influx of Pacific seawater into the Atlantic Ocean ca. 41-37 Ma (Scher and Martin, 2006; Livermore et al., 2007). However, relative sea level highs around Antarctica due to near-field processes during glaciation (e.g., Stocchi et al., 2013) may have also affected sea level in southeastern Patagonia prior to a global sea level decrease through the Oligocene.

New geochronological data from the overlying fluvial Río Guillermo Formation suggest its deposition took place between latest Chattian through Aquitanian time ca. 24-21 Ma (Fig. 5). These radiometric results revise the previously accepted biostratigraphic upper Eocene to lower Oligocene age (Malumián and Caramés, 1997; Vento et al., 2017) and the interpretation that the Río Guillermo Formation predates a rejuvenated phase of Andean orogenesis. These coarse-

grained strata reflect the first Cenozoic fully continental conditions on the Patagonian foredeep depocenter (c.f. Varela et al., 2019) in the area. The onset of fluvial deposition coincides with ca. 27-21 Ma fault motion on the Río El Ríncon-Castillo thrusts (Fosdick et al., 2011), suggesting these deposits reflect increased supply of tectonically generated sediment (c.f., Armitage et al., 2011) during structural uplift and unroofing of the Patagonian orogen. This interpretation is consistent with published subsurface data just to the south of our study area (Fig. 1) that record latest Eocene through early Miocene prograding clastic strata (Gallardo, 2015; Gallardo Jara et al., 2019).

REORGANIZATION OF SEDIMENT PROVENANCE AND ROUTING

Detrital provenance data from the Upper Cretaceous – Miocene basin infill track changes in relative proportions of zircon age groups for pre-Cenozoic age groups (Fig. 2). A comparison with the Upper Cretaceous basin record and our new data show the upsection rise and subsequent loss of Jurassic – Early Cretaceous (J-K1) grains (blue wedge), a progressive loss of Precambrian and Paleozoic grains (browns and pink wedges), and an overall increase in Late Cretaceous and Cenozoic igneous sources (gray and white wedges). Notably, the Paleocene Cerro Dorotea Formation maintains similar provenance and gross depositional character to the underlying Dorotea Formation. This similarity indicates little to no drainage divide reorganization nor exposure of new sources during southward building of the continental shelf (Schwartz and Graham, 2015) from Maastrichtian to earliest Selandian time. Moreover, this observation is noteworthy because of the discontinuous nature of the Cerro Dorotea Formation along the frontal monocline, which has invited debate regarding its original lateral extent and subsequent erosion versus heterogeneous depositional footprint (e.g., Fosdick et al., 2015). The Paleocene foreland basin phase along this sector of the basin may have once been more geographically widespread

prior to erosional removal and resumed deposition with the middle Eocene Río Turbio Formation that forms the Paleogene unconformity (Fig. 6).

The largest shift in sediment provenance signature occurred across the Paleocene Cerro Dorotea and the middle Eocene Río Turbio Formation boundary, marked by a conspicuous decline of Late Jurassic and Paleozoic zircons (Figs. 2 and 4). Zircons of these ages are sourced from hinterland thrust sheets (Fig. 1) that expose the Upper Jurassic volcanic Tobífera Formation (Pankhurst et al., 2000; Calderón et al., 2007) and Paleozoic basement (Hervé et al., 2003; Lacassie et al., 2006; Pankhurst et al., 2006). The concurrent increase in Cenozoic zircons from the Patagonian Batholith may act to swamp out the signal from these older zircon sources. However, a comparison of relative proportion of pre-66 Ma age groups show similar trends in the rise and decline of the Jurassic and Paleozoic age groups (Fig. 4). We interpret this initial shift as likely a consequence of tectonic changes in sediment routing between ca. 60 and 44 Ma, when the basin became topographically isolated from northwestern hinterland sources during deformation and widening across the external fold-thrust belt.

Our age control of the Paleogene unconformity in our study area improves upon the work of Fosdick et al. (2015) who compared provenance and burial histories of the Dorotea Formation with the upper Río Turbio Formation, but lacked higher provenance resolution from intervening deposits. Additionally, the ca. 15 m.y. hiatus estimated by our model partially matches recently published ages in Sierra Baguales and Río Las Chinas, ~40 km north of our study area (Gutiérrez et al., 2017; George et al., 2020). There, a ca. 20 m.y. hiatus across the Paleogene unconformity has been proposed by George et al. (2020), also based on detrital zircon U-Pb geochronology. Evidence of coeval basin burial thermal heating (Fosdick et al., 2015; Süssenberger et al., 2017) in the central thrust belt and development of a basin-wide foreland unconformity is consistent

445 with this timeframe. New provenance data sheds light on the timing of Tenerife thrusting (Fig. 6)
446 and further supports an Eocene phase of orogenesis that is well-documented in the Fuegian
447 Andes (Biddle et al., 1986; Ghiglione and Ramos, 2005; Barbeau et al., 2009), but remains
448 enigmatic in the Southern Patagonian Andes. This finding suggests that, rather than being an
449 inactive foreland basin during this time (Sachse et al., 2015; Horton and Fuentes, 2016), a more
450 continuous fold-and-thrust belt and basin depocenter connected the Patagonian and Fuegian
451 Andes during development of the Fuegian orocline (Ghiglione et al., 2010).

452 These upsection trends continue into late Eocene-Oligocene time when sediment
453 provenance of the upper Río Turbio Formation reflects predominantly Cretaceous and younger
454 age peaks. Prominent Eocene and Late Cretaceous age clusters include two prominent new
455 populations – denoted here as K4 (ca. 80-66 Ma) and P2 (ca. 35-25 Ma) – that are not well-
456 recognized in in-situ batholith geochronology datasets (Hervé et al., 2007) and extend the record
457 of pulsed activity of arc magmatism (Fig. 2). In the most comprehensive summary of the
458 Southern Patagonian Batholith magmatism, Hervé et al (2007) document a Paleogene phase of
459 magmatism from 67-40 Ma, and a Neogene phase from 25-16 Ma. These detrital findings of K4
460 and P2 zircon populations highlight the value of the sedimentary archive in recognizing phases
461 of magmatism not represented in available bedrock records. By ca. 26 Ma and the end of the
462 marine sedimentation at this latitude, detrital zircons derived from the Late Jurassic Tobífera
463 thrust sheets (Fig. 1), which were once a dominant sediment source to the Cenomanian-
464 Paleocene basin, are virtually absent in the basin fill. Synchronous with this change in
465 depositional environment is a marked provenance shift to increased mafic volcanic and recycled
466 sedimentary sources, suggesting the change in environment is linked to upland tectonic/climate
467 changes with a lesser control from low-stand in global sea level (Leonard, 2017; Leonard et al.,

2020). This timing of transition to fully continental sedimentation coincides with deformation in the fold-and-thrust belt at Río El Rincon thrust and related structures (Fosdick et al., 2011). We suggest the Río Guillermo Formation represents tectonically generated sediment (e.g., Horton et al., 2004; Armitage et al., 2011) associated with this phase of deformation.

Fluvial sedimentation was temporarily disrupted by flooding of the foreland basin by the *Leonense* marine incursion (Ameghino, 1906; Cuitiño and Scasso, 2010; Parras et al., 2012, 2020; Cuitiño et al., 2012), which may have been further enhanced by subsidence loading during Toro thrust faulting (Fig. 6). Resumed fluvial deposition of the Santa Cruz Formation is classically cited as the molasse deposits of the main phase of early Miocene Andean orogenesis and surface uplift (e.g., Blisniuk et al., 2005; Ramos, 2005; Bostelmann et al., 2013; Cuitiño et al., 2016; Raigemborn et al., 2018). Published detrital geochronology from the overlying early Miocene Santa Cruz Formation yields dominantly (>70%) Late Cretaceous zircons (Fosdick et al., 2015). Based on modeling of detrital zircon U-Pb-He thermochronological data, Fosdick et al. (2015) suggested these grains were recycled from the Upper Cretaceous clastic wedge rather than direct sourcing of the Mesozoic batholith. Our data from underlying strata corroborate this interpretation and capture a more complete transition of provenance loss of the Jurassic and Paleozoic age groups.

General provenance and sediment recycling

The rise and subsequent isolation of diagnostic sediment sources or detrital zircon age groups bears on resolving complexities from sediment recycling (Schmitt and Steidtmann, 1990; Dickinson et al., 2009) and variability in zircon fertility (Moecher and Samson, 2006). As such, a geologically diagnostic age source – especially one with smaller and/or more fragile grains (e.g.,

volcanics) – is a useful tracer for identifying primary versus recycled sources and constraints on movement of orogenic drainage divides during changes in orogenic wedge behavior. The Eocene-through Oligocene upsection depletion of Jurassic and Paleozoic sources near 51°S, concurrent with sustained dominance of plutonic arc-derived Cretaceous zircons (Fig. 4), suggests recycling of the Cretaceous strata in the Río Turbio Formation and winnowing of the smaller and more fragile Jurassic volcanic and Paleozoic zircons during sediment transport. Moreover, the isolation of hinterland and primary Cretaceous batholith sources requires a cratonward shift in the drainage divide by ca. 44 Ma. This change in sediment routing was followed by subsequent hinterland shift in the drainage divide that occurred sometime after ca. 18 Ma, at which point sedimentation shifted to a more distal, offshore location (Ghiglione et al., 2016b).

This synchronous adjustment in retroarc basin configuration has been observed along >600 km length of the Patagonian and Fuegian Andes (Blisniuk et al., 2005, 2006; Boutonnet et al., 2010; Cuitiño et al., 2016), with multiple mechanisms considered, including: 1) a reduction in sediment supply to the retroarc foreland basin caused by fold-and-thrust belt deformation and growth of an orographic rain shadow (Blisniuk et al., 2005, 2006), 2) effects of a shallowing slab geometry and associated eastward arc-migration between 14-12 Ma (e.g., Espinoza et al., 2010; Boutonnet et al., 2010) and subduction erosion without changes in the slab dip (e.g., Ramírez de Arellano et al., 2012), and 3) regional surface uplift in response to formation of the Chile Ridge slab window beneath Patagonia (Fig. 6; Guillaume et al., 2009; Dávila et al., 2019). Today, the hinterland high peaks of the Patagonian Andes constitute the upland sediment sources to rivers and glacial valleys that drain both sides of the Andes and Tobífera thrusts (Fig. 1; Pepper et al., 2016).

SUMMARY AND IMPLICATIONS

In summary, new estimates of maximum depositional ages from detrital geochronology data require a revised chronostratigraphy of the middle Cenozoic strata. Our study confirms a Selandian maximum depositional age for the Cerro Dorotea Formation, previously constrained by biostratigraphy to the Danian. Sediment provenance data from the Cenozoic Magallanes-Austral Basin at 51°S track the decline of once prominent hinterland sources between ca. 60-44 Ma. We suggest a major change in sediment routing and paleogeography during this time that we attribute to a phase of Eocene orogenesis and uplift of a topographic barrier that isolated the basin from Paleozoic and Late Jurassic-Early Cretaceous sources (Fig. 6). We also identify a previously unrecognized latest Eocene through Oligocene period of marine deposition from ca. 37 to 27 Ma in the proximal foredeep depozone (upper Río Turbio Formation), followed by a major change to nonmarine sedimentation ca. 24.3 Ma. Here, we propose that the upper Río Turbio and Río Guillermo Formations, together, reflect a genetically linked stratigraphic pair that show Oligocene basin deepening and subsequent latest Oligocene - early Miocene deposition of coarse-grained sediments derived from the Patagonian hinterland, during a renewed phase of orogenesis (Fig. 6).

Moreover, an eastward incursion of an embayed foredeep trough may link the upper Río Turbio Formation to the distal El Huemul Formation and potentially the San Julián Formation, suggesting a tectonic loading origin for the *Juliense* phase of the Patagonian Sea. Additional stratigraphic correlation to the Atlantic margin is needed to test this hypothesis. The late Oligocene – early Miocene synchronicity of (1) proximal fluvial facies (Río Guillermo Formation) and distal marine facies (*Juliense* and *Leonense*), (2) active orogenic deformation (Río El Rincon and Toro thrust faults), and (3) sustained global sea level highstand, taken

536 together, indicates high sediment supply during shortening of the thrust-belt (Fig. 6). In the case
537 of the Oligocene – early Miocene Patagonian record, we suggest that the combined effects of
538 tectonics – flexural loading of the upper plate and increased sediment supply from actively
539 exhuming orogenic sources – are primary drivers for marine incursions.

540 Rejuvenated late Oligocene through early Miocene retroarc foreland sedimentation in
541 southern Patagonia – and elsewhere along the Andean margin (e.g., Carrapa et al., 2005; Perez
542 and Horton, 2014; Horton and Fuentes, 2016; Fosdick et al., 2017) – may signal a Cordilleran-
543 scale upper plate transition to a dominantly compressional margin and active retroarc foreland
544 basin systems (Horton, 2018; Chen et al., 2019) that include the southern Patagonian Andes
545 sector. This response was likely due to increased plate convergence (Somoza and Ghidella,
546 2012) and initiation of the Nazca plate subduction regime (e.g., Barckhausen et al., 2008). In
547 Patagonia, regional retroarc deformation and basin development may have been enhanced by
548 three-dimensional stress from transpressional tectonics along the North Scotia Ridge (Bry et al.,
549 2004; Ramos and Ghiglione, 2008; Lagabrielle et al., 2009). These findings underscore central
550 requirements of detailed chronology and provenance to develop basin age models and
551 understanding of long-term changes in sources that reflect orogen-scale responses to tectonics,
552 climate, and eustasy.

553 **ACKNOWLEDGMENTS**

554 Research was supported by the U.S. National Science Foundation Award EAR-1649585
555 to JCF, the Robert R. Shrock Foundation at Indiana University, faculty research funds from the
556 University of Connecticut, and Project Anillo de Investigación en Ciencia Antártica (ATC-105).
557 JEBT expresses his gratitude to Proyecto Anillo ACT-172099. T. Schwartz, S. Casadío, and A.
558 Parras contributed to fruitful discussions on Patagonian geology. La Cumbre Baguales Geo-
559 Paleontological Park, Hotel Remota, the Torres del Paine Municipality, Hielos Patagónicos,
560 Mountain Travel, at Puerto Natales, and N. Raffer provided logistical support. We thank S.F

Alvarez for permission to conduct fieldwork at the Estancia Cancha Carrera. The Arizona LaserChron Center (NSF Award EAR-1338583) provided expert analytical assistance. Reviews on previous manuscript versions by N. Perez, A. Stevens Goddard, D. Barbeau, and G. Dix greatly improved the scope of our work. We thank Lithosphere Editor L. Godin for careful handling of our manuscript, and two anonymous reviewers for their constructive reviews.

REFERENCES CITED

Acosta, M.C., Mathiasen, P., and Premoli, A.C., 2014, Retracing the evolutionary history of Nothofagus in its geo-climatic context: New developments in the emerging field of phylogeology: Geobiology, v. 12, p. 497–510, doi:10.1111/gbi.12098.

Ameghino, F., 1906, Les formations sédimentaires du Crétacé Supérieur et du Tertiaire de Patagonie avec un parallelé entre leurs faunes mammalogiques et celles de l´ancien continent: Anales del Museo Nacional de Buenos Aires (tercera serie), v. 8, p. 1–568.

Antoine, P.-O. et al., 2016, A 60-million-year Cenozoic history of western Amazonian ecosystems in Contamana, eastern Peru: Gondwana Research, v. 31, p. 30–59, doi:10.1016/j.gr.2015.11.001.

Aramendía, I., Cuitiño, J.I., Ghiglione, M., and Bouza, P.J., 2019, Tectonostratigraphic significance of the Neogene sedimentary record of northwestern Austral-Magallanes basin, Argentinean Patagonia: Latin American Journal of Sedimentology and Basin Analysis, v. 26, p. 99–126.

Armitage, J.J., Duller, R.A., Whittaker, A.C., and Allen, P.A., 2011, Transformation of tectonic and climatic signals from source to sedimentary archive: Nature Geoscience, v. 4, p. 231–235, doi:10.1038/ngeo1087.

Barbeau, D.L., Olivero, E.B., Swanson-Hysell, N.L., Zahid, K.M., Murray, K.E., and Gehrels, G.E., 2009, Detrital-zircon geochronology of the eastern Magallanes foreland basin: Implications for Eocene kinematics of the northern Scotia Arc and Drake Passage: Earth and Planetary Science Letters, v. 284, p. 489–503, doi:10.1016/j.epsl.2009.05.014.

Barckhausen, U., Ranero, C.R., Cande, S.C., Engels, M., and Weinrebe, W., 2008, Birth of an intraoceanic spreading center: Geology, v. 36, p. 767–770, doi:10.1130/g25056a.1.

Beaumont, C., Fullsack, P., and Hamilton, J., 1992, Erosional control of active compressional orogens, *in* McClay, K.R. ed., Thrust Tectonics, Chapman and Hall, p. 1–18.

Bechis, F., Encinas, A., Concheyro, A., Litvak, V.D., Aguirre-Urreta, B., and Ramos, V.A., 2014, New age constraints for the Cenozoic marine transgressions of northwestern Patagonia, Argentina (41°-43° S): Paleogeographic andtectonic implications: Journal of South American Earth Sciences, v. 52, p. 72–93, doi:10.1016/j.jsames.2014.02.003.

Bernhardt, A., Jobe, Z.R., Grove, M., and Lowe, D.R., 2012, Palaeogeography and diachronous

infill of an ancient deep-marine foreland basin, Upper Cretaceous Cerro Toro Formation, Magallanes Basin: Basin Research, v. 24, p. 269–294, doi:10.1111/j.1365-2117.2011.00528.x.

Biddle, K.T., Uliana, M.A., Mitchum, R.M., Fitzgerald, M.G., and Wright, R.C., 1986, The stratigraphic and structural evolution of the central and eastern Magallanes Basin, southern South America, *in* Allen, P.A. and Homewood, P. eds., Foreland Basins, Oxford, UK, Blackwell Publishing Ltd., v. 8, p. 41–61, doi:doi: 10.1002/9781444303810.ch2.

Blisniuk, P.M., Stern, L.A., Chamberlain, C.P., Idleman, B., and Zeitler, P.K., 2005, Climatic and ecologic changes during Miocene surface uplift in the Southern Patagonian Andes: Earth and Planetary Science Letters, v. 230, p. 125–142, doi:10.1016/j.epsl.2004.11.015.

Blisniuk, P.M., Stern, L.A., Chamberlain, C.P., Zeitler, P.K., Ramos, V.A., Sobel, E.R., Haschke, M., Strecker, M.R., and Warkus, F., 2006, Links between mountain uplift, climate, and surface processes in the southern Patagonian Andes, *in* The Andes, p. 429–440, doi:10.1007/978-3-540-48684-8_20.

Bonnet, S., and Crave, A., 2003, Landscape response to climate change: Insights from experimental modeling and implications for tectonic versus climatic uplift of topography: Geology, v. 31, p. 123–126, doi:10.1130/0091-7613(2003)031<0123:LRTCCI>2.0.CO.

Bostelmann, J.E., Le Roux, J.P., Vasquez, A., Gutiérrez, N.M., Oyarzún, J.L., Carreño, C., Torres, T., Otero, R., Llanos, A., Fanning, C.M., and Hervé, F., 2013, Burdigalian deposits of the Santa Cruz Formation in the Sierra Baguales, Austral (Magallanes) Basin: Age, depositional environment and vertebrate fossils: Andean Geology, v. 40, p. 458–489, doi:10.5027/andgeoV40n3-a04.

Boutonnet, E., Arnaud, N., Guivel, C., Lagabrielle, Y., Scalabrino, B., and Espinoza, F., 2010, Subduction of the South Chile active spreading ridge: A 17 Ma to 3 Ma magmatic record in central Patagonia (western edge of Meseta del Lago Buenos Aires, Argentina): Journal of Volcanology and Geothermal Research, v. 189, p. 319–339, doi:10.1016/j.jvolgeores.2009.11.022.

Breitsprecher, K., and Thorkelson, D.J., 2009, Neogene kinematic history of Nazca–Antarctic–Phoenix slab windows beneath Patagonia and the Antarctic Peninsula: Tectonophysics, v. 464, p. 10–20, doi:10.1016/j.tecto.2008.02.013.

Browning, J. V., Miller, K.G., McLaughlin, P.P., Kominz, M.A., Sugarman, P.J., Monteverde, D., Feigenson, M.D., and Hernández, J.C., 2006, Quantification of the effects of eustasy, subsidence, and sediment supply on Miocene sequences, mid-Atlantic margin of the United States: Bulletin of the Geological Society of America, v. 118, p. 567–588, doi:10.1130/B25551.1.

Bry, M., White, N., Singh, S., England, R., and Trowell, C., 2004, Anatomy and formation of oblique continental collision: South Falkland basin: Tectonics, v. 23, p. 1–20, doi:10.1029/2002TC001482.

634 Calderón, M., Fildani, A., Hervé, F., Fanning, C.M.M., Weislogel, A., and Cordani, U., 2007,
635 Late Jurassic bimodal magmatism in the northern sea-floor remnant of the Rocas Verdes
636 basin, southern Patagonian Andes: Journal of the Geological Society, v. 164, p. 1011–1022,
637 doi:10.1144/0016-76492006-102.

638 Carrapa, B., Adelmann, D., Hilley, G.E., Mortimer, E., Sobel, E.R., and Strecker, M.R., 2005,
639 Oligocene range uplift and development of plateau morphology in the southern central
640 Andes: Tectonics, v. 24, p. 1–19, doi:10.1029/2004TC001762.

641 Casadío, S., Griffin, M., Marenssi, S., Net, L., Parras, A., Rodríguez Raising, M.E., and
642 Santillana, S., 2009, Paleontology and sedimentology of Middle Eocene rocks in Lago
643 Argentino area, Santa Cruz Province, Argentina: Ameghiniana, v. 46, p. 27–47.

644 Chen, Y.-W., Wu, J., and Suppe, J., 2019, Southward propagation of Nazca subduction along the
645 Andes: Nature, v. 565, p. 441–447, doi:10.1038/s41586-018-0860-1.

646 Christie-Blick, N., 1991, Onlap, offlap, and the origin of unconformity-bounded depositional
647 sequences: Marine Geology, v. 97, p. 35–56, doi:10.1016/0025-3227(91)90018-Y.

648 Clift, P.D., Shimizu, N., D, L.G., Blusztaign, J.S., Gaedicke, C., Schluter, H.-H., Clark, M.K.,
649 and Amjad, S., 2001, Development of the Indus Fan and its significance for the erosional
650 history development of the Indus Fan and its significance for the erosional history of the
651 Western Himalaya and Karakoram: Geological Society of America Bulletin, v. 113, p.
652 1039–1051, doi:10.1130/0016-7606(2001)113<1039.

653 Cox, R., Lowe, D.R., and Cullers, R.L., 1995, The influence of sediment recycling and basement
654 composition on evolution of mudrock chemistry in the southwestern United States:
655 Geochimica et Cosmochimica Acta, v. 59, p. 2919–2940, doi:10.1016/0016-
656 7037(95)00185-9.

657 Cruz, L., Malinski, J., Hernandez, M., Take, A., and Hilley, G.E., 2011, Erosional control of the
658 kinematics of the Aconcagua fold-and-thrust belt from numerical simulations and physical
659 experiments: Geology, v. 39, p. 439–442, doi:10.1130/G31675.1.

660 Cuitiño, J.I., Fernicola, J.C., Kohn, M.J., Trayler, R., Naipauer, M., Bargo, M.S., Kay, R.F., and
661 Vizcaíno, S.F., 2016, U-Pb geochronology of the Santa Cruz Formation (early Miocene) at
662 the Río Bote and Río Santa Cruz (southernmost Patagonia, Argentina): Implications for the
663 correlation of fossil vertebrate localities: Journal of South American Earth Sciences, v. 70,
664 p. 198–210, doi:10.1016/j.jsames.2016.05.007.

665 Cuitiño, J.I., Pimentel, M.M., Ventura Santos, R., and Scasso, R. a., 2012, High resolution
666 isotopic ages for the early Miocene “Patagoniense” transgression in Southwest Patagonia:
667 Stratigraphic implications: Journal of South American Earth Sciences, v. 38, p. 110–122,
668 doi:10.1016/j.jsames.2012.06.008.

669 Cuitiño, J.I., and Scasso, R.A., 2010, Sedimentología y paleoambientes del Patagoniano y su
670 transición a la Formatión Santa Cruz al sur del Lago Argentino, Patagonia Austral: Revista
671 de la Asociación Geológica Argentina, v. 66, p. 406–417,

672 doi:http://hdl.handle.net/11336/16534.

673 Cuitiño, J.I., Varela, A.N., Ghiglione, M.C., Richiano, S., and Poiré, D.G., 2019, The Austral-
674 Magallanes Basin (southern Patagonia): A synthesis of its stratigraphy and evolution: Latin
675 American Journal of Sedimentology and Basin Analysis, v. 26, p. 155–166.

676 Dahlen, F.A., Suppe, J., and Davis, D., 1984, Mechanics of fold-and-thrust belts and accretionary
677 wedges Cohesive Coulomb theory: Journal of Geophysical Research, v. 89, p. 10087–
678 10101, doi:10.1029/JB089iB12p10087.

679 Dávila, F.M., Ávila, P., and Martina, F., 2019, Relative contributions of tectonics and dynamic
680 topography to the Mesozoic-Cenozoic subsidence of southern Patagonia: Journal of South
681 American Earth Sciences, v. 93, p. 412–423, doi:10.1016/j.jsames.2019.05.010.

682 Dickinson, W.R., Lawton, T.F., and Gehrels, G.E., 2009, Recycling detrital zircons: A case study
683 from the Cretaceous Bisbee Group of southern Arizona: Geology, v. 37, p. 503–506,
684 doi:10.1130/G25646A.1.

685 Dix, G.R., and Parras, A., 2014, Integrated diagenetic and sequence stratigraphy of a late
686 Oligocene-early Miocene, mixed-sediment platform (Austral Basin, southern Patagonia):
687 Resolving base-level and paleoceanographic changes, and paleoaquifer characteristics:
688 Sedimentary Geology, v. 307, p. 17–33, doi:10.1016/j.sedgeo.2014.04.003.

689 Espinoza, F., Morata, D., Polvé, M., Lagabrielle, Y., Maury, R., de la Rupelle, A., Guivel, C.,
690 Cotten, J., Bellon, H., and Suárez, M., 2010, Middle Miocene calc-alkaline volcanism in
691 Central Patagonia (47°S): petrogenesis and implication for slab dynamics: Andean Geology,
692 v. 37, p. 300–328.

693 Fildani, A., Cope, T.D., Graham, S.A., and Wooden, J.L., 2003, Initiation of the Magallanes
694 foreland basin: Timing of the southernmost Patagonian Andes orogeny revised by detrital
695 zircon provenance analysis: Geology, v. 31, p. 1081–1084.

696 Flemings, P.B., and Jordan, T.E., 1989, A synthetic stratigraphic model of foreland basin
697 development: Journal of Geophysical Research, v. 94, p. 3851–3866.

698 Fosdick, J.C., Graham, S.A., and Hilley, G.E., 2014, Influence of attenuated lithosphere and
699 sediment loading on flexure of the deep-water Magallanes retroarc foreland basin, Southern
700 Andes: Tectonics, v. 33, p. 2505–2525, doi:10.1002/2014TC003684.

701 Fosdick, J.C., Grove, M., Graham, S.A., Hourigan, J.K., Lovera, O., and Romans, B.W., 2015,
702 Detrital thermochronologic record of burial heating and sediment recycling in the
703 Magallanes foreland basin, Patagonian Andes: Basin Research, v. 27, p. 546–572,
704 doi:10.1111/bre.12088.

705 Fosdick, J.C., Reat, E.J., Carrapa, B., Ortiz, G., and Alvarado, P.M., 2017, Retroarc basin
706 reorganization and aridification during Paleogene uplift of the southern central Andes:
707 Tectonics, v. 36, p. 493–514, doi:10.1002/2016TC004400.

Fosdick, J.C., Romans, B.W., Fildani, A., Bernhardt, A., Calderón, M., and Graham, S.A., 2011, Kinematic evolution of the Patagonian retroarc fold-and-thrust belt and Magallanes foreland basin, Chile and Argentina, 51°30'S: Geological Society of America Bulletin, v. 123, p. 1679–1698.

Francis, J.E, Marenssi, S., Levy, R., Hambrey, M., Thorn, V.C., Mohr, B., Brinkhuis, H., Warnaar, J., Zachos, J., Bohaty, S., and DeConto, R., 2008, Chapter 8. From Greenhouse to Icehouse - The Eocene/Oligocene in Antarctica: Developments in Earth and Environmental Sciences, v. 8, p. 309–368, doi:10.1016/S1571-9197(08)00008-6.

Furque, G., and Camacho, H.H., 1972, El Cretácico Superior y Terciario de la región Austral del Lago Argentino (Provincia de Santa Cruz): Jornadas Geológicas Argentinas, Actas, v. 4, p. 61–76.

Galeazzi, J.S., 1998, Structural and stratigraphic evolution of the western Malvinas Basin, Argentina: American Association of Petroleum Geologists Bulletin, v. 82, p. 596–636, doi:10.1306/1D9BC5C5-172D-11D7-8645000102C1865D.

Gallardo, R.E., 2015, Seismic sequence stratigraphy of a foreland unit in the Magallanes-Austral Basin, Dorado Riquelme Block, Chile: Implications for deep-marine reservoirs: Latin American Journal of Sedimentology and Basin Analysis, v. 21, p. 49–64.

Gallardo Jara, R.E., Ghiglione, M.C., and Rojas Galliani, L., 2019, Tectonic evolution of the southern Austral-Magallanes Basin in Tierra del Fuego: Latin American Journal of Sedimentology and Basin Analysis, v. 16, p. 57–74.

Gehrels, G., 2011, Detrital Zircon U-Pb Geochronology: Current Methods and New Opportunities: Tectonics of Sedimentary Basins, p. 45–62, doi:10.1002/9781444347166.ch2.

Gehrels, G.E., Valencia, V.A., and Ruiz, J., 2008, Enhanced precision, accuracy, efficiency, and spatial resolution of U-Pb ages by laser ablation-multicollector-inductively coupled plasma-mass spectrometry: Geochemistry, Geophysics, Geosystems, v. 9, p. 1–13, doi:10.1029/2007GC001805.

George, S.W.M., Davis, S.N., Fernández, R.A., Manríquez, L.M.E., Leppe, M.A., Horton, B.K., and Clarke, J.A., 2020, Chronology of deposition and unconformity development across the Cretaceous–Paleogene boundary, Magallanes-Austral Basin, Patagonian Andes: Journal of South American Earth Sciences, v. 97, 102237, doi:10.1016/j.jsames.2019.102237.

Ghiglione, M.C., Quinteros, J., Yagupsky, D., Bonillo-Martínez, P., Hlebszevtich, J., Ramos, V.A., Vergani, G., Figueroa, D., Quesada, S., and Zapata, Y.T., 2010, Structure and tectonic history of the foreland basins of southernmost South America: Journal of South American Earth Sciences, v. 29, p. 262–277, doi:10.1016/j.jsames.2009.07.006.

Ghiglione, M.C., and Ramos, V.A., 2005, Progression of deformation and sedimentation in the southernmost Andes: Tectonophysics, v. 405, p. 25–46, doi:10.1016/j.tecto.2005.05.004.

Ghiglione, M.C., Ramos, V., Cuitiño, J., and Barberón, V., 2016a, Growth of the Southern Patagonian Andes (46–53°S) and its relation with subduction processes, *in* Folguera, A., Naipauer, M., Sagripanti, L., Ghiglione, M.C., Orts, D.L., and Giambiagi, L. eds., Growth of the Southern Andes, Berlin, Springer, p. 201–240.

Ghiglione, M.C., Sue, C., Ramos, M.E., Tobal, J.E., and Gallardo, R.E., 2016b, The relation between Neogene denudation of the Southernmost Andes and sedimentation in the offshore Argentine and Malvinas Basins during the opening of the Drake Passage, *in* Geodynamic Evolution of the Southernmost Andes, p. 109–135.

Ghiglione, M.C., Yagupsky, D., Ghidella, M., and Ramos, V.A., 2008, Continental stretching preceding the opening of the Drake Passage: Evidence from Tierra del Fuego: Geology, v. 36, p. 643–646, doi:10.1130/G24857A.1.

González, E.R., 2015, Estratigrafía secuencial y sedimentología de la Formación Dorotea (Maastrichtiano), sector Río de las Chinas, Región de Magallanes y Antártica Chilena, Chile (50°S), Undergraduate thesis: Universidad de Chile, 153 p.

González Estebenet, M.S., Guerstein, G.R., and Casadío, S., 2015, Estudio bioestratigráfico y paleoambiental de la Formación Río Turbio (Eoceno medio a tardío) en el sudoeste de Patagonia (Argentina) basado en quistes de dinoflagelados: Revista Brasilera de Paleontología, v. 18, p. 429–442, doi:10.4072/rbp.2015.3.08.

González Estebenet, M.S., Guerstein, G.R., Rodríguez Raising, M.E., Ponce, J.J., and Alperín, M.I., 2017, Dinoflagellate cyst zonation for the middle to upper Eocene in the Austral Basin, southwestern Atlantic Ocean: implications for regional and global correlation: Geological Magazine, v. 154, p. 1022–1036, doi:10.1017/S0016756816000601.

Griffin, M., 1991, Bivalves from the Río Turbio Formation, Eocene southwestern Patagonia (Argentina): Journal of Paleontology, v. 65, p. 119–146, doi:10.1017/S0022336000020254.

Guerstein, G.R., González Estebenet, M.S., Alperín, M.I., Casadío, S.A., and Archangelsky, S., 2014, Correlation and paleoenvironments of middle Paleogene marine beds based on dinoflagellate cysts in southwestern Patagonia, Argentina: Journal of South American Earth Sciences, v. 52, p. 166–178, doi:10.1016/j.jsames.2014.02.011.

Guillaume, B., Martinod, J., Husson, L., Roddaz, M., and Riquelme, R., 2009, Neogene uplift of central eastern Patagonia: Dynamic response to active spreading ridge subduction? Tectonics, v. 28, p. 1–19, doi:10.1029/2008TC002324.

Gutiérrez, N.M., Le Roux, J.P., Vásquez, A., Carreño, C., Pedroza, V., Araos, J., Oyarzún, J.L., Pino, J.P., Rivera, H.A., and Hinojosa, L.F., 2017, Tectonic events reflected by palaeocurrents, zircon geochronology, and palaeobotany in the Sierra Baguales of Chilean Patagonia: Tectonophysics, v. 695, p. 76–99, doi:10.1016/j.tecto.2016.12.014.

Heller, P.L., Angevine, C.L., Winslow, N.S., and Paola, C., 1988, Two-phase stratigraphie model of foreland-basin sequences: Geology, v. 16, p. 501–504, doi:10.1130/0091-7613(1988)016<0501:TPSMOF>2.3.CO;2.

783 Hervé, F., Fanning, C.M., and Pankhurst, R.J., 2003, Detrital zircon age patterns and provenance
784 of the metamorphic complexes of southern Chile: Journal of South American Earth
785 Sciences, v. 16, p. 107–123, doi:10.1016/S0895-9811(03)00022-1.

786 Hodgson, D.M., Bernhardt, A., Clare, M.A., Da Silva, A.C., Fosdick, J.C., Mauz, B.,
787 Midtkandal, I., Owen, A., and Romans, B.W., 2018, Grand challenges (and great
788 opportunities) in sedimentology, stratigraphy, and diagenesis research: Frontiers in Earth
789 Science, v. 6, p. 1–9, doi:10.3389/feart.2018.00173.

790 Hoorn, C. et al., 2010, Amazonia through time: Andean uplift, climate change, landscape
791 evolution, and biodiversity: Science, v. 330, p. 927–931, doi:10.1126/science.1194585.

792 Horton, B.K., 2018, Sedimentary record of Andean mountain building: Earth-Science Reviews,
793 v. 178, p. 279–309, doi:10.1016/j.earscirev.2017.11.025.

794 Horton, B.K., Constenius, K.N., and DeCelles, P.G., 2004, Tectonic control on coarse-grained
795 foreland-basin sequences: An example from the Cordilleran foreland basin, Utah: Geology,
796 v. 32, p. 637, doi:10.1130/G20407.1.

797 Horton, B.K., and Fuentes, F., 2016, Sedimentary record of plate coupling and decoupling during
798 growth of the Andes: Geology, v. 44, p. 647–650, doi:10.1130/G37918.1.

799 Houben, A.J.P., Bijl, P.K., Pross, J., Bohaty, S.M., Passchier, S., Stickley, C.E., et al., 2013,
800 Reorganization of Southern Ocean plankton ecosystem at the onset of Antarctic glaciation:
801 Science, v. 340, p. 341–344, doi:doi:10.1126/science.1223646.

802 Houston, W.S., Huntoon, J.E., and Kamola, D.L., 2000, Modeling of Cretaceous foreland-basin
803 parasequences, Utah, with implications for timing of Sevier thrusting: Geology, v. 28, p.
804 267–270, doi:10.1130/0091-7613(2000)28<267:MOCFPU>2.0.CO;2.

805 Hünicken, M.A., 1955, Depósitos Neocretácicos y Terciarios del extremo SSW de Santa Cruz
806 (Cuenca Carbonífera de Río Turbio): Revista del Instituto Nacional de Investigaciones en
807 Ciencias Naturales, Ciencias Geológicas, v. 4, p. 1–161.

808 Johnsson, M.J., and Basu, A., 1993, Processes Controlling the Composition of Clastic
809 Sediments: Geological Society of America Special Paper, v. 284, doi:10.1130/SPE284.

810 Jordan, T.E., Allmendinger, R.W., Damanti, J.F., and Drake, R.E., 1993, Chronology of motion
811 in a complete thrust belt: The Precordillera, 30-31°S, Andes Mountains: The Journal of
812 Geology, v. 101, p. 135–156, doi:10.1086/648213.

813 Lacassie, J.P., Hervé, F., and Roser, B., 2006, Sedimentary provenance study of the post-Early
814 Permian to pre-Early Cretaceous metasedimentary Duque de York Complex, Chile: Revista
815 Geologica de Chile, v. 33, p. 199–219.

816 Lagabrielle, Y., Goddéris, Y., Donnadieu, Y., Malavieille, J., and Suarez, M., 2009, The tectonic
817 history of Drake Passage and its possible impacts on global climate: Earth and Planetary
818 Science Letters, v. 279, p. 197–211, doi:10.1016/j.epsl.2008.12.037.

819 Leeder, M.R., 1993, Tectonic controls upon drainage basin development, river channel migration
820 and alluvial architecture: implications for hydrocarbon reservoir development and
821 characterization: Geological Society Special Publication, v. 73, p. 7–22,
822 doi:10.1144/GSL.SP.1993.073.01.02.

823 Leonard, J.S., 2017, Miocene growth of the Patagonian Andes revealed by sedimentary
824 provenance of the Río Guillermo Formation, Magallanes-Austral Basin, Chile and
825 Argentina (51°30'S): M.S. Thesis, Indiana University, 55 p.

826 Leonard, J.S., Fosdick, J.C., and VanderLeest, R.A., 2020, Erosional and tectonic evolution of a
827 retroarc orogenic wedge as revealed by sedimentary provenance: case of the Oligocene –
828 Miocene Patagonian Andes: Frontiers in Earth Science, v. 7, p. 1–20,
829 doi:10.3389/feart.2019.00353.

830 Limonta, M., Garzanti, E., Resentini, A., Andò, S., Boni, M., and Bechstädt, T., 2015,
831 Multicyclic sediment transfer along and across convergent plate boundaries (Barbados,
832 Lesser Antilles): Basin Research, v. 27, p. 696–713, doi:10.1111/bre.12095.

833 Livermore, R., Hillenbrand, C.-D., Meredith, M., and Eagles, G., 2007, Drake Passage and
834 Cenozoic climate: An open and shut case? Geochemistry Geophysics Geosystems, v. 8,
835 doi:10.1029/2005GC001224.

836 Ludwig, K.R., 2008, User's Manual for Isoplot 3.60 - A Geochronological Toolkit for Microsoft
837 Excel: Berkeley Geochronology Center Special Publication, v. 4, p. 77.

838 Macellari, C.E., Barrio, C.A., and Manassero, M.J., 1989, Upper Cretaceous to Paleocene
839 depositional sequences and standstone petrography of southwestern Patagonia (Argentina
840 and Chile): Journal of South American Earth Sciences, v. 2, p. 223–239, doi:10.1016/0895-
841 9811(89)90031-X.

842 Malkowski, M.A., Grove, M.J., and Graham, S.A., 2015, Unzipping the Patagonian Andes—
843 Long-lived influence of rifting history on foreland basin evolution: Lithosphere, v. 8, p. 23–
844 28.

845 Malkowski, M.A., Schwartz, T.M., Sharman, G.R., Sickmann, Z.T., and Graham, S.A., 2017a,
846 Stratigraphic and provenance variations in the early evolution of the Magallanes-Austral
847 foreland basin: Implications for the role of longitudinal versus transverse sediment dispersal
848 during arc-continent collision: Geological Society of America Bulletin, v. 129, p. 349–371,
849 doi:10.1130/B31549.1.

850 Malkowski, M.A., Sharman, G.R., Graham, S.A., and Fildani, A., 2017b, Characterization and
851 diachronous initiation of coarse clastic deposition in the Magallanes-Austral foreland basin,
852 Patagonian Andes: Basin Research, v. 29, p. 298–326, doi:10.1111/bre.12150.

853 Malkowski, M.A., Sharman, G.R., Schwartz, T.M., and Graham, S.A., 2013, Spatial variations in
854 deposional setting during foreland basin initiation, Magallanes-Austral basin, Patagonia:
855 linking ancient deep-water lobes to their shelfal source, *in* Stanford Project on Deepwater
856 Depositional Systems Consortium Report, p. 43.

Malumián, N., and Caramés, A., 1997, Upper Campanian-Paleogene from the Río Turbio coal measures in southern Argentina: micropaleontology and the Paleocene/Eocene boundary: Journal of South American Earth Sciences, v. 10, p. 189–201, doi:10.1016/S0895-9811(97)00015-1.

Malumián, N., and Náñez, C., 2011, The Late Cretaceous-Cenozoic transgressions in Patagonia and the Fuegian Andes: foraminifera, palaeoecology, and palaeogeography: Biological Journal of the Linnean Society, v. 103, p. 269–288, doi:10.1111/j.1095-8312.2011.01649.x.

Malumián, N., Panza, J.L., Parisi, C., Naňez, C., Caramés, A., and Torre, A., 2000, Hoja Geológica 5172-III, Yacimiento Río Turbio (1:250,000): Servicio Geológico Minero Argentino, Boletin, v. 247, p. 180.

Manríquez, L.M.E., Lavina, E.L.C., Fernández, R.A., Trevisan, C., and Leppe, M.A., 2019, Campanian-Maastrichtian and Eocene stratigraphic architecture, facies analysis, and paleoenvironmental evolution of the northern Magallanes Basin (Chilean Patagonia): Journal of South American Earth Sciences, v. 93, p. 102–118, doi:10.1016/j.jsames.2019.04.010.

Marenssi, S.A., Casadío, S., and Santillana, S., 2002, La Formación Man Aike al sur de El Calafate (Provincia de Santa Cruz) y su relación con la discordancia del Eoceno medio en la cuenca Austral: Revista de la Asociación Geológica Argentina, v. 57, p. 341–344.

Marshall, L.G., Webb, S.D., Sepkoski, J.J., and Raup, D.M., 1982, Mammalian evolution and the Great American Interchange: Science, v. 215, p. 1351–1357, doi:10.1126/science.215.4538.1351.

Martínez, S., and del Río, C.J., 2002, Late Miocene mollusks from the southwestern Atlantic Ocean (Argentina and Uruguay): A palaeobiogeographic analysis: Palaeogeography, Palaeoclimatology, Palaeoecology, v. 188, p. 167–187, doi:10.1016/S0031-0182(02)00551-5.

Miller, K.G., and Gornitz, V., 2008, Sea level change, last 250 million years: Encyclopedia of Paleoclimatology and Ancient Environments, v. 1, p. 879–887.

Miller, K.G., Kominz, M.A., Browning, J. V, Wright, J.D., Mountain, G.S., Katz, M.E., Sugarman, P.J., Cramer, B.S., Christie-Blick, N., and Pekar, S.F., 2005, The Phanerozoic record of global sea-level change.: Science, v. 310, p. 1293–1298, doi:10.1126/science.1116412.

Moecher, D.P., and Samson, S.D., 2006, Differential zircon fertility of source terranes and natural bias in the detrital zircon record: Implications for sedimentary provenance analysis: Earth and Planetary Science Letters, v. 247, p. 252–266, doi:10.1016/j.epsl.2006.04.035.

Moyano Paz, D., Richiano, S., Varela, A.N., Gómez Dacal, A., and Poiré, D.G., 2020, Ichnological signatures from wave- and fluvial-dominated deltas: The La Anita formation, Upper Cretaceous, Austral-Magallanes Basin, Patagonia: Marine and Petroleum Geology, v. 113, p. 104169, doi:10.1016/j.marpetgeo.2019.104168.

Moyano Paz, D., Tettamanti, C., Varela, A.N., Cereceda, A., and Poiré, D.G., 2018, Depositional processes and stratigraphic evolution of the Campanian deltaic system of La Anita Formation, Austral-Magallanes Basin, Patagonia, Argentina: Latin American Journal of Sedimentology and Basin Analysis, v. 25, p. 69–92.

Natland, M.L., Gonzales, E.P., Cañon, A., and Ernst, M., 1974, A system of stages for correlation of Magallanes Basin sediments: Geological Society of America, Memoir, v. 139, p. 1–73, doi:10.1130/MEM139-p1.

Nie, J., Horton, B.K., Saylor, J.E., Mora, A.A., Mange, M., Garzione, C.N., Basu, A., Moreno, C.J., Caballero, V., and Parra, M., 2012, Integrated provenance analysis of a convergent retroarc foreland system: U-Pb ages, heavy minerals, Nd isotopes, and sandstone compositions of the Middle Magdalena Valley basin, northern Andes, Colombia: Earth-Science Reviews, v. 110, p. 111–126, doi:10.1016/j.earscirev.2011.11.002.

Nullo, F., and Combina, A., 2011, Patagonian continental deposits (Cretaceous-Tertiary): Biological Journal of the Linnean Society, v. 103, p. 289–304, doi:10.1111/j.1095-8312.2011.01654.x.

Olivero, E.B., and Malumián, N., 2008, Mesozoic-Cenozoic stratigraphy of the Fuegian Andes, Argentina: Geologica Acta, v. 6, p. 5–18, doi:10.1344/105.

Otero, R.A., Oyarzún, J.L., Soto-Acuña, S., Yury-Yáñez, R.E., Gutiérrez, N.M., Le Roux, J.P., Torres, T., and Hervé, F., 2013, Neoselachians and Chimaeriformes (Chondrichthyes) from the latest Cretaceous-Paleogene of Sierra Baguales, southernmost Chile. chronostratigraphic, paleobiogeographic and paleoenvironmental implications: Journal of South American Earth Sciences, v. 48, p. 13–30, doi:10.1016/j.jsames.2013.07.013.

Otero, R.A., and Soto-Acuña, S., 2015, Nuevos condrictios de niveles Bartoniano-priabonianos de Río de Las Minas y Sierra Dorotea, Cuenca de Magallanes, Patagonia Chilena: Andean Geology, v. 42, p. 268–283, doi:10.5027/andgeoV42n2-a06.

Painter, C.S., and Carrapa, B., 2013, Flexural versus dynamic processes of subsidence in the North American Cordillera foreland basin: Geophysical Research Letters, v. 40, p. 4249–4253, doi:10.1002/grl.50831.

Pankhurst, R.J., Rapela, C.W., Fanning, C.M., and Márquez, M., 2006, Gondwanide continental collision and the origin of Patagonia: Earth-Science Reviews, v. 76, p. 235–257, doi:10.1016/j.earscirev.2006.02.001.

Pankhurst, R.J., Riley, T.R., Fanning, C.M., and Kelley, S.P., 2000, Episodic silicic volcanism in Patagonia and the Antarctic Peninsula: Chronology of magmatism associated with the break-up of Gondwana: Journal of Petrology, v. 41, p. 605–625.

Panti, C., 2020, Fossil leaves of subtropical lineages in the Eocene–?Oligocene of southern Patagonia: Historical Biology, v. 32, p. 252–266, doi:10.1080/08912963.2018.1488934.

Panti, C., 2014, Myrtaceae fossil leaves from the Río Turbio Formation (Middle Eocene), Santa

Cruz Province, Argentina: Historical Biology, v. 28, p. 459–469, doi:10.1080/08912963.2014.976635.

Panti, C., 2019, Southern beech (Nothofagaceae) fossil leaves from the Río Turbio Formation (Eocene-? Oligocene), Santa Cruz Province, Argentina: Revista del Museo Argentino de Ciencias Naturales, Nueva Serie, v. 21, p. 69–85, doi:10.22179/REVMACN.21.626.

Paredes, J.M., Foix, N., Guerstein, G.R., Guler, M. V., Irigoyen, M., Moscoso, P., and Giordano, S., 2015, A late Eocene-early Oligocene transgressive event in the Golfo San Jorge basin: Palynological results and stratigraphic implications: Journal of South American Earth Sciences, v. 63, p. 293–309, doi:10.1016/j.jsames.2015.08.009.

Parras, A., and Cuitiño, J.I., 2018, The stratigraphic and paleoenvironmental significance of the regressive Monte Observación member, Early Miocene of the Austral Basin, Patagonia: Latin American Journal of Sedimentology and Basin Analysis, v. 25, p. 93–115.

Parras, A., Dix, G.R., and Griffin, M., 2012, Sr-isotope chronostratigraphy of Paleogene-Neogene marine deposits: Austral Basin, southern Patagonia (Argentina): Journal of South American Earth Sciences, v. 37, p. 122–135, doi:10.1016/j.jsames.2012.02.007.

Parras, A., Griffin, M., Feldmann, R., Casadío, S., Schweitzer, C., and Marenssi, S., 2008, Correlation of marine beds based on Sr- and Ar-date determinations and faunal affinities across the Paleogene/Neogene boundary in southern Patagonia, Argentina: Journal of South American Earth Sciences, v. 26, p. 204–216, doi:10.1016/j.jsames.2008.03.006.

Parras, A., Guerstein, G.R., Panera, J.P.P., Náñez, C., Cusminsky, G., and Quiroga, A., 2020, Integrated stratigraphy and paleontology of the lower Miocene Monte León Formation, southeastern Patagonia, Argentina: Unraveling paleonvironmental changes and factors controlling sedimentation: Palaeogeography, Palaeoclimatology, Palaeoecology, p. 109701, doi:10.1016/j.palaeo.2020.109701.

Pearson, N.J., Mángano, M.G., Buatois, L.A., Casadío, S., and Rodríguez Raising, M., 2012, Ichnology, sedimentology, and sequence stratigraphy of outer-estuarine and coastal-plain deposits: Implications for the distinction between allogenic and autogenic expressions of the Glossifungites Ichnofacies: Palaeogeography, Palaeoclimatology, Palaeoecology, v. 333–334, p. 192–217, doi:10.1016/j.palaeo.2012.03.031.

Pepper, M., Gehrels, G., Pullen, A., Ibanez-Mejia, M., Ward, K.M., and Kapp, P., 2016, Magmatic history and crustal genesis of western South America: Constraints from U-Pb ages and Hf isotopes of detrital zircons in modern rivers: Geosphere, v. 12, p. 1532–1555, doi:10.1130/GES01315.1.

Perez, N.D., and Horton, B.K., 2014, Oligocene-Miocene deformational and depositional history of the Andean hinterland basin in the northern Altiplano Plateau, southern Perú: Tectonics, v. 33, p. 1819–1847, doi:10.1002/2014TC003647.

Perkins, M.E., Fleagle, J.G., Heizler, M.T., Nash, B., Bown, T.M., Tauber, A. a, and Dozo, M.T., 2012, Tephrochronology of the Miocene Santa Cruz and Pinturas Formations, Argentina: in

970 Early Miocene Paleobiology in Patagonia: High-Latitude Paleocommunities of the Santa
971 Cruz Formation, p. 23–40.

972 Pujana, R.R., and Ruiz, D.P., 2019, Fossil woods from the Eocene–Oligocene (Río Turbio
973 Formation) of southwestern Patagonia (Santa Cruz province, Argentina): IAWA Journal, v.
974 40, p. 596-S3, doi:10.1163/22941932-40190253.

975 Raigemborn, M.S., Krapovickas, V., Zucol, A.F., Zapata, L., Beilinson, E., Toledo, N., Perry, J.,
976 Lizzoli, S., Martegani, L., Tineo, D.E., and Passeggi, E., 2018, Paleosols and related soil-
977 biota of the early Miocene Santa Cruz Formation (Austral-Magallanes Basin, Argentina): a
978 multidisciplinary approach to reconstructing ancient terrestrial landscapes: Latin American
979 Journal of Sedimentology and Basin Analysis, v. 25, p. 117–148.

980 Ramírez de Arellano, C., Putlitz, B., Müntener, O., and Ovtcharova, M., 2012, High precision
981 U/Pb zircon dating of the Chaltén Plutonic Complex (Cerro Fitz Roy, Patagonia) and its
982 relationship to arc migration in the southernmost Andes: Tectonics, v. 31,
983 doi:10.1029/2011TC003048.

984 Ramos, V.A., 2005, Seismic ridge subduction and topography: Foreland deformation in the
985 Patagonian Andes: Tectonophysics, v. 399, p. 73–86, doi:10.1016/j.tecto.2004.12.016.

986 Ramos, V.A., and Ghiglione, M.C., 2008, Tectonic evolution of the Patagonian Andes:
987 Developments in Quaternary Science, v. 11, p. 57–71, doi:10.1016/S1571-0866(07)10004-
988 X.

989 Rehak, K., Bookhagen, B., Strecker, M.R., and Echtler, H.P., 2010, The topographic imprint of a
990 transient climate episode: The western Andean flank between 15°5’ and 41°5’S: Earth
991 Surface Processes and Landforms, v. 35, p. 1516–1534, doi:10.1002/esp.1992.

992 Riccardi, A., and Rolleri, E., 1980, Cordillera Patagónica Austral: Academia Nacional de
993 Ciencias, v. 2, p. 1173–1306.

994 Rodríguez Raising, M., 2010, Estratigrafía secuencial de los depósitos marinos y continentales
995 del Eoceno – Oligoceno temprano de la cuenca Austral, suroeste de la provincia de Santa
996 Cruz: PhD thesis, Universidad Nacional del Sur, Buenos Aires, Argentina, 202 p.

997 Roe, G.H., Whipple, K.X., and Fletcher, J.K., 2008, Feedbacks among climate, erosion, and
998 tectonics in a critical wedge orogen: American Journal of Science, v. 308, p. 815–842,
999 doi:10.2475/07.2008.01.

1000 Romans, B.W., Fildani, A., Graham, S.A., Hubbard, S.M., and Covault, J.A., 2010, Importance
1001 of predecessor basin history on the sedimentary fill of a retroarc foreland basin: provenance
1002 analysis of the Cretaceous Magallanes: Basin Research, v. 22, p. 640–658,
1003 doi:10.1111/j.1365-2117.2009.00443.x.

1004 Romans, B.W., Fildani, A., Hubbard, S.M., Covault, J.A., Fosdick, J.C., and Graham, S.A.,
1005 2011, Evolution of deep-water stratigraphic architecture, Magallanes Basin, Chile: Marine
1006 and Petroleum Geology, v. 28, p. 612–628, doi:10.1016/j.marpetgeo.2010.05.002.

1007 Romans, B.W., and Graham, S.A., 2013, A deep-time perspective of land-ocean linkages in the
1008 sedimentary record.: Annual review of marine science, v. 5, p. 69–94, doi:10.1146/annurev-
1009 marine-121211-172426.

1010 Sachse, V.F., Strozyk, F., Anka, Z., Rodriguez, J.F., and di Primio, R., 2015, The tectono-
1011 stratigraphic evolution of the Austral Basin and adjacent areas against the background of
1012 Andean tectonics, southern Argentina, South America: Basin Research, v. 26, p. 462–482,
1013 doi:10.1111/bre.12118.

1014 Sánchez, A., Pavlishina, P., Godoy, E., Hervé, F., and Fanning, C.M., 2010, On the presence of
1015 Upper Paleocene rocks in the foreland succsion at Cabo Nariz, Tierra del Fuego, Chile:
1016 geology and new palynological and U-Pb data: Andean Geology, v. 37, p. 413–432.

1017 Scher, H.D., and Martin, E.E., 2006, Timing and climatic consequences of the opening of Drake
1018 Passage: Science, v. 312, p. 428–430, doi:10.1126/science.1120044.

1019 Schmitt, J.G., and Steidtmann, J.R., 1990, Interior ramp-supported uplifts: Implications for
1020 sediment provenance in foreland basins: Geological Society of America Bulletin, v. 102, p.
1021 494–201.

1022 Schwartz, T.M., Fosdick, J.C., and Graham, S.A., 2016, Using detrital zircon U-Pb ages to
1023 calculate Late Cretaceous sedimentation rates in the Magallanes-Austral basin, Patagonia:
1024 Basin Research, v. 29, p. 725–746, doi:10.1111/bre.12198.

1025 Schwartz, T.M., and Graham, S.A., 2015, Stratigraphic architecture of a tide-influenced shelf-
1026 edge delta, Upper Cretaceous Dorotea Formation, Magallanes-Austral Basin, Patagonia:
1027 Sedimentology, v. 62, p. 1039–1077, doi:10.1111/sed.12176.

1028 Schweitzer, C.E., Feldmann, R.M., Casadío, S., and Rodríguez Raising, M., 2012, Eocene
1029 decapod crustacea (Thalassinidea and Brachyura) from Patagonia, Argentina: Annals of
1030 Carnegie Museum, v. 80, p. 173–186.

1031 Sepkoski, J.J., 1996, Patterns of Phanerozoic extinction: a perspective from global data bases, *in*
1032 Walliser, D.H. ed., Global events and event stratigraphy in the Phanerozoic, Berlin,
1033 Springer, p. 35–51.

1034 SERNAGEOMIN, 2003, Mapa Geológico de Chile: versión digital. Servicio Nacional de
1035 Geología y Minería, Publicación Geológica Digital, No. 4 (CD-ROM, versión 1.0).:

1036 Sickmann, Z.T., Schwartz, T.M., and Graham, S.A., 2018, Refining stratigraphy and tectonic
1037 history using detrital zircon maximum depositional age: an example from the Cerro
1038 Fortaleza Formation, Austral Basin, southern Patagonia: Basin Research, v. 30, p. 708–729,
1039 doi:10.1111/bre.12272.

1040 Simpson, G.D.H., 2006, Modelling interactions between fold-thrust belt deformation, foreland
1041 flexure and surface mass transport: Basin Research, v. 18, p. 125–143, doi:10.1111/j.1365-
1042 2117.2006.00287.x.

1043 Sommerfield, C.K., and Wheatcroft, R.A., 2007, Late Holocene sediment accumulation on the
1044 northern California shelf: Oceanic, fluvial, and anthropogenic influences: Bulletin of the
1045 Geological Society of America, v. 119, p. 1120–1134, doi:10.1130/B26019.1.

1046 Somoza, R., and Ghidella, M.E., 2012, Late Cretaceous to recent plate motions in western South
1047 America revisited: Earth and Planetary Science Letters, v. 331–332, p. 152–163,
1048 doi:10.1016/j.epsl.2012.03.003.

1049 Stevens Goddard, A.L., and Fosdick, J.C., 2019, Multichronometer thermochronologic modeling
1050 of migrating spreading ridge subduction in southern Patagonia: Geology, v. 47, p. 555–558.

1051 Stocchi, P., Escutia, C., Houben, A.J.P., Vermeersen, B.L.A., Bijl, P.K., Brinkhuis, H., DeConto,
1052 R.M., Galeotti, S., Passchier, S., Pollard, D., and IODP Expedition 318 scientists, 2013,
1053 Relative sea-level rise around East Antarctica during Oligocene glaciation: Nature
1054 Geoscience, v. 6, p. 380–384, doi:10.1038/NGEO1783.

1055 Süssenberger, A., Schmidt, S.T., Wemmer, K., Baumgartner, L.P., and Grobéty, B., 2017,
1056 Timing and thermal evolution of fold-and-thrust belt formation in the Última Esperanza
1057 District, 51°S Chile: Constraints from K-Ar dating and illite characterization: Geological
1058 Society Of America Bulletin, v. 130, p. 975–998.

1059 Tettamanti, C., Moyano Paz, D., Varela, A.N., Gomez-Peral, L.E., Poiré, D.G., Cereceda, A.,
1060 and Odino Barreto, L.A., 2018, Sedimentology and stratigraphy of the uppermost
1061 Cretaceous continental deposits of the Austral-Magallanes Basin, Patagonia, Argentina:
1062 Latin American Journal of Sedimentology and Basin Analysi, v. 25, p. 149–168.

1063 Torres Carbonell, P.J., and Olivero, E.B., 2019, Tectonic control on the evolution of depositional
1064 systems in a fossil, marine foreland basin: Example from the SE Austral Basin, Tierra del
1065 Fuego, Argentina: Marine and Petroleum Geology, v. 104, p. 40–60,
1066 doi:10.1016/j.marpetgeo.2019.03.022.

1067 Ugalde, R.A., 2014, Contribución al conocimiento de la estratigrafia cenozoica de la Sierra
1068 Baguales: La Formación Man Aike (“Las Flores”), Provincia de Última Esperanza,
1069 Magallanes: Universidad de Chile, 82 p.

1070 Ugalde, R., 2019, Petrografía, quimioestratigrafía y proveniencia sedimentaria de la Formación
1071 Camacho (Mioceno), Uruguay: Universidad de la República, Montevideo, Uruguay, 222 p.

1072 Varela, A.N., Poiré, D.G., Martin, T., Gerdes, A., Goin, F.J., Gelfo, J.N., and Hoffmann, S.,
1073 2012, U-Pb zircon constraints on the age of the Cretaceous Mata Amarilla Formation,
1074 Southern Patagonia, Argentina: its relationship with the evolution of the Austral Basin:
1075 Andean Geology, v. 39, p. 359–379, doi:10.5027/andgeoV39n3-a01.

1076 Varela, A.N., Richiano, S., D´Elia, L., Moyano Paz, D., Tettamanti, C., and Poiré, D.G., 2019,
1077 Sedimentology and stratigraphy of the Puesto El Moro Formation, Patagonia, Argentina:
1078 Implications for Upper Cretaceous paleogeographic reconstruction and
1079 compartmentalization of the Austral-Magallanes Basin: Journal of South American Earth
1080 Sciences, v. 92, p. 466–480, doi:10.1016/j.jsames.2019.03.030.

1081 Vento, B., Gandolfo, M.A., Nixon, K.C., and Prámparo, M., 2017, Paleofloristic assemblage
1082 from the Paleogene Río Guillermo Formation, Argentina: preliminary results of
1083 phylogenetic relationships of Nothofagus in South America: Historical Biology, v. 29, p.
1084 93–107, doi:10.1080/08912963.2015.1136930.

1085 Vento, B., and Prámparo, M., 2018, Angiosperm association from the Río Turbio Formation
1086 (Eocene–?Oligocene) Santa Cruz, Argentina: revision of Hünicken's (1955) fossil leaves
1087 collection: Alcheringa: An Australasian Journal of Palaeontology, v. 42, p. 125–153,
1088 doi:10.1080/03115518.2017.1408854.

1089 Wilf, P., Cúneo, N.R., Johnson, K.R., Hicks, J.F., Wing, S.L., and Obradovich, J.D., 2003, High
1090 plant diversity in Eocene South America: evidence from Patagonia: Science, v. 300, p. 122–
1091 125, doi:10.1126/science.1080475.

1092 Willett, S.D., 1999, Orogeny and orography: The effects of erosion on the structure of mountain
1093 belts: Journal of Geophysical Research, v. 104, p. 28957–28981,
1094 doi:10.1029/1999JB900248.

1095 Zachos, J.C., Dickens, G.R., and Zeebe, R.E., 2008, An early Cenozoic perspective on
1096 greenhouse warming and carbon-cycle dynamics.: Nature, v. 451, p. 279–283,
1097 doi:10.1038/nature06588.

1098 Zachos, J., Pagani, M., Sloan, L., Thomas, E., and Billups, K., 2001, Trends, rhythms, and
1099 aberrations in global climate 65 Ma to present.: Science, v. 292, p. 686–93,
1100 doi:10.1126/science.1059412.

1101 **TABLE CAPTIONS**

1102 **Table 1.** Sample information and calculated maximum depositional ages from the Magallanes-
1103 Austral Basin for detrital zircon U-Pb LA-ICP-MS geochronology.

1104 **FIGURE CAPTIONS**

1105 **Figure 1.** (A) Tectonic setting of the Magallanes-Austral Basin and other Cenozoic depocenters
1106 (yellow) in relation to key southern plate boundary features (after Galeazzi, 1998; Ghiglione et
1107 al., 2010; Fosdick et al., 2011). Global Multi-Resolution Topography (GMRT) base map from
1108 GeoMapApp©. Black stars denote stratigraphic areas discussed in the text: CC – Cerro Castillo,
1109 SJ – San Julián. NP – Nazca plate; NSR – North Scotia Ridge; MFFZ – Magallanes-Fagnano
1110 Fault Zone; SFZ – Shackleton Fracture Zone. (B) Location of the Cerro Castillo – Cancha
1111 Carrera study area within the Cenozoic Magallanes-Austral Basin outcrop belt along the eastern
1112 margins of the Patagonian thrust belt. Geologic map compiled from Malumián et al. (2000),
1113 SERNAGEOMIN (2003), and Fosdick et al. (2011). Zircon crystallization ages are summarized
1114 from igneous and recycled sediment sources (Fosdick et al., 2015).

Figure 2. Detrital zircon U-Pb geochronology data compiled by formation (<600 Ma only), showing probability density plots of Upper Cretaceous through lower Miocene stratigraphy. For each formation, N refers to the number of individual samples included in the formation, followed by number of total grains analyzed. Published data from the Santa Cruz, Dorotea, Tres Pasos, and Punta Barrosa Formations are included for comparison (Fildani et al., 2003; Romans et al., 2010; Bernhardt et al., 2012; Fosdick et al., 2015). Note break in scale at 360-600 Ma and change of scale after 600 Ma. Southern Patagonian Batholith age groups after Hervé et al. (2007): N = Neogene, P = Paleogene, K1 = Cretaceous I, K2 = Cretaceous II, K3 = Cretaceous III, and J = Jurassic. PZ = Paleozoic. We identify 'K4' and 'P2' age groups in our detrital datasets.

Figure 3. Maximum depositional ages (MDA) interpreted from the youngest detrital zircon U-Pb data from each sample (individual analyses shown at 2σ uncertainty). MDA are the error-weighted mean age (± 2σ uncertainty) of all grains (n) that define the youngest age cluster represented by the horizontal gray bars.

Figure 4. Changes in relative proportions of zircon age groups for pre-Cenozoic age groups. Results show upsection rise and subsequent loss of Jurassic – Early Cretaceous (J-K1) grains, a progressive loss of Paleozoic grains, and an overall increase in Paleogene igneous sources. The largest shift in provenance signature occurred across the Paleocene Cerro Dorotea Formation - middle Eocene Río Turbio Formation boundary.

Figure 5. Summary of new depositional age constraints and paleoenvironmental context in the Magallanes-Austral Basin near 51°S. Cenozoic stratigraphy and revised timing of sedimentation based on new maximum depositional ages (MDA) calculated from youngest detrital zircon U-Pb age cluster from each sample.

Figure 6. Implications for revised timing of sedimentation of the middle Cenozoic Magallanes-Austral Basin strata compared to changes in regional tectonics (Breitsprecher and Thorkelson, 2009; Lagabrielle et al., 2009; Fosdick et al., 2011), plate convergence rate (Somoza and Ghidella, 2012), global climate (Zachos et al., 2008), and eustatic sea level (Miller and Gornitz, 2008). Published chronostratigraphy of proximal foothills compiled from Malumián et al. (2000), Malumián and Náñez, (2011), Perkins et al. (2012), and references therein. Chronostratigraphy of the San Julián sector of the Atlantic coast from Parras et al. (2008) and (2012). New age estimates and sediment provenance highlight (1) isolation of Jurassic and Paleozoic zircon sources and disruption of the foreland basin system across the Paleogene foreland unconformity, (2) a potential foreland younging transgression caused by flexural deepening during Tenerife thrusting and synchronous basin subsidence in Tierra del Fuego, and (3) accelerated sediment supply of the Río Guillermo Formation linked to retroarc deformation and unroofing along the El Ríncon thrusts.

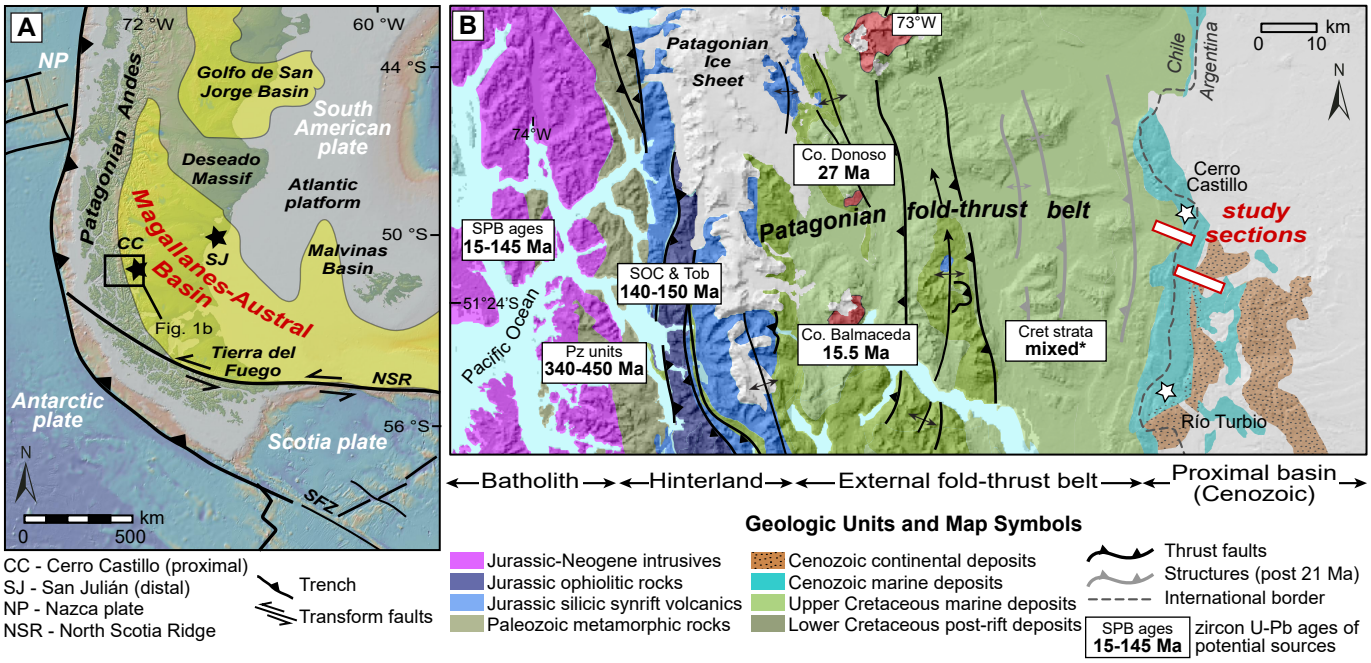
A
72 °W
60 °W
44 °S
50 °S
56 °S
NP
Golfo de San Jorge Basin
South American plate
Deseado Massif
Atlantic platform
Patagonian Andes
Magallanes-Austral Basin
CC
SJ
Malvinas Basin
Fig. 1b
Tierra del Fuego
NSR
Antarctic plate
Scotia plate
SFZ
N
km
0
500
CC - Cerro Castillo (proximal)
SJ - San Julián (distal)
NP - Nazca plate
NSR - North Scotia Ridge
Trench
Transform faults
B
73°W
74°W
51°24'S
Patagonian Ice Sheet
Pacific Ocean
Chile
Argentina
km
0
10
N
Co. Donoso
27 Ma
SPB ages
15-145 Ma
SOC & Tob
140-150 Ma
Pz units
340-450 Ma
Co. Balmaceda
15.5 Ma
Cret strata
mixed*
Patagonian fold-thrust belt
Cerro Castillo
study sections
Río Turbio
Batholith
Hinterland
External fold-thrust belt
Proximal basin (Cenozoic)
Geologic Units and Map Symbols
Jurassic-Neogene intrusives
Jurassic ophiolitic rocks
Jurassic silicic synrift volcanics
Paleozoic metamorphic rocks
Cenozoic continental deposits
Cenozoic marine deposits
Upper Cretaceous marine deposits
Lower Cretaceous post-rift deposits
Thrust faults
Structures (post 21 Ma)
International border
SPB ages
15-145 Ma
zircon U-Pb ages of potential sources

Figure 1.

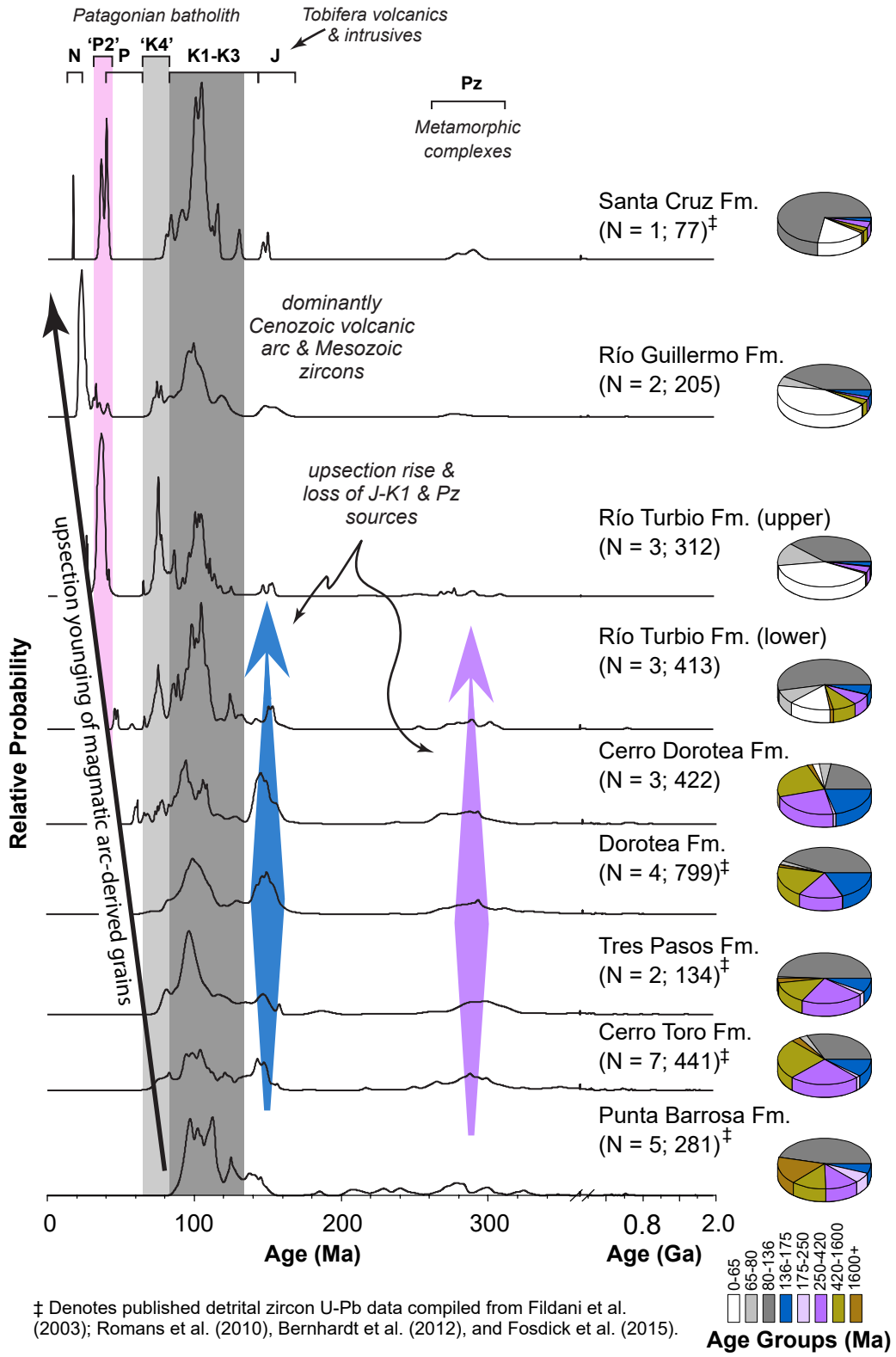

‡ Denotes published detrital zircon U-Pb data compiled from Fildani et al. (2003); Romans et al. (2010), Bernhardt et al. (2012), and Fosdick et al. (2015).

Figure 2.

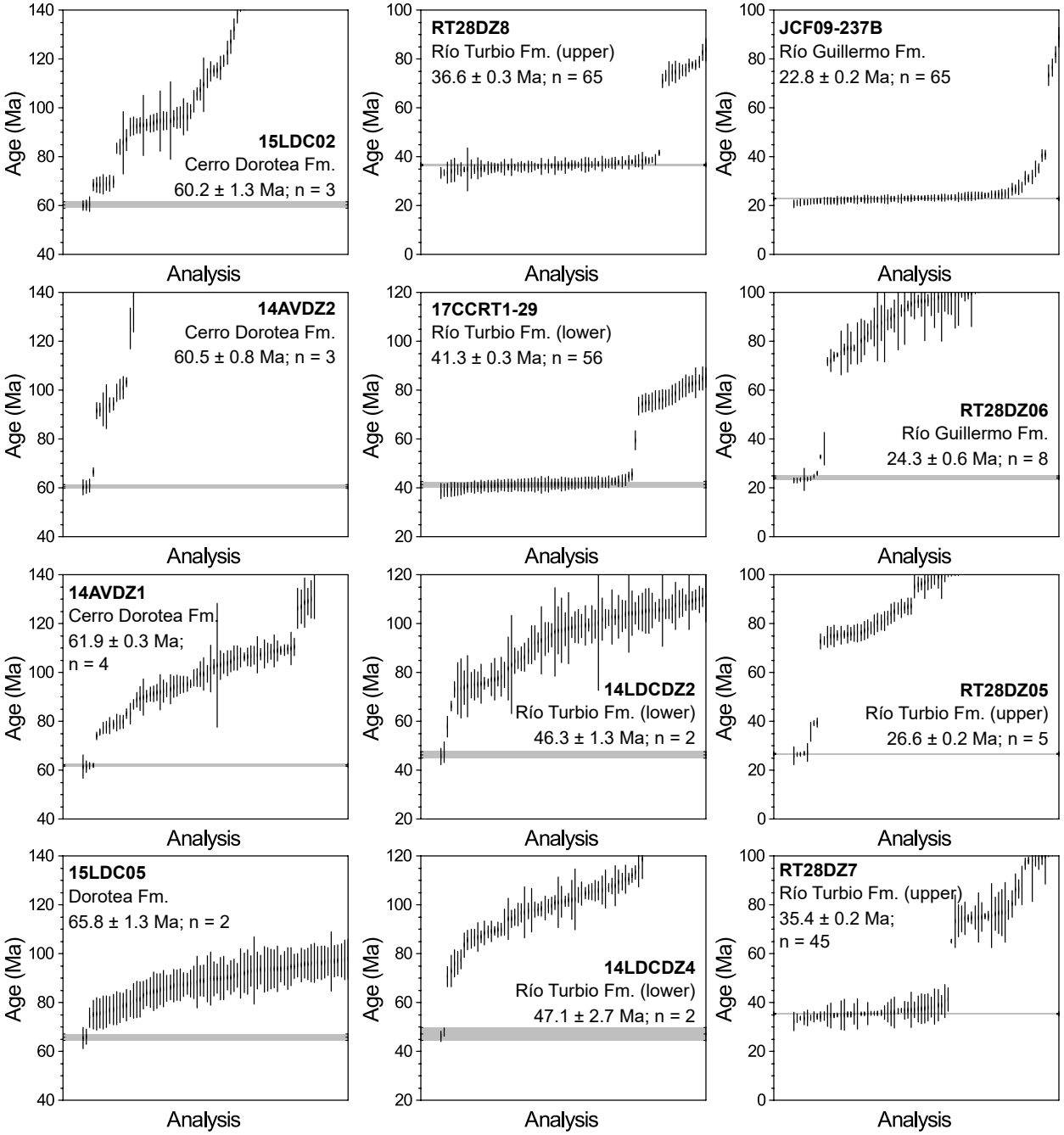
15LDC02
Cerro Dorotea Fm.
60.2 ± 1.3 Ma; n = 3
RT28DZ8
Río Turbio Fm. (upper)
36.6 ± 0.3 Ma; n = 65
JCF09-237B
Río Guillermo Fm.
22.8 ± 0.2 Ma; n = 65
14AVDZ2
Cerro Dorotea Fm.
60.5 ± 0.8 Ma; n = 3
17CCRT1-29
Río Turbio Fm. (lower)
41.3 ± 0.3 Ma; n = 56
RT28DZ06
Río Guillermo Fm.
24.3 ± 0.6 Ma; n = 8
14AVDZ1
Cerro Dorotea Fm.
61.9 ± 0.3 Ma;
n = 4
14LDCDZ2
Río Turbio Fm. (lower)
46.3 ± 1.3 Ma; n = 2
RT28DZ05
Río Turbio Fm. (upper)
26.6 ± 0.2 Ma; n = 5
15LDC05
Dorotea Fm.
65.8 ± 1.3 Ma; n = 2
14LDCDZ4
Río Turbio Fm. (lower)
47.1 ± 2.7 Ma; n = 2
RT28DZ7
Río Turbio Fm. (upper)
35.4 ± 0.2 Ma;
n = 45
Age (Ma)
Analysis

Figure 3.

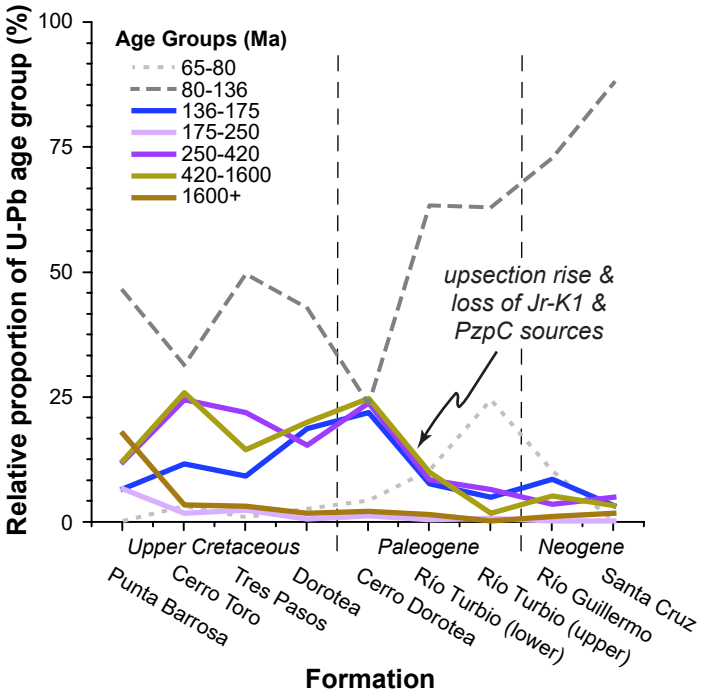
Relative proportion of U-Pb age group (%)
100
75
50
25
0
Age Groups (Ma)
65-80
80-136
136-175
175-250
250-420
420-1600
1600+
upsection rise &
loss of Jr-K1 &
PzpC sources
Upper Cretaceous
Paleogene
Neogene
Punta Barrosa
Cerro Toro
Tres Pasos
Dorotea
Cerro Dorotea
Río Turbio (lower)
Río Turbio (upper)
Río Guillermo
Santa Cruz
Formation

Figure 4.

Chronostratigraphy and composite section at Cerro Castillo and Cancha Carrera

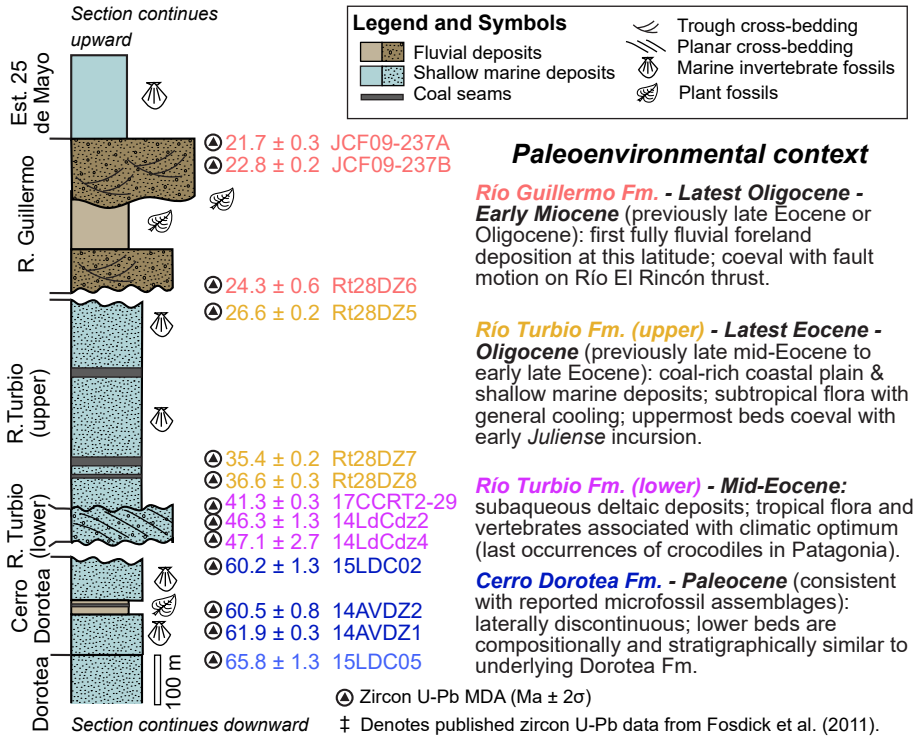

Paleoenvironmental context

Río Guillermo Fm.* - *Latest Oligocene - Early Miocene (previously late Eocene or Oligocene): first fully fluvial foreland deposition at this latitude; coeval with fault motion on Río El Rincón thrust.

Río Turbio Fm. (upper)* - *Latest Eocene - Oligocene (previously late mid-Eocene to early late Eocene): coal-rich coastal plain & shallow marine deposits; subtropical flora with general cooling; uppermost beds coeval with early *Juliense* incursion.

Río Turbio Fm. (lower)* - *Mid-Eocene: subaqueous deltaic deposits; tropical flora and vertebrates associated with climatic optimum (last occurrences of crocodiles in Patagonia).

Cerro Dorotea Fm.* - *Paleocene (consistent with reported microfossil assemblages): laterally discontinuous; lower beds are compositionally and stratigraphically similar to underlying Dorotea Fm.

▲ Zircon U-Pb MDA (Ma ± 2σ)

‡ Denotes published zircon U-Pb data from Fosdick et al. (2011).

Figure 5.

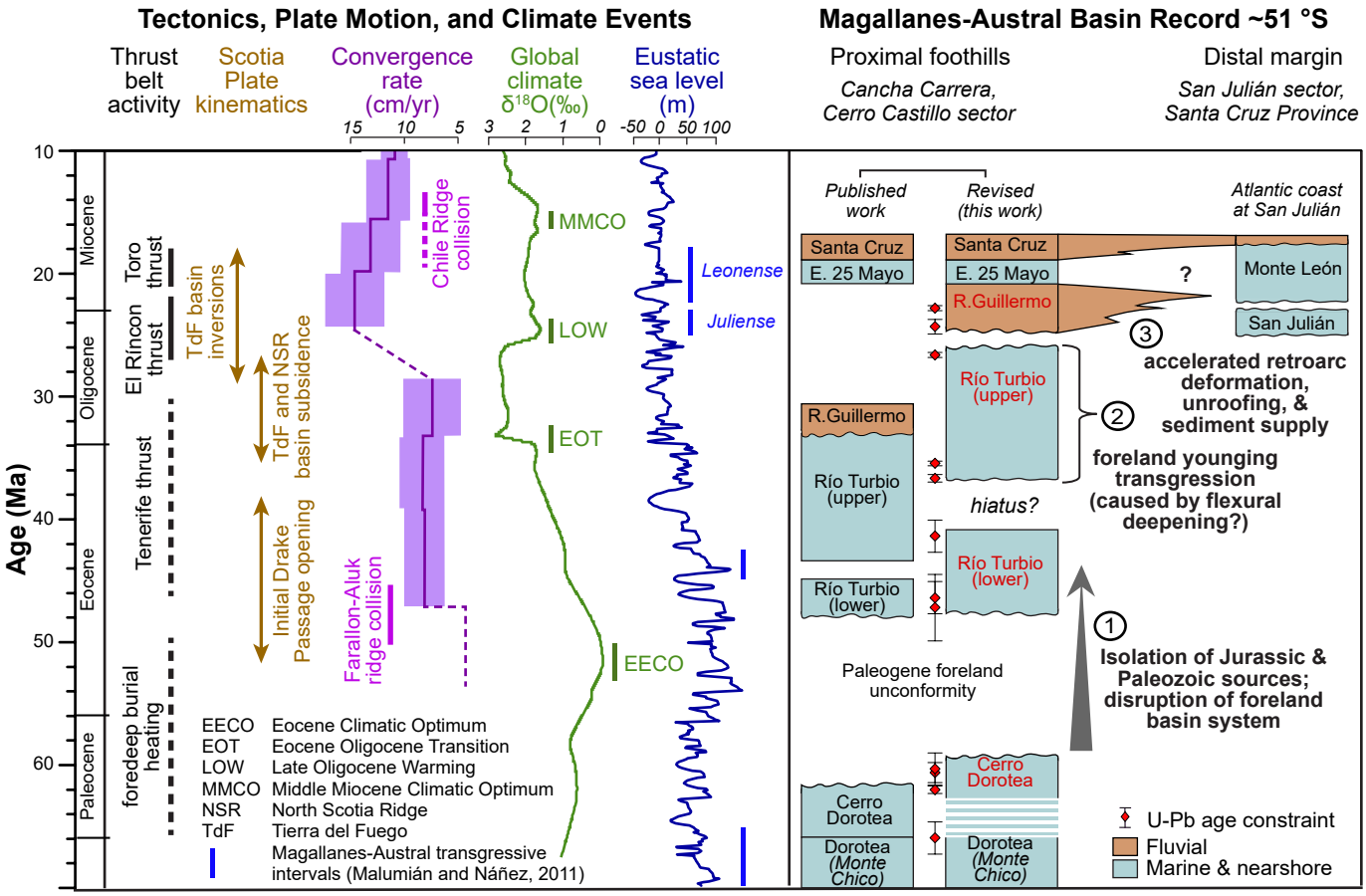
Tectonics, Plate Motion, and Climate Events
Magallanes-Austral Basin Record ~51 °S
Thrust belt activity
Scotia Plate kinematics
Convergence rate (cm/yr)
Global climate δ18O(‰)
Eustatic sea level (m)
Proximal foothills
Cancha Carrera, Cerro Castillo sector
Distal margin
San Julián sector, Santa Cruz Province
Age (Ma)
Miocene
Oligocene
Eocene
Paleocene
Toro thrust
El Rincon thrust
Tenerife thrust
foredeep burial heating
TdF basin inversions
TdF and NSR basin subsidence
Initial Drake Passage opening
Chile Ridge collision
Farallon-Aluk ridge collision
MMCO
LOW
EOT
EECO
Leonense
Juliense
EECO Eocene Climatic Optimum
EOT Eocene Oligocene Transition
LOW Late Oligocene Warming
MMCO Middle Miocene Climatic Optimum
NSR North Scotia Ridge
TdF Tierra del Fuego
Magallanes-Austral transgressive intervals (Malumián and Náñez, 2011)
Published work
Revised (this work)
Atlantic coast at San Julián
Santa Cruz
E. 25 Mayo
R.Guillermo
Río Turbio (upper)
Río Turbio (lower)
Monte León
San Julián
?
3
accelerated retroarc deformation, unroofing, & sediment supply
2
foreland younging transgression (caused by flexural deepening?)
hiatus?
1
Isolation of Jurassic & Paleozoic sources; disruption of foreland basin system
Paleogene foreland unconformity
Cerro Dorotea
Dorotea (Monte Chico)
U-Pb age constraint
Fluvial
Marine & nearshore

Figure 6.

TABLE 1. SAMPLE INFORMATION AND CALCULATED MAXIMUM DEPOSITIONAL AGES FROM THE MAGALLANES BASIN FOR DETRITAL ZIRCON U-Pb LA-ICP-MS GEOCHRONOLOGY

Sample	Formation	Latitude (°N)	Longitude (°W)	Elevation (m)	# grains analyzed	Interpreted maximum depositional age (± 2σ)
JCF09-237B	Río Guillermo	-51.30338	-72.18670	389	115	22.8 ± 0.2 Ma (n = 65)
Rt28DZ6	Río Guillermo	-51.31163	-72.22042	346	94	24.3 ± 0.6 Ma (n = 8)
Rt28DZ5	Río Turbio (upper)	-51.31373	-72.21932	323	103	26.6 ± 0.5 Ma (n = 5)
Rt28DZ7	Río Turbio (upper)	-51.29761	-72.23581	349	101	35.4 ± 0.2 Ma (n = 45)
Rt28DZ8	Río Turbio (upper)	-51.29667	-72.23819	282	110	36.6 ± 0.3 Ma (n = 65)
17CCRT2-29	Río Turbio (lower)	-51.31735	-72.29126	464	157	41.3 ± 0.3 Ma (n = 56)
14LdCdz2	Río Turbio (lower)	-51.28071	-72.28936	443	106	46.3 ± 1.3 Ma (n = 2)
14LdCdz4	Río Turbio (lower)	-51.27997	-72.28916	411	108	47.1 ± 2.7 Ma (n = 2)
15LDC02/14DZ3	Cerro Dorotea	-51.28001	-72.28927	351	227	60.2 ± 1.3 Ma (n = 3)
14AVDZ2	Cerro Dorotea	-51.28475	-72.30764	433	107	60.5 ± 0.8 Ma (n = 3)
14AVDZ1	Cerro Dorotea	-51.28473	-72.30828	434	103	61.9 ± 0.3 Ma (n = 4)
15LDC05	Dorotea	-51.27793	-72.31254	312	212	65.8 ± 1.3 Ma (n = 2)

Revised timing of Cenozoic Atlantic incursions and changing hinterland sediment sources during southern Patagonian orogenesis

Data Repository

U-Pb geochronologic analyses of detrital zircon (Nu HR ICPMS)

Detrital zircons were extracted from ~5 kg medium-grained sandstone hand-samples using standard mineral separation techniques at the ZirChron, LLC. (Tucson, Arizona), including crushing and grinding, fractionation of magnetic minerals with a Frantz isodynamic magnetic separator, and settling through heavy liquids to exclude phases with densities less than 3.3 g/cm^3. Final zircon separates were mounted in epoxy resin together with fragments of the Sri Lanka standard zircon. The mounts are polished to a depth of ~20 μm, imaged, and cleaned prior to isotopic analysis.

U-Pb geochronology of zircons is conducted by laser ablation multicollector inductively coupled plasma mass spectrometry (LA-MC-ICPMS) at the Arizona LaserChron Center (Gehrels et al., 2008; Gehrels, 2012). The analyses involve ablation of zircon with a Photon Machines Analyte G2 excimer laser using a spot diameter of 30 μm. The ablated material is carried in helium into the plasma source of a Nu HR ICPMS, which is equipped with a flight tube of sufficient width that U, Th, and Pb isotopes are measured simultaneously. All measurements are made in static mode, using Faraday detectors with 3x10^{11} ohm resistors for ^{238}U, ^{232}Th, ^{208}Pb-^{206}Pb, and discrete dynode ion counters for ^{204}Pb and ^{202}Hg. Ion yields are ~0.8 mv per ppm. Each analysis consists of one 15-second integration on peaks with the laser off (for backgrounds), 15 one-second integrations with the laser firing, and a 30 second delay to purge the previous sample and prepare for the next analysis. The ablation pit is ~15 μm in depth.

For each analysis, the errors in determining ^{206}Pb/^{238}U and ^{206}Pb/^{204}Pb result in a measurement error of ~1-2% (at 2σ level) in the ^{206}Pb/^{238}U age. The errors in measurement of ^{206}Pb/^{207}Pb and ^{206}Pb/^{204}Pb also result in ~1-2% (at 2σ level) uncertainty in age for grains that are >1.0 Ga, but are substantially larger for younger grains due to low intensity of the ^{207}Pb signal. For most analyses, the cross-over in precision of ^{206}Pb/^{238}U and ^{206}Pb/^{207}Pb ages occurs at ~1.0 Ga. ^{204}Hg interference with ^{204}Pb is accounted for measurement of ^{202}Hg during laser ablation and subtraction of ^{204}Hg according to the natural ^{202}Hg/^{204}Hg of 4.35. This Hg is correction is

not significant for most analyses because our Hg backgrounds are low (generally ~150 cps at mass 204). Common Pb correction is accomplished by using the Hg-corrected ^{204}Pb and assuming an initial Pb composition (Stacey and Kramers, 1975). Uncertainties of 1.5 for ^{206}Pb/^{204}Pb and 0.3 for ^{207}Pb/^{204}Pb are applied to these compositional values based on the variation in Pb isotopic composition in modern crystal rocks. Inter-element fractionation of Pb/U is generally ~5%, whereas apparent fractionation of Pb isotopes is generally <0.2%. In-run analysis of fragments of a large zircon crystal (generally every fifth measurement) with known age of 563.5 ± 3.2 Ma (2σ error) is used to correct for this fractionation. The uncertainty resulting from the calibration correction is generally 1-2% (2σ) for both ^{206}Pb/^{207}Pb and ^{206}Pb/^{238}U ages. Concentrations of U and Th are calibrated relative to Sri Lanka zircon, which contains ~518 ppm of U and 68 ppm Th.

The analytical data are reported in Table A1. Preferred calculated U-Pb ages use the ^{204}Pb corrected ^{206}Pb/^{238}U ratio for <1.0 Ga grains and the ^{204}Pb corrected ^{206}Pb/^{207}Pb ratio for >900 Ma grains. Uncertainties shown in these tables are at the 1σ level, and include only measurement errors. Analyses that are >20% discordant or >5% reverse discordant (by comparison of ^{206}Pb/^{238}U and ^{206}Pb/^{207}Pb ages) were excluded from provenance interpretations and maximum depositional age calculations. Pb*/U concordia diagrams (Fig. A1) and probability density plots (Figs. A2 and A3) were generated using the routines in Isoplot (Ludwig, 2008). The age-probability diagrams show each age and its uncertainty (for measurement error only) as a normal distribution, and sum all ages from a sample into a single curve. For samples that yielded youngest age groups that could represent conceivable maximum depositional ages, we calculated error-weighted mean ages (Table 1) based on the following criteria: age clusters contained at least 2 overlapping concordant grains at 2σ uncertainty. For published samples from collected within the latitude of our study area from the Punta Barrosa, Cerro Toro, Tres Pasos, Dorotea, and Santa Cruz Formations (Fig. 2 and Fig. 4), we recalculated relative probability density curves from published detrital zircon U-Pb geochronological data (Fildani et al., 2003; Romans et al., 2010; Bernhardt et al., 2012; Fosdick et al., 2015): Punta Barrosa Formation samples included in data comparison are: *Pb0104, 2/21-3, 2/6-3, 3/5-3*, and *3/11-3* (Fildani et al., 2003). Cerro Toro Formation samples included in data comparison are: *CC* and *VC* (Romans et al., 2010) and *SS-Ndskld, CB-C, SdT-Co, SdT-Wc, SS_PehoeA* (Bernhardt et al., 2012). Tres Pasos Formation samples included in data comparison are: *F04* and *F05-1* (Romans et al., 2010).

Dorotea Formation samples included in data comparison are: *CCS-01* and *CM-1* (Romans et al., 2010) and *JCF09-226* (Fosdick et al., 2015). Santa Cruz Formation samples included in data comparison are: *JCF09-235* (Fosdick et al., 2015).

REFERENCES

Bernhardt, A., Jobe, Z.R., Grove, M., and Lowe, D.R., 2012, Palaeogeography and diachronous infill of an ancient deep-marine foreland basin, Upper Cretaceous Cerro Toro Formation, Magallanes Basin: Basin Research, v. 24, p. 269–294.

Fildani, A., Cope, T.D., Graham, S.A., and Wooden, J.L., 2003, Initiation of the Magallanes foreland basin: Timing of the southernmost Patagonian Andes orogeny revised by detrital zircon provenance analysis: Geology, v. 31, p. 1081–1084.

Fosdick, J.C., Grove, M., Graham, S.A., Hourigan, J.K., Lovera, O., and Romans, B.W., 2015, Detrital thermochronologic record of burial heating and sediment recycling in the Magallanes foreland basin, Patagonian Andes: Basin Research, v. 27, p. 546–572.

Gehrels, G., 2012, Detrital Zircon U-Pb Geochronology: Current Methods and New Opportunities: Tectonics of Sedimentary Basins, p. 45–62, doi:10.1002/9781444347166.ch2.

Gehrels, G.E., Valencia, V.A., and Ruiz, J., 2008, Enhanced precision, accuracy, efficiency, and spatial resolution of U-Pb ages by laser ablation-multicollector-inductively coupled plasma-mass spectrometry: Geochemistry, Geophysics, Geosystems, v. 9, p. 1–13.

Ludwig, K.R., 2008, User's Manual for Isoplot 3.60 - A Geochronological Toolkit for Microsoft Excel: Berkeley Geochronology Center Special Publication, v. 4, p. 77.

Romans, B.W., Fildani, A., Graham, S.A., Hubbard, S.M., and Covault, J.A., 2010, Importance of predecessor basin history on the sedimentary fill of a retroarc foreland basin: provenance analysis of the Cretaceous Magallanes: Basin Research, v. 22, p. 640–658.

Stacey, J.S., and Kramers, J.D., 1975, Approximation of terrestrial lead on a subset of magmatic rocks and isotope evolution by a two-stage model: Earth and Planetary Science Letters, v. 26, p. 207–221.

TABLES

Table A1. Zircon U-Pb LA-MC-ICPMS geochronological data.

FIGURES

Figure A1. Zircon U-Pb concordia diagrams for individual samples. Ellipses show 2σ uncertainty. n denotes the total number of analyzed grains per sample.

Figure A2. Relative probability plots of detrital zircon U-Pb ages for individual samples (0 to 2500 Ma). n denotes the total number of analyzed grains per sample.

Figure A3. Relative probability plots of detrital zircon U-Pb ages for individual samples (0 to 600 Ma).

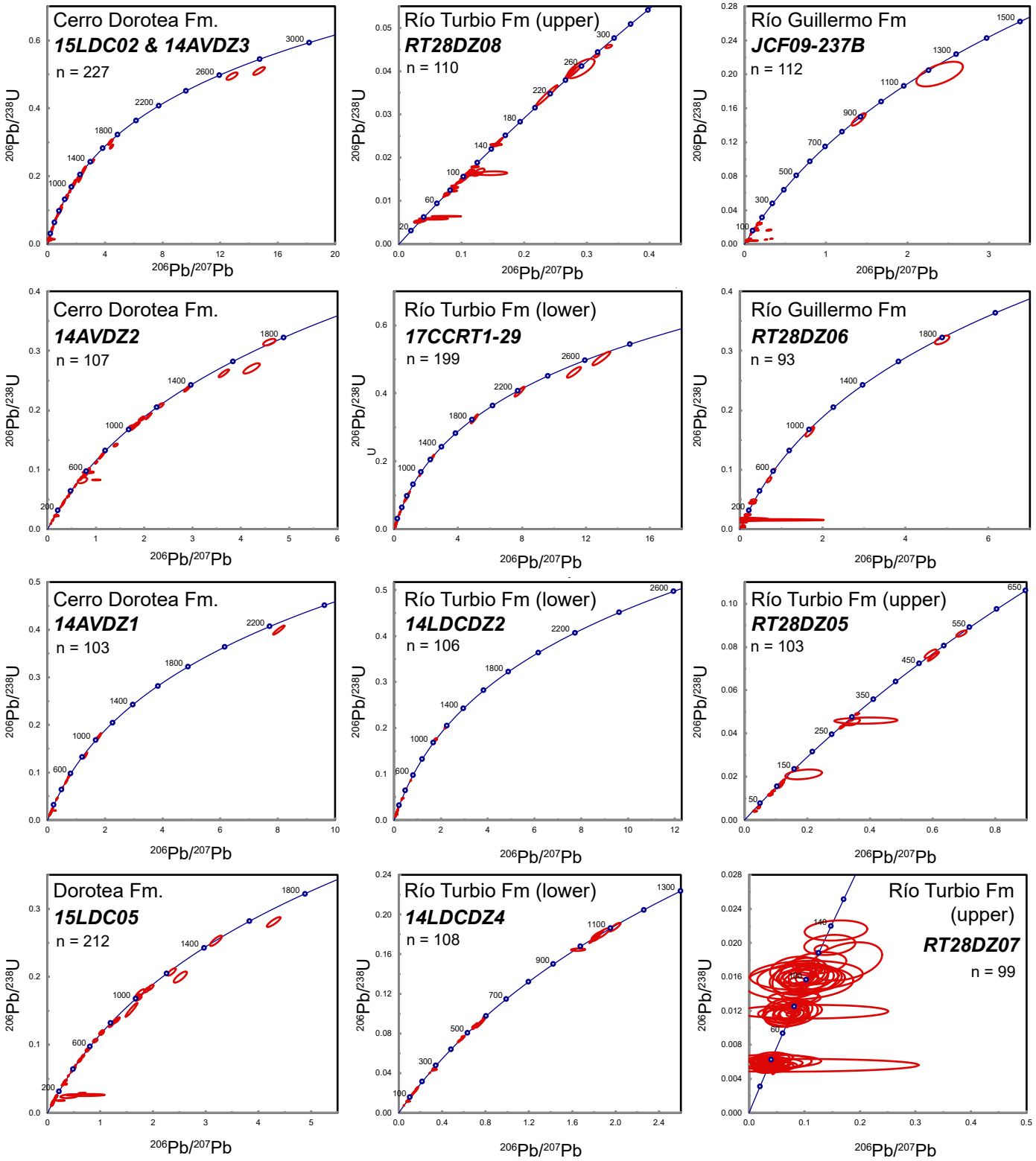

Figure A1. Zircon U-Pb concordia diagrams for individual samples. Ellipses show 2σ uncertainty. n denotes the total number of analyzed grains per sample.

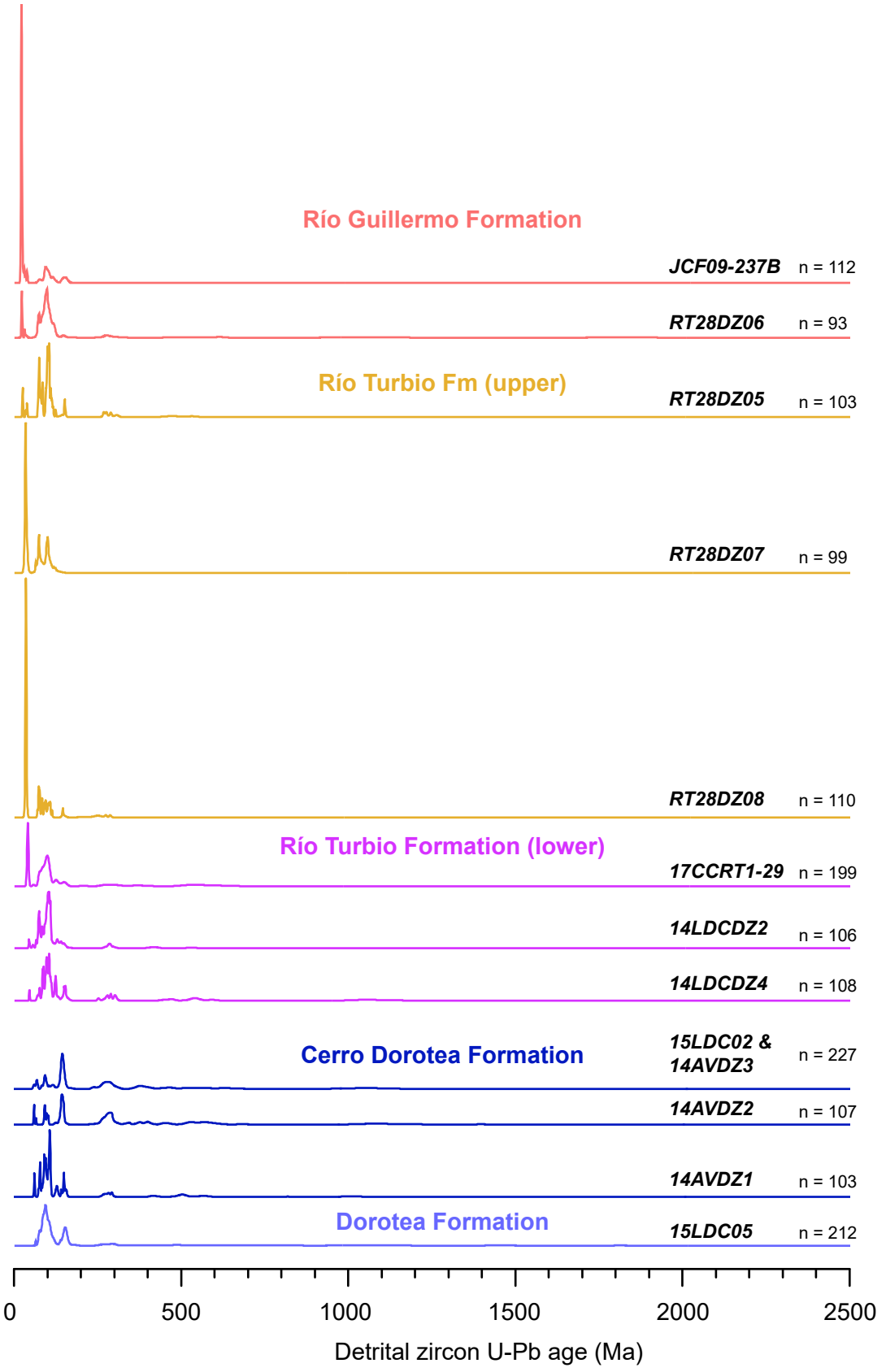

Figure A2. Relative probability plots of detrital zircon U-Pb ages for individual samples (0 to 2500 Ma). n denotes total number of analyzed grains per sample

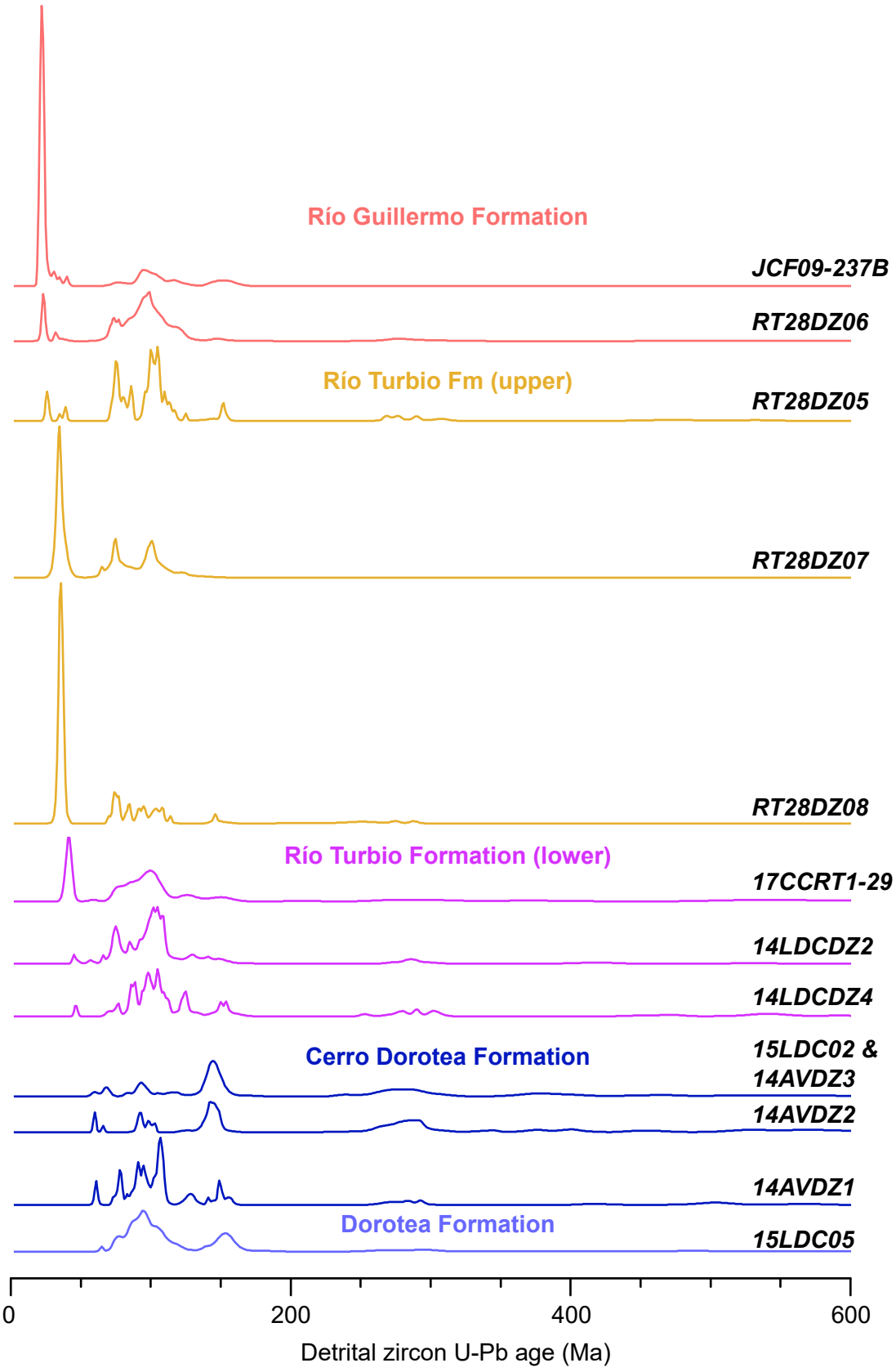

Figure A3. Relative probability plots of detrital zircon U-Pb ages for individual samples (0 to 600 Ma).

TABLE A1. ZIRCON U-Pb LA-ICP-MS GEOCHRONOLOGICAL DATA

Analysis	Isotope ratios										Apparent ages (Ma)								
	U (ppm)	$^{206}Pb/^{204}Pb$	U/Th	$^{206}Pb^*/^{207}Pb^*$	± (%)	$^{207}Pb^*/^{235}U^*$	± (%)	$^{206}Pb^*/^{238}U$	± (%)	error corr.	$^{206}Pb^*/^{238}U^*$	± (Ma)	$^{207}Pb^*/^{235}U$	± (Ma)	$^{206}Pb^*/^{207}Pb^*$	± (Ma)	Best age (Ma)	± (Ma)	Conc (%)
Sample 15LDC05 (Dorotea Formation)																			
15LDC05-100	168	13352	1.7	17.4714	8.1	0.0805	8.3	0.0102	1.7	0.20	65.4	1.1	78.6	6.3	500.7	179.2	65.4	1.1	NA
15LDC05-24	686	30189	1.5	21.6317	2.4	0.0656	2.7	0.0103	1.2	0.45	66.0	0.8	64.5	1.7	9.5	58.4	66.0	0.8	NA
15LDC05-195	271	22339	1.0	20.7702	3.6	0.0764	3.9	0.0115	1.4	0.36	73.8	1.0	74.8	2.8	106.4	85.2	73.8	1.0	NA
15LDC05-158	239	55224	1.4	20.8756	4.3	0.0773	4.7	0.0117	2.0	0.41	75.0	1.5	75.6	3.5	94.5	102.4	75.0	1.5	NA
15LDC05-88	255	38181	1.9	20.4784	4.3	0.0792	4.8	0.0118	2.2	0.46	75.4	1.7	77.4	3.6	139.8	101.0	75.4	1.7	NA
15LDC05-143	157	26161	1.4	21.4783	4.4	0.0756	4.9	0.0118	2.0	0.41	75.5	1.5	74.0	3.5	26.6	106.4	75.5	1.5	NA
15LDC05-147	170	101484	1.2	19.9545	5.5	0.0818	6.0	0.0118	2.2	0.37	75.8	1.7	79.8	4.6	200.3	128.7	75.8	1.7	NA
15LDC05-1	242	31704	2.0	17.7081	6.9	0.0927	7.3	0.0119	2.1	0.29	76.3	1.6	90.0	6.3	471.0	153.9	76.3	1.6	NA
15LDC05-141	602	33833	1.3	21.6353	3.3	0.0765	3.8	0.0120	1.8	0.48	76.9	1.4	74.9	2.7	9.1	80.5	76.9	1.4	NA
15LDC05-175	105	13045	1.3	19.9475	7.0	0.0832	7.3	0.0120	2.0	0.28	77.1	1.6	81.2	5.7	201.1	162.8	77.1	1.6	NA
15LDC05-140	120	9298	1.5	22.2731	5.6	0.0750	6.0	0.0121	2.2	0.37	77.7	1.7	73.5	4.3	61.2	136.2	77.7	1.7	NA
15LDC05-26	135	26071	1.5	20.4350	5.1	0.0819	5.4	0.0121	2.0	0.37	77.8	1.5	80.0	4.2	144.7	118.9	77.8	1.5	NA
15LDC05-67	301	100716	0.9	21.0860	3.7	0.0803	4.0	0.0123	1.6	0.39	78.7	1.2	78.4	3.1	70.7	88.4	78.7	1.2	NA
15LDC05-111	233	27652	1.2	21.5391	4.2	0.0788	4.7	0.0123	2.1	0.44	78.9	1.6	77.1	3.5	19.9	101.4	78.9	1.6	NA
15LDC05-65	227	31865	1.0	20.8829	4.1	0.0820	4.4	0.0124	1.7	0.38	79.6	1.3	80.1	3.4	93.7	96.2	79.6	1.3	NA
15LDC05-34	247	51143	2.8	21.0830	4.8	0.0823	5.3	0.0126	2.2	0.42	80.7	1.8	80.3	4.1	71.0	114.4	80.7	1.8	NA
15LDC05-188	716	42463	1.0	20.9690	2.6	0.0833	3.5	0.0127	2.3	0.66	81.2	1.8	81.3	2.7	83.9	61.5	81.2	1.8	NA
15LDC05-112	117	6377	1.4	22.1081	5.0	0.0791	5.5	0.0127	2.2	0.41	81.3	1.8	77.3	4.1	43.1	121.4	81.3	1.8	NA
15LDC05-98	848	97540	1.0	21.0459	2.4	0.0849	2.9	0.0130	1.7	0.59	83.0	1.4	82.7	2.3	75.2	56.6	83.0	1.4	NA
15LDC05-218	236	34323	1.4	21.2723	3.9	0.0850	4.2	0.0131	1.6	0.37	84.0	1.3	82.9	3.4	49.7	93.5	84.0	1.3	NA
15LDC05-142	177	28097	1.7	20.5219	3.7	0.0882	4.2	0.0131	1.9	0.44	84.1	1.5	85.9	3.4	134.8	88.1	84.1	1.5	NA
15LDC05-110	246	9791	1.7	20.9815	4.0	0.0867	4.7	0.0132	2.4	0.51	84.5	2.0	84.5	3.8	82.5	95.3	84.5	2.0	NA
15LDC05-101	534	46496	1.4	20.6657	3.0	0.0882	3.6	0.0132	2.1	0.58	84.6	1.8	85.8	3.0	118.4	70.0	84.6	1.8	NA
15LDC05-55	298	44469	1.2	21.3444	3.1	0.0861	3.6	0.0133	1.9	0.52	85.3	1.6	83.9	2.9	41.6	73.9	85.3	1.6	NA
15LDC05-124	300	16034	1.2	20.4663	4.1	0.0901	4.7	0.0134	2.2	0.47	85.7	1.9	87.6	3.9	141.2	97.0	85.7	1.9	NA
15LDC05-11	155	12379	1.4	21.4855	3.9	0.0860	4.2	0.0134	1.6	0.37	85.8	1.3	83.8	3.4	25.9	94.1	85.8	1.3	NA
15LDC05-190	146	25471	1.1	21.8904	4.1	0.0848	4.4	0.0135	1.5	0.34	86.2	1.3	82.6	3.5	19.1	100.3	86.2	1.3	NA
15LDC05-156	215	40934	0.8	20.5998	4.1	0.0907	4.5	0.0136	1.9	0.43	86.8	1.7	88.2	3.8	125.8	95.5	86.8	1.7	NA
15LDC05-52	210	27551	2.1	21.3746	4.1	0.0878	4.4	0.0136	1.8	0.40	87.1	1.5	85.4	3.6	38.2	97.3	87.1	1.5	NA
15LDC05-16	154	30153	2.0	21.2418	4.8	0.0884	5.2	0.0136	1.9	0.36	87.2	1.6	86.0	4.3	53.1	114.8	87.2	1.6	NA
15LDC05-15	2504	83370	1.2	21.0201	1.5	0.0895	2.0	0.0136	1.4	0.69	87.4	1.2	87.1	1.7	78.1	35.1	87.4	1.2	NA
15LDC05-135	720	60369	1.7	19.9542	2.0	0.0945	2.3	0.0137	1.3	0.53	87.6	1.1	91.7	2.1	200.3	46.0	87.6	1.1	NA

15LDC05-133	915	59552	1.9	20.5792	1.7	0.0918	2.4	0.0137	1.6	0.68	87.7	1.4	89.2	2.0	128.2	40.7	87.7	1.4	NA
15LDC05-71	193	32290	0.9	21.5723	4.9	0.0881	5.3	0.0138	1.9	0.36	88.2	1.7	85.7	4.3	16.2	118.0	88.2	1.7	NA
15LDC05-202	228	14756	2.5	20.6972	4.5	0.0919	5.4	0.0138	3.0	0.56	88.3	2.6	89.3	4.6	114.7	106.6	88.3	2.6	NA
15LDC05-53	378	69984	0.9	20.7508	3.6	0.0922	4.0	0.0139	1.8	0.44	88.8	1.6	89.5	3.4	108.7	84.7	88.8	1.6	NA
15LDC05-144	137	32647	1.7	19.9802	4.8	0.0958	5.1	0.0139	1.8	0.36	88.9	1.6	92.9	4.6	197.3	111.7	88.9	1.6	NA
15LDC05-186	80	14825	1.1	21.0972	6.0	0.0915	6.6	0.0140	2.6	0.40	89.6	2.3	88.9	5.6	69.4	143.2	89.6	2.3	NA
15LDC05-121	62	4428	1.9	20.0242	6.7	0.0965	7.4	0.0140	3.1	0.42	89.7	2.7	93.5	6.6	192.2	156.0	89.7	2.7	NA
15LDC05-161	541	40136	1.2	18.2795	4.2	0.1057	4.6	0.0140	2.0	0.43	89.7	1.8	102.1	4.5	400.2	93.9	89.7	1.8	NA
15LDC05-213	167	42285	1.6	20.7543	4.6	0.0931	4.9	0.0140	1.7	0.34	89.8	1.5	90.4	4.2	108.2	108.5	89.8	1.5	NA
15LDC05-194	91	27192	1.6	20.7011	5.2	0.0934	5.8	0.0140	2.4	0.42	89.8	2.2	90.7	5.0	114.3	123.3	89.8	2.2	NA
15LDC05-72	117	12496	1.4	20.6192	5.4	0.0940	5.9	0.0141	2.5	0.42	90.0	2.2	91.3	5.2	123.6	126.4	90.0	2.2	NA
15LDC05-38	377	29327	1.1	21.4405	2.4	0.0906	2.8	0.0141	1.4	0.51	90.2	1.3	88.0	2.4	30.9	57.7	90.2	1.3	NA
15LDC05-92	236	13895	1.7	21.7047	5.2	0.0895	5.6	0.0141	1.9	0.35	90.2	1.7	87.1	4.7	1.4	126.4	90.2	1.7	NA
15LDC05-35	103	33623	1.7	18.9739	5.4	0.1034	5.7	0.0142	1.8	0.32	91.1	1.7	99.9	5.4	316.0	123.4	91.1	1.7	NA
15LDC05-153	347	247805	0.8	20.9711	3.4	0.0936	3.6	0.0142	1.3	0.37	91.1	1.2	90.8	3.1	83.6	79.6	91.1	1.2	NA
15LDC05-126	68	3937	1.5	19.4011	7.2	0.1020	7.7	0.0143	2.8	0.36	91.8	2.5	98.6	7.2	265.2	165.0	91.8	2.5	NA
15LDC05-196	86	16098	1.2	21.0600	6.2	0.0942	6.6	0.0144	2.2	0.33	92.1	2.0	91.4	5.8	73.6	148.2	92.1	2.0	NA
15LDC05-102	103	77537	1.4	19.3858	4.1	0.1027	4.8	0.0144	2.5	0.52	92.4	2.3	99.3	4.5	267.0	93.7	92.4	2.3	NA
15LDC05-6	127	11284	1.6	23.8381	5.0	0.0839	5.3	0.0145	1.7	0.32	92.9	1.6	81.8	4.2	229.5	126.6	92.9	1.6	NA
15LDC05-5	255	30270	1.6	19.5611	5.9	0.1024	7.0	0.0145	3.7	0.53	93.0	3.4	99.0	6.6	246.3	136.5	93.0	3.4	NA
15LDC05-178	78	13512	1.8	20.6183	5.7	0.0972	6.1	0.0145	2.1	0.34	93.1	1.9	94.2	5.5	123.7	135.3	93.1	1.9	NA
15LDC05-89	216	12602	1.3	21.3537	3.9	0.0944	4.2	0.0146	1.6	0.38	93.5	1.5	91.6	3.7	40.6	93.0	93.5	1.5	NA
15LDC05-154	285	46541	1.3	20.5977	3.3	0.0979	4.2	0.0146	2.5	0.60	93.6	2.3	94.8	3.8	126.1	78.6	93.6	2.3	NA
15LDC05-197	76	13847	1.7	20.0694	7.1	0.1005	7.5	0.0146	2.4	0.32	93.6	2.2	97.2	6.9	186.9	164.3	93.6	2.2	NA
15LDC05-165	53	10801	1.3	19.2112	7.4	0.1050	7.7	0.0146	2.2	0.28	93.6	2.0	101.4	7.4	287.7	169.4	93.6	2.0	NA
15LDC05-32	95	11566	1.6	21.1836	6.4	0.0954	6.7	0.0147	2.1	0.31	93.8	1.9	92.5	5.9	59.7	152.1	93.8	1.9	NA
15LDC05-189	59	4722	1.6	20.1360	6.4	0.1003	6.9	0.0147	2.5	0.36	93.8	2.3	97.1	6.4	179.2	150.4	93.8	2.3	NA
15LDC05-123	834	36351	1.7	20.9925	2.2	0.0963	2.7	0.0147	1.5	0.55	93.9	1.4	93.4	2.4	81.2	52.6	93.9	1.4	NA
15LDC05-61	122	208804	1.0	21.0863	5.2	0.0960	5.5	0.0147	1.8	0.33	94.0	1.7	93.1	4.9	70.6	123.5	94.0	1.7	NA
15LDC05-7	213	32137	2.3	20.4699	3.9	0.0989	4.5	0.0147	2.3	0.51	94.0	2.1	95.8	4.1	140.8	91.4	94.0	2.1	NA
15LDC05-211	99	65864	2.4	20.6015	5.5	0.0991	5.9	0.0148	2.1	0.35	94.7	1.9	95.9	5.4	125.7	129.7	94.7	1.9	NA
15LDC05-193	183	18807	1.2	21.4316	4.0	0.0953	4.2	0.0148	1.3	0.32	94.8	1.3	92.4	3.7	31.9	95.6	94.8	1.3	NA
15LDC05-44	879	82969	1.7	20.6176	1.7	0.0995	2.1	0.0149	1.3	0.59	95.2	1.2	96.3	2.0	123.8	41.0	95.2	1.2	NA
15LDC05-113	189	24134	1.2	19.4278	4.1	0.1058	4.5	0.0149	1.8	0.41	95.4	1.7	102.1	4.3	262.1	93.8	95.4	1.7	NA
15LDC05-167	275	117536	1.2	20.6462	3.6	0.0999	3.9	0.0150	1.5	0.39	95.7	1.5	96.7	3.6	120.6	84.1	95.7	1.5	NA
15LDC05-182	306	25225	3.9	20.1084	3.0	0.1027	3.4	0.0150	1.7	0.49	95.8	1.6	99.2	3.3	182.4	70.0	95.8	1.6	NA
15LDC05-187	95	10674	1.7	19.9376	5.3	0.1039	5.7	0.0150	2.0	0.35	96.1	1.9	100.3	5.4	202.2	124.1	96.1	1.9	NA
15LDC05-23	254	26873	2.9	20.1640	3.6	0.1027	4.2	0.0150	2.1	0.50	96.1	2.0	99.3	4.0	175.9	84.9	96.1	2.0	NA
15LDC05-39	332	34799	1.4	20.7852	3.9	0.0999	4.3	0.0151	1.7	0.40	96.3	1.7	96.6	3.9	104.7	92.6	96.3	1.7	NA

15LDC05-73	84	13158	1.5	20.0786	5.6	0.1034	5.9	0.0151	1.8	0.30	96.3	1.7	99.9	5.6	185.9	131.1	96.3	1.7	NA
15LDC05-18	183	30519	1.8	19.9817	4.5	0.1042	4.8	0.0151	1.7	0.36	96.6	1.6	100.6	4.6	197.1	105.0	96.6	1.6	NA
15LDC05-45	303	17577	2.0	20.3886	3.3	0.1023	3.6	0.0151	1.5	0.41	96.8	1.4	98.9	3.4	150.1	77.6	96.8	1.4	NA
15LDC05-85	89	58719	2.1	21.1492	6.2	0.0986	7.0	0.0151	3.2	0.45	96.8	3.0	95.5	6.4	63.6	148.8	96.8	3.0	NA
15LDC05-106	77	18944	1.9	19.7672	5.9	0.1056	6.1	0.0151	1.7	0.27	96.9	1.6	101.9	5.9	222.2	135.5	96.9	1.6	NA
15LDC05-216	266	96433	4.3	19.8823	3.4	0.1053	3.8	0.0152	1.6	0.44	97.1	1.6	101.6	3.6	208.7	78.7	97.1	1.6	NA
15LDC05-128	565	33035	1.9	21.0551	2.3	0.0995	2.9	0.0152	1.7	0.61	97.2	1.7	96.3	2.6	74.2	54.0	97.2	1.7	NA
15LDC05-25	91	12958	2.2	20.0807	5.7	0.1046	6.1	0.0152	2.1	0.35	97.5	2.0	101.0	5.8	185.6	132.6	97.5	2.0	NA
15LDC05-159	158	26290	1.1	21.0826	4.2	0.0999	4.7	0.0153	2.1	0.45	97.7	2.0	96.6	4.3	71.1	99.8	97.7	2.0	NA
15LDC05-9	312	37328	1.8	20.6944	3.1	0.1018	3.6	0.0153	1.8	0.50	97.7	1.7	98.4	3.4	115.0	73.0	97.7	1.7	NA
15LDC05-118	1094	169571	1.1	20.3483	1.6	0.1040	2.0	0.0153	1.3	0.62	98.2	1.2	100.4	1.9	154.7	37.4	98.2	1.2	NA
15LDC05-173	240	151824	4.2	20.9796	3.3	0.1011	3.7	0.0154	1.8	0.48	98.4	1.8	97.7	3.5	82.7	77.3	98.4	1.8	NA
15LDC05-64	779	27553	1.6	20.8246	2.4	0.1018	2.9	0.0154	1.6	0.54	98.4	1.5	98.4	2.7	100.2	57.9	98.4	1.5	NA
15LDC05-87	578	44245	1.6	21.1964	2.8	0.1001	3.3	0.0154	1.8	0.54	98.4	1.7	96.9	3.0	58.2	65.7	98.4	1.7	NA
15LDC05-109	483	43182	3.3	20.6821	3.1	0.1038	3.7	0.0156	2.1	0.57	99.6	2.1	100.3	3.6	116.5	72.2	99.6	2.1	NA
15LDC05-99	40	1448	1.8	18.6817	7.3	0.1150	7.8	0.0156	2.8	0.36	99.6	2.8	110.5	8.2	351.3	164.3	99.6	2.8	NA
15LDC05-163	321	45227	4.7	21.0689	2.9	0.1021	3.3	0.0156	1.6	0.47	99.8	1.6	98.7	3.1	72.6	69.8	99.8	1.6	NA
15LDC05-138	106	31821	1.6	19.3085	5.3	0.1115	5.7	0.0156	2.0	0.36	99.9	2.0	107.4	5.8	276.2	121.1	99.9	2.0	NA
15LDC05-160	199	31105	4.7	20.2136	2.8	0.1074	3.7	0.0157	2.3	0.64	100.7	2.3	103.6	3.6	170.2	65.9	100.7	2.3	NA
15LDC05-68	145	28573	1.4	19.9420	4.9	0.1093	5.2	0.0158	1.6	0.32	101.1	1.7	105.3	5.2	201.8	113.8	101.1	1.7	NA
15LDC05-105	219	34182	1.1	20.4998	3.9	0.1071	4.2	0.0159	1.4	0.34	101.9	1.4	103.3	4.1	137.3	92.1	101.9	1.4	NA
15LDC05-117	57	2664	2.2	21.0727	5.6	0.1046	6.3	0.0160	2.9	0.46	102.3	2.9	101.1	6.1	72.2	133.0	102.3	2.9	NA
15LDC05-198	240	21085	2.0	21.1062	3.8	0.1055	4.3	0.0162	2.0	0.47	103.3	2.1	101.8	4.2	68.4	90.7	103.3	2.1	NA
15LDC05-205	87	8044	2.2	21.3546	4.7	0.1045	5.2	0.0162	2.1	0.40	103.5	2.1	101.0	5.0	40.5	113.3	103.5	2.1	NA
15LDC05-31	262	18326	1.5	21.1986	3.1	0.1058	3.7	0.0163	1.9	0.52	104.0	2.0	102.1	3.6	58.0	74.8	104.0	2.0	NA
15LDC05-86	1152	52546	1.2	20.7329	2.0	0.1084	2.5	0.0163	1.4	0.56	104.2	1.4	104.5	2.5	110.7	48.2	104.2	1.4	NA
15LDC05-166	59	25303	1.2	19.6595	6.6	0.1143	7.0	0.0163	2.5	0.36	104.2	2.6	109.9	7.3	234.8	151.3	104.2	2.6	NA
15LDC05-54	142	26696	3.4	21.0027	5.2	0.1070	5.5	0.0163	1.8	0.33	104.2	1.9	103.2	5.4	80.1	123.6	104.2	1.9	NA
15LDC05-94	104	5641	2.1	21.7898	5.3	0.1034	5.7	0.0163	2.0	0.35	104.5	2.1	99.9	5.4	8.0	128.0	104.5	2.1	NA
15LDC05-131	84	30487	1.7	21.3831	5.7	0.1054	6.1	0.0163	2.1	0.35	104.5	2.2	101.8	5.9	37.3	137.0	104.5	2.2	NA
15LDC05-206	33	1970	1.5	23.2735	9.2	0.0976	9.8	0.0165	3.3	0.34	105.3	3.4	94.5	8.8	169.5	229.2	105.3	3.4	NA
15LDC05-132	367	100251	2.3	20.6335	3.1	0.1104	3.5	0.0165	1.6	0.46	105.6	1.7	106.3	3.5	122.0	73.3	105.6	1.7	NA
15LDC05-56	82	3577	2.0	22.7315	5.7	0.1002	6.1	0.0165	2.3	0.37	105.7	2.4	97.0	5.7	111.1	140.2	105.7	2.4	NA
15LDC05-77	418	29987	2.2	20.9659	3.1	0.1088	3.6	0.0165	1.9	0.52	105.8	2.0	104.9	3.6	84.2	74.1	105.8	2.0	NA
15LDC05-172	176	26450	1.0	19.8630	3.4	0.1156	4.0	0.0166	2.0	0.50	106.4	2.1	111.0	4.2	210.9	79.4	106.4	2.1	NA
15LDC05-103	273	33655	2.6	20.0070	3.5	0.1148	4.1	0.0167	2.1	0.50	106.5	2.2	110.3	4.3	194.2	82.3	106.5	2.2	NA
15LDC05-14	54	16906	1.8	21.0081	5.5	0.1095	6.0	0.0167	2.4	0.40	106.6	2.5	105.5	6.0	79.5	131.5	106.6	2.5	NA
15LDC05-119	119	42952	3.1	21.3885	3.9	0.1076	4.5	0.0167	2.2	0.50	106.7	2.4	103.7	4.4	36.7	92.4	106.7	2.4	NA
15LDC05-82	295	46807	1.8	20.5429	2.9	0.1122	3.4	0.0167	1.7	0.50	106.8	1.8	107.9	3.4	132.4	68.7	106.8	1.8	NA

15LDC05-108	109	28859	2.6	21.1516	4.1	0.1093	4.7	0.0168	2.3	0.49	107.2	2.5	105.3	4.7	63.3	97.7	107.2	2.5	NA
15LDC05-91	109	205652	1.5	21.5049	4.5	0.1081	5.3	0.0169	2.8	0.52	107.7	2.9	104.2	5.2	23.7	107.5	107.7	2.9	NA
15LDC05-40	740	66594	2.2	20.4309	2.0	0.1141	2.5	0.0169	1.5	0.59	108.1	1.6	109.7	2.6	145.2	47.5	108.1	1.6	NA
15LDC05-179	203	41016	1.6	20.3101	3.6	0.1156	4.1	0.0170	1.9	0.46	108.8	2.1	111.1	4.3	159.1	85.2	108.8	2.1	NA
15LDC05-157	123	11739	1.6	20.4788	4.8	0.1153	5.2	0.0171	2.0	0.39	109.4	2.2	110.8	5.4	139.7	112.3	109.4	2.2	NA
15LDC05-152	136	11273	1.6	20.1950	4.9	0.1174	5.3	0.0172	1.9	0.36	109.9	2.0	112.7	5.6	172.4	114.7	109.9	2.0	NA
15LDC05-151	283	37855	4.0	20.5615	4.2	0.1156	4.5	0.0172	1.4	0.31	110.2	1.5	111.1	4.7	130.2	99.8	110.2	1.5	NA
15LDC05-21	66	11892	2.7	20.4484	6.0	0.1167	6.5	0.0173	2.5	0.38	110.6	2.7	112.1	6.9	143.2	141.9	110.6	2.7	NA
15LDC05-27	406	30565	2.2	20.7630	2.9	0.1153	3.4	0.0174	1.9	0.54	111.0	2.0	110.8	3.6	107.3	68.7	111.0	2.0	NA
15LDC05-162	342	19859	1.7	21.2074	2.7	0.1130	3.4	0.0174	2.2	0.63	111.1	2.4	108.7	3.5	57.0	63.4	111.1	2.4	NA
15LDC05-107	483	54930	8.2	21.1350	3.1	0.1135	3.6	0.0174	1.8	0.49	111.2	2.0	109.1	3.7	65.2	74.8	111.2	2.0	NA
15LDC05-177	58	4754	1.8	21.1822	6.2	0.1151	7.0	0.0177	3.3	0.48	113.0	3.8	110.6	7.4	59.9	147.1	113.0	3.8	NA
15LDC05-93	70	22755	3.2	9.9063	19.1	0.2498	19.3	0.0179	2.8	0.15	114.7	3.2	226.4	39.2	1641.6	357.6	114.7	3.2	NA
15LDC05-36	548	168290	1.7	20.3163	2.6	0.1234	3.3	0.0182	2.0	0.61	116.2	2.3	118.2	3.6	158.4	60.2	116.2	2.3	NA
15LDC05-69	2897	137221	6.2	20.2273	1.2	0.1242	1.9	0.0182	1.4	0.75	116.4	1.6	118.9	2.1	168.6	28.7	116.4	1.6	NA
15LDC05-122	1445	193382	1.1	19.2486	1.8	0.1315	2.5	0.0184	1.8	0.70	117.2	2.1	125.4	3.0	283.3	41.2	117.2	2.1	NA
15LDC05-79	260	36024	2.1	18.6634	5.9	0.1360	6.2	0.0184	1.6	0.27	117.6	1.9	129.5	7.5	353.5	134.3	117.6	1.9	NA
15LDC05-200	314	33279	1.8	20.2738	3.3	0.1262	3.8	0.0186	1.8	0.48	118.5	2.2	120.7	4.3	163.3	77.8	118.5	2.2	NA
15LDC05-2	206	80264	2.0	21.1154	4.1	0.1240	4.5	0.0190	1.8	0.40	121.3	2.2	118.7	5.0	67.3	97.3	121.3	2.2	NA
15LDC05-204	311	46653	1.1	21.3518	2.4	0.1230	2.9	0.0190	1.6	0.54	121.6	1.9	117.7	3.2	40.8	57.8	121.6	1.9	NA
15LDC05-58	188	26685	2.0	20.1669	3.7	0.1337	4.2	0.0196	1.8	0.44	124.8	2.3	127.4	5.0	175.6	87.3	124.8	2.3	NA
15LDC05-46	247	26632	2.2	20.7883	3.0	0.1353	3.4	0.0204	1.6	0.47	130.2	2.1	128.8	4.1	104.4	70.9	130.2	2.1	NA
15LDC05-30	432	52206	1.8	20.8077	2.4	0.1453	2.6	0.0219	1.0	0.38	139.8	1.4	137.8	3.4	102.2	57.2	139.8	1.4	NA
15LDC05-146	234	19450	2.6	21.1046	3.0	0.1433	3.4	0.0219	1.7	0.50	139.8	2.4	135.9	4.4	68.6	70.5	139.8	2.4	NA
15LDC05-42	641	99653	2.1	20.4583	2.0	0.1496	2.6	0.0222	1.7	0.65	141.5	2.4	141.5	3.4	142.1	46.4	141.5	2.4	NA
15LDC05-201	223	33987	3.7	20.8269	2.4	0.1489	3.2	0.0225	2.1	0.65	143.4	2.9	140.9	4.2	100.0	57.5	143.4	2.9	NA
15LDC05-209	76	16930	2.6	20.6615	4.4	0.1524	4.9	0.0228	2.2	0.45	145.6	3.1	144.1	6.5	118.8	102.7	145.6	3.1	NA
15LDC05-183	505	40326	1.6	19.8534	2.1	0.1599	2.6	0.0230	1.6	0.60	146.7	2.3	150.6	3.7	212.0	48.4	146.7	2.3	NA
15LDC05-134	343	56754	2.7	19.2062	4.0	0.1653	7.2	0.0230	6.0	0.84	146.8	8.7	155.3	10.4	288.3	90.5	146.8	8.7	NA
15LDC05-43	546	173334	1.1	20.9571	2.2	0.1534	3.0	0.0233	2.0	0.67	148.6	2.9	144.9	4.0	85.3	52.2	148.6	2.9	NA
15LDC05-96	1294	134509	3.7	20.5030	1.9	0.1578	2.3	0.0235	1.4	0.61	149.5	2.1	148.7	3.2	137.0	43.5	149.5	2.1	NA
15LDC05-219	131	39985	1.2	20.0936	3.8	0.1613	4.0	0.0235	1.4	0.34	149.8	2.0	151.9	5.7	184.1	88.5	149.8	2.0	NA
15LDC05-74	151	38649	1.2	19.5303	4.4	0.1664	4.8	0.0236	1.9	0.40	150.2	2.9	156.3	7.0	249.9	101.7	150.2	2.9	NA
15LDC05-125	237	37840	1.9	20.0780	3.7	0.1620	4.1	0.0236	1.6	0.39	150.3	2.3	152.5	5.8	185.9	87.3	150.3	2.3	NA
15LDC05-29	524	51064	3.7	20.0234	2.1	0.1630	2.9	0.0237	2.0	0.69	150.8	3.0	153.3	4.1	192.3	48.9	150.8	3.0	NA
15LDC05-176	194	41965	1.4	20.2679	2.5	0.1619	3.0	0.0238	1.7	0.56	151.6	2.5	152.4	4.3	163.9	58.5	151.6	2.5	NA
15LDC05-130	219	156993	2.0	20.6236	2.3	0.1593	3.2	0.0238	2.2	0.70	151.8	3.4	150.1	4.5	123.1	54.4	151.8	3.4	NA
15LDC05-47	854	194646	1.1	20.5927	1.6	0.1596	2.1	0.0238	1.3	0.63	151.8	1.9	150.3	2.9	126.7	37.7	151.8	1.9	NA
15LDC05-184	300	43981	2.3	20.6415	2.1	0.1602	2.5	0.0240	1.4	0.54	152.8	2.1	150.9	3.5	121.1	49.9	152.8	2.1	NA

15LDC05-129	339	28919	2.0	19.8291	2.2	0.1669	2.7	0.0240	1.5	0.55	152.9	2.2	156.7	3.9	214.9	51.5	152.9	2.2	NA
15LDC05-181	801	32580	2.5	20.0380	2.0	0.1652	2.5	0.0240	1.4	0.59	153.0	2.2	155.3	3.5	190.6	46.3	153.0	2.2	NA
15LDC05-199	188	25421	1.3	20.8286	3.6	0.1594	4.0	0.0241	1.7	0.43	153.4	2.6	150.2	5.6	99.8	85.2	153.4	2.6	NA
15LDC05-37	325	31497	1.3	20.8570	2.3	0.1597	2.8	0.0242	1.6	0.57	153.9	2.4	150.4	3.9	96.6	55.0	153.9	2.4	NA
15LDC05-19	326	27213	1.2	20.9314	2.6	0.1597	3.1	0.0242	1.7	0.57	154.4	2.7	150.4	4.3	88.2	60.5	154.4	2.7	NA
15LDC05-49	1560	158633	2.3	19.8734	1.3	0.1685	2.0	0.0243	1.5	0.76	154.7	2.3	158.2	2.9	209.7	30.0	154.7	2.3	NA
15LDC05-170	375	88041	2.6	20.1338	2.2	0.1668	2.7	0.0244	1.6	0.60	155.1	2.5	156.6	3.9	179.5	50.2	155.1	2.5	NA
15LDC05-59	153	12110	2.2	8.1772	25.4	0.4110	26.4	0.0244	7.2	0.27	155.2	11.1	349.6	78.2	1989.9	459.0	155.2	11.1	NA
15LDC05-10	415	92788	2.3	20.6930	2.2	0.1631	2.6	0.0245	1.4	0.53	155.9	2.1	153.4	3.7	115.3	52.0	155.9	2.1	NA
15LDC05-149	579	44255	1.9	20.0877	1.9	0.1682	2.4	0.0245	1.5	0.62	156.1	2.3	157.9	3.6	184.8	44.8	156.1	2.3	NA
15LDC05-174	199	51105	2.9	20.5767	2.4	0.1645	2.7	0.0246	1.3	0.47	156.4	2.0	154.7	3.9	128.5	56.4	156.4	2.0	NA
15LDC05-97	2393	311187	14.1	20.1899	1.3	0.1678	2.4	0.0246	2.0	0.82	156.5	3.0	157.5	3.5	173.0	31.5	156.5	3.0	NA
15LDC05-17	221	1038603	3.4	20.4528	2.5	0.1658	3.0	0.0246	1.7	0.55	156.6	2.6	155.7	4.4	142.7	59.6	156.6	2.6	NA
15LDC05-120	222	30344	1.7	20.1070	2.9	0.1690	3.3	0.0247	1.6	0.47	157.0	2.4	158.6	4.8	182.6	67.1	157.0	2.4	NA
15LDC05-76	77	30915	1.9	20.0701	5.9	0.1699	6.4	0.0247	2.3	0.36	157.5	3.6	159.3	9.4	186.8	138.4	157.5	3.6	NA
15LDC05-214	193	68718	1.6	20.4671	3.0	0.1667	3.4	0.0247	1.7	0.50	157.6	2.7	156.5	5.0	141.1	69.4	157.6	2.7	NA
15LDC05-4	1019	79460	4.3	20.4932	1.8	0.1681	2.4	0.0250	1.6	0.66	159.1	2.5	157.7	3.5	138.1	42.4	159.1	2.5	NA
15LDC05-60	275	149763	2.4	21.0387	2.9	0.1642	3.2	0.0251	1.5	0.47	159.5	2.4	154.4	4.6	76.0	68.0	159.5	2.4	NA
15LDC05-208	173	44606	2.8	19.7421	2.9	0.1750	3.2	0.0251	1.3	0.41	159.6	2.0	163.8	4.8	225.1	67.5	159.6	2.0	NA
15LDC05-51	1788	109229	2.0	20.1688	1.5	0.1721	3.0	0.0252	2.6	0.86	160.2	4.0	161.2	4.4	175.4	35.1	160.2	4.0	NA
15LDC05-13	348	151178	2.4	20.5794	1.6	0.1732	2.2	0.0258	1.6	0.70	164.5	2.5	162.2	3.4	128.2	37.6	164.5	2.5	NA
15LDC05-220	260	6265	0.9	5.0369	32.7	0.7185	33.0	0.0262	3.9	0.12	167.0	6.4	549.8	140.9	2814.2	552.2	167.0	6.4	NA
15LDC05-185	77	5029	1.2	6.0945	6.4	0.6534	6.7	0.0289	2.0	0.29	183.6	3.5	510.6	27.0	2498.2	108.5	183.6	3.5	NA
15LDC05-137	77	15322	1.6	19.7780	3.9	0.2850	4.3	0.0409	1.8	0.43	258.3	4.6	254.6	9.6	220.9	89.6	258.3	4.6	NA
15LDC05-115	627	194198	8.5	16.3621	1.7	0.3530	2.3	0.0419	1.5	0.65	264.5	3.8	306.9	6.0	643.4	37.4	264.5	3.8	NA
15LDC05-114	195	95824	2.1	19.4642	2.7	0.3062	3.4	0.0432	2.0	0.60	272.8	5.4	271.2	8.1	257.8	62.1	272.8	5.4	NA
15LDC05-75	185	38196	2.2	19.4645	2.6	0.3093	3.1	0.0437	1.6	0.52	275.5	4.4	273.6	7.4	257.7	60.9	275.5	4.4	NA
15LDC05-81	100	30400	2.2	19.2921	3.3	0.3167	3.9	0.0443	2.0	0.53	279.5	5.6	279.4	9.5	278.1	75.7	279.5	5.6	NA
15LDC05-83	191	140087	2.7	19.3593	2.8	0.3258	3.3	0.0457	1.9	0.56	288.3	5.3	286.3	8.3	270.1	63.2	288.3	5.3	NA
15LDC05-28	161	49561	2.7	18.7250	2.5	0.3440	3.2	0.0467	1.9	0.61	294.4	5.6	300.2	8.3	346.0	57.2	294.4	5.6	NA
15LDC05-139	486	4270710	1.6	19.3300	2.0	0.3372	2.5	0.0473	1.6	0.62	297.8	4.6	295.1	6.5	273.6	45.3	297.8	4.6	NA
15LDC05-84	319	29382	2.9	19.2274	1.6	0.3409	2.1	0.0475	1.4	0.65	299.4	4.0	297.8	5.4	285.8	36.4	299.4	4.0	NA
15LDC05-155	167	34438	1.1	18.9720	2.1	0.3470	2.7	0.0478	1.7	0.62	300.7	4.9	302.5	7.0	316.3	47.4	300.7	4.9	NA
15LDC05-116	732	181992	2.0	19.0210	1.6	0.3935	2.2	0.0543	1.5	0.68	340.8	5.0	336.9	6.3	310.4	36.4	340.8	5.0	NA
15LDC05-207	747	78066	48.8	18.4991	1.5	0.4531	2.2	0.0608	1.7	0.75	380.5	6.1	379.5	7.0	373.4	33.0	380.5	6.1	NA
15LDC05-63	1498	72180	15.8	17.4881	1.2	0.5163	2.0	0.0655	1.6	0.79	408.9	6.3	422.7	6.9	498.5	27.1	408.9	6.3	3%
15LDC05-66	453	61963	1.5	18.2018	1.3	0.5202	2.5	0.0687	2.2	0.86	428.1	8.9	425.3	8.7	409.7	28.0	428.1	8.9	-1%
15LDC05-90	377	85121	2.4	17.5613	1.9	0.5973	2.8	0.0761	2.0	0.74	472.7	9.3	475.5	10.5	489.4	41.2	472.7	9.3	1%
15LDC05-148	256	66102	1.9	17.2585	1.6	0.6150	2.5	0.0770	1.9	0.77	478.1	8.8	486.7	9.6	527.6	35.0	478.1	8.8	2%

15LDC05-150	412	190464	1.8	17.6245	1.2	0.6146	1.8	0.0786	1.4	0.76	487.5	6.5	486.5	7.1	481.4	26.5	487.5	6.5	0%
15LDC05-95	374	126397	5.0	17.1734	1.6	0.6669	2.3	0.0831	1.6	0.71	514.4	8.1	518.9	9.4	538.4	35.4	514.4	8.1	1%
15LDC05-169	390	104635	4.3	16.9180	1.2	0.6790	2.0	0.0833	1.6	0.79	515.9	8.0	526.2	8.3	571.1	26.9	515.9	8.0	2%
15LDC05-164	155	90896	6.7	16.8255	1.8	0.7535	2.5	0.0920	1.8	0.72	567.1	10.0	570.3	11.1	583.0	38.1	567.1	10.0	1%
15LDC05-57	325	136560	4.2	17.1202	1.6	0.7473	2.3	0.0928	1.6	0.71	572.0	8.9	566.7	10.0	545.2	35.5	572.0	8.9	-1%
15LDC05-78	488	97909	3.5	16.5827	1.7	0.7826	2.9	0.0941	2.4	0.83	579.9	13.4	587.0	13.1	614.5	35.7	579.9	13.4	1%
15LDC05-3	72	27455	1.0	16.2474	2.8	0.9021	3.2	0.1063	1.7	0.52	651.3	10.5	652.9	15.6	658.4	59.2	651.3	10.5	0%
15LDC05-192	259	121841	3.8	15.5984	1.4	1.0383	2.1	0.1175	1.6	0.75	716.0	10.8	723.1	11.0	745.2	29.9	716.0	10.8	1%
15LDC05-191	105	207971	1.1	15.9860	1.8	1.0206	2.6	0.1183	1.9	0.73	720.9	12.9	714.2	13.3	693.1	38.1	720.9	12.9	-1%
15LDC05-136	249	93452	4.1	14.8118	1.6	1.1993	2.3	0.1288	1.6	0.71	781.2	12.0	800.3	12.8	853.6	34.0	781.2	12.0	2%
15LDC05-20	259	50129	2.6	14.4690	1.6	1.2908	2.4	0.1355	1.9	0.76	818.9	14.2	841.6	14.0	902.1	32.9	818.9	14.2	3%
15LDC05-33	487	72676	10.3	14.2116	1.3	1.3276	2.1	0.1368	1.6	0.79	826.8	12.6	857.9	11.9	939.0	26.0	826.8	12.6	4%
15LDC05-62	71	52899	7.8	13.7922	1.9	1.7482	3.3	0.1749	2.7	0.81	1038.9	25.4	1026.5	21.2	1000.1	39.1	1000.1	39.1	-1%
15LDC05-217	180	4831501	1.1	13.7915	1.5	1.7002	2.3	0.1701	1.7	0.77	1012.5	16.4	1008.6	14.6	1000.2	29.6	1000.2	29.6	0%
15LDC05-210	49	87876	2.6	13.5249	1.9	1.7200	2.3	0.1687	1.3	0.58	1005.0	12.4	1016.0	14.7	1039.7	37.7	1039.7	37.7	1%
15LDC05-41	698	146082	2.8	13.5099	1.1	1.7150	1.8	0.1680	1.4	0.77	1001.3	12.7	1014.2	11.3	1042.0	22.7	1042.0	22.7	1%
15LDC05-80	480	79536	4.4	13.2318	1.2	1.8842	1.9	0.1808	1.4	0.76	1071.5	14.3	1075.6	12.7	1083.8	25.0	1083.8	25.0	0%
15LDC05-171	223	253015	0.2	13.1117	1.4	1.5911	4.7	0.1513	4.5	0.96	908.3	37.7	966.7	29.0	1102.1	27.3	1102.1	27.3	6%
15LDC05-180	127	180970	3.4	13.0163	1.3	1.9544	1.9	0.1845	1.4	0.72	1091.5	13.6	1099.9	12.6	1116.7	25.8	1116.7	25.8	1%
15LDC05-70	390	161904	1.9	12.1173	1.3	2.3564	2.2	0.2071	1.7	0.78	1213.3	18.8	1229.5	15.5	1258.1	26.3	1258.1	26.3	1%
15LDC05-48	61	36538	1.2	10.9416	1.9	2.5157	3.3	0.1996	2.6	0.81	1173.4	28.2	1276.6	23.7	1454.8	36.7	1454.8	36.7	8%
15LDC05-203	81	130664	0.5	10.9293	1.3	3.1936	2.3	0.2531	1.9	0.84	1454.7	25.2	1455.6	17.8	1457.0	23.9	1457.0	23.9	0%
15LDC05-168	212	65733	0.9	9.0213	1.0	4.2883	2.0	0.2806	1.8	0.87	1594.3	24.9	1691.1	16.7	1813.4	18.5	1813.4	18.5	6%
15LDC05-215	41	71147	1.2	3.2709	1.0	26.6508	1.9	0.6322	1.6	0.84	3158.4	39.2	3370.7	18.4	3499.5	16.0	3499.5	16.0	6%
Sample 14AVDZ1 (Cerro Dorotea Formation)																			
14AVDZ1-57	90	3444	0.8	19.1998	8.3	0.0688	8.5	0.0096	2.0	0.23	61.4	1.2	67.5	5.6	289.1	189.6	61.4	1.2	NA
14AVDZ1-12	165	12084	0.8	20.4084	1.1	0.0647	1.5	0.0096	0.9	0.63	61.4	0.6	63.7	0.9	147.8	26.8	61.4	0.6	NA
14AVDZ1-67	261	31130	0.7	20.7405	0.8	0.0640	1.0	0.0096	0.6	0.59	61.8	0.4	63.0	0.6	109.8	18.8	61.8	0.4	NA
14AVDZ1-42	94	8903	1.1	20.1935	2.1	0.0660	2.1	0.0097	0.3	0.15	62.0	0.2	64.9	1.3	172.5	48.3	62.0	0.2	NA
14AVDZ1-16	255	13255	1.1	20.4546	1.1	0.0778	1.2	0.0115	0.6	0.46	74.0	0.4	76.1	0.9	142.5	25.4	74.0	0.4	NA
14AVDZ1-52	176	8208	1.6	20.5058	1.4	0.0793	1.4	0.0118	0.4	0.31	75.6	0.3	77.5	1.1	136.6	31.8	75.6	0.3	NA
14AVDZ1-60	178	15805	0.6	19.9328	3.1	0.0835	3.2	0.0121	0.8	0.23	77.3	0.6	81.4	2.5	202.8	72.7	77.3	0.6	NA
14AVDZ1-20	414	190129	3.1	20.3840	1.0	0.0819	1.3	0.0121	0.8	0.62	77.6	0.6	79.9	1.0	150.6	23.0	77.6	0.6	NA
14AVDZ1-6	390	49449	1.0	20.5751	0.8	0.0818	1.3	0.0122	1.1	0.80	78.2	0.8	79.8	1.0	128.7	19.0	78.2	0.8	NA
14AVDZ1-65	42	2166	1.1	20.4985	1.0	0.0826	1.2	0.0123	0.5	0.46	78.7	0.4	80.6	0.9	137.5	24.4	78.7	0.4	NA
14AVDZ1-1	327	16505	1.8	20.4922	1.0	0.0834	1.5	0.0124	1.1	0.74	79.4	0.9	81.3	1.2	138.2	23.3	79.4	0.9	NA
14AVDZ1-103	292	26599	1.8	20.4291	0.6	0.0840	1.1	0.0124	0.9	0.82	79.7	0.7	81.9	0.8	145.4	14.6	79.7	0.7	NA
14AVDZ1-27	124	5589	1.1	20.9108	1.2	0.0821	1.4	0.0125	0.8	0.57	79.8	0.7	80.1	1.1	90.5	28.3	79.8	0.7	NA

14AVDZ1-45	66	7473	1.4	20.3980	2.4	0.0876	2.5	0.0130	0.6	0.24	83.0	0.5	85.3	2.1	149.0	57.4	83.0	0.5	NA
14AVDZ1-85	206	38637	1.2	20.3796	1.3	0.0879	1.8	0.0130	1.3	0.69	83.2	1.1	85.5	1.5	151.1	31.0	83.2	1.1	NA
14AVDZ1-51	264	15813	1.1	20.2781	0.6	0.0922	0.8	0.0136	0.6	0.69	86.8	0.5	89.5	0.7	162.8	14.1	86.8	0.5	NA
14AVDZ1-35	285	27169	0.9	20.2740	0.9	0.0943	1.2	0.0139	0.8	0.69	88.7	0.7	91.5	1.1	163.3	20.4	88.7	0.7	NA
14AVDZ1-92	98	8169	1.3	20.2951	1.5	0.0948	2.0	0.0140	1.4	0.68	89.3	1.2	92.0	1.8	160.9	35.0	89.3	1.2	NA
14AVDZ1-39	46	3103	1.2	20.6216	2.2	0.0939	3.0	0.0140	2.1	0.68	89.9	1.8	91.1	2.6	123.4	52.2	89.9	1.8	NA
14AVDZ1-93	191	22815	1.2	20.2809	0.8	0.0957	1.0	0.0141	0.7	0.65	90.1	0.6	92.8	0.9	162.5	18.5	90.1	0.6	NA
14AVDZ1-89	144	34293	1.5	20.2116	1.2	0.0971	1.4	0.0142	0.8	0.56	91.1	0.7	94.1	1.3	170.5	27.8	91.1	0.7	NA
14AVDZ1-101	47	4947	1.3	20.0194	1.7	0.0982	1.9	0.0143	0.9	0.47	91.3	0.8	95.1	1.7	192.8	39.5	91.3	0.8	NA
14AVDZ1-63	46	9205	1.1	18.3346	7.6	0.1079	7.7	0.0143	0.9	0.12	91.8	0.8	104.1	7.6	393.5	170.8	91.8	0.8	NA
14AVDZ1-90	88	7375	0.8	20.1440	1.3	0.0983	2.4	0.0144	2.0	0.83	91.9	1.8	95.2	2.1	178.3	30.6	91.9	1.8	NA
14AVDZ1-34	60	17635	1.1	20.0480	2.2	0.0992	2.6	0.0144	1.2	0.48	92.3	1.1	96.1	2.4	189.4	52.3	92.3	1.1	NA
14AVDZ1-36	35	3983	1.0	20.0169	2.7	0.1001	2.9	0.0145	0.8	0.27	93.0	0.7	96.8	2.6	193.1	63.9	93.0	0.7	NA
14AVDZ1-26	51	5251	1.5	20.3229	1.7	0.0987	2.3	0.0145	1.6	0.70	93.1	1.5	95.6	2.1	157.6	39.2	93.1	1.5	NA
14AVDZ1-100	69	5289	0.9	20.1927	1.6	0.1004	2.0	0.0147	1.2	0.61	94.1	1.1	97.1	1.8	172.6	36.3	94.1	1.1	NA
14AVDZ1-33	440	52719	1.5	20.4823	0.6	0.0995	1.3	0.0148	1.1	0.89	94.5	1.1	96.3	1.2	139.3	13.5	94.5	1.1	NA
14AVDZ1-24	715	55275	1.2	20.5137	1.0	0.0996	1.3	0.0148	0.9	0.69	94.9	0.9	96.4	1.2	135.7	22.8	94.9	0.9	NA
14AVDZ1-49	291	11719	2.0	19.8029	0.8	0.1034	1.2	0.0149	0.9	0.75	95.1	0.8	100.0	1.1	218.0	18.4	95.1	0.8	NA
14AVDZ1-5	160	17226	2.3	20.6610	0.7	0.0993	1.0	0.0149	0.8	0.77	95.2	0.7	96.1	0.9	118.9	15.4	95.2	0.7	NA
14AVDZ1-64	144	24017	2.4	20.0813	1.0	0.1022	1.1	0.0149	0.4	0.39	95.3	0.4	98.8	1.0	185.5	22.5	95.3	0.4	NA
14AVDZ1-7	345	62897	1.8	20.3734	1.1	0.1034	1.4	0.0153	0.9	0.62	97.8	0.8	99.9	1.3	151.8	25.9	97.8	0.8	NA
14AVDZ1-79	69	12810	1.5	18.1460	5.1	0.1162	5.1	0.0153	0.9	0.18	97.8	0.9	111.6	5.4	416.6	113.0	97.8	0.9	NA
14AVDZ1-41	50	5809	1.6	18.4747	7.5	0.1158	7.6	0.0155	1.3	0.17	99.3	1.3	111.3	8.0	376.4	168.3	99.3	1.3	NA
14AVDZ1-69	266	24951	2.6	20.6956	1.3	0.1034	2.2	0.0155	1.7	0.79	99.3	1.7	99.9	2.1	114.9	31.5	99.3	1.7	NA
14AVDZ1-21	48	5830	1.5	20.0492	2.7	0.1069	2.9	0.0155	0.9	0.31	99.5	0.9	103.1	2.8	189.3	63.2	99.5	0.9	NA
14AVDZ1-32	123	12121	1.6	20.4422	1.0	0.1071	2.6	0.0159	2.4	0.92	101.6	2.4	103.3	2.5	143.9	24.3	101.6	2.4	NA
14AVDZ1-18	58	4160	1.7	19.9839	1.8	0.1104	1.9	0.0160	0.7	0.38	102.3	0.7	106.3	2.0	196.9	41.6	102.3	0.7	NA
14AVDZ1-62	82	6525	1.5	20.7205	1.3	0.1070	6.4	0.0161	6.2	0.98	102.8	6.3	103.2	6.2	112.1	30.8	102.8	6.3	NA
14AVDZ1-72	187	25153	1.4	20.3412	0.7	0.1092	1.6	0.0161	1.4	0.91	103.0	1.5	105.2	1.6	155.5	15.5	103.0	1.5	NA
14AVDZ1-30	406	29984	1.6	20.5179	1.0	0.1090	1.4	0.0162	1.0	0.72	103.7	1.0	105.1	1.4	135.2	22.8	103.7	1.0	NA
14AVDZ1-77	337	21842	1.0	20.4525	0.8	0.1094	1.5	0.0162	1.3	0.84	103.7	1.3	105.4	1.5	142.7	19.0	103.7	1.3	NA
14AVDZ1-55	182	26112	1.4	20.5265	1.6	0.1098	1.9	0.0163	1.0	0.53	104.5	1.1	105.7	1.9	134.3	38.5	104.5	1.1	NA
14AVDZ1-82	624	95703	1.6	20.3806	0.5	0.1120	1.3	0.0166	1.2	0.91	105.8	1.3	107.8	1.3	151.0	12.8	105.8	1.3	NA
14AVDZ1-94	53	5631	1.4	20.2628	2.1	0.1127	2.4	0.0166	1.2	0.48	105.9	1.2	108.4	2.5	164.5	49.5	105.9	1.2	NA
14AVDZ1-11	65	20296	0.9	19.8823	1.3	0.1152	1.6	0.0166	0.9	0.59	106.2	1.0	110.7	1.6	208.7	29.2	106.2	1.0	NA
14AVDZ1-23	529	30150	1.7	20.0665	1.0	0.1143	1.1	0.0166	0.4	0.38	106.3	0.4	109.9	1.1	187.3	23.3	106.3	0.4	NA
14AVDZ1-98	47	4961	1.8	19.0966	1.4	0.1201	1.6	0.0166	0.9	0.55	106.3	0.9	115.2	1.8	301.4	31.0	106.3	0.9	NA
14AVDZ1-96	396	36278	1.0	20.1673	1.0	0.1140	1.4	0.0167	1.0	0.71	106.6	1.1	109.6	1.5	175.6	23.3	106.6	1.1	NA
14AVDZ1-25	283	21661	1.5	20.3023	0.7	0.1137	1.1	0.0167	0.9	0.76	107.0	0.9	109.3	1.2	160.0	17.1	107.0	0.9	NA

14AVDZ1-102	27	3050	1.4	20.4410	2.6	0.1131	3.2	0.0168	1.7	0.55	107.2	1.8	108.8	3.3	144.1	62.1	107.2	1.8	NA
14AVDZ1-87	57	17060	1.4	20.1013	2.2	0.1153	2.3	0.0168	0.6	0.25	107.4	0.6	110.8	2.4	183.2	50.8	107.4	0.6	NA
14AVDZ1-37	239	112043	1.4	20.1424	0.9	0.1152	1.6	0.0168	1.3	0.83	107.6	1.4	110.7	1.7	178.5	21.1	107.6	1.4	NA
14AVDZ1-78	90	24974	1.6	20.0072	1.1	0.1164	1.4	0.0169	0.9	0.65	108.0	1.0	111.8	1.5	194.2	25.5	108.0	1.0	NA
14AVDZ1-86	65	16866	1.4	20.2206	1.3	0.1157	1.5	0.0170	0.7	0.50	108.4	0.8	111.1	1.5	169.4	29.7	108.4	0.8	NA
14AVDZ1-104	74	7619	1.5	20.0526	0.7	0.1170	1.7	0.0170	1.5	0.90	108.7	1.6	112.3	1.8	188.9	16.7	108.7	1.6	NA
14AVDZ1-71	314	37745	1.4	20.3272	0.7	0.1154	1.2	0.0170	1.0	0.80	108.8	1.0	110.9	1.2	157.1	16.7	108.8	1.0	NA
14AVDZ1-17	170	23214	1.8	20.0402	0.7	0.1173	0.8	0.0170	0.4	0.46	109.0	0.4	112.6	0.9	190.3	16.8	109.0	0.4	NA
14AVDZ1-40	45	5478	1.7	19.8301	2.8	0.1187	2.9	0.0171	0.5	0.18	109.2	0.5	113.9	3.1	214.8	65.7	109.2	0.5	NA
14AVDZ1-74	257	23306	1.5	20.4667	0.9	0.1154	1.0	0.0171	0.4	0.44	109.5	0.5	110.9	1.0	141.1	20.8	109.5	0.5	NA
14AVDZ1-96	49	4579	1.5	20.4974	3.1	0.1155	3.5	0.0172	1.5	0.44	109.8	1.7	111.0	3.7	137.6	73.2	109.8	1.7	NA
14AVDZ1-56	213	14688	1.8	19.3969	2.4	0.1229	2.6	0.0173	0.8	0.32	110.5	0.9	117.7	2.8	265.7	55.5	110.5	0.9	NA
14AVDZ1-99	683	55746	0.9	20.2456	0.7	0.1346	1.8	0.0198	1.6	0.92	126.1	2.1	128.2	2.1	166.5	16.0	126.1	2.1	NA
14AVDZ1-19	440	45790	1.0	19.9648	0.7	0.1373	1.5	0.0199	1.4	0.88	126.9	1.7	130.6	1.9	199.1	16.7	126.9	1.7	NA
14AVDZ1-84	289	83265	1.0	20.2398	0.9	0.1372	2.2	0.0201	2.0	0.91	128.6	2.5	130.6	2.7	167.2	20.7	128.6	2.5	NA
14AVDZ1-9	22	2046	1.1	18.5318	2.9	0.1504	3.1	0.0202	1.1	0.34	129.0	1.4	142.3	4.2	369.4	66.3	129.0	1.4	NA
14AVDZ1-81	87	1567	0.7	11.7645	14.5	0.2387	14.6	0.0204	1.5	0.10	130.0	1.9	217.3	28.6	1315.6	283.5	130.0	1.9	NA
14AVDZ1-14	235	10085	1.9	17.9182	9.9	0.1592	10.1	0.0207	1.9	0.19	132.0	2.5	150.0	14.0	444.8	220.1	132.0	2.5	NA
14AVDZ1-2	90	21048	1.9	19.7273	1.3	0.1552	1.5	0.0222	0.7	0.45	141.6	0.9	146.5	2.0	226.8	30.7	141.6	0.9	NA
14AVDZ1-68	997	203731	0.7	20.2196	1.0	0.1559	1.3	0.0229	0.8	0.64	145.8	1.2	147.1	1.8	169.5	23.3	145.8	1.2	NA
14AVDZ1-88	80	10915	1.5	19.8803	1.2	0.1625	2.0	0.0234	1.7	0.81	149.3	2.4	152.9	2.9	208.9	27.5	149.3	2.4	NA
14AVDZ1-50	97	10145	2.2	19.7902	1.7	0.1635	1.8	0.0235	0.5	0.27	149.5	0.7	153.7	2.5	219.5	39.2	149.5	0.7	NA
14AVDZ1-8	264	70980	1.8	19.8995	0.8	0.1628	1.1	0.0235	0.7	0.62	149.7	1.0	153.1	1.5	206.7	19.7	149.7	1.0	NA
14AVDZ1-75	200	94982	1.8	20.0639	0.8	0.1614	1.0	0.0235	0.7	0.64	149.7	1.0	152.0	1.5	187.6	18.6	149.7	1.0	NA
14AVDZ1-13	417	47356	0.6	20.0044	1.0	0.1634	1.1	0.0237	0.4	0.37	151.0	0.6	153.7	1.5	194.5	23.0	151.0	0.6	NA
14AVDZ1-10	2526	1083822	1.3	20.1788	1.7	0.1666	2.3	0.0244	1.6	0.69	155.3	2.4	156.4	3.3	174.2	38.9	155.3	2.4	NA
14AVDZ1-15	135	31091	1.4	19.8535	1.2	0.1705	1.4	0.0245	0.7	0.53	156.3	1.1	159.8	2.1	212.0	27.4	156.3	1.1	NA
14AVDZ1-3	535	120786	1.5	19.9095	0.7	0.1702	1.2	0.0246	1.0	0.82	156.5	1.6	159.6	1.8	205.5	16.5	156.5	1.6	NA
14AVDZ1-80	91	27455	1.0	18.7989	1.0	0.3138	1.7	0.0428	1.4	0.82	270.1	3.7	277.1	4.2	337.1	22.5	270.1	3.7	NA
14AVDZ1-28	63	20488	0.9	18.9061	0.6	0.3159	1.8	0.0433	1.7	0.94	273.3	4.6	278.7	4.4	324.2	14.3	273.3	4.6	NA
14AVDZ1-54	573	193204	1.8	19.2183	0.7	0.3117	1.6	0.0435	1.4	0.90	274.2	3.8	275.5	3.8	286.9	15.5	274.2	3.8	NA
14AVDZ1-22	65	20777	0.8	18.8836	0.8	0.3243	3.1	0.0444	3.0	0.97	280.2	8.2	285.2	7.7	326.9	18.2	280.2	8.2	NA
14AVDZ1-31	145	52588	0.8	19.2163	0.6	0.3243	0.9	0.0452	0.7	0.75	284.9	2.0	285.2	2.3	287.1	14.2	284.9	2.0	NA
14AVDZ1-29	334	110542	1.3	18.7689	0.7	0.3395	1.5	0.0462	1.4	0.90	291.3	3.9	296.8	3.9	340.7	14.8	291.3	3.9	NA
14AVDZ1-95	108	28506	1.4	18.8650	1.0	0.3401	1.0	0.0465	0.4	0.38	293.2	1.1	297.2	2.7	329.1	21.9	293.2	1.1	NA
14AVDZ1-83	361	301797	12.3	17.8334	0.8	0.5150	1.5	0.0666	1.2	0.82	415.7	4.9	421.8	5.1	455.3	18.5	415.7	4.9	1%
14AVDZ1-73	581	249366	1.9	17.7123	1.2	0.5290	2.1	0.0680	1.7	0.81	423.8	7.2	431.1	7.5	470.4	27.6	423.8	7.2	2%
14AVDZ1-105	205	136417	1.3	17.2713	0.7	0.6246	2.3	0.0782	2.1	0.95	485.6	10.0	492.7	8.8	526.0	15.8	485.6	10.0	1%
14AVDZ1-76	54	26569	0.9	17.2596	0.9	0.6489	1.4	0.0812	1.0	0.75	503.4	5.0	507.8	5.5	527.5	20.2	503.4	5.0	1%

14AVDZ1-58	164	102646	3.2	17.0481	0.8	0.6586	1.5	0.0814	1.2	0.84	504.7	6.0	513.8	5.9	554.4	17.6	504.7	6.0	2%
14AVDZ1-38	481	135926	1.9	17.0538	1.0	0.6588	1.6	0.0815	1.2	0.75	505.0	5.8	513.9	6.4	553.7	22.8	505.0	5.8	2%
14AVDZ1-47	78	27226	1.6	16.9573	0.8	0.6641	3.2	0.0817	3.1	0.96	506.1	15.1	517.1	13.0	566.1	18.4	506.1	15.1	2%
14AVDZ1-70	304	145960	6.8	17.0894	0.6	0.7051	2.4	0.0874	2.3	0.97	540.1	11.9	541.8	9.9	549.1	12.8	540.1	11.9	0%
14AVDZ1-43	543	243127	10.6	16.8622	1.4	0.7463	1.9	0.0913	1.3	0.69	563.1	7.1	566.1	8.4	578.3	30.4	563.1	7.1	1%
14AVDZ1-46	785	596784	14.0	17.1936	1.6	0.7517	2.0	0.0937	1.2	0.60	577.6	6.8	569.2	8.8	535.8	35.5	577.6	6.8	-1%
14AVDZ1-59	25	21706	1.2	14.1008	0.8	1.3160	2.6	0.1346	2.4	0.95	814.0	18.7	852.8	14.8	955.0	15.6	814.0	18.7	5%
14AVDZ1-4	414	263018	2.6	14.1516	0.9	1.3305	2.6	0.1366	2.4	0.93	825.2	18.6	859.1	15.0	947.7	19.3	825.2	18.6	4%
14AVDZ1-66	140	113346	1.3	13.7911	0.6	1.6861	1.1	0.1686	0.9	0.84	1004.6	8.4	1003.3	6.9	1000.3	11.9	1000.3	11.9	0%
14AVDZ1-44	290	321214	1.5	13.7162	1.0	1.7435	1.4	0.1734	0.9	0.69	1031.0	8.9	1024.8	8.7	1011.3	19.8	1011.3	19.8	-1%
14AVDZ1-61	310	282268	1.4	13.5067	1.0	1.7883	3.0	0.1752	2.9	0.94	1040.6	27.4	1041.2	19.8	1042.5	20.9	1042.5	20.9	0%
14AVDZ1-53	52	166854	2.3	6.8460	0.6	8.0416	1.6	0.3993	1.5	0.93	2165.7	28.2	2235.7	14.9	2300.4	10.2	2300.4	10.2	3%
Sample 14AVDZ2 (Cerro Dorotea Formation)																			
AVDZ2-73	229	16639	1.1	19.5348	4.6	0.0662	4.8	0.0094	1.3	0.27	60.2	0.8	65.1	3.0	249.4	106.9	60.2	0.8	NA
AVDZ2-11	145	10687	0.8	20.4438	1.5	0.0635	1.8	0.0094	1.1	0.58	60.4	0.6	62.5	1.1	143.7	35.4	60.4	0.6	NA
AVDZ2-17	218	13823	1.3	20.3759	1.1	0.0642	1.6	0.0095	1.1	0.71	60.9	0.7	63.2	1.0	151.5	25.6	60.9	0.7	NA
AVDZ2-108	138	11657	1.2	20.1785	0.9	0.0708	1.1	0.0104	0.7	0.62	66.5	0.5	69.5	0.8	174.3	20.9	66.5	0.5	NA
AVDZ2-105	480	69902	0.8	20.3372	0.6	0.0970	1.1	0.0143	0.9	0.82	91.6	0.8	94.0	1.0	156.0	14.7	91.6	0.8	NA
AVDZ2-3	91	10621	0.9	20.1067	1.3	0.0987	1.5	0.0144	0.7	0.49	92.1	0.7	95.5	1.4	182.6	30.1	92.1	0.7	NA
AVDZ2-72	88	7913	1.3	20.1833	1.1	0.0983	2.1	0.0144	1.8	0.86	92.1	1.7	95.2	1.9	173.7	25.4	92.1	1.7	NA
AVDZ2-40	141	17319	1.3	20.2148	1.3	0.0993	2.8	0.0146	2.4	0.88	93.2	2.2	96.2	2.5	170.1	31.1	93.2	2.2	NA
AVDZ2-42	106	8898	1.0	20.3726	1.5	0.0993	1.7	0.0147	0.8	0.48	93.9	0.7	96.1	1.5	151.9	34.2	93.9	0.7	NA
AVDZ2-36	244	29573	1.1	20.5180	0.7	0.0991	1.0	0.0147	0.7	0.70	94.4	0.6	95.9	0.9	135.2	16.2	94.4	0.6	NA
AVDZ2-106	49	4122	1.5	19.7887	2.2	0.1077	2.4	0.0155	0.9	0.38	98.9	0.9	103.8	2.4	219.6	51.2	98.9	0.9	NA
AVDZ2-92	30	2926	1.7	20.5376	3.3	0.1054	3.5	0.0157	1.0	0.29	100.4	1.0	101.7	3.4	133.0	78.7	100.4	1.0	NA
AVDZ2-48	56	5287	1.4	20.0135	1.7	0.1088	2.1	0.0158	1.1	0.55	101.0	1.1	104.8	2.1	193.5	40.1	101.0	1.1	NA
AVDZ2-37	72	9876	1.0	19.9904	1.1	0.1114	1.2	0.0161	0.4	0.37	103.2	0.4	107.2	1.2	196.1	25.4	103.2	0.4	NA
AVDZ2-2	110	12438	1.5	20.1374	1.0	0.1343	2.0	0.0196	1.7	0.85	125.2	2.1	127.9	2.4	179.0	24.0	125.2	2.1	NA
AVDZ2-1	178	37707	1.3	19.9854	0.6	0.1495	2.7	0.0217	2.6	0.97	138.2	3.6	141.5	3.6	196.7	14.5	138.2	3.6	NA
AVDZ2-38	198	23611	1.8	19.8917	0.8	0.1532	1.5	0.0221	1.3	0.84	140.9	1.8	144.7	2.0	207.6	18.7	140.9	1.8	NA
AVDZ2-55	296	34483	0.7	19.2845	6.2	0.1580	6.4	0.0221	1.8	0.28	140.9	2.5	149.0	8.9	279.0	141.0	140.9	2.5	NA
AVDZ2-107	205	56497	1.5	19.6824	0.7	0.1552	2.1	0.0222	2.0	0.95	141.2	2.8	146.5	2.9	232.1	15.5	141.2	2.8	NA
AVDZ2-4	422	73581	1.1	19.9021	1.0	0.1539	1.6	0.0222	1.3	0.80	141.6	1.8	145.3	2.2	206.4	22.5	141.6	1.8	NA
AVDZ2-49	303	27004	1.0	19.6916	2.3	0.1557	2.7	0.0222	1.4	0.51	141.8	2.0	147.0	3.7	231.0	53.9	141.8	2.0	NA
AVDZ2-71	67	7096	0.8	16.6729	16.9	0.1848	17.0	0.0223	1.5	0.09	142.5	2.1	172.2	26.9	602.7	368.3	142.5	2.1	NA
AVDZ2-80	204	39021	1.1	20.3201	0.7	0.1520	0.9	0.0224	0.5	0.56	142.8	0.7	143.7	1.2	158.0	16.9	142.8	0.7	NA
AVDZ2-99	137	18766	1.1	20.0302	1.0	0.1551	2.0	0.0225	1.7	0.87	143.6	2.5	146.4	2.7	191.5	22.6	143.6	2.5	NA
AVDZ2-34	308	47790	1.7	19.9869	0.8	0.1554	1.4	0.0225	1.1	0.80	143.6	1.5	146.7	1.9	196.5	19.1	143.6	1.5	NA

AVDZ2-103	156	11885	1.9	18.7319	6.7	0.1675	7.2	0.0228	2.6	0.36	145.1	3.7	157.3	10.5	345.2	151.5	145.1	3.7	NA
AVDZ2-35	355	71727	1.4	19.9798	0.6	0.1577	1.3	0.0229	1.1	0.90	145.7	1.6	148.7	1.8	197.3	13.1	145.7	1.6	NA
AVDZ2-63	229	34538	0.8	19.7054	0.8	0.1601	1.3	0.0229	0.9	0.75	145.9	1.4	150.8	1.8	229.4	19.1	145.9	1.4	NA
AVDZ2-95	230	18197	1.5	19.9020	0.8	0.1590	1.5	0.0229	1.2	0.83	146.2	1.7	149.8	2.0	206.4	18.7	146.2	1.7	NA
AVDZ2-67	189	39289	1.0	19.7537	0.6	0.1606	1.5	0.0230	1.4	0.92	146.6	2.0	151.2	2.1	223.7	14.0	146.6	2.0	NA
AVDZ2-100	343	18079	1.1	17.7096	14.4	0.1793	14.7	0.0230	3.0	0.20	146.7	4.4	167.4	22.6	470.8	319.2	146.7	4.4	NA
AVDZ2-54	254	32386	1.5	20.0831	0.8	0.1581	1.3	0.0230	1.0	0.76	146.7	1.4	149.0	1.7	185.3	18.8	146.7	1.4	NA
AVDZ2-22	232	20950	2.0	20.3064	0.8	0.1566	1.4	0.0231	1.1	0.80	147.0	1.6	147.7	1.9	159.5	19.4	147.0	1.6	NA
AVDZ2-59	257	57884	1.7	19.7862	1.0	0.1615	1.8	0.0232	1.5	0.83	147.7	2.1	152.0	2.5	219.9	22.5	147.7	2.1	NA
AVDZ2-66	138	7356	1.7	17.2125	10.4	0.1859	10.5	0.0232	1.3	0.12	147.9	1.9	173.1	16.7	533.4	229.1	147.9	1.9	NA
AVDZ2-56	320	54503	1.5	19.9002	0.9	0.1628	1.1	0.0235	0.7	0.60	149.7	1.0	153.1	1.6	206.6	20.9	149.7	1.0	NA
AVDZ2-91	324	30880	1.5	20.0080	0.8	0.1660	2.6	0.0241	2.5	0.95	153.4	3.7	155.9	3.8	194.1	19.0	153.4	3.7	NA
AVDZ2-16	150	39931	1.1	19.0282	0.6	0.2707	2.4	0.0374	2.3	0.96	236.4	5.3	243.2	5.1	309.6	14.6	236.4	5.3	NA
AVDZ2-88	39	28619	0.9	18.4798	2.5	0.3048	3.3	0.0409	2.2	0.66	258.1	5.5	270.2	7.9	375.7	56.6	258.1	5.5	NA
AVDZ2-33	108	40446	1.0	19.0128	1.0	0.3035	1.6	0.0419	1.2	0.77	264.3	3.1	269.1	3.7	311.4	22.8	264.3	3.1	NA
AVDZ2-58	92	20340	1.3	18.8399	0.8	0.3077	2.0	0.0420	1.8	0.92	265.5	4.7	272.4	4.7	332.2	17.2	265.5	4.7	NA
AVDZ2-52	81	30285	2.9	18.9809	0.8	0.3080	1.4	0.0424	1.2	0.83	267.7	3.0	272.6	3.3	315.2	17.7	267.7	3.0	NA
AVDZ2-28	149	42537	1.3	18.7414	1.2	0.3133	1.9	0.0426	1.5	0.79	268.9	3.9	276.8	4.5	344.0	26.2	268.9	3.9	NA
AVDZ2-97	205	34599	1.3	18.8526	1.3	0.3116	1.9	0.0426	1.5	0.76	268.9	3.9	275.4	4.7	330.7	28.5	268.9	3.9	NA
AVDZ2-27	42	7097	1.0	18.5588	1.8	0.3206	2.3	0.0432	1.4	0.62	272.4	3.8	282.4	5.6	366.1	40.4	272.4	3.8	NA
AVDZ2-110	170	65892	2.1	18.7991	0.7	0.3233	1.2	0.0441	0.9	0.82	278.1	2.6	284.5	2.9	337.1	15.1	278.1	2.6	NA
AVDZ2-86	175	47991	0.8	18.2948	1.0	0.3327	1.5	0.0441	1.2	0.75	278.5	3.2	291.6	3.9	398.3	23.1	278.5	3.2	NA
AVDZ2-77	42	6556	0.6	18.7752	1.8	0.3259	2.1	0.0444	1.1	0.53	279.9	3.0	286.4	5.2	340.0	39.7	279.9	3.0	NA
AVDZ2-96	91	47419	0.8	18.6681	0.7	0.3283	1.7	0.0445	1.5	0.90	280.4	4.2	288.3	4.2	352.9	16.4	280.4	4.2	NA
AVDZ2-57	169	51371	0.8	18.7088	0.6	0.3289	1.2	0.0446	1.0	0.87	281.5	2.8	288.8	3.0	348.0	13.1	281.5	2.8	NA
AVDZ2-93	289	87742	1.0	18.7311	1.0	0.3301	1.3	0.0448	0.8	0.60	282.8	2.2	289.7	3.3	345.3	23.4	282.8	2.2	NA
AVDZ2-104	572	212170	1.7	18.9439	1.1	0.3280	1.8	0.0451	1.3	0.75	284.1	3.7	288.0	4.4	319.7	26.1	284.1	3.7	NA
AVDZ2-23	164	56028	0.5	18.8739	1.0	0.3299	1.5	0.0452	1.1	0.76	284.7	3.2	289.5	3.8	328.1	22.2	284.7	3.2	NA
AVDZ2-78	145	32901	1.1	18.5897	0.8	0.3383	1.0	0.0456	0.6	0.56	287.5	1.6	295.9	2.6	362.4	19.1	287.5	1.6	NA
AVDZ2-9	107	49219	2.1	18.8463	0.7	0.3351	1.0	0.0458	0.7	0.71	288.7	2.0	293.5	2.6	331.4	15.9	288.7	2.0	NA
AVDZ2-30	137	26036	1.2	18.5214	0.5	0.3440	0.8	0.0462	0.7	0.80	291.2	1.9	300.2	2.2	370.7	11.5	291.2	1.9	NA
AVDZ2-8	54	19243	1.1	18.7251	0.6	0.3426	1.3	0.0465	1.2	0.90	293.1	3.5	299.1	3.5	346.0	13.4	293.1	3.5	NA
AVDZ2-76	337	157145	1.8	18.7785	0.7	0.3419	0.8	0.0466	0.5	0.55	293.4	1.3	298.6	2.2	339.6	15.9	293.4	1.3	NA
AVDZ2-6	191	55832	1.5	18.7958	0.7	0.3418	1.2	0.0466	0.9	0.78	293.6	2.7	298.5	3.1	337.5	17.0	293.6	2.7	NA
AVDZ2-70	277	58443	1.1	18.9260	0.6	0.3414	2.6	0.0469	2.6	0.98	295.2	7.4	298.2	6.8	321.8	12.9	295.2	7.4	NA
AVDZ2-84	114	78117	1.4	18.8720	0.8	0.3447	2.7	0.0472	2.6	0.96	297.2	7.6	300.7	7.1	328.3	17.3	297.2	7.6	NA
AVDZ2-41	250	116118	1.0	18.7087	0.5	0.3509	1.5	0.0476	1.4	0.94	299.9	4.2	305.4	4.1	348.0	12.0	299.9	4.2	NA
AVDZ2-25	71	19379	1.3	18.7499	0.9	0.3610	1.7	0.0491	1.4	0.84	308.9	4.2	312.9	4.5	343.0	20.3	308.9	4.2	NA
AVDZ2-89	217	64570	3.6	18.1526	0.7	0.4059	1.1	0.0534	0.9	0.81	335.6	3.0	346.0	3.3	415.8	15.0	335.6	3.0	NA

AVDZ2-29	19	5957	1.3	17.8338	3.2	0.4255	3.3	0.0550	0.7	0.20	345.4	2.3	360.0	10.1	455.3	72.1	345.4	2.3	NA
AVDZ2-60	213	116384	11.4	18.1639	0.7	0.4471	1.4	0.0589	1.2	0.88	368.9	4.4	375.3	4.4	414.4	14.6	368.9	4.4	NA
AVDZ2-101	253	83338	1.3	18.0331	0.6	0.4594	1.0	0.0601	0.8	0.78	376.1	2.8	383.8	3.2	430.5	13.8	376.1	2.8	NA
AVDZ2-81	269	106829	3.5	17.8559	2.1	0.4704	4.0	0.0609	3.4	0.85	381.2	12.4	391.5	12.9	452.5	46.6	381.2	12.4	NA
AVDZ2-7	565	181265	1.7	18.3201	1.2	0.4671	1.7	0.0621	1.3	0.73	388.1	4.7	389.2	5.6	395.2	26.4	388.1	4.7	NA
AVDZ2-98	275	72047	2.4	17.9001	0.6	0.4945	1.0	0.0642	0.7	0.77	401.1	2.9	408.0	3.3	447.0	13.9	401.1	2.9	2%
AVDZ2-75	182	69461	2.9	17.7569	0.6	0.4997	1.6	0.0644	1.5	0.92	402.0	5.7	411.5	5.4	464.9	13.7	402.0	5.7	2%
AVDZ2-5	142	38829	2.3	17.7091	0.5	0.5055	1.7	0.0649	1.7	0.96	405.5	6.6	415.4	5.9	470.8	11.2	405.5	6.6	2%
AVDZ2-102	241	102023	3.3	17.4726	0.7	0.5634	1.1	0.0714	0.8	0.75	444.6	3.6	453.8	4.0	500.5	16.0	444.6	3.6	2%
AVDZ2-53	396	101707	0.9	17.5153	0.8	0.5818	1.2	0.0739	0.9	0.74	459.6	4.0	465.6	4.6	495.1	18.0	459.6	4.0	1%
AVDZ2-19	210	68551	6.6	17.6408	0.5	0.5832	1.5	0.0746	1.4	0.94	463.9	6.2	466.5	5.5	479.4	11.3	463.9	6.2	1%
AVDZ2-10	111	26433	1.8	15.7514	8.0	0.7215	8.9	0.0824	3.8	0.43	510.6	18.7	551.5	37.7	724.5	169.8	510.6	18.7	7%
AVDZ2-32	216	192920	1.3	17.1832	0.9	0.6744	1.8	0.0840	1.6	0.86	520.2	7.9	523.4	7.5	537.2	20.4	520.2	7.9	1%
AVDZ2-94	191	53615	1.7	16.9262	1.1	0.6881	1.7	0.0845	1.4	0.79	522.8	6.9	531.7	7.2	570.1	23.1	522.8	6.9	2%
AVDZ2-12	94	125532	1.9	16.8179	0.7	0.6951	1.4	0.0848	1.2	0.84	524.6	5.8	535.9	5.7	584.0	15.9	524.6	5.8	2%
AVDZ2-20	285	155717	1.1	17.1646	0.8	0.6972	1.5	0.0868	1.3	0.84	536.5	6.5	537.1	6.2	539.5	17.8	536.5	6.5	0%
AVDZ2-51	199	376887	0.9	17.0205	0.6	0.7054	1.3	0.0871	1.2	0.90	538.2	6.0	542.0	5.4	557.9	12.1	538.2	6.0	1%
AVDZ2-82	38	22041	0.6	16.5343	1.2	0.7601	1.7	0.0912	1.3	0.73	562.4	6.9	574.1	7.6	620.8	25.5	562.4	6.9	2%
AVDZ2-87	56	24831	0.6	16.2103	3.0	0.7757	3.3	0.0912	1.4	0.42	562.6	7.4	583.0	14.7	663.3	64.4	562.6	7.4	4%
AVDZ2-46	272	172768	6.5	16.4814	1.9	0.7720	2.1	0.0923	1.0	0.47	569.0	5.5	580.9	9.4	627.7	40.6	569.0	5.5	2%
AVDZ2-61	85	48288	1.0	16.4451	0.8	0.7815	1.8	0.0932	1.7	0.90	574.5	9.1	586.3	8.2	632.5	16.9	574.5	9.1	2%
AVDZ2-109	239	158995	0.7	16.3585	0.5	0.7868	2.0	0.0934	1.9	0.96	575.3	10.4	589.4	8.8	643.8	11.6	575.3	10.4	2%
AVDZ2-15	349	62149	22.4	15.6393	9.2	0.8420	9.3	0.0955	1.2	0.13	588.0	6.6	620.3	43.0	739.7	194.7	588.0	6.6	5%
AVDZ2-47	315	104975	165.6	16.6230	1.1	0.8121	1.8	0.0979	1.5	0.82	602.1	8.7	603.6	8.4	609.2	22.9	602.1	8.7	0%
AVDZ2-90	74	56575	2.2	16.0486	0.9	0.8462	2.3	0.0985	2.1	0.92	605.6	12.3	622.5	10.7	684.8	19.0	605.6	12.3	3%
AVDZ2-65	253	192856	1.8	16.4681	0.7	0.8320	2.5	0.0994	2.5	0.96	610.8	14.3	614.7	11.8	629.4	14.5	610.8	14.3	1%
AVDZ2-39	120	63308	1.5	15.3339	0.9	1.0058	1.5	0.1119	1.3	0.83	683.5	8.2	706.8	7.8	781.3	18.1	683.5	8.2	3%
AVDZ2-13	345	220214	1.6	15.2572	1.2	1.1246	3.5	0.1244	3.3	0.94	756.1	23.4	765.2	18.7	791.8	25.2	756.1	23.4	1%
AVDZ2-85	194	196982	2.8	13.8782	1.8	1.4080	2.1	0.1417	1.1	0.53	854.4	8.9	892.3	12.4	987.5	36.0	987.5	36.0	4%
AVDZ2-79	442	483407	1.6	13.6841	1.9	1.7260	2.4	0.1713	1.4	0.59	1019.2	13.4	1018.2	15.4	1016.1	39.2	1016.1	39.2	0%
AVDZ2-24	292	338195	3.0	13.3272	1.4	1.7913	2.8	0.1731	2.4	0.87	1029.4	22.9	1042.3	18.0	1069.5	27.4	1069.5	27.4	1%
AVDZ2-68	130	309061	2.1	13.2733	0.8	1.7997	1.5	0.1733	1.3	0.85	1030.0	12.0	1045.4	9.7	1077.6	15.8	1077.6	15.8	1%
AVDZ2-14	129	99045	1.9	13.2456	0.9	1.9217	1.3	0.1846	0.9	0.68	1092.1	8.7	1088.7	8.5	1081.8	18.6	1081.8	18.6	0%
AVDZ2-45	165	307055	1.6	13.1984	1.0	1.9388	1.9	0.1856	1.6	0.83	1097.4	15.9	1094.6	12.7	1088.9	20.9	1088.9	20.9	0%
AVDZ2-18	204	316819	1.8	13.1649	1.2	1.8528	1.6	0.1769	1.1	0.69	1050.0	11.1	1064.4	10.9	1094.0	23.7	1094.0	23.7	1%
AVDZ2-69	63	62495	12.3	13.0391	0.9	1.9671	1.2	0.1860	0.8	0.68	1099.8	8.5	1104.3	8.4	1113.2	18.2	1113.2	18.2	0%
AVDZ2-64	114	138543	2.3	12.5249	0.6	2.0917	1.9	0.1900	1.8	0.95	1121.4	18.1	1146.1	12.7	1193.1	11.8	1193.1	11.8	2%
AVDZ2-31	160	208109	1.9	12.2800	1.3	2.3382	1.8	0.2082	1.2	0.67	1219.5	13.1	1224.0	12.6	1231.9	25.9	1231.9	25.9	0%
AVDZ2-74	115	2549	2.4	11.3727	5.6	1.0078	5.6	0.0831	0.5	0.09	514.8	2.5	707.8	28.5	1380.9	107.2	1380.9	107.2	27%

AVDZ2-83	107	141895	1.2	11.2770	0.6	2.8970	1.6	0.2369	1.5	0.92	1370.8	18.3	1381.1	12.2	1397.2	12.2	1397.2	12.2	1%
AVDZ2-43	118	150371	0.8	9.9160	0.9	3.6460	1.9	0.2622	1.7	0.88	1501.2	22.2	1559.6	15.0	1639.7	16.6	1639.7	16.6	4%
AVDZ2-44	222	951248	3.0	9.4503	1.5	4.5889	1.9	0.3145	1.1	0.61	1762.9	17.7	1747.2	15.7	1728.5	27.4	1728.5	27.4	-1%
AVDZ2-21	301	359753	1.1	8.8264	1.6	4.2208	2.6	0.2702	2.1	0.79	1541.8	28.7	1678.1	21.7	1852.9	29.0	1852.9	29.0	8%
Sample 15LDC02/14DZ3 (Cerro Dorotea Formation)																			
15LDC03-30	75	4894	1.2	21.6207	5.1	0.0596	5.4	0.0094	1.7	0.31	60.0	1.0	58.8	3.1	10.8	123.1	60.0	1.0	NA
15LDC03-31	119	15706	2.3	21.1922	4.4	0.0610	4.8	0.0094	1.7	0.37	60.2	1.0	60.2	2.8	58.7	105.6	60.2	1.0	NA
15LDC03-215	41	8641	3.3	20.5589	6.6	0.0633	7.1	0.0094	2.5	0.35	60.6	1.5	62.3	4.3	130.5	155.9	60.6	1.5	NA
15LDC03-133	130	41858	1.4	20.8043	3.9	0.0707	4.3	0.0107	1.7	0.39	68.4	1.1	69.3	2.9	102.6	92.8	68.4	1.1	NA
15LDC03-142	53	5108	2.3	20.2849	5.9	0.0725	6.3	0.0107	2.3	0.36	68.4	1.6	71.0	4.3	162.0	137.3	68.4	1.6	NA
15LDC03-202	55	12513	1.3	19.9956	7.1	0.0737	7.5	0.0107	2.4	0.32	68.5	1.6	72.2	5.2	195.5	164.5	68.5	1.6	NA
15LDC03-35	110	5306	1.6	7.9347	11.7	0.1858	12.0	0.0107	2.9	0.24	68.6	2.0	173.1	19.2	2043.3	207.2	68.6	2.0	NA
15LDC03-122	78	7188	1.1	21.3692	5.9	0.0693	6.3	0.0107	2.0	0.32	68.9	1.4	68.1	4.1	38.8	141.9	68.9	1.4	NA
15LDC03-79	35	3384	1.7	22.3882	7.4	0.0664	7.8	0.0108	2.4	0.31	69.1	1.6	65.3	4.9	73.8	180.5	69.1	1.6	NA
15LDC03-138	166	21130	1.5	21.9322	3.3	0.0684	3.7	0.0109	1.7	0.45	69.7	1.2	67.2	2.4	23.7	78.8	69.7	1.2	NA
15LDC03-12	641	39179	0.6	20.6931	2.4	0.0868	2.8	0.0130	1.3	0.46	83.5	1.1	84.5	2.2	115.2	57.6	83.5	1.1	NA
15LDC03-155	289	26662	1.5	21.7247	2.8	0.0833	3.3	0.0131	1.8	0.55	84.0	1.5	81.2	2.6	0.8	67.1	84.0	1.5	NA
LDCDZ3-10	135	7424	1.1	22.3762	23.3	0.0825	24.5	0.0134	7.5	0.31	85.7	6.4	80.5	19.0	-72.5	576.9	85.7	6.4	NA
15LDC03-39	91	15809	1.9	21.2360	4.4	0.0880	5.1	0.0136	2.6	0.51	86.8	2.2	85.7	4.2	53.8	104.0	86.8	2.2	NA
15LDC03-16	95	14451	1.1	19.7309	3.7	0.1005	4.2	0.0144	2.0	0.47	92.1	1.8	97.2	3.9	226.4	86.1	92.1	1.8	NA
15LDC03-96	157	24258	1.8	21.4188	4.0	0.0931	4.5	0.0145	2.0	0.45	92.5	1.9	90.4	3.9	33.3	95.5	92.5	1.9	NA
15LDC03-209	209	101993	1.3	20.4751	3.2	0.0974	3.6	0.0145	1.7	0.46	92.5	1.5	94.3	3.3	140.2	76.2	92.5	1.5	NA
15LDC03-1	122	26629	1.6	20.3857	4.1	0.0981	4.4	0.0145	1.7	0.39	92.8	1.6	95.0	4.0	150.4	95.6	92.8	1.6	NA
LDCDZ3-13	59	1822	0.9	14.4342	90.2	0.1386	90.5	0.0145	6.7	0.07	92.9	6.2	131.8	112.3	907.1	299.5	92.9	6.2	NA
15LDC03-131	325	51974	1.7	20.6850	2.5	0.0969	2.7	0.0145	1.2	0.44	93.0	1.1	93.9	2.5	116.2	57.8	93.0	1.1	NA
15LDC03-151	227	47731	1.9	20.4301	3.0	0.0985	3.5	0.0146	1.9	0.53	93.4	1.8	95.4	3.2	145.3	70.2	93.4	1.8	NA
15LDC03-148	108	92530	1.0	20.6421	4.3	0.0979	4.7	0.0147	1.9	0.40	93.8	1.8	94.8	4.2	121.1	100.7	93.8	1.8	NA
15LDC03-75	117	31505	1.7	20.0568	2.6	0.1014	3.2	0.0147	1.8	0.57	94.4	1.7	98.1	3.0	188.4	61.3	94.4	1.7	NA
LDCDZ3-14	81	5178	1.1	25.1850	43.4	0.0809	43.9	0.0148	6.6	0.15	94.6	6.2	79.0	33.4	-370.0	1171.8	94.6	6.2	NA
15LDC03-184	50	41767	1.7	18.6347	5.8	0.1094	6.2	0.0148	2.0	0.33	94.7	1.9	105.5	6.2	356.9	131.5	94.7	1.9	NA
15LDC03-204	118	112319	1.5	20.7401	4.5	0.0984	4.9	0.0148	1.9	0.39	94.7	1.8	95.3	4.5	109.9	106.6	94.7	1.8	NA
LDCDZ3-9	47	3681	1.3	13.8314	154.7	0.1476	154.9	0.0148	8.5	0.05	94.7	7.9	139.8	205.1	994.4	666.0	94.7	7.9	NA
15LDC03-190	213	74903	1.8	20.7391	3.7	0.0993	4.1	0.0149	1.8	0.44	95.6	1.7	96.1	3.7	110.0	86.5	95.6	1.7	NA
15LDC03-214	73	6607	1.6	20.7224	5.3	0.0997	5.8	0.0150	2.3	0.40	95.9	2.2	96.5	5.3	111.9	125.4	95.9	2.2	NA
15LDC03-191	54	30203	1.4	20.2137	7.0	0.1026	7.4	0.0150	2.3	0.31	96.2	2.2	99.1	7.0	170.2	164.0	96.2	2.2	NA
LDCDZ3-12	102	5445	1.3	26.5653	18.7	0.0781	19.1	0.0150	3.9	0.20	96.3	3.7	76.4	14.1	-510.3	503.6	96.3	3.7	NA
LDCDZ3-7	152	7875	1.5	19.6975	22.0	0.1054	22.2	0.0151	3.0	0.13	96.3	2.8	101.7	21.5	230.3	513.7	96.3	2.8	NA
15LDC03-118	120	10324	2.7	21.7026	4.5	0.0977	4.7	0.0154	1.5	0.31	98.4	1.4	94.7	4.2	1.7	107.4	98.4	1.4	NA

15LDC03-29	72	7321	1.6	21.2203	5.0	0.1042	5.4	0.0160	2.2	0.41	102.6	2.2	100.7	5.2	55.6	118.3	102.6	2.2	NA
15LDC03-81	206	21537	2.3	20.7304	3.0	0.1099	3.2	0.0165	1.3	0.39	105.7	1.3	105.9	3.2	111.0	69.7	105.7	1.3	NA
15LDC03-80	60	213360	1.4	21.8476	5.2	0.1060	5.5	0.0168	2.0	0.35	107.3	2.1	102.3	5.4	14.4	124.7	107.3	2.1	NA
LDCDZ3-15	111	5229	2.0	27.2312	24.9	0.0868	25.4	0.0171	5.1	0.20	109.5	5.5	84.5	20.6	-576.8	681.2	109.5	5.5	NA
15LDC03-152	60	23247	2.3	20.9429	5.2	0.1155	5.5	0.0175	1.8	0.33	112.1	2.0	110.9	5.7	86.9	122.3	112.1	2.0	NA
15LDC03-116	196	25743	1.9	21.2119	3.4	0.1169	3.8	0.0180	1.8	0.47	114.9	2.0	112.3	4.0	56.5	80.3	114.9	2.0	NA
LDCDZ3-2	902	31596	0.8	20.8429	2.5	0.1192	2.7	0.0180	1.0	0.36	115.1	1.1	114.3	3.0	98.2	60.3	115.1	1.1	NA
15LDC03-95	363	45539	1.7	20.6671	2.3	0.1204	2.7	0.0180	1.4	0.51	115.3	1.6	115.4	2.9	118.2	54.0	115.3	1.6	NA
15LDC03-50	292	71546	5.1	21.3666	3.4	0.1175	4.0	0.0182	2.1	0.52	116.3	2.4	112.8	4.3	39.2	82.3	116.3	2.4	NA
15LDC03-213	176	56048	1.6	20.2615	3.1	0.1270	3.2	0.0187	1.0	0.30	119.2	1.2	121.4	3.7	164.7	71.8	119.2	1.2	NA
15LDC03-193	150	27649	1.6	20.4997	2.9	0.1291	3.5	0.0192	2.0	0.56	122.6	2.4	123.3	4.1	137.4	68.3	122.6	2.4	NA
15LDC03-206	131	42628	2.1	21.7204	3.0	0.1263	3.6	0.0199	1.9	0.52	127.0	2.3	120.8	4.1	0.3	73.5	127.0	2.3	NA
15LDC03-74	132	51185	1.6	20.0793	2.9	0.1423	3.3	0.0207	1.6	0.47	132.2	2.1	135.1	4.2	185.8	68.5	132.2	2.1	NA
15LDC03-100	347	35493	3.4	20.2537	2.3	0.1481	2.7	0.0218	1.5	0.54	138.7	2.0	140.2	3.6	165.6	53.7	138.7	2.0	NA
15LDC03-83	398	190348	1.5	20.3043	2.0	0.1492	2.4	0.0220	1.4	0.58	140.1	1.9	141.2	3.1	159.8	45.6	140.1	1.9	NA
15LDC03-36	1112	65187	2.3	20.5283	1.2	0.1485	2.0	0.0221	1.5	0.77	141.0	2.1	140.6	2.6	134.0	29.3	141.0	2.1	NA
15LDC03-183	178	41006	1.2	20.8648	2.4	0.1473	2.8	0.0223	1.4	0.49	142.2	1.9	139.6	3.6	95.7	57.0	142.2	1.9	NA
15LDC03-60	429	59977	2.0	20.5326	1.9	0.1500	2.5	0.0223	1.6	0.66	142.4	2.3	141.9	3.3	133.6	44.1	142.4	2.3	NA
15LDC03-85	257	82947	2.9	20.2310	2.0	0.1525	2.5	0.0224	1.5	0.61	142.6	2.2	144.1	3.3	168.2	45.8	142.6	2.2	NA
15LDC03-110	344	58260	1.9	19.0604	2.7	0.1619	3.0	0.0224	1.4	0.46	142.7	2.0	152.4	4.3	305.7	61.8	142.7	2.0	NA
15LDC03-173	235	29089	2.3	20.3577	3.9	0.1518	4.4	0.0224	2.1	0.47	142.8	2.9	143.5	5.9	153.6	91.2	142.8	2.9	NA
15LDC03-121	243	25099	0.8	20.6898	2.3	0.1495	2.8	0.0224	1.6	0.55	143.0	2.2	141.4	3.7	115.6	55.4	143.0	2.2	NA
15LDC03-150	632	94228	2.4	20.3945	1.4	0.1520	1.9	0.0225	1.3	0.70	143.3	1.9	143.7	2.6	149.4	32.5	143.3	1.9	NA
15LDC03-196	193	17914	2.2	21.0042	2.9	0.1478	3.3	0.0225	1.7	0.50	143.5	2.4	140.0	4.4	79.9	68.2	143.5	2.4	NA
15LDC03-97	160	36432	1.8	20.2553	2.8	0.1534	3.1	0.0225	1.3	0.42	143.7	1.8	144.9	4.1	165.4	64.7	143.7	1.8	NA
15LDC03-161	295	147028	1.3	19.6302	2.9	0.1586	3.4	0.0226	1.9	0.54	143.9	2.6	149.5	4.8	238.2	66.8	143.9	2.6	NA
15LDC03-132	174	21991	2.4	20.6053	2.7	0.1511	3.2	0.0226	1.7	0.54	144.0	2.5	142.9	4.3	125.2	64.1	144.0	2.5	NA
15LDC03-2	288	48119	2.8	20.5858	2.0	0.1514	2.7	0.0226	1.9	0.68	144.1	2.6	143.1	3.7	127.5	47.7	144.1	2.6	NA
15LDC03-139	565	101362	2.2	20.1600	1.7	0.1546	2.2	0.0226	1.4	0.66	144.1	2.0	146.0	3.0	176.4	38.6	144.1	2.0	NA
15LDC03-84	102	16184	2.7	20.4802	3.1	0.1524	3.4	0.0226	1.4	0.40	144.3	1.9	144.0	4.6	139.6	73.0	144.3	1.9	NA
15LDC03-65	211	40460	2.1	20.7366	2.6	0.1505	3.3	0.0226	2.0	0.61	144.3	2.8	142.4	4.3	110.3	61.5	144.3	2.8	NA
15LDC03-59	116	22810	3.1	20.4428	3.7	0.1528	4.2	0.0227	2.1	0.50	144.4	3.0	144.4	5.7	143.8	86.2	144.4	3.0	NA
15LDC03-218	595	73251	1.3	19.9684	1.6	0.1564	1.9	0.0227	1.1	0.55	144.4	1.5	147.6	2.7	198.7	37.7	144.4	1.5	NA
15LDC03-141	251	243456	1.9	19.9259	2.8	0.1568	3.3	0.0227	1.6	0.50	144.5	2.3	147.9	4.5	203.6	65.6	144.5	2.3	NA
15LDC03-175	934	91638	3.3	20.5695	1.4	0.1520	1.8	0.0227	1.1	0.63	144.5	1.6	143.7	2.4	129.4	33.2	144.5	1.6	NA
15LDC03-86	265	73102	2.6	21.0156	2.8	0.1488	3.3	0.0227	1.8	0.54	144.6	2.6	140.9	4.4	78.6	67.2	144.6	2.6	NA
15LDC03-181	92	100088	2.1	19.9942	3.5	0.1565	4.0	0.0227	1.8	0.46	144.7	2.6	147.7	5.4	195.7	81.5	144.7	2.6	NA
15LDC03-179	253	27406	2.3	20.2420	1.9	0.1549	2.5	0.0227	1.6	0.66	144.9	2.4	146.2	3.4	166.9	43.8	144.9	2.4	NA
15LDC03-194	453	54995	1.5	20.4397	2.3	0.1534	2.7	0.0227	1.4	0.52	144.9	2.0	144.9	3.6	144.2	53.1	144.9	2.0	NA

15LDC03-129	310	27023	1.4	20.6315	1.9	0.1521	2.5	0.0228	1.6	0.66	145.1	2.3	143.8	3.3	122.3	43.6	145.1	2.3	NA
15LDC03-134	163	68798	1.8	20.4282	3.3	0.1539	4.1	0.0228	2.4	0.58	145.3	3.4	145.3	5.5	145.5	78.0	145.3	3.4	NA
15LDC03-176	387	37756	1.7	20.2948	1.7	0.1549	2.3	0.0228	1.5	0.68	145.3	2.2	146.2	3.1	160.9	39.1	145.3	2.2	NA
15LDC03-49	1981	2235447	2.2	20.5487	1.2	0.1530	2.2	0.0228	1.9	0.85	145.4	2.7	144.6	3.0	131.7	27.2	145.4	2.7	NA
15LDC03-52	445	49925	1.9	20.7943	1.7	0.1515	2.5	0.0228	1.8	0.74	145.6	2.6	143.2	3.3	103.7	39.4	145.6	2.6	NA
15LDC03-159	325	50879	1.8	20.4732	2.7	0.1539	3.2	0.0228	1.8	0.56	145.6	2.6	145.3	4.3	140.3	62.4	145.6	2.6	NA
15LDC03-25	258	41493	1.5	20.2896	1.8	0.1557	2.3	0.0229	1.4	0.62	146.0	2.0	146.9	3.1	161.5	41.7	146.0	2.0	NA
15LDC03-114	78	30784	3.7	20.5690	4.1	0.1537	4.7	0.0229	2.1	0.45	146.2	3.0	145.2	6.3	129.4	97.6	146.2	3.0	NA
15LDC03-195	406	28849	1.4	20.3612	1.6	0.1559	2.2	0.0230	1.4	0.65	146.7	2.1	147.1	3.0	153.2	38.5	146.7	2.1	NA
15LDC03-136	129	77458	1.7	19.8290	3.0	0.1602	3.3	0.0230	1.4	0.43	146.8	2.1	150.9	4.6	214.9	69.1	146.8	2.1	NA
15LDC03-178	219	32999	2.3	20.3318	2.7	0.1563	3.1	0.0231	1.6	0.50	146.9	2.3	147.5	4.3	156.6	63.2	146.9	2.3	NA
15LDC03-34	132	15995	4.4	20.6400	3.0	0.1541	3.4	0.0231	1.7	0.50	147.0	2.5	145.5	4.6	121.3	69.8	147.0	2.5	NA
15LDC03-77	1450	141442	2.0	20.3513	1.6	0.1564	2.2	0.0231	1.5	0.70	147.1	2.3	147.5	3.0	154.3	36.5	147.1	2.3	NA
15LDC03-53	58	25276	2.3	20.1789	5.1	0.1585	5.4	0.0232	1.9	0.35	147.8	2.7	149.4	7.5	174.2	118.5	147.8	2.7	NA
15LDC03-182	785	53941	1.0	20.4401	1.5	0.1565	2.5	0.0232	1.9	0.79	147.8	2.8	147.6	3.4	144.1	35.4	147.8	2.8	NA
15LDC03-27	583	47218	3.2	20.5311	1.5	0.1560	2.2	0.0232	1.6	0.73	148.1	2.4	147.2	3.1	133.7	36.0	148.1	2.4	NA
15LDC03-154	295	78177	2.4	20.7426	1.8	0.1546	2.5	0.0233	1.8	0.71	148.2	2.6	146.0	3.4	109.6	41.6	148.2	2.6	NA
15LDC03-200	247	33110	2.4	21.0028	2.6	0.1530	3.2	0.0233	1.9	0.58	148.5	2.7	144.6	4.3	80.0	61.9	148.5	2.7	NA
15LDC03-51	483	84024	1.3	20.4549	1.4	0.1572	2.0	0.0233	1.4	0.70	148.6	2.1	148.2	2.8	142.4	33.4	148.6	2.1	NA
15LDC03-145	276	98065	2.8	19.9115	2.6	0.1616	2.9	0.0233	1.2	0.43	148.7	1.8	152.1	4.0	205.3	59.7	148.7	1.8	NA
15LDC03-62	194	87567	3.4	20.3504	1.6	0.1581	2.1	0.0233	1.4	0.65	148.7	2.0	149.0	3.0	154.5	38.2	148.7	2.0	NA
15LDC03-162	648	232099	2.2	20.2873	1.7	0.1587	2.2	0.0234	1.4	0.63	148.8	2.1	149.6	3.1	161.8	40.2	148.8	2.1	NA
15LDC03-56	456	52830	1.1	19.7863	1.9	0.1636	2.3	0.0235	1.4	0.58	149.6	2.0	153.8	3.3	219.9	43.8	149.6	2.0	NA
15LDC03-94	239	59247	2.8	21.1882	2.3	0.1536	2.9	0.0236	1.7	0.59	150.4	2.5	145.1	3.9	59.2	55.6	150.4	2.5	NA
15LDC03-88	29	13342	2.9	22.0566	5.6	0.1489	5.9	0.0238	1.9	0.32	151.8	2.8	140.9	7.7	37.4	135.4	151.8	2.8	NA
15LDC03-167	578	107790	0.9	20.6460	1.9	0.1596	2.5	0.0239	1.7	0.66	152.3	2.5	150.4	3.5	120.6	44.3	152.3	2.5	NA
15LDC03-174	548	189348	3.2	20.2125	1.6	0.1633	2.1	0.0239	1.4	0.67	152.5	2.2	153.6	3.0	170.3	37.1	152.5	2.2	NA
15LDC03-78	704	210608	1.7	20.4716	1.6	0.1614	2.5	0.0240	1.8	0.74	152.7	2.7	152.0	3.5	140.5	38.7	152.7	2.7	NA
LDCDZ3-6	279	12038	1.6	20.5004	5.9	0.1613	6.4	0.0240	2.5	0.39	152.8	3.8	151.9	9.1	137.3	138.8	152.8	3.8	NA
LDCDZ3-3	196	13088	2.3	20.5631	6.9	0.1632	7.1	0.0243	1.6	0.22	155.0	2.4	153.5	10.1	130.1	162.4	155.0	2.4	NA
15LDC03-165	853	169207	1.0	20.3118	1.1	0.1694	1.8	0.0250	1.4	0.78	158.9	2.2	158.9	2.6	158.9	26.4	158.9	2.2	NA
15LDC03-28	76	24969	1.5	20.3443	3.5	0.1785	3.8	0.0263	1.6	0.42	167.6	2.6	166.8	5.9	155.2	81.4	167.6	2.6	NA
15LDC03-42	152	68273	3.3	19.8468	2.4	0.1906	3.3	0.0274	2.3	0.70	174.5	4.0	177.2	5.4	212.8	54.7	174.5	4.0	NA
15LDC03-123	440	106620	1.4	19.4312	1.7	0.2651	2.1	0.0374	1.2	0.59	236.4	2.9	238.8	4.5	261.6	39.0	236.4	2.9	NA
15LDC03-189	161	111264	2.5	17.2364	2.1	0.3020	2.5	0.0378	1.4	0.55	238.9	3.3	268.0	6.0	530.4	46.6	238.9	3.3	NA
15LDC03-156	174	37826	1.2	19.8385	2.2	0.2670	2.7	0.0384	1.5	0.55	243.0	3.5	240.3	5.7	213.8	51.8	243.0	3.5	NA
15LDC03-98	206	93498	0.8	19.3295	1.9	0.2823	2.7	0.0396	1.9	0.69	250.2	4.6	252.5	6.0	273.7	44.6	250.2	4.6	NA
15LDC03-127	174	45310	2.8	19.3271	2.0	0.2825	2.6	0.0396	1.6	0.62	250.3	4.0	252.6	5.8	273.9	46.7	250.3	4.0	NA
15LDC03-124	279	207348	1.4	19.4752	1.3	0.2948	2.0	0.0416	1.5	0.75	263.0	3.9	262.3	4.7	256.5	30.9	263.0	3.9	NA

15LDC03-46	234	40090	1.6	18.9933	1.7	0.3044	2.2	0.0419	1.4	0.62	264.8	3.6	269.9	5.3	313.8	39.6	264.8	3.6	NA
15LDC03-112	54	11412	1.1	19.4630	3.5	0.2990	4.0	0.0422	2.0	0.50	266.5	5.2	265.6	9.3	257.9	79.3	266.5	5.2	NA
15LDC03-109	810	82243	15.5	18.9803	1.2	0.3077	1.8	0.0424	1.3	0.73	267.4	3.5	272.4	4.4	315.3	28.4	267.4	3.5	NA
15LDC03-21	483	197952	1.4	19.4162	1.7	0.3017	2.0	0.0425	1.2	0.57	268.3	3.0	267.8	4.8	263.4	38.2	268.3	3.0	NA
15LDC03-120	71	74310	2.0	19.7576	3.2	0.2968	3.9	0.0425	2.3	0.59	268.5	6.0	263.9	9.1	223.3	73.0	268.5	6.0	NA
15LDC03-158	365	57113	1.4	19.0968	1.3	0.3072	2.1	0.0426	1.6	0.77	268.6	4.3	272.0	5.1	301.4	30.7	268.6	4.3	NA
15LDC03-9	334	225426	1.1	19.3952	1.3	0.3037	2.0	0.0427	1.5	0.75	269.7	3.9	269.3	4.7	265.9	30.4	269.7	3.9	NA
15LDC03-92	314	97032	1.9	19.1337	2.0	0.3083	2.5	0.0428	1.4	0.57	270.0	3.7	272.9	5.9	297.0	46.0	270.0	3.7	NA
15LDC03-43	31	9472	2.3	19.8476	4.7	0.2985	5.1	0.0430	2.0	0.39	271.2	5.3	265.2	11.9	212.7	108.6	271.2	5.3	NA
15LDC03-73	217	210150	2.6	19.3892	1.9	0.3081	2.5	0.0433	1.7	0.67	273.4	4.6	272.7	6.1	266.6	43.1	273.4	4.6	NA
15LDC03-14	125	38880	6.5	19.7035	1.7	0.3034	2.2	0.0434	1.4	0.63	273.6	3.7	269.1	5.3	229.6	40.0	273.6	3.7	NA
15LDC03-15	114	38452	1.2	19.2955	2.1	0.3108	2.8	0.0435	1.8	0.65	274.4	4.8	274.8	6.7	277.7	48.4	274.4	4.8	NA
15LDC03-107	177	236595	1.4	18.2798	2.1	0.3290	2.6	0.0436	1.6	0.62	275.2	4.4	288.8	6.6	400.2	46.5	275.2	4.4	NA
15LDC03-68	335	87128	1.2	19.1950	1.8	0.3166	2.5	0.0441	1.7	0.70	278.0	4.7	279.3	6.0	289.7	40.3	278.0	4.7	NA
15LDC03-185	101	41683	1.4	18.9127	2.4	0.3248	2.9	0.0446	1.6	0.55	281.0	4.3	285.6	7.1	323.4	54.2	281.0	4.3	NA
15LDC03-69	110	69647	2.0	19.0712	1.9	0.3235	2.5	0.0447	1.6	0.64	282.2	4.4	284.6	6.2	304.4	43.6	282.2	4.4	NA
15LDC03-54	85	47769	1.4	19.2955	2.8	0.3211	3.2	0.0449	1.5	0.46	283.4	4.1	282.8	7.9	277.7	65.1	283.4	4.1	NA
15LDC03-211	88	28555	2.3	19.4883	2.8	0.3191	3.4	0.0451	2.0	0.59	284.4	5.6	281.2	8.4	254.9	63.7	284.4	5.6	NA
15LDC03-40	43	48216	1.5	19.5533	4.2	0.3196	4.8	0.0453	2.3	0.47	285.8	6.3	281.6	11.8	247.2	97.3	285.8	6.3	NA
15LDC03-45	78	83585	2.9	19.0775	2.7	0.3282	3.2	0.0454	1.7	0.54	286.3	4.9	288.2	8.1	303.7	61.6	286.3	4.9	NA
15LDC03-26	100	48147	1.6	19.3420	2.5	0.3245	2.9	0.0455	1.5	0.51	287.0	4.1	285.4	7.2	272.2	57.1	287.0	4.1	NA
15LDC03-119	64	25954	3.3	19.4113	2.6	0.3239	3.0	0.0456	1.5	0.50	287.5	4.2	284.9	7.5	264.0	60.0	287.5	4.2	NA
15LDC03-212	106	35656	1.4	19.3921	3.0	0.3245	3.3	0.0456	1.1	0.35	287.7	3.2	285.3	8.1	266.3	70.0	287.7	3.2	NA
15LDC03-102	42	35107	1.9	19.5069	3.4	0.3228	3.8	0.0457	1.7	0.45	287.9	4.9	284.0	9.5	252.7	78.7	287.9	4.9	NA
15LDC03-140	160	40175	4.9	19.2233	1.9	0.3277	2.5	0.0457	1.5	0.62	288.0	4.3	287.8	6.2	286.3	44.3	288.0	4.3	NA
15LDC03-103	154	99069	2.0	19.3357	2.0	0.3274	2.4	0.0459	1.3	0.54	289.3	3.7	287.5	6.1	272.9	46.8	289.3	3.7	NA
15LDC03-104	294	57147	2.4	19.0864	1.4	0.3333	2.0	0.0461	1.4	0.71	290.8	4.0	292.1	5.1	302.6	32.0	290.8	4.0	NA
15LDC03-41	101	45523	1.3	19.5483	2.9	0.3267	3.5	0.0463	1.9	0.54	291.8	5.4	287.0	8.7	247.8	67.4	291.8	5.4	NA
15LDC03-101	432	140184	1.2	19.1105	1.7	0.3359	2.3	0.0466	1.6	0.68	293.3	4.5	294.1	5.9	299.7	38.8	293.3	4.5	NA
15LDC03-168	141	35591	1.8	19.3435	2.2	0.3385	2.8	0.0475	1.7	0.61	299.1	5.1	296.0	7.3	272.0	51.5	299.1	5.1	NA
15LDC03-10	123	231561	1.6	19.3750	2.4	0.3401	2.9	0.0478	1.7	0.59	301.0	5.1	297.3	7.5	268.3	54.4	301.0	5.1	NA
15LDC03-197	236	97189	1.5	19.1611	2.0	0.3466	2.4	0.0482	1.4	0.59	303.3	4.3	302.2	6.4	293.7	45.0	303.3	4.3	NA
15LDC03-126	30	16325	2.8	19.5610	4.9	0.3400	5.3	0.0482	2.2	0.40	303.7	6.4	297.2	13.8	246.3	112.6	303.7	6.4	NA
15LDC03-143	82	48552	1.3	18.7455	3.2	0.3606	3.5	0.0490	1.3	0.37	308.6	3.9	312.7	9.4	343.5	73.1	308.6	3.9	NA
15LDC03-20	511	125210	39.9	18.9958	1.3	0.3636	1.9	0.0501	1.4	0.72	315.1	4.3	314.9	5.2	313.4	30.6	315.1	4.3	NA
15LDC03-17	536	100872	128.4	18.3977	1.0	0.4253	1.7	0.0567	1.4	0.81	355.8	4.8	359.8	5.1	385.8	22.3	355.8	4.8	NA
15LDC03-137	83	25018	4.0	18.8244	2.3	0.4298	2.7	0.0587	1.6	0.57	367.6	5.5	363.0	8.4	334.0	51.3	367.6	5.5	NA
15LDC03-106	324	129534	5.1	18.5942	1.5	0.4364	2.2	0.0588	1.5	0.71	368.6	5.5	367.7	6.7	361.8	34.4	368.6	5.5	NA
15LDC03-4	754	118265	39.9	18.4140	1.2	0.4447	1.8	0.0594	1.4	0.76	371.9	5.0	373.5	5.7	383.8	26.7	371.9	5.0	NA

15LDC03-128	300	596599	51.0	18.2560	1.4	0.4536	1.9	0.0601	1.3	0.68	376.0	4.7	379.8	5.9	403.1	30.4	376.0	4.7	NA
15LDC03-144	66	33900	1.3	19.2797	2.8	0.4313	3.1	0.0603	1.3	0.42	377.5	4.8	364.1	9.5	279.6	64.8	377.5	4.8	NA
15LDC03-166	251	43649	4.0	18.8160	1.2	0.4421	1.8	0.0603	1.4	0.77	377.6	5.1	371.7	5.7	335.0	26.5	377.6	5.1	NA
15LDC03-8	455	102288	9.3	18.0549	1.2	0.4623	1.9	0.0605	1.4	0.77	378.9	5.3	385.8	6.0	427.8	26.5	378.9	5.3	NA
15LDC03-37	410	55163	35.1	18.3558	1.6	0.4568	2.4	0.0608	1.8	0.75	380.6	6.5	382.1	7.5	390.9	35.1	380.6	6.5	NA
15LDC03-169	144	76187	3.0	18.7514	2.0	0.4501	2.5	0.0612	1.5	0.60	383.0	5.7	377.4	8.0	342.8	46.2	383.0	5.7	NA
15LDC03-82	71	130008	1.5	18.2409	2.2	0.4653	2.6	0.0616	1.5	0.57	385.1	5.7	387.9	8.5	404.9	48.4	385.1	5.7	NA
15LDC03-186	218	83425	1.9	17.7751	1.5	0.4872	2.0	0.0628	1.3	0.64	392.7	4.9	403.0	6.6	462.6	33.9	392.7	4.9	NA
15LDC03-220	196	69960	2.2	17.9779	1.5	0.4873	2.0	0.0635	1.3	0.65	397.1	5.0	403.0	6.6	437.4	33.6	397.1	5.0	NA
15LDC03-115	214	1007236	2.3	18.2733	1.5	0.4819	2.2	0.0639	1.5	0.70	399.1	5.9	399.4	7.1	401.0	34.3	399.1	5.9	NA
15LDC03-90	437	163742	4.0	18.3380	1.1	0.4826	2.0	0.0642	1.6	0.82	401.1	6.3	399.9	6.5	393.0	25.4	401.1	6.3	0%
15LDC03-91	198	262373	1.4	18.2634	1.4	0.4896	1.8	0.0648	1.1	0.62	405.1	4.3	404.6	6.0	402.2	31.5	405.1	4.3	0%
15LDC03-11	66	104596	2.6	18.0761	2.6	0.5102	3.0	0.0669	1.4	0.46	417.4	5.6	418.6	10.3	425.2	59.1	417.4	5.6	0%
15LDC03-153	177	124687	2.2	18.1292	1.6	0.5284	2.2	0.0695	1.5	0.68	433.0	6.2	430.7	7.7	418.7	35.8	433.0	6.2	-1%
15LDC03-58	434	70173	4.7	17.9739	1.7	0.5434	2.2	0.0708	1.4	0.64	441.2	5.9	440.7	7.8	437.9	37.4	441.2	5.9	0%
15LDC03-135	125	110234	4.1	17.9594	1.5	0.5657	1.9	0.0737	1.3	0.65	458.3	5.6	455.3	7.1	439.7	32.7	458.3	5.6	-1%
15LDC03-170	466	207573	18.1	17.4259	1.6	0.5887	2.3	0.0744	1.6	0.70	462.7	7.2	470.1	8.6	506.4	35.9	462.7	7.2	2%
15LDC03-157	184	126976	2.3	17.5735	1.7	0.5842	2.4	0.0745	1.6	0.67	462.9	7.1	467.1	8.8	487.8	38.6	462.9	7.1	1%
15LDC03-93	48	28623	4.8	17.8523	2.5	0.5812	3.0	0.0752	1.6	0.52	467.7	7.1	465.2	11.1	452.9	56.3	467.7	7.1	-1%
15LDC03-201	141	56600	3.4	17.7072	1.9	0.5917	2.5	0.0760	1.6	0.63	472.1	7.1	472.0	9.3	471.1	42.7	472.1	7.1	0%
15LDC03-113	419	95268	8.9	17.5848	1.3	0.5977	1.8	0.0762	1.3	0.70	473.6	5.8	475.8	6.8	486.4	28.2	473.6	5.8	0%
15LDC03-188	582	125173	1.2	17.2283	1.3	0.6469	2.0	0.0808	1.5	0.76	501.1	7.4	506.6	8.0	531.4	28.5	501.1	7.4	1%
15LDC03-208	1054	150572	17.5	16.8532	0.8	0.6750	1.6	0.0825	1.5	0.88	511.1	7.1	523.8	6.7	579.5	16.9	511.1	7.1	2%
15LDC03-13	79	25224	2.6	17.2580	1.8	0.6600	2.2	0.0826	1.2	0.57	511.7	6.1	514.6	8.7	527.7	39.0	511.7	6.1	1%
15LDC03-217	1335	689330	2.8	17.0423	0.9	0.6914	1.8	0.0855	1.5	0.85	528.6	7.6	533.6	7.3	555.1	20.2	528.6	7.6	1%
15LDC03-198	143	71422	4.0	16.7784	2.0	0.7080	2.5	0.0862	1.4	0.58	532.8	7.3	543.6	10.4	589.1	43.7	532.8	7.3	2%
15LDC03-55	700	265063	2.6	17.0369	1.4	0.7052	2.4	0.0871	1.9	0.82	538.6	10.0	541.9	9.9	555.9	29.5	538.6	10.0	1%
15LDC03-108	76	57412	2.6	16.8767	1.9	0.7240	2.4	0.0886	1.5	0.63	547.4	8.1	553.0	10.4	576.4	41.0	547.4	8.1	1%
15LDC03-171	223	201653	3.9	17.1191	1.8	0.7220	2.3	0.0896	1.4	0.61	553.4	7.5	551.8	9.8	545.3	39.7	553.4	7.5	0%
15LDC03-219	16	62191	0.7	16.1141	3.8	0.7787	4.1	0.0910	1.7	0.42	561.5	9.4	584.7	18.4	676.1	80.4	561.5	9.4	4%
LDCDZ3-16	290	63915	13.6	16.4859	1.1	0.7677	2.8	0.0918	2.5	0.91	566.1	13.7	578.4	12.3	627.1	24.7	566.1	13.7	2%
15LDC03-44	311	83559	1.9	16.9206	1.3	0.7489	1.9	0.0919	1.5	0.76	566.8	7.9	567.6	8.4	570.8	27.3	566.8	7.9	0%
15LDC03-192	343	98789	3.2	16.5288	1.4	0.7862	2.0	0.0942	1.4	0.72	580.6	7.9	589.0	8.9	621.5	29.7	580.6	7.9	1%
15LDC03-172	347	57399	13.7	16.8726	1.5	0.7760	2.1	0.0950	1.4	0.68	584.8	7.9	583.2	9.2	577.0	33.2	584.8	7.9	0%
15LDC03-125	160	70827	3.7	16.8081	1.7	0.7893	2.6	0.0962	2.0	0.75	592.2	11.1	590.8	11.8	585.3	37.7	592.2	11.1	0%
15LDC03-57	227	88870	2.4	16.3522	1.1	0.8561	2.5	0.1015	2.3	0.89	623.4	13.4	628.0	11.9	644.7	24.5	623.4	13.4	1%
LDCDZ3-1	159	27370	4.0	15.4016	3.9	0.9127	6.3	0.1019	4.9	0.78	625.8	29.0	658.5	30.3	772.0	82.9	625.8	29.0	5%
15LDC03-187	293	146252	15.2	15.6333	2.0	0.9021	2.7	0.1023	1.7	0.64	627.8	10.2	652.8	12.8	740.5	42.9	627.8	10.2	4%
15LDC03-160	108	197851	2.5	16.5607	1.5	0.8541	2.3	0.1026	1.7	0.75	629.5	10.5	626.9	10.8	617.3	32.8	629.5	10.5	0%

15LDC03-66	467	395316	18.5	16.4511	1.0	0.8606	1.7	0.1027	1.4	0.82	630.1	8.4	630.5	8.0	631.7	20.9	630.1	8.4	0%
15LDC03-146	269	4676970	2.3	16.5882	1.3	0.8577	2.0	0.1032	1.5	0.75	633.1	9.1	628.9	9.3	613.8	28.3	633.1	9.1	-1%
15LDC03-48	461	99187	21.9	16.1189	1.6	0.9009	2.4	0.1053	1.7	0.74	645.5	10.7	652.2	11.3	675.5	33.7	645.5	10.7	1%
15LDC03-24	180	77485	5.2	16.2821	1.4	0.9365	2.3	0.1106	1.8	0.79	676.2	11.8	671.1	11.5	653.9	31.0	676.2	11.8	-1%
15LDC03-71	243	58187	5.5	15.8978	1.1	0.9844	1.9	0.1135	1.6	0.81	693.1	10.3	695.9	9.7	704.9	24.3	693.1	10.3	0%
LDCDZ3-4	288	101568	6.3	14.7895	1.2	1.2592	5.0	0.1351	4.9	0.97	816.7	37.2	827.5	28.3	856.8	25.4	816.7	37.2	1%
15LDC03-23	325	50771	2.4	14.2735	1.0	1.3799	1.8	0.1428	1.6	0.84	860.7	12.5	880.4	10.8	930.1	20.2	860.7	12.5	2%
15LDC03-99	47	63822	4.4	13.9223	1.9	1.5411	2.5	0.1556	1.7	0.67	932.3	14.5	946.9	15.4	981.1	37.7	981.1	37.7	2%
LDCDZ3-5	152	64511	1.5	13.8381	0.8	1.6669	2.0	0.1673	1.9	0.92	997.2	17.1	996.0	12.8	993.4	16.1	993.4	16.1	0%
15LDC03-19	233	452811	1.6	13.8000	1.2	1.4087	1.8	0.1410	1.3	0.75	850.3	10.7	892.6	10.7	999.0	24.4	999.0	24.4	5%
15LDC03-61	120	78983	3.6	13.7461	1.5	1.7285	2.0	0.1723	1.4	0.70	1024.9	13.3	1019.2	13.0	1006.9	29.5	1006.9	29.5	-1%
15LDC03-64	463	262017	1.9	13.7357	1.2	1.3417	1.8	0.1337	1.4	0.78	808.7	10.9	863.9	10.7	1008.5	23.5	1008.5	23.5	6%
15LDC03-6	69	157199	2.3	13.7202	1.7	1.7699	2.1	0.1761	1.2	0.57	1045.7	11.3	1034.5	13.4	1010.7	34.4	1010.7	34.4	-1%
15LDC03-38	287	111625	2.3	13.7150	1.2	1.6731	1.7	0.1664	1.3	0.73	992.4	11.5	998.4	10.8	1011.5	23.5	1011.5	23.5	1%
15LDC03-72	118	36007	1.9	13.7021	1.1	1.7034	2.1	0.1693	1.8	0.85	1008.1	16.6	1009.8	13.3	1013.4	21.9	1013.4	21.9	0%
15LDC03-203	71	51902	1.4	13.6074	1.7	1.7754	2.6	0.1752	2.0	0.76	1040.8	19.3	1036.5	17.1	1027.5	34.5	1027.5	34.5	0%
15LDC03-117	48	134652	3.2	13.5869	2.0	1.7357	2.5	0.1710	1.4	0.58	1017.8	13.4	1021.9	16.0	1030.5	41.0	1030.5	41.0	0%
LDCDZ3-8	133	40717	2.4	13.4880	1.1	1.8806	1.9	0.1840	1.6	0.82	1088.6	15.8	1074.3	12.8	1045.3	22.5	1045.3	22.5	-1%
15LDC03-177	526	230323	1.9	13.4603	1.0	1.7580	1.8	0.1716	1.6	0.85	1021.1	14.8	1030.1	12.0	1049.5	19.8	1049.5	19.8	1%
15LDC03-207	247	213666	16.0	13.3907	1.2	1.7776	2.0	0.1726	1.6	0.80	1026.7	15.3	1037.3	13.2	1059.9	24.7	1059.9	24.7	1%
15LDC03-76	116	58957	2.6	13.2900	1.5	1.8817	2.2	0.1814	1.6	0.73	1074.5	15.6	1074.7	14.3	1075.1	29.5	1075.1	29.5	0%
15LDC03-32	54	64697	1.3	13.2676	1.8	1.7571	2.4	0.1691	1.6	0.68	1007.0	15.2	1029.8	15.5	1078.4	35.2	1078.4	35.2	2%
15LDC03-87	482	551729	4.5	13.2663	0.9	1.8889	1.7	0.1817	1.5	0.85	1076.5	14.7	1077.2	11.6	1078.6	18.7	1078.6	18.7	0%
15LDC03-205	41	71301	2.8	13.1977	1.6	1.8445	2.6	0.1766	2.0	0.78	1048.1	19.5	1061.5	17.0	1089.0	32.4	1089.0	32.4	1%
15LDC03-216	254	74641	3.1	13.1701	1.1	1.9591	1.6	0.1871	1.2	0.73	1105.8	11.9	1101.6	10.8	1093.2	22.0	1093.2	22.0	0%
15LDC03-147	269	86950	2.7	13.1604	1.0	1.8971	1.7	0.1811	1.4	0.82	1072.8	13.6	1080.1	11.2	1094.7	19.4	1094.7	19.4	1%
15LDC03-33	192	147088	2.4	13.1193	1.2	1.8737	2.1	0.1783	1.8	0.84	1057.6	17.5	1071.8	14.2	1100.9	23.4	1100.9	23.4	1%
15LDC03-7	309	217396	2.4	12.7536	1.2	2.1078	2.1	0.1950	1.7	0.82	1148.2	18.2	1151.4	14.6	1157.2	24.3	1157.2	24.3	0%
15LDC03-111	88	65436	2.7	12.0060	1.7	2.4912	2.3	0.2169	1.5	0.67	1265.6	17.7	1269.5	16.8	1276.0	33.6	1276.0	33.6	0%
15LDC03-199	147	204966	1.4	11.9822	1.1	2.3590	2.0	0.2050	1.7	0.83	1202.1	18.2	1230.3	14.3	1279.9	21.9	1279.9	21.9	2%
15LDC03-67	646	376610	2.8	11.9070	1.0	2.4247	1.8	0.2094	1.5	0.82	1225.6	16.7	1249.9	13.1	1292.2	20.2	1292.2	20.2	2%
15LDC03-149	61	55322	2.2	11.8606	1.6	2.5772	2.5	0.2217	1.9	0.78	1290.8	22.7	1294.2	18.3	1299.8	30.7	1299.8	30.7	0%
15LDC03-47	49	131570	2.8	11.7643	1.8	2.2561	4.0	0.1925	3.5	0.89	1134.9	36.8	1198.7	28.0	1315.6	35.2	1315.6	35.2	5%
15LDC03-163	228	252143	0.9	10.6310	0.9	3.1684	1.6	0.2443	1.4	0.84	1409.0	17.3	1449.5	12.6	1509.4	16.8	1509.4	16.8	3%
15LDC03-63	142	123229	2.9	9.4775	1.3	4.3707	2.3	0.3004	1.9	0.83	1693.4	28.7	1706.8	19.1	1723.3	23.5	1723.3	23.5	1%
15LDC03-18	266	215936	2.1	8.9012	1.1	4.4466	1.8	0.2871	1.4	0.79	1626.8	20.0	1721.1	14.6	1837.7	19.4	1837.7	19.4	5%
15LDC03-210	62	133681	1.6	5.3133	1.3	12.8275	2.0	0.4943	1.5	0.74	2589.3	31.2	2667.1	18.5	2726.6	21.7	2726.6	21.7	3%
15LDC03-70	218	187822	10.5	4.7798	1.0	14.7087	1.8	0.5099	1.5	0.82	2656.2	32.0	2796.6	17.1	2899.4	16.7	2899.4	16.7	5%

Sample 14LDC-DZ4 (Río Turbio Formation - lower)																			
LDCDZ4-67	290	9339	0.6	20.7009	0.8	0.0478	1.4	0.0072	1.1	0.82	46.1	0.5	47.4	0.6	114.3	18.8	46.1	0.5	NA
LDCDZ4-56	71	1885	1.1	21.4860	1.7	0.0479	2.0	0.0075	0.9	0.46	47.9	0.4	47.5	0.9	25.8	41.8	47.9	0.4	NA
LDCDZ4-35	177	8159	1.4	20.6405	1.1	0.0736	1.8	0.0110	1.5	0.80	70.6	1.0	72.1	1.3	121.2	25.4	70.6	1.0	NA
LDCDZ4-76	43	1739	1.0	18.2479	13.0	0.0860	13.2	0.0114	2.2	0.17	72.9	1.6	83.7	10.6	404.1	292.0	72.9	1.6	NA
LDCDZ4-38	105	6839	0.6	20.7085	2.1	0.0790	2.8	0.0119	1.8	0.66	76.0	1.4	77.2	2.1	113.5	49.8	76.0	1.4	NA
LDCDZ4-7	384	15191	0.5	20.6525	0.7	0.0794	1.7	0.0119	1.5	0.91	76.2	1.2	77.5	1.3	119.8	16.1	76.2	1.2	NA
LDCDZ4-81	50	2083	0.9	20.9860	2.1	0.0796	2.4	0.0121	1.3	0.52	77.6	1.0	77.8	1.8	81.9	49.2	77.6	1.0	NA
LDCDZ4-59	432	19297	0.9	21.0414	0.8	0.0854	1.7	0.0130	1.5	0.89	83.5	1.2	83.2	1.3	75.7	18.2	83.5	1.2	NA
LDCDZ4-6	53	2718	1.1	20.7039	2.0	0.0891	2.3	0.0134	1.2	0.51	85.6	1.0	86.6	1.9	114.0	46.8	85.6	1.0	NA
LDCDZ4-106	167	12657	0.7	20.4872	0.7	0.0905	1.3	0.0134	1.1	0.86	86.1	1.0	88.0	1.1	138.7	16.2	86.1	1.0	NA
LDCDZ4-17	102	3750	1.1	21.0313	2.1	0.0886	2.3	0.0135	1.0	0.43	86.6	0.9	86.2	1.9	76.8	49.8	86.6	0.9	NA
LDCDZ4-40	88	6604	0.7	20.3423	2.9	0.0918	3.4	0.0136	1.7	0.51	86.8	1.5	89.2	2.9	155.4	68.7	86.8	1.5	NA
LDCDZ4-68	85	12137	0.7	20.0920	2.2	0.0932	2.3	0.0136	0.7	0.30	87.0	0.6	90.5	2.0	184.3	51.7	87.0	0.6	NA
LDCDZ4-84	65	3419	0.7	20.6955	2.2	0.0920	2.7	0.0138	1.4	0.53	88.5	1.2	89.4	2.3	114.9	52.9	88.5	1.2	NA
LDCDZ4-36	64	5563	1.4	20.8184	2.9	0.0919	3.0	0.0139	0.7	0.22	88.9	0.6	89.3	2.6	101.0	69.5	88.9	0.6	NA
LDCDZ4-11	165	6086	1.4	21.0677	1.4	0.0910	1.8	0.0139	1.2	0.67	89.1	1.1	88.5	1.5	72.7	32.2	89.1	1.1	NA
LDCDZ4-95	330	19371	0.7	20.8062	0.6	0.0925	0.8	0.0140	0.5	0.69	89.3	0.5	89.8	0.7	102.4	13.0	89.3	0.5	NA
LDCDZ4-63	178	12074	1.0	20.7309	1.6	0.0934	1.9	0.0140	0.9	0.47	89.9	0.8	90.6	1.6	110.9	38.6	89.9	0.8	NA
LDCDZ4-98	436	63966	0.6	20.7082	0.9	0.0935	1.1	0.0140	0.7	0.63	89.9	0.6	90.7	1.0	113.5	20.5	89.9	0.6	NA
LDCDZ4-66	489	16025	2.3	20.7714	0.7	0.0964	1.6	0.0145	1.4	0.91	93.0	1.3	93.5	1.4	106.3	15.6	93.0	1.3	NA
LDCDZ4-105	279	14346	2.1	20.4845	0.6	0.0991	2.4	0.0147	2.3	0.96	94.2	2.1	96.0	2.2	139.1	14.7	94.2	2.1	NA
LDCDZ4-33	57	3682	0.8	20.9145	1.6	0.0971	1.8	0.0147	0.9	0.51	94.2	0.9	94.1	1.6	90.1	36.9	94.2	0.9	NA
LDCDZ4-78	371	22700	1.7	20.6787	1.1	0.0989	1.4	0.0148	0.9	0.62	94.9	0.8	95.7	1.3	116.9	26.5	94.9	0.8	NA
LDCDZ4-94	402	18438	1.2	20.7373	0.6	0.0997	1.4	0.0150	1.2	0.89	96.0	1.2	96.5	1.3	110.2	15.2	96.0	1.2	NA
LDCDZ4-10	49	4372	1.1	20.2244	2.2	0.1030	2.4	0.0151	1.0	0.40	96.7	0.9	99.6	2.3	169.0	51.1	96.7	0.9	NA
LDCDZ4-48	51	5404	1.3	20.1423	3.1	0.1037	4.1	0.0151	2.7	0.66	96.9	2.6	100.2	3.9	178.5	71.7	96.9	2.6	NA
LDCDZ4-29	377	17652	0.5	20.9201	1.2	0.1004	1.5	0.0152	0.9	0.58	97.5	0.8	97.1	1.4	89.4	28.1	97.5	0.8	NA
LDCDZ4-74	288	14315	1.4	20.6622	1.1	0.1019	2.5	0.0153	2.3	0.90	97.7	2.2	98.6	2.4	118.7	25.3	97.7	2.2	NA
LDCDZ4-108	41	2220	1.3	21.0045	2.8	0.1004	2.9	0.0153	0.8	0.27	97.9	0.8	97.2	2.7	79.9	66.9	97.9	0.8	NA
LDCDZ4-2	498	14423	1.5	19.2379	3.4	0.1099	3.5	0.0153	0.6	0.18	98.1	0.6	105.8	3.5	284.6	77.9	98.1	0.6	NA
LDCDZ4-91	52	3218	1.6	20.7380	1.9	0.1022	2.0	0.0154	0.8	0.37	98.4	0.7	98.8	1.9	110.1	45.0	98.4	0.7	NA
LDCDZ4-47	119	10029	1.1	20.4783	1.8	0.1039	2.2	0.0154	1.3	0.58	98.7	1.2	100.3	2.1	139.8	41.8	98.7	1.2	NA
LDCDZ4-85	28	2299	1.5	20.3450	4.8	0.1054	4.8	0.0155	0.7	0.15	99.4	0.7	101.7	4.7	155.1	111.5	99.4	0.7	NA
LDCDZ4-30	752	57607	0.5	20.8084	0.7	0.1031	1.1	0.0156	0.9	0.80	99.6	0.9	99.7	1.1	102.1	16.0	99.6	0.9	NA
LDCDZ4-44	145	10241	1.7	20.8523	1.8	0.1042	1.9	0.0158	0.7	0.38	100.8	0.7	100.7	1.8	97.1	42.1	100.8	0.7	NA
LDCDZ4-46	347	19169	1.7	20.7059	0.6	0.1051	2.6	0.0158	2.6	0.97	100.9	2.6	101.5	2.5	113.8	13.9	100.9	2.6	NA
LDCDZ4-41	56	3013	1.6	20.5427	3.3	0.1062	3.6	0.0158	1.6	0.44	101.2	1.6	102.5	3.5	132.4	76.5	101.2	1.6	NA
LDCDZ4-24	50	2504	1.3	20.5886	2.1	0.1062	2.1	0.0159	0.5	0.25	101.4	0.5	102.5	2.1	127.2	48.6	101.4	0.5	NA

LDCDZ4-25	27	3167	1.3	19.4878	2.7	0.1128	2.8	0.0159	0.7	0.24	101.9	0.7	108.5	2.9	255.0	62.1	101.9	0.7	NA
LDCDZ4-18	4716	338107	5.5	20.9070	2.0	0.1052	2.8	0.0160	2.0	0.69	102.0	2.0	101.6	2.8	90.9	48.5	102.0	2.0	NA
LDCDZ4-72	53	2557	1.5	20.0503	2.6	0.1099	4.0	0.0160	3.1	0.76	102.2	3.1	105.9	4.0	189.1	60.5	102.2	3.1	NA
LDCDZ4-88	167	9266	0.8	20.9568	0.6	0.1069	1.0	0.0163	0.8	0.77	103.9	0.8	103.1	1.0	85.3	14.9	103.9	0.8	NA
LDCDZ4-16	28	1494	1.4	21.0906	1.5	0.1069	1.9	0.0164	1.1	0.59	104.6	1.2	103.1	1.9	70.1	36.8	104.6	1.2	NA
LDCDZ4-69	66	10849	1.1	20.2263	1.3	0.1117	1.4	0.0164	0.6	0.39	104.8	0.6	107.5	1.4	168.8	30.4	104.8	0.6	NA
LDCDZ4-83	94	11727	1.3	20.6566	2.3	0.1098	2.4	0.0164	0.7	0.30	105.2	0.7	105.8	2.4	119.4	53.8	105.2	0.7	NA
LDCDZ4-52	51	3789	1.0	20.1965	2.0	0.1125	2.2	0.0165	0.8	0.37	105.4	0.8	108.3	2.2	172.2	46.6	105.4	0.8	NA
LDCDZ4-9	294	18236	1.0	20.3320	0.7	0.1122	1.2	0.0165	1.0	0.82	105.8	1.1	108.0	1.3	156.6	16.7	105.8	1.1	NA
LDCDZ4-14	129	14811	0.9	20.7117	2.1	0.1102	2.3	0.0166	0.9	0.39	105.8	0.9	106.1	2.3	113.1	49.6	105.8	0.9	NA
LDCDZ4-62	134	7747	1.6	20.8044	0.5	0.1099	1.5	0.0166	1.4	0.93	106.1	1.5	105.9	1.5	102.6	12.5	106.1	1.5	NA
LDCDZ4-90	158	9683	1.7	20.5855	0.9	0.1115	2.1	0.0166	1.9	0.91	106.4	2.0	107.3	2.1	127.5	20.3	106.4	2.0	NA
LDCDZ4-51	75	5441	0.8	20.4486	1.2	0.1128	1.3	0.0167	0.4	0.32	107.0	0.4	108.5	1.3	143.2	28.1	107.0	0.4	NA
LDCDZ4-45	387	28941	1.1	20.5859	1.0	0.1128	1.3	0.0168	0.8	0.58	107.7	0.8	108.5	1.3	127.5	24.5	107.7	0.8	NA
LDCDZ4-109	99	7902	1.4	20.2051	1.7	0.1150	2.6	0.0169	1.9	0.75	107.8	2.0	110.6	2.7	171.2	39.6	107.8	2.0	NA
LDCDZ4-80	166	14965	1.1	20.3434	1.4	0.1160	1.8	0.0171	1.1	0.61	109.4	1.2	111.4	1.9	155.3	33.9	109.4	1.2	NA
LDCDZ4-71	87	6307	2.1	21.1603	1.2	0.1115	1.5	0.0171	0.8	0.53	109.4	0.9	107.4	1.5	62.3	29.8	109.4	0.9	NA
LDCDZ4-73	73	5187	2.0	20.5845	1.6	0.1158	2.0	0.0173	1.3	0.64	110.5	1.4	111.2	2.1	127.6	36.7	110.5	1.4	NA
LDCDZ4-79	88	8081	1.8	20.3832	2.9	0.1170	2.9	0.0173	0.5	0.19	110.5	0.6	112.3	3.1	150.7	67.7	110.5	0.6	NA
LDCDZ4-19	315	32237	1.6	20.8526	1.0	0.1159	1.2	0.0175	0.6	0.54	112.0	0.7	111.4	1.2	97.1	23.5	112.0	0.7	NA
LDCDZ4-53	75	3909	1.8	20.4664	1.8	0.1194	1.9	0.0177	0.6	0.33	113.3	0.7	114.6	2.1	141.2	42.3	113.3	0.7	NA
LDCDZ4-96	254	15819	0.9	20.7140	0.9	0.1202	2.0	0.0181	1.8	0.89	115.4	2.0	115.2	2.1	112.9	21.1	115.4	2.0	NA
LDCDZ4-93	741	45919	1.5	20.5192	0.6	0.1249	1.8	0.0186	1.7	0.94	118.7	2.0	119.5	2.1	135.1	14.6	118.7	2.0	NA
LDCDZ4-70	88	3900	1.4	20.4550	2.4	0.1296	2.5	0.0192	0.8	0.31	122.8	1.0	123.8	2.9	142.4	56.3	122.8	1.0	NA
LDCDZ4-103	133	9832	1.2	20.3756	1.0	0.1321	1.1	0.0195	0.4	0.39	124.6	0.5	125.9	1.3	151.6	23.2	124.6	0.5	NA
LDCDZ4-89	93	13102	1.8	20.4689	1.6	0.1316	1.8	0.0195	0.8	0.47	124.7	1.0	125.5	2.1	140.9	37.0	124.7	1.0	NA
LDCDZ4-107	154	21398	1.2	20.0262	1.4	0.1346	1.8	0.0195	1.2	0.67	124.8	1.5	128.2	2.2	192.0	31.6	124.8	1.5	NA
LDCDZ4-100	124	7634	1.6	20.6336	1.0	0.1307	1.7	0.0196	1.4	0.82	124.8	1.7	124.7	2.0	122.0	22.9	124.8	1.7	NA
LDCDZ4-1	53	3560	1.3	20.2877	1.9	0.1338	2.0	0.0197	0.6	0.28	125.6	0.7	127.5	2.4	161.7	45.2	125.6	0.7	NA
LDCDZ4-5	70	9200	1.1	19.9495	1.8	0.1366	2.6	0.0198	1.8	0.70	126.2	2.2	130.0	3.1	200.9	42.6	126.2	2.2	NA
LDCDZ4-32	158	12578	1.4	20.4157	0.9	0.1343	1.0	0.0199	0.6	0.53	126.9	0.7	127.9	1.2	147.0	20.7	126.9	0.7	NA
LDCDZ4-92	306	21026	1.2	20.3189	0.8	0.1370	2.7	0.0202	2.5	0.96	128.8	3.3	130.3	3.3	158.1	18.1	128.8	3.3	NA
LDCDZ4-60	283	25063	0.7	20.4860	0.8	0.1406	1.6	0.0209	1.3	0.84	133.3	1.8	133.6	2.0	138.9	19.8	133.3	1.8	NA
LDCDZ4-42	345	26973	1.6	20.3275	0.5	0.1536	1.5	0.0226	1.4	0.93	144.3	1.9	145.1	2.0	157.1	12.1	144.3	1.9	NA
LDCDZ4-55	124	9865	2.0	19.6243	2.1	0.1592	6.1	0.0227	5.7	0.94	144.5	8.2	150.0	8.5	238.9	47.3	144.5	8.2	NA
LDCDZ4-87	182	20632	1.9	20.4690	0.9	0.1584	1.3	0.0235	0.9	0.70	149.8	1.4	149.3	1.8	140.9	21.9	149.8	1.4	NA
LDCDZ4-22	290	21433	0.7	20.4780	0.6	0.1595	0.8	0.0237	0.5	0.66	150.9	0.7	150.2	1.1	139.8	13.5	150.9	0.7	NA
LDCDZ4-61	87	14094	0.9	19.9073	1.5	0.1667	1.7	0.0241	0.7	0.41	153.3	1.0	156.5	2.5	205.8	35.8	153.3	1.0	NA
LDCDZ4-23	181	20174	2.2	20.1806	0.9	0.1647	1.5	0.0241	1.1	0.78	153.5	1.7	154.8	2.1	174.0	21.2	153.5	1.7	NA

LDCDZ4-64	520	40610	1.4	20.2081	1.3	0.1654	1.4	0.0242	0.5	0.35	154.4	0.8	155.4	2.1	170.9	31.5	154.4	0.8	NA
LDCDZ4-57	193	20656	1.1	20.1615	1.3	0.1658	2.7	0.0242	2.3	0.87	154.4	3.6	155.8	3.9	176.2	30.6	154.4	3.6	NA
LDCDZ4-99	1122	128377	0.7	20.3713	0.8	0.1656	1.8	0.0245	1.6	0.90	155.9	2.5	155.6	2.7	152.0	19.2	155.9	2.5	NA
LDCDZ4-65	192	14904	1.7	20.2612	1.1	0.1722	2.0	0.0253	1.6	0.82	161.1	2.6	161.3	2.9	164.7	26.1	161.1	2.6	NA
LDCDZ4-39	69	11734	0.8	19.3463	0.6	0.2862	1.0	0.0402	0.8	0.78	253.8	2.0	255.6	2.3	271.7	14.6	253.8	2.0	NA
LDCDZ4-49	386	48266	1.2	19.0033	0.9	0.3156	1.8	0.0435	1.6	0.87	274.5	4.2	278.5	4.4	312.6	19.9	274.5	4.2	NA
LDCDZ4-8	196	21027	0.7	18.1903	3.9	0.3302	4.1	0.0436	1.3	0.31	274.9	3.5	289.7	10.4	411.2	87.8	274.9	3.5	NA
LDCDZ4-97	176	110960	1.2	19.2312	0.9	0.3189	1.2	0.0445	0.7	0.62	280.6	2.0	281.1	2.9	285.3	21.0	280.6	2.0	NA
LDCDZ4-4	111	19900	0.9	19.0201	0.9	0.3228	1.2	0.0445	0.8	0.69	280.9	2.3	284.1	3.0	310.5	20.2	280.9	2.3	NA
LDCDZ4-77	137	27359	2.1	18.9814	0.6	0.3337	0.8	0.0459	0.5	0.62	289.6	1.4	292.4	2.0	315.2	14.0	289.6	1.4	NA
LDCDZ4-3	147	36488	1.5	18.9051	0.7	0.3371	0.9	0.0462	0.5	0.60	291.3	1.5	295.0	2.2	324.3	15.5	291.3	1.5	NA
LDCDZ4-15	235	55790	1.5	19.0048	0.9	0.3417	1.5	0.0471	1.2	0.79	296.7	3.4	298.4	3.9	312.4	20.7	296.7	3.4	NA
LDCDZ4-50	227	45478	1.0	19.1364	0.7	0.3456	1.0	0.0480	0.7	0.69	302.0	2.0	301.4	2.5	296.6	16.0	302.0	2.0	NA
LDCDZ4-28	81	16559	1.1	18.8863	0.6	0.3515	0.9	0.0481	0.7	0.75	303.1	1.9	305.8	2.3	326.6	13.2	303.1	1.9	NA
LDCDZ4-43	472	79078	0.9	19.1356	0.6	0.3518	0.9	0.0488	0.7	0.72	307.3	2.0	306.1	2.5	296.8	14.8	307.3	2.0	NA
LDCDZ4-27	436	100806	1.3	17.9897	0.8	0.5559	1.6	0.0725	1.4	0.85	451.4	6.0	448.9	5.8	435.9	18.9	451.4	6.0	-1%
LDCDZ4-102	107	31505	1.6	17.6829	0.8	0.5815	1.5	0.0746	1.3	0.85	463.7	5.8	465.4	5.7	474.1	17.9	463.7	5.8	0%
LDCDZ4-86	546	181248	3.9	17.7749	1.4	0.5943	1.7	0.0766	0.9	0.51	475.9	3.9	473.6	6.3	462.6	31.8	475.9	3.9	0%
LDCDZ4-82	62	28536	2.0	17.0690	0.7	0.6998	1.9	0.0866	1.8	0.93	535.6	9.1	538.7	8.0	551.8	15.4	535.6	9.1	1%
LDCDZ4-31	55	15916	1.3	17.3054	1.2	0.6935	1.6	0.0870	1.1	0.67	538.0	5.6	534.9	6.8	521.6	26.4	538.0	5.6	-1%
LDCDZ4-104	37	19162	1.2	16.8476	0.6	0.7162	1.1	0.0875	1.0	0.85	540.8	5.0	548.4	4.8	580.2	13.2	540.8	5.0	1%
LDCDZ4-21	211	75363	1.1	17.2559	0.8	0.7042	2.0	0.0881	1.9	0.93	544.5	9.8	541.3	8.5	527.9	16.5	544.5	9.8	-1%
LDCDZ4-101	110	41361	2.2	17.0081	0.8	0.7185	1.4	0.0886	1.1	0.82	547.5	5.9	549.8	5.9	559.5	17.3	547.5	5.9	0%
LDCDZ4-110	31	9007	1.2	16.6105	1.0	0.7575	3.8	0.0913	3.7	0.97	562.9	20.0	572.5	16.8	610.9	21.7	562.9	20.0	2%
LDCDZ4-26	47	14575	0.2	16.8302	0.7	0.7901	1.2	0.0964	1.0	0.82	593.5	5.4	591.2	5.2	582.4	14.6	593.5	5.4	0%
LDCDZ4-13	225	174274	1.9	13.7114	2.5	1.6538	2.6	0.1645	0.5	0.18	981.5	4.3	991.0	16.3	1012.0	51.5	1012.0	51.5	1%
LDCDZ4-37	100	96904	2.2	13.5222	0.8	1.8217	1.6	0.1787	1.3	0.86	1059.6	13.0	1053.3	10.2	1040.2	16.2	1040.2	16.2	-1%
LDCDZ4-75	111	103370	2.1	13.4534	0.5	1.8209	2.4	0.1777	2.3	0.97	1054.2	22.6	1053.0	15.6	1050.5	10.7	1050.5	10.7	0%
LDCDZ4-12	68	107444	2.0	13.3290	0.7	1.8195	1.2	0.1759	1.0	0.81	1044.5	9.3	1052.5	7.8	1069.2	14.2	1069.2	14.2	1%
LDCDZ4-58	278	211377	3.9	13.2914	1.2	1.8778	2.2	0.1810	1.9	0.83	1072.5	18.3	1073.3	14.8	1074.8	24.8	1074.8	24.8	0%
LDCDZ4-54	124	82404	1.3	12.9556	0.9	1.9919	1.8	0.1872	1.5	0.85	1106.0	15.5	1112.8	12.1	1126.0	18.6	1126.0	18.6	1%
Sample 14LDC-DZ2 (Río Turbio Formation - lower)																			
LDCDZ2-93	61	908	1.6	21.8993	2.3	0.0447	3.0	0.0071	1.8	0.62	45.7	0.8	44.5	1.3	-20.1	56.5	45.7	0.8	NA
LDCDZ2-11	124	2016	2.0	20.6820	2.4	0.0491	3.3	0.0074	2.3	0.68	47.3	1.1	48.7	1.6	116.5	57.4	47.3	1.1	NA
LDCDZ2-80	51	1025	1.0	22.0946	4.4	0.0562	4.8	0.0090	1.9	0.39	57.8	1.1	55.5	2.6	-41.6	107.3	57.8	1.1	NA
LDCDZ2-59	60	1574	0.9	21.7236	2.2	0.0656	2.4	0.0103	0.8	0.32	66.3	0.5	64.5	1.5	-0.6	54.1	66.3	0.5	NA
LDCDZ2-100	257	9217	1.0	20.5294	1.1	0.0765	1.6	0.0114	1.1	0.71	73.0	0.8	74.8	1.1	133.9	25.9	73.0	0.8	NA
LDCDZ2-12	76	2118	0.7	20.8892	2.3	0.0756	4.3	0.0115	3.6	0.84	73.4	2.7	74.0	3.1	92.9	54.9	73.4	2.7	NA

LDCDZ2-41	280	9057	1.0	21.4188	1.9	0.0738	4.5	0.0115	4.1	0.91	73.4	3.0	72.3	3.2	33.3	46.2	73.4	3.0	NA
LDCDZ2-68	110	3841	0.7	21.0255	1.3	0.0755	2.7	0.0115	2.3	0.88	73.8	1.7	73.9	1.9	77.5	30.4	73.8	1.7	NA
LDCDZ2-75	64	3137	0.7	21.2568	2.5	0.0753	4.9	0.0116	4.2	0.86	74.4	3.1	73.7	3.5	51.5	59.8	74.4	3.1	NA
LDCDZ2-25	259	6878	0.5	20.7606	1.4	0.0775	2.2	0.0117	1.7	0.79	74.7	1.3	75.8	1.6	107.6	32.0	74.7	1.3	NA
LDCDZ2-81	191	5173	1.3	21.3119	1.7	0.0757	2.7	0.0117	2.1	0.78	75.0	1.6	74.1	1.9	45.2	39.5	75.0	1.6	NA
LDCDZ2-39	77	1946	0.7	21.5519	3.4	0.0749	3.8	0.0117	1.7	0.46	75.0	1.3	73.3	2.7	18.5	81.1	75.0	1.3	NA
LDCDZ2-71	43	2368	1.4	20.4304	3.3	0.0793	4.2	0.0117	2.7	0.63	75.3	2.0	77.5	3.1	145.3	76.9	75.3	2.0	NA
LDCDZ2-60	280	9120	0.8	21.0637	1.2	0.0772	1.4	0.0118	0.8	0.58	75.6	0.6	75.5	1.0	73.2	28.0	75.6	0.6	NA
LDCDZ2-70	200	7306	0.7	20.7398	0.9	0.0786	1.0	0.0118	0.5	0.51	75.8	0.4	76.8	0.7	109.9	20.1	75.8	0.4	NA
LDCDZ2-92	30	1179	1.1	17.0098	4.9	0.0975	5.4	0.0120	2.2	0.41	77.1	1.7	94.5	4.9	559.3	107.2	77.1	1.7	NA
LDCDZ2-89	227	3242	0.5	15.4522	19.4	0.1075	19.6	0.0120	2.8	0.14	77.2	2.1	103.7	19.3	765.1	412.0	77.2	2.1	NA
LDCDZ2-30	294	9009	1.8	20.6853	1.6	0.0808	1.9	0.0121	1.0	0.54	77.6	0.8	78.9	1.4	116.1	36.9	77.6	0.8	NA
LDCDZ2-101	434	11719	0.7	21.0677	1.1	0.0799	2.8	0.0122	2.6	0.93	78.2	2.0	78.0	2.1	72.7	25.1	78.2	2.0	NA
LDCDZ2-65	572	24941	0.9	20.6532	0.7	0.0824	1.8	0.0123	1.6	0.92	79.0	1.3	80.4	1.4	119.8	16.9	79.0	1.3	NA
LDCDZ2-72	224	8281	1.4	20.7465	1.3	0.0846	4.2	0.0127	4.0	0.95	81.5	3.2	82.4	3.3	109.1	31.3	81.5	3.2	NA
LDCDZ2-17	55	1362	1.3	21.6211	3.0	0.0828	6.8	0.0130	6.1	0.90	83.2	5.0	80.8	5.2	10.7	71.8	83.2	5.0	NA
LDCDZ2-4	73	2199	0.9	20.7654	3.2	0.0879	3.6	0.0132	1.6	0.44	84.8	1.3	85.5	2.9	107.0	75.5	84.8	1.3	NA
LDCDZ2-19	42	1152	0.8	21.2735	2.9	0.0861	3.1	0.0133	1.0	0.33	85.1	0.9	83.9	2.5	49.6	69.4	85.1	0.9	NA
LDCDZ2-48	60	1642	1.1	21.7439	1.8	0.0847	2.3	0.0134	1.4	0.62	85.5	1.2	82.5	1.8	-2.9	43.8	85.5	1.2	NA
LDCDZ2-95	144	5013	1.9	20.5925	2.0	0.0902	2.6	0.0135	1.7	0.64	86.2	1.4	87.7	2.2	126.7	47.1	86.2	1.4	NA
LDCDZ2-28	112	3342	0.7	21.4277	1.7	0.0892	2.3	0.0139	1.5	0.65	88.8	1.3	86.8	1.9	32.3	41.2	88.8	1.3	NA
LDCDZ2-43	46	1474	0.9	21.1117	1.1	0.0931	2.4	0.0143	2.1	0.89	91.3	1.9	90.4	2.1	67.8	26.4	91.3	1.9	NA
LDCDZ2-58	464	21491	1.5	20.8497	0.6	0.0952	2.0	0.0144	1.9	0.95	92.2	1.7	92.4	1.8	97.4	14.6	92.2	1.7	NA
LDCDZ2-3	47	1460	1.3	21.0993	2.6	0.0942	2.8	0.0144	1.1	0.38	92.2	1.0	91.4	2.5	69.2	62.4	92.2	1.0	NA
LDCDZ2-57	35	1463	2.0	21.3412	4.3	0.0940	5.7	0.0146	3.7	0.65	93.1	3.4	91.2	5.0	42.0	103.3	93.1	3.4	NA
LDCDZ2-97	96	3204	1.2	20.5993	4.5	0.0980	4.8	0.0146	1.8	0.38	93.7	1.7	94.9	4.4	125.9	105.3	93.7	1.7	NA
LDCDZ2-33	94	3418	1.5	20.7725	1.2	0.0978	2.0	0.0147	1.6	0.80	94.3	1.5	94.8	1.8	106.2	28.2	94.3	1.5	NA
LDCDZ2-73	204	10359	1.6	20.5753	1.5	0.0998	2.0	0.0149	1.3	0.63	95.3	1.2	96.6	1.8	128.7	36.5	95.3	1.2	NA
LDCDZ2-98	50	3064	1.9	20.1884	1.8	0.1031	5.1	0.0151	4.7	0.94	96.6	4.5	99.6	4.8	173.1	41.3	96.6	4.5	NA
LDCDZ2-79	18	701	2.2	21.8410	4.8	0.0959	5.4	0.0152	2.5	0.46	97.2	2.4	93.0	4.8	-13.6	115.8	97.2	2.4	NA
LDCDZ2-14	71	2033	1.7	21.3413	1.2	0.0981	3.6	0.0152	3.4	0.95	97.2	3.3	95.1	3.3	42.0	27.7	97.2	3.3	NA
LDCDZ2-13	574	15123	1.0	20.8065	1.1	0.1011	2.1	0.0153	1.8	0.85	97.6	1.7	97.8	1.9	102.3	26.2	97.6	1.7	NA
LDCDZ2-21	27	1747	1.3	20.3859	3.0	0.1037	4.8	0.0153	3.7	0.78	98.1	3.6	100.2	4.6	150.4	69.8	98.1	3.6	NA
LDCDZ2-44	31	1357	1.6	21.3421	3.0	0.0995	3.2	0.0154	1.1	0.34	98.5	1.0	96.3	2.9	41.9	71.5	98.5	1.0	NA
LDCDZ2-103	61	2490	1.5	20.9300	1.3	0.1015	2.1	0.0154	1.6	0.77	98.6	1.6	98.2	1.9	88.3	31.1	98.6	1.6	NA
LDCDZ2-76	130	11672	2.4	20.7534	1.5	0.1027	2.3	0.0155	1.7	0.76	98.9	1.7	99.3	2.2	108.4	34.7	98.9	1.7	NA
LDCDZ2-82	220	11885	1.5	20.7110	0.8	0.1031	1.5	0.0155	1.2	0.82	99.0	1.2	99.6	1.4	113.2	19.9	99.0	1.2	NA
LDCDZ2-88	17	728	1.6	22.1319	4.7	0.0966	5.1	0.0155	2.1	0.40	99.2	2.0	93.7	4.6	-45.7	114.2	99.2	2.0	NA
LDCDZ2-105	103	3812	1.1	20.4988	1.3	0.1045	1.5	0.0155	0.6	0.44	99.4	0.6	100.9	1.4	137.5	31.2	99.4	0.6	NA

LDCDZ2-9	42	2073	2.1	20.3379	3.1	0.1056	3.7	0.0156	1.9	0.53	99.7	1.9	101.9	3.6	155.9	73.0	99.7	1.9	NA
LDCDZ2-69	225	13864	1.3	20.5224	1.3	0.1047	1.9	0.0156	1.5	0.76	99.7	1.4	101.1	1.9	134.7	29.7	99.7	1.4	NA
LDCDZ2-99	355	18256	1.4	20.3499	1.1	0.1062	7.0	0.0157	6.9	0.99	100.3	6.9	102.5	6.9	154.5	26.7	100.3	6.9	NA
LDCDZ2-62	93	4236	1.7	20.6916	1.5	0.1060	2.6	0.0159	2.2	0.82	101.8	2.2	102.3	2.6	115.4	35.8	101.8	2.2	NA
LDCDZ2-23	69	2567	1.3	20.7089	1.7	0.1060	1.9	0.0159	1.0	0.50	101.8	1.0	102.3	1.9	113.4	39.7	101.8	1.0	NA
LDCDZ2-77	52	2581	0.9	20.5821	4.3	0.1072	4.4	0.0160	0.8	0.18	102.4	0.8	103.4	4.3	127.9	102.4	102.4	0.8	NA
LDCDZ2-84	213	6676	1.6	20.7975	1.2	0.1064	3.0	0.0160	2.7	0.91	102.6	2.8	102.6	2.9	103.3	28.8	102.6	2.8	NA
LDCDZ2-36	44	1564	1.4	22.1310	2.0	0.1000	2.1	0.0161	0.8	0.36	102.7	0.8	96.8	2.0	-45.6	48.3	102.7	0.8	NA
LDCDZ2-2	70	2390	1.6	20.9018	2.8	0.1060	3.5	0.0161	2.1	0.61	102.7	2.2	102.3	3.4	91.5	65.4	102.7	2.2	NA
LDCDZ2-46	68	2799	1.1	21.1237	1.6	0.1052	2.2	0.0161	1.6	0.71	103.1	1.6	101.6	2.1	66.4	37.1	103.1	1.6	NA
LDCDZ2-96	479	20636	0.9	20.9075	0.8	0.1069	1.6	0.0162	1.4	0.87	103.7	1.4	103.2	1.6	90.9	18.8	103.7	1.4	NA
LDCDZ2-40	349	14309	1.3	20.8427	1.0	0.1077	3.9	0.0163	3.8	0.97	104.1	3.9	103.9	3.9	98.2	22.6	104.1	3.9	NA
LDCDZ2-34	26	1290	2.0	21.0807	3.4	0.1066	4.1	0.0163	2.2	0.54	104.3	2.3	102.9	4.0	71.3	81.5	104.3	2.3	NA
LDCDZ2-55	126	5326	0.9	20.4916	1.8	0.1097	2.1	0.0163	1.1	0.52	104.3	1.1	105.7	2.1	138.2	42.1	104.3	1.1	NA
LDCDZ2-1	53	2102	1.2	20.6248	1.8	0.1092	2.5	0.0163	1.7	0.68	104.5	1.7	105.3	2.5	123.0	42.4	104.5	1.7	NA
LDCDZ2-31	175	6350	1.6	20.7082	1.0	0.1089	2.1	0.0164	1.9	0.88	104.6	1.9	105.0	2.1	113.5	24.0	104.6	1.9	NA
LDCDZ2-20	130	3904	1.8	20.1462	3.3	0.1125	4.0	0.0164	2.2	0.55	105.1	2.3	108.2	4.1	178.0	76.9	105.1	2.3	NA
LDCDZ2-32	91	2732	1.7	21.4092	1.3	0.1060	2.5	0.0165	2.2	0.86	105.2	2.3	102.3	2.5	34.3	31.1	105.2	2.3	NA
LDCDZ2-63	125	6127	0.9	20.6812	1.5	0.1099	2.3	0.0165	1.7	0.74	105.4	1.8	105.8	2.3	116.6	36.5	105.4	1.8	NA
LDCDZ2-47	169	5549	1.7	20.1047	2.4	0.1131	2.5	0.0165	0.8	0.31	105.4	0.8	108.8	2.6	182.8	55.9	105.4	0.8	NA
LDCDZ2-61	277	11203	1.5	20.5387	0.8	0.1108	1.3	0.0165	1.1	0.81	105.5	1.1	106.7	1.4	132.9	18.5	105.5	1.1	NA
LDCDZ2-5	149	5114	1.6	20.4765	1.0	0.1113	3.7	0.0165	3.6	0.96	105.7	3.8	107.2	3.8	140.0	24.0	105.7	3.8	NA
LDCDZ2-49	47	1786	1.2	20.9600	5.4	0.1090	5.4	0.0166	0.9	0.17	105.9	1.0	105.0	5.4	84.9	127.4	105.9	1.0	NA
LDCDZ2-104	334	13743	1.4	20.2733	0.6	0.1127	1.2	0.0166	1.0	0.84	106.0	1.0	108.5	1.2	163.3	14.7	106.0	1.0	NA
LDCDZ2-42	61	1858	1.7	20.9985	1.9	0.1089	2.4	0.0166	1.4	0.58	106.0	1.5	105.0	2.4	80.5	45.9	106.0	1.5	NA
LDCDZ2-22	131	4089	1.5	21.0077	1.6	0.1101	2.8	0.0168	2.3	0.82	107.2	2.4	106.0	2.8	79.5	37.5	107.2	2.4	NA
LDCDZ2-29	48	2114	1.7	20.6612	2.5	0.1128	2.8	0.0169	1.3	0.46	108.0	1.4	108.5	2.9	118.9	58.5	108.0	1.4	NA
LDCDZ2-91	124	13461	2.1	20.7575	0.9	0.1128	1.6	0.0170	1.3	0.83	108.6	1.4	108.5	1.6	107.9	21.3	108.6	1.4	NA
LDCDZ2-87	214	6975	1.9	20.6559	0.8	0.1134	1.1	0.0170	0.8	0.67	108.6	0.8	109.1	1.2	119.5	19.4	108.6	0.8	NA
LDCDZ2-16	106	5139	3.1	21.0889	1.9	0.1112	3.2	0.0170	2.6	0.80	108.7	2.8	107.1	3.3	70.3	45.3	108.7	2.8	NA
LDCDZ2-78	342	13476	1.2	20.6470	0.9	0.1143	1.3	0.0171	0.9	0.70	109.4	1.0	109.9	1.3	120.5	21.1	109.4	1.0	NA
LDCDZ2-64	122	4531	1.9	21.0085	1.4	0.1127	1.7	0.0172	0.9	0.55	109.7	1.0	108.4	1.7	79.4	32.9	109.7	1.0	NA
LDCDZ2-24	63	1804	1.5	21.0722	1.9	0.1126	2.3	0.0172	1.3	0.55	110.0	1.4	108.3	2.3	72.2	45.2	110.0	1.4	NA
LDCDZ2-52	420	17291	1.1	20.6315	0.5	0.1158	1.0	0.0173	0.9	0.86	110.7	1.0	111.2	1.1	122.3	12.4	110.7	1.0	NA
LDCDZ2-67	33	1610	2.1	21.5265	2.7	0.1116	3.6	0.0174	2.4	0.67	111.3	2.7	107.4	3.7	21.3	64.0	111.3	2.7	NA
LDCDZ2-7	70	2316	1.7	21.1783	2.2	0.1144	3.1	0.0176	2.2	0.71	112.3	2.4	110.0	3.2	60.3	51.7	112.3	2.4	NA
LDCDZ2-18	378	19247	1.7	20.4983	0.7	0.1258	1.9	0.0187	1.8	0.94	119.5	2.1	120.4	2.2	137.5	15.8	119.5	2.1	NA
LDCDZ2-37	103	4159	1.9	20.7653	1.4	0.1243	2.5	0.0187	2.1	0.84	119.5	2.5	118.9	2.8	107.0	32.4	119.5	2.5	NA
LDCDZ2-45	28	1381	1.1	20.5007	2.3	0.1319	3.4	0.0196	2.5	0.73	125.2	3.1	125.8	4.1	137.2	54.9	125.2	3.1	NA

LDCDZ2-6	165	10307	1.8	20.5458	0.9	0.1340	1.7	0.0200	1.5	0.86	127.4	1.9	127.7	2.1	132.0	20.8	127.4	1.9	NA
LDCDZ2-10	401	12211	1.0	20.4270	0.8	0.1378	1.1	0.0204	0.8	0.72	130.3	1.1	131.1	1.4	145.7	18.7	130.3	1.1	NA
LDCDZ2-86	42	3198	1.8	20.3499	1.9	0.1398	2.5	0.0206	1.7	0.68	131.7	2.2	132.9	3.2	154.5	43.7	131.7	2.2	NA
LDCDZ2-102	41	2545	1.4	20.5487	1.8	0.1393	2.6	0.0208	1.9	0.73	132.5	2.5	132.4	3.2	131.7	41.6	132.5	2.5	NA
LDCDZ2-53	169	7858	1.4	20.4717	1.3	0.1446	1.8	0.0215	1.3	0.72	137.0	1.8	137.2	2.3	140.5	29.8	137.0	1.8	NA
LDCDZ2-54	111	5571	2.0	20.3753	0.8	0.1507	1.3	0.0223	1.0	0.79	142.0	1.4	142.5	1.7	151.6	18.3	142.0	1.4	NA
LDCDZ2-51	88	4991	1.5	20.3308	2.8	0.1525	3.4	0.0225	2.0	0.58	143.3	2.8	144.1	4.6	156.7	65.8	143.3	2.8	NA
LDCDZ2-85	162	18217	1.1	20.0944	1.7	0.1585	3.3	0.0231	2.9	0.87	147.2	4.2	149.4	4.6	184.0	38.9	147.2	4.2	NA
LDCDZ2-15	216	10390	1.7	20.3789	1.2	0.1575	2.0	0.0233	1.6	0.80	148.4	2.3	148.5	2.7	151.2	27.6	148.4	2.3	NA
LDCDZ2-27	695	34907	2.9	20.5226	1.3	0.1614	2.0	0.0240	1.6	0.79	153.0	2.5	151.9	2.9	134.7	29.4	153.0	2.5	NA
LDCDZ2-66	99	7180	1.6	20.5219	0.8	0.1659	4.3	0.0247	4.2	0.98	157.3	6.5	155.9	6.2	134.8	19.3	157.3	6.5	NA
LDCDZ2-50	452	57189	1.5	19.1008	0.9	0.3134	1.3	0.0434	0.9	0.74	274.0	2.5	276.8	3.1	300.9	19.4	274.0	2.5	NA
LDCDZ2-35	661	59517	0.7	19.0840	1.2	0.3269	1.4	0.0452	0.8	0.54	285.3	2.1	287.2	3.5	302.9	26.8	285.3	2.1	NA
LDCDZ2-8	469	55044	2.8	19.1200	1.0	0.3278	1.3	0.0455	0.8	0.64	286.6	2.3	287.9	3.2	298.6	22.2	286.6	2.3	NA
LDCDZ2-56	201	18612	1.4	19.5019	1.0	0.3249	1.5	0.0460	1.1	0.75	289.6	3.2	285.7	3.7	253.3	22.7	289.6	3.2	NA
LDCDZ2-94	54	7640	1.4	17.4989	5.1	0.3743	5.3	0.0475	1.3	0.24	299.2	3.7	322.8	14.6	497.2	113.0	299.2	3.7	NA
LDCDZ2-R33	44	6225	1.4	18.1116	0.9	0.5000	1.7	0.0657	1.5	0.87	410.0	6.0	411.7	5.9	420.8	19.2	410.0	6.0	0%
LDCDZ2-R33	142	23303	0.8	18.1500	0.5	0.5186	1.4	0.0683	1.3	0.92	425.7	5.3	424.2	4.8	416.1	12.0	425.7	5.3	0%
LDCDZ2-90	22	5739	0.9	16.7546	0.8	0.7067	1.7	0.0859	1.5	0.88	531.1	7.4	542.8	6.9	592.2	16.8	531.1	7.4	2%
LDCDZ2-38	359	116584	8.4	13.6204	1.8	1.7692	2.1	0.1748	1.1	0.52	1038.3	10.6	1034.2	13.8	1025.5	37.0	1025.5	37.0	0%
LDCDZ2-74	133	54745	2.2	12.6274	1.0	2.1944	1.3	0.2010	0.8	0.64	1180.5	8.8	1179.3	8.9	1177.0	19.3	1177.0	19.3	0%
LDCDZ2-26	96	86577	1.1	5.8560	1.2	9.8836	1.9	0.4198	1.5	0.78	2259.4	28.2	2424.0	17.4	2565.1	19.6	2565.1	19.6	7%
Sample 17CCRT-29 (Río Turbio Formation - lower)																			
17CCRT1-29-167	55	624	2.5	37.7650	9.7	0.0220	10.5	0.0060	4.0	0.38	38.7	1.5	22.1	2.3	NA	NA	38.7	1.5	NA
17CCRT1-29-132	56	923	2.3	26.1073	5.9	0.0321	6.7	0.0061	3.2	0.48	39.0	1.3	32.0	2.1	NA	NA	39.0	1.3	NA
17CCRT1-29-105	58	1283	1.3	24.6131	4.7	0.0342	5.8	0.0061	3.4	0.59	39.2	1.3	34.1	1.9	NA	NA	39.2	1.3	NA
17CCRT1-29-190	55	1319	2.4	25.9131	11.4	0.0325	12.0	0.0061	3.7	0.31	39.3	1.4	32.5	3.8	NA	NA	39.3	1.4	NA
17CCRT1-29-150	41	1039	2.0	33.1663	6.6	0.0255	7.5	0.0061	3.4	0.46	39.4	1.3	25.6	1.9	NA	NA	39.4	1.3	NA
17CCRT1-29-137	57	767	1.2	33.8095	8.8	0.0250	9.4	0.0061	3.2	0.35	39.5	1.3	25.1	2.3	NA	NA	39.5	1.3	NA
17CCRT1-29-170	36	3965	3.3	26.7320	5.5	0.0317	6.3	0.0061	3.1	0.49	39.5	1.2	31.7	2.0	NA	NA	39.5	1.2	NA
17CCRT1-29-133	69	5913	2.4	21.6531	4.3	0.0394	5.1	0.0062	2.7	0.54	39.8	1.1	39.2	2.0	7.2	102.7	39.8	1.1	NA
17CCRT1-29-37	139	1305	2.2	27.5612	11.5	0.0313	11.8	0.0063	2.5	0.21	40.2	1.0	31.3	3.6	NA	NA	40.2	1.0	NA
17CCRT1-29-56	148	1646	2.0	22.4952	5.2	0.0384	5.8	0.0063	2.6	0.44	40.3	1.0	38.3	2.2	NA	NA	40.3	1.0	NA
17CCRT1-29-86	64	2655	2.9	25.4021	4.9	0.0340	5.9	0.0063	3.2	0.54	40.3	1.3	34.0	2.0	NA	NA	40.3	1.3	NA
17CCRT1-29-87	68	3858	2.4	18.2337	6.0	0.0475	6.4	0.0063	2.3	0.36	40.4	0.9	47.1	2.9	405.8	133.6	40.4	0.9	NA
17CCRT1-29-91	50	9835	2.5	22.5150	4.7	0.0385	5.7	0.0063	3.3	0.57	40.4	1.3	38.4	2.1	NA	NA	40.4	1.3	NA
17CCRT1-29-14	134	5561	1.6	20.1066	2.8	0.0434	3.7	0.0063	2.5	0.67	40.7	1.0	43.1	1.6	182.6	64.5	40.7	1.0	NA
17CCRT1-29-128	103	2548	2.3	22.1589	4.4	0.0394	5.3	0.0063	3.0	0.56	40.7	1.2	39.2	2.1	NA	NA	40.7	1.2	NA

17CCRT1-29-130	107	1093	2.5	28.7722	20.3	0.0303	20.5	0.0063	2.8	0.14	40.7	1.1	30.4	6.1	NA	NA	40.7	1.1	NA
17CCRT1-29-76	92	2589	3.1	24.0107	3.9	0.0365	4.8	0.0064	2.8	0.58	40.8	1.1	36.4	1.7	NA	NA	40.8	1.1	NA
17CCRT1-29-123	49	3294	1.9	24.8370	5.5	0.0353	6.4	0.0064	3.3	0.52	40.8	1.3	35.2	2.2	NA	NA	40.8	1.3	NA
17CCRT1-29-92	81	1305	1.5	27.8376	9.2	0.0316	9.6	0.0064	2.6	0.27	41.0	1.1	31.5	3.0	NA	NA	41.0	1.1	NA
17CCRT1-29-143	119	1042	1.7	28.9466	4.0	0.0303	4.9	0.0064	2.9	0.59	41.0	1.2	30.4	1.5	NA	NA	41.0	1.2	NA
17CCRT1-29-157	65	6899	2.0	24.8606	4.7	0.0354	5.6	0.0064	3.0	0.54	41.0	1.2	35.3	2.0	NA	NA	41.0	1.2	NA
17CCRT1-29-65	129	15209	1.9	20.4846	3.7	0.0430	4.9	0.0064	3.2	0.65	41.0	1.3	42.7	2.0	139.1	87.2	41.0	1.3	NA
17CCRT1-29-151	61	672	2.5	35.3153	6.7	0.0250	7.1	0.0064	2.3	0.33	41.1	0.9	25.0	1.8	NA	NA	41.1	0.9	NA
17CCRT1-29-113	107	3097	2.2	22.3107	3.3	0.0395	4.5	0.0064	3.1	0.69	41.1	1.3	39.4	1.7	NA	NA	41.1	1.3	NA
17CCRT1-29-75	93	6173	1.8	21.4261	3.7	0.0412	4.8	0.0064	3.0	0.64	41.1	1.2	41.0	1.9	32.5	88.1	41.1	1.2	NA
17CCRT1-29-138	87	20150	2.2	21.3760	4.1	0.0413	5.3	0.0064	3.2	0.61	41.1	1.3	41.1	2.1	38.1	99.2	41.1	1.3	NA
17CCRT1-29-95	91	3803	2.6	21.6368	4.4	0.0408	5.4	0.0064	3.1	0.58	41.2	1.3	40.6	2.1	9.0	105.8	41.2	1.3	NA
17CCRT1-29-52	76	2492	2.8	25.5276	4.8	0.0346	5.8	0.0064	3.3	0.56	41.2	1.3	34.6	2.0	NA	NA	41.2	1.3	NA
17CCRT1-29-15	75	1962	1.8	25.5564	5.3	0.0346	6.4	0.0064	3.6	0.56	41.2	1.5	34.6	2.2	NA	NA	41.2	1.5	NA
17CCRT1-29-1	273	7987	1.0	20.7307	3.1	0.0427	4.3	0.0064	2.9	0.68	41.3	1.2	42.5	1.8	110.9	73.9	41.3	1.2	NA
17CCRT1-29-168	216	5355	2.0	21.3603	3.3	0.0415	5.3	0.0064	4.2	0.78	41.3	1.7	41.3	2.2	39.9	79.3	41.3	1.7	NA
17CCRT1-29-156	86	1618	2.2	22.7484	11.2	0.0391	11.6	0.0064	3.2	0.28	41.4	1.3	38.9	4.4	NA	NA	41.4	1.3	NA
17CCRT1-29-152	46	903	3.0	48.2320	3.9	0.0184	5.6	0.0064	4.0	0.71	41.4	1.6	18.5	1.0	NA	NA	41.4	1.6	NA
17CCRT1-29-112	156	2549	2.6	22.9929	3.6	0.0387	4.4	0.0065	2.5	0.56	41.5	1.0	38.5	1.7	NA	NA	41.5	1.0	NA
17CCRT1-29-69	156	79793	1.4	20.4061	3.2	0.0436	4.2	0.0065	2.7	0.64	41.5	1.1	43.3	1.8	148.0	75.8	41.5	1.1	NA
17CCRT1-29-107	219	5170	1.6	21.5730	2.6	0.0413	3.6	0.0065	2.4	0.68	41.5	1.0	41.1	1.4	16.1	62.9	41.5	1.0	NA
17CCRT1-29-187	68	715	1.8	36.8952	10.1	0.0241	10.7	0.0065	3.5	0.33	41.5	1.5	24.2	2.6	NA	NA	41.5	1.5	NA
17CCRT1-29-189	55	758	2.2	26.6379	5.5	0.0334	6.4	0.0065	3.3	0.51	41.5	1.4	33.4	2.1	NA	NA	41.5	1.4	NA
17CCRT1-29-103	199	188095	1.5	19.6006	3.1	0.0456	4.2	0.0065	2.9	0.69	41.7	1.2	45.3	1.9	241.7	70.5	41.7	1.2	NA
17CCRT1-29-64	129	1422	1.5	21.1412	4.9	0.0423	5.5	0.0065	2.5	0.46	41.7	1.1	42.1	2.3	64.4	117.6	41.7	1.1	NA
17CCRT1-29-7	80	4663	2.3	21.4395	4.1	0.0418	5.0	0.0065	2.8	0.57	41.8	1.2	41.6	2.0	31.0	98.5	41.8	1.2	NA
17CCRT1-29-196	93	6023	1.3	20.5049	4.4	0.0438	5.1	0.0065	2.5	0.50	41.9	1.1	43.5	2.2	136.7	104.3	41.9	1.1	NA
17CCRT1-29-77	191	1806	1.7	23.8988	3.1	0.0377	4.1	0.0065	2.7	0.66	42.0	1.1	37.5	1.5	NA	NA	42.0	1.1	NA
17CCRT1-29-171	79	1764	2.3	22.4452	7.2	0.0401	7.8	0.0065	3.0	0.39	42.0	1.3	40.0	3.1	NA	NA	42.0	1.3	NA
17CCRT1-29-27	72	6401	1.6	22.3543	4.2	0.0403	5.0	0.0065	2.7	0.55	42.0	1.1	40.2	2.0	NA	NA	42.0	1.1	NA
17CCRT1-29-192	129	3267	1.5	22.5370	3.7	0.0401	4.7	0.0066	2.9	0.62	42.1	1.2	39.9	1.8	NA	NA	42.1	1.2	NA
17CCRT1-29-121	114	1445	1.4	26.5648	8.0	0.0340	8.4	0.0066	2.6	0.31	42.1	1.1	33.9	2.8	NA	NA	42.1	1.1	NA
17CCRT1-29-73	152	13115	1.7	19.9237	3.1	0.0454	4.4	0.0066	3.1	0.71	42.2	1.3	45.1	1.9	203.8	72.1	42.2	1.3	NA
17CCRT1-29-66	255	4662	1.5	22.0160	2.1	0.0411	3.2	0.0066	2.4	0.76	42.2	1.0	40.9	1.3	NA	NA	42.2	1.0	NA
17CCRT1-29-114	182	38543	1.0	18.8113	3.3	0.0482	4.1	0.0066	2.4	0.59	42.3	1.0	47.8	1.9	335.6	75.0	42.3	1.0	NA
17CCRT1-29-175	156	94883	3.3	19.6500	2.8	0.0463	4.0	0.0066	2.9	0.73	42.5	1.2	46.0	1.8	235.9	63.5	42.5	1.2	NA
17CCRT1-29-145	218	21957	1.9	19.7519	2.7	0.0462	3.2	0.0066	1.7	0.53	42.6	0.7	45.9	1.4	223.9	62.0	42.6	0.7	NA
17CCRT1-29-30	193	3031	2.7	23.0389	5.8	0.0397	6.0	0.0066	1.8	0.30	42.6	0.8	39.5	2.3	NA	NA	42.6	0.8	NA
17CCRT1-29-185	97	2718	1.3	25.3096	4.9	0.0361	5.5	0.0066	2.6	0.47	42.7	1.1	36.1	2.0	NA	NA	42.7	1.1	NA

17CCRT1-29-25	137	4968	1.3	22.9036	3.4	0.0401	4.4	0.0067	2.8	0.63	42.9	1.2	40.0	1.7	NA	NA	42.9	1.2	NA
17CCRT1-29-195	80	21567	2.0	21.1588	4.5	0.0438	5.2	0.0067	2.6	0.51	43.2	1.1	43.6	2.2	62.5	107.0	43.2	1.1	NA
17CCRT1-29-186	223	3404	2.3	21.2866	4.6	0.0449	5.1	0.0069	2.1	0.41	44.6	0.9	44.6	2.2	48.1	110.7	44.6	0.9	NA
17CCRT1-29-11	116	2873	1.3	22.9753	5.7	0.0425	6.3	0.0071	2.6	0.42	45.5	1.2	42.3	2.6	NA	NA	45.5	1.2	NA
17CCRT1-29-182	88	9259	1.0	19.9983	3.1	0.0638	4.6	0.0093	3.4	0.73	59.4	2.0	62.8	2.8	195.2	72.2	59.4	2.0	NA
17CCRT1-29-124	282	7827	0.9	20.1686	2.5	0.0783	3.5	0.0115	2.5	0.71	73.4	1.8	76.5	2.6	175.4	58.3	73.4	1.8	NA
17CCRT1-29-82	115	5086	1.0	18.1479	4.6	0.0882	5.2	0.0116	2.4	0.46	74.5	1.8	85.9	4.3	416.4	103.8	74.5	1.8	NA
17CCRT1-29-89	159	1743	0.8	24.9455	3.1	0.0646	4.0	0.0117	2.5	0.63	74.9	1.9	63.5	2.4	NA	NA	74.9	1.9	NA
17CCRT1-29-183	124	82661	0.9	20.7533	2.9	0.0776	3.6	0.0117	2.1	0.59	74.9	1.6	75.9	2.6	108.4	68.3	74.9	1.6	NA
17CCRT1-29-74	349	6995	0.8	21.4067	1.8	0.0754	3.2	0.0117	2.6	0.82	75.0	2.0	73.8	2.3	34.6	43.3	75.0	2.0	NA
17CCRT1-29-84	82	2638	0.8	23.6119	3.7	0.0691	4.5	0.0118	2.6	0.57	75.8	1.9	67.8	2.9	NA	NA	75.8	1.9	NA
17CCRT1-29-79	518	25486	0.8	20.6947	1.5	0.0790	2.9	0.0119	2.5	0.86	76.0	1.9	77.2	2.2	115.0	35.3	76.0	1.9	NA
17CCRT1-29-96	298	32245	1.2	18.7577	1.5	0.0874	3.0	0.0119	2.6	0.86	76.2	2.0	85.0	2.5	342.1	34.8	76.2	2.0	NA
17CCRT1-29-39	173	3805	0.7	22.1434	4.9	0.0744	5.3	0.0120	2.2	0.42	76.6	1.7	72.9	3.8	NA	NA	76.6	1.7	NA
17CCRT1-29-16	305	6002	0.8	20.3854	1.9	0.0813	2.8	0.0120	2.1	0.74	77.0	1.6	79.3	2.2	150.4	44.5	77.0	1.6	NA
17CCRT1-29-148	236	114837	1.2	21.1044	1.9	0.0796	3.2	0.0122	2.6	0.81	78.1	2.0	77.7	2.4	68.6	44.4	78.1	2.0	NA
17CCRT1-29-110	332	4126	0.7	21.4568	1.9	0.0789	3.1	0.0123	2.5	0.81	78.7	2.0	77.1	2.3	29.0	44.5	78.7	2.0	NA
17CCRT1-29-141	1141	62385	1.7	20.9253	1.5	0.0820	2.8	0.0125	2.3	0.84	79.8	1.9	80.0	2.1	88.9	36.0	79.8	1.9	NA
17CCRT1-29-80	138	1663	1.7	25.7861	2.2	0.0675	3.2	0.0126	2.3	0.73	80.9	1.9	66.3	2.1	NA	NA	80.9	1.9	NA
17CCRT1-29-54	489	9884	1.8	21.2812	1.8	0.0826	3.2	0.0128	2.7	0.83	81.7	2.2	80.6	2.5	48.7	43.3	81.7	2.2	NA
17CCRT1-29-118	159	11331	1.7	20.3665	1.7	0.0869	2.7	0.0128	2.0	0.76	82.2	1.6	84.6	2.2	152.6	40.7	82.2	1.6	NA
17CCRT1-29-139	204	54384	1.2	20.2416	1.9	0.0879	2.8	0.0129	2.1	0.74	82.7	1.7	85.5	2.3	167.0	44.8	82.7	1.7	NA
17CCRT1-29-181	69	2251	1.0	22.9641	4.2	0.0778	5.6	0.0130	3.7	0.66	83.0	3.0	76.1	4.1	NA	NA	83.0	3.0	NA
17CCRT1-29-127	389	9537	1.3	20.3565	1.6	0.0879	2.5	0.0130	1.8	0.75	83.1	1.5	85.5	2.0	153.8	37.8	83.1	1.5	NA
17CCRT1-29-174	224	15223	2.1	21.3844	1.8	0.0853	3.4	0.0132	2.9	0.85	84.7	2.4	83.1	2.7	37.1	42.9	84.7	2.4	NA
17CCRT1-29-120	100	14689	1.4	19.7455	3.4	0.0928	4.2	0.0133	2.4	0.57	85.1	2.0	90.1	3.6	224.7	79.6	85.1	2.0	NA
17CCRT1-29-146	115	5932	1.5	22.0755	3.6	0.0831	4.1	0.0133	2.1	0.52	85.3	1.8	81.1	3.2	NA	NA	85.3	1.8	NA
17CCRT1-29-117	97	16103	1.3	20.3135	2.6	0.0906	3.5	0.0134	2.4	0.69	85.5	2.1	88.0	3.0	158.7	59.8	85.5	2.1	NA
17CCRT1-29-58	148	2599	1.2	21.9531	5.1	0.0839	5.5	0.0134	2.1	0.38	85.5	1.8	81.8	4.4	NA	NA	85.5	1.8	NA
17CCRT1-29-164	130	9334	0.7	19.6717	3.2	0.0944	4.0	0.0135	2.4	0.61	86.2	2.1	91.6	3.5	233.3	73.0	86.2	2.1	NA
17CCRT1-29-126	191	3410	1.0	23.0885	3.5	0.0807	4.0	0.0135	2.0	0.50	86.6	1.7	78.8	3.0	NA	NA	86.6	1.7	NA
17CCRT1-29-24	185	36257	0.8	20.0818	2.1	0.0934	3.0	0.0136	2.2	0.73	87.2	1.9	90.7	2.6	185.5	48.3	87.2	1.9	NA
17CCRT1-29-45	220	61871	0.8	20.7417	2.1	0.0915	3.1	0.0138	2.3	0.73	88.2	2.0	88.9	2.6	109.7	50.5	88.2	2.0	NA
17CCRT1-29-154	313	9739	1.7	21.2032	1.7	0.0895	3.3	0.0138	2.8	0.85	88.2	2.4	87.1	2.7	57.5	40.9	88.2	2.4	NA
17CCRT1-29-72	71	108982	2.2	19.7021	3.0	0.0973	4.2	0.0139	3.0	0.71	89.1	2.6	94.3	3.8	229.7	69.4	89.1	2.6	NA
17CCRT1-29-17	53	6776	2.0	19.7629	3.4	0.0981	4.3	0.0141	2.7	0.62	90.1	2.4	95.0	3.9	222.6	78.8	90.1	2.4	NA
17CCRT1-29-28	265	11008	1.1	20.9030	2.0	0.0930	2.8	0.0141	1.9	0.68	90.2	1.7	90.3	2.4	91.4	48.0	90.2	1.7	NA
17CCRT1-29-109	80	2142	1.5	24.1584	4.0	0.0804	4.6	0.0141	2.2	0.48	90.2	2.0	78.5	3.5	NA	NA	90.2	2.0	NA
17CCRT1-29-18	353	7816	3.7	21.1980	2.6	0.0918	3.3	0.0141	2.1	0.62	90.3	1.9	89.1	2.9	58.0	62.6	90.3	1.9	NA

17CCRT1-29-48	104	2262	1.0	22.2368	3.9	0.0882	4.7	0.0142	2.6	0.56	91.1	2.4	85.8	3.9	NA	NA	91.1	2.4	NA
17CCRT1-29-198	100	11498	1.2	20.2865	2.8	0.0987	3.6	0.0145	2.3	0.64	93.0	2.1	95.6	3.3	161.8	64.4	93.0	2.1	NA
17CCRT1-29-13	189	7203	2.7	20.3360	2.0	0.0986	2.9	0.0145	2.0	0.71	93.1	1.9	95.5	2.6	156.1	47.2	93.1	1.9	NA
17CCRT1-29-71	93	3877	2.0	21.5304	2.3	0.0948	3.8	0.0148	3.0	0.79	94.7	2.8	91.9	3.3	20.8	55.2	94.7	2.8	NA
17CCRT1-29-9	350	5519	2.0	21.0451	1.5	0.0978	2.3	0.0149	1.8	0.76	95.6	1.7	94.8	2.1	75.3	36.1	95.6	1.7	NA
17CCRT1-29-38	100	2240	2.5	21.4990	7.7	0.0958	8.1	0.0149	2.5	0.31	95.6	2.4	92.9	7.2	24.3	185.3	95.6	2.4	NA
17CCRT1-29-173	64	1231	2.4	26.6929	3.3	0.0772	4.1	0.0150	2.4	0.60	95.7	2.3	75.5	3.0	NA	NA	95.7	2.3	NA
17CCRT1-29-116	94	8408	2.4	19.9246	2.6	0.1040	3.4	0.0150	2.1	0.63	96.2	2.0	100.5	3.2	203.7	61.4	96.2	2.0	NA
17CCRT1-29-142	54	21142	2.2	20.0182	3.3	0.1037	4.1	0.0151	2.4	0.58	96.4	2.3	100.2	3.9	192.9	76.5	96.4	2.3	NA
17CCRT1-29-188	66	7845	2.4	21.4129	3.9	0.0970	4.7	0.0151	2.5	0.54	96.4	2.4	94.0	4.2	34.0	93.9	96.4	2.4	NA
17CCRT1-29-81	102	86257	2.9	14.7134	5.4	0.1414	6.0	0.0151	2.5	0.42	96.6	2.4	134.3	7.5	867.5	112.1	96.6	2.4	NA
17CCRT1-29-5	147	24110	1.4	19.3372	1.8	0.1077	2.9	0.0151	2.3	0.79	96.7	2.2	103.9	2.9	272.7	41.0	96.7	2.2	NA
17CCRT1-29-60	136	4116	1.9	21.8939	3.0	0.0951	4.2	0.0151	3.0	0.71	96.7	2.9	92.3	3.7	NA	NA	96.7	2.9	NA
17CCRT1-29-165	63	2458	2.5	24.2514	4.0	0.0862	4.7	0.0152	2.6	0.55	97.1	2.5	84.0	3.8	NA	NA	97.1	2.5	NA
17CCRT1-29-125	127	3790	1.2	21.9182	3.0	0.0955	3.8	0.0152	2.2	0.59	97.2	2.1	92.6	3.3	NA	NA	97.2	2.1	NA
17CCRT1-29-147	124	4792	2.2	20.8710	3.4	0.1008	4.2	0.0153	2.4	0.58	97.7	2.4	97.5	3.9	95.0	80.9	97.7	2.4	NA
17CCRT1-29-31	104	4324	1.2	20.7101	2.8	0.1017	3.8	0.0153	2.6	0.68	97.8	2.5	98.3	3.6	113.3	66.2	97.8	2.5	NA
17CCRT1-29-191	165	4583	1.2	22.3375	2.3	0.0943	3.6	0.0153	2.8	0.78	97.8	2.7	91.5	3.1	NA	NA	97.8	2.7	NA
17CCRT1-29-119	74	3453	1.8	20.7167	5.2	0.1018	5.6	0.0153	2.2	0.39	97.9	2.1	98.5	5.3	112.5	122.6	97.9	2.1	NA
17CCRT1-29-49	42	1447	1.9	28.0987	11.3	0.0759	11.6	0.0155	2.8	0.24	99.0	2.8	74.3	8.3	NA	NA	99.0	2.8	NA
17CCRT1-29-68	216	14339	1.4	20.1980	1.9	0.1061	3.5	0.0155	2.9	0.84	99.4	2.9	102.4	3.4	172.0	43.5	99.4	2.9	NA
17CCRT1-29-34	445	40025	1.2	20.4354	1.5	0.1050	2.6	0.0156	2.1	0.82	99.6	2.1	101.4	2.5	144.7	34.7	99.6	2.1	NA
17CCRT1-29-102	160	32083	1.4	20.3168	1.9	0.1057	2.6	0.0156	1.8	0.70	99.7	1.8	102.0	2.5	158.3	43.6	99.7	1.8	NA
17CCRT1-29-12	96	12304	2.3	17.0754	2.4	0.1263	3.4	0.0156	2.4	0.71	100.1	2.4	120.7	3.8	550.9	51.6	100.1	2.4	NA
17CCRT1-29-33	119	1771	2.6	22.4153	2.3	0.0965	3.4	0.0157	2.5	0.73	100.4	2.4	93.5	3.0	NA	NA	100.4	2.4	NA
17CCRT1-29-178	67	2572	1.7	21.5706	4.9	0.1004	5.3	0.0157	2.0	0.39	100.5	2.0	97.1	4.9	16.3	117.1	100.5	2.0	NA
17CCRT1-29-159	91	28381	1.7	20.6623	2.7	0.1049	3.6	0.0157	2.5	0.68	100.6	2.5	101.3	3.5	118.7	63.3	100.6	2.5	NA
17CCRT1-29-61	272	6788	2.1	21.1944	1.7	0.1024	2.8	0.0158	2.2	0.79	100.8	2.2	99.0	2.6	58.5	40.8	100.8	2.2	NA
17CCRT1-29-197	64	115127	2.2	14.4363	4.3	0.1505	5.0	0.0158	2.6	0.51	100.8	2.6	142.4	6.7	906.8	89.5	100.8	2.6	NA
17CCRT1-29-78	165	2589	2.2	22.8288	4.2	0.0953	5.1	0.0158	3.0	0.59	101.0	3.0	92.4	4.5	NA	NA	101.0	3.0	NA
17CCRT1-29-6	48	3366	2.2	18.6284	3.3	0.1169	4.8	0.0158	3.5	0.73	101.1	3.5	112.3	5.1	357.7	73.5	101.1	3.5	NA
17CCRT1-29-50	88	1799	1.8	23.4850	3.2	0.0934	4.0	0.0159	2.4	0.60	101.8	2.4	90.7	3.5	NA	NA	101.8	2.4	NA
17CCRT1-29-193	125	10578	1.3	20.2002	2.1	0.1087	3.8	0.0159	3.2	0.84	101.9	3.3	104.8	3.8	171.8	48.4	101.9	3.3	NA
17CCRT1-29-106	148	32969	0.9	19.9440	1.7	0.1103	2.7	0.0160	2.1	0.77	102.0	2.1	106.2	2.7	201.5	39.1	102.0	2.1	NA
17CCRT1-29-153	130	12951	1.4	20.3432	2.7	0.1084	3.9	0.0160	2.7	0.71	102.3	2.8	104.5	3.8	155.3	64.1	102.3	2.8	NA
17CCRT1-29-162	101	9094	0.9	21.1477	2.7	0.1043	3.6	0.0160	2.4	0.66	102.4	2.4	100.8	3.4	63.7	64.6	102.4	2.4	NA
17CCRT1-29-62	108	7552	2.1	17.9892	3.9	0.1231	5.0	0.0161	3.1	0.62	102.8	3.2	117.9	5.5	436.0	87.0	102.8	3.2	NA
17CCRT1-29-21	71	14923	1.3	19.5008	2.4	0.1138	3.4	0.0161	2.4	0.71	103.0	2.5	109.5	3.6	253.4	55.9	103.0	2.5	NA
17CCRT1-29-199	92	4797	1.2	21.3508	3.0	0.1040	3.9	0.0161	2.5	0.65	103.1	2.6	100.5	3.7	40.9	71.0	103.1	2.6	NA

17CCRT1-29-67	343	18242	1.6	20.6939	1.5	0.1079	2.9	0.0162	2.5	0.86	103.6	2.6	104.1	2.9	115.2	35.3	103.6	2.6	NA
17CCRT1-29-23	197	28523	1.1	20.1117	1.7	0.1113	3.5	0.0162	3.1	0.87	103.8	3.1	107.1	3.6	182.0	39.6	103.8	3.1	NA
17CCRT1-29-176	79	7522	1.6	20.0467	3.5	0.1117	3.9	0.0162	1.8	0.46	103.9	1.9	107.5	4.0	189.5	81.0	103.9	1.9	NA
17CCRT1-29-35	111	3836	2.2	22.7104	3.4	0.0991	4.4	0.0163	2.8	0.64	104.4	2.9	96.0	4.0	NA	NA	104.4	2.9	NA
17CCRT1-29-194	827	689036	4.6	20.4220	1.3	0.1103	2.7	0.0163	2.4	0.88	104.5	2.5	106.3	2.7	146.3	29.7	104.5	2.5	NA
17CCRT1-29-40	126	16159	1.5	19.4632	2.5	0.1159	3.4	0.0164	2.3	0.68	104.6	2.4	111.3	3.5	257.8	56.9	104.6	2.4	NA
17CCRT1-29-140	85	14371	1.4	19.3590	2.4	0.1166	3.3	0.0164	2.2	0.69	104.7	2.3	112.0	3.5	270.2	54.5	104.7	2.3	NA
17CCRT1-29-70	226	16000	1.1	20.5259	2.0	0.1112	3.2	0.0166	2.5	0.78	105.9	2.6	107.1	3.3	134.3	47.5	105.9	2.6	NA
17CCRT1-29-134	252	3423	2.4	21.7930	5.0	0.1056	5.4	0.0167	2.2	0.40	106.7	2.3	101.9	5.3	NA	NA	106.7	2.3	NA
17CCRT1-29-172	377	6167	2.8	20.9287	2.7	0.1106	3.5	0.0168	2.2	0.63	107.4	2.4	106.5	3.6	88.5	64.8	107.4	2.4	NA
17CCRT1-29-29	239	72423	1.8	20.5079	1.8	0.1132	2.7	0.0168	2.0	0.76	107.7	2.2	108.9	2.8	136.4	41.4	107.7	2.2	NA
17CCRT1-29-63	300	7077	2.5	16.2011	3.9	0.1436	4.5	0.0169	2.2	0.50	107.9	2.4	136.2	5.7	664.6	82.6	107.9	2.4	NA
17CCRT1-29-163	867	98532	2.3	20.4179	1.5	0.1152	3.2	0.0171	2.8	0.87	109.1	3.0	110.7	3.3	146.7	36.2	109.1	3.0	NA
17CCRT1-29-10	203	27246	1.6	20.1356	2.0	0.1170	3.1	0.0171	2.3	0.75	109.3	2.5	112.4	3.2	179.2	46.7	109.3	2.5	NA
17CCRT1-29-42	101	4802	2.2	22.0369	3.1	0.1083	3.8	0.0173	2.2	0.58	110.7	2.4	104.4	3.8	NA	NA	110.7	2.4	NA
17CCRT1-29-122	200	15268	2.0	21.0924	1.5	0.1174	2.8	0.0180	2.3	0.83	114.8	2.6	112.7	3.0	70.0	36.7	114.8	2.6	NA
17CCRT1-29-94	663	50042	1.0	20.6551	1.4	0.1282	2.4	0.0192	2.0	0.82	122.7	2.4	122.5	2.8	119.6	32.8	122.7	2.4	NA
17CCRT1-29-155	155	10758	1.8	20.9752	1.9	0.1282	3.2	0.0195	2.6	0.82	124.6	3.2	122.5	3.7	83.2	44.0	124.6	3.2	NA
17CCRT1-29-111	76	10053	2.2	20.2637	3.3	0.1339	4.3	0.0197	2.8	0.64	125.7	3.4	127.6	5.2	164.4	78.1	125.7	3.4	NA
17CCRT1-29-43	230	9266	2.1	20.5251	1.3	0.1328	2.5	0.0198	2.1	0.85	126.3	2.6	126.6	2.9	134.4	31.1	126.3	2.6	NA
17CCRT1-29-85	486	21341	1.0	20.3404	1.2	0.1352	2.4	0.0200	2.0	0.86	127.3	2.5	128.7	2.9	155.6	28.6	127.3	2.5	NA
17CCRT1-29-136	1095	427416	1.2	20.4627	1.3	0.1352	2.4	0.0201	2.0	0.84	128.1	2.6	128.8	2.9	141.6	30.6	128.1	2.6	NA
17CCRT1-29-41	122	7023	2.5	21.3511	2.9	0.1304	3.9	0.0202	2.6	0.66	128.9	3.3	124.4	4.5	40.9	69.1	128.9	3.3	NA
17CCRT1-29-97	199	6832	2.2	20.5977	2.4	0.1356	3.4	0.0203	2.5	0.72	129.3	3.1	129.1	4.2	126.1	56.3	129.3	3.1	NA
17CCRT1-29-160	208	4957	1.2	21.1839	1.7	0.1399	2.6	0.0215	1.9	0.75	137.2	2.6	133.0	3.2	59.7	40.7	137.2	2.6	NA
17CCRT1-29-19	471	5580	1.1	14.8497	2.7	0.2023	3.7	0.0218	2.6	0.70	139.0	3.6	187.0	6.3	848.3	55.3	139.0	3.6	NA
17CCRT1-29-99	94	2625	1.5	21.3969	2.8	0.1445	3.6	0.0224	2.3	0.64	143.1	3.3	137.1	4.6	35.7	66.6	143.1	3.3	NA
17CCRT1-29-20	261	9176	1.2	20.7212	1.9	0.1528	3.3	0.0230	2.7	0.82	146.4	3.9	144.3	4.5	112.0	44.9	146.4	3.9	NA
17CCRT1-29-47	387	105990	1.9	20.3586	1.4	0.1583	2.5	0.0234	2.1	0.83	149.0	3.1	149.2	3.5	153.5	32.8	149.0	3.1	NA
17CCRT1-29-108	334	97602	2.4	19.9965	1.3	0.1641	2.5	0.0238	2.1	0.84	151.7	3.1	154.3	3.5	195.4	31.2	151.7	3.1	NA
17CCRT1-29-57	667	260074	2.1	20.1917	0.9	0.1641	2.7	0.0240	2.5	0.95	153.1	3.9	154.3	3.8	172.8	20.0	153.1	3.9	NA
17CCRT1-29-4	592	57660	1.9	19.7684	1.3	0.1692	2.6	0.0243	2.3	0.87	154.5	3.5	158.7	3.8	222.0	29.5	154.5	3.5	NA
17CCRT1-29-115	388	26623	2.8	20.4660	1.6	0.1638	2.8	0.0243	2.3	0.82	155.0	3.6	154.1	4.0	141.2	37.6	155.0	3.6	NA
17CCRT1-29-8	200	18494	0.5	19.8380	1.6	0.2285	3.0	0.0329	2.6	0.85	208.7	5.3	209.0	5.7	213.9	36.5	208.7	5.3	NA
17CCRT1-29-129	195	21025	1.0	19.2909	1.4	0.3015	2.4	0.0422	2.0	0.82	266.4	5.1	267.5	5.6	278.3	31.7	266.4	5.1	NA
17CCRT1-29-59	205	72082	3.0	18.9600	1.2	0.3158	2.7	0.0434	2.4	0.89	274.1	6.5	278.7	6.6	317.7	28.0	274.1	6.5	NA
17CCRT1-29-179	361	131553	1.9	18.9768	1.2	0.3177	2.9	0.0437	2.6	0.91	276.0	7.1	280.1	7.1	315.7	26.7	276.0	7.1	NA
17CCRT1-29-26	241	19109	1.3	19.3530	1.2	0.3187	2.8	0.0448	2.5	0.90	282.3	7.0	280.9	6.9	270.9	27.6	282.3	7.0	NA
17CCRT1-29-100	63	9837	1.7	18.5282	1.7	0.3579	3.2	0.0481	2.7	0.84	302.9	7.9	310.6	8.5	369.9	38.5	302.9	7.9	NA

17CCRT1-29-184	78	59594	1.4	18.4637	1.9	0.3619	2.7	0.0485	1.9	0.69	305.2	5.6	313.6	7.3	377.7	43.8	305.2	5.6	NA
17CCRT1-29-32	207	84686	1.9	18.4626	1.4	0.3657	2.9	0.0490	2.6	0.88	308.3	7.8	316.5	7.9	377.8	30.6	308.3	7.8	NA
17CCRT1-29-90	96	27687	1.2	18.1603	1.2	0.3938	2.9	0.0519	2.6	0.91	326.1	8.3	337.1	8.2	414.9	26.6	326.1	8.3	NA
17CCRT1-29-53	133	21983	1.6	18.1290	1.5	0.4379	2.8	0.0576	2.3	0.85	361.0	8.2	368.8	8.6	418.7	32.9	361.0	8.2	NA
17CCRT1-29-149	142	163056	9.4	17.9455	1.2	0.4507	2.6	0.0587	2.3	0.88	367.7	8.2	377.8	8.2	441.4	27.6	367.7	8.2	NA
17CCRT1-29-131	1341	523134	3.9	18.3683	1.0	0.4537	2.6	0.0605	2.4	0.93	378.5	8.8	379.9	8.2	389.3	21.9	378.5	8.8	NA
17CCRT1-29-177	804	103986	2.1	18.3294	0.9	0.4832	2.8	0.0643	2.6	0.95	401.5	10.2	400.3	9.2	394.1	19.9	401.5	10.2	0%
17CCRT1-29-104	276	95228	1.9	17.3052	1.0	0.6557	2.5	0.0823	2.3	0.92	510.0	11.4	512.0	10.2	521.6	22.0	510.0	11.4	0%
17CCRT1-29-88	363	69314	1.8	17.2265	1.1	0.6667	2.5	0.0833	2.2	0.89	515.9	10.9	518.7	10.0	531.7	24.8	515.9	10.9	1%
17CCRT1-29-135	1083	77501	3.5	17.2786	1.0	0.6759	2.5	0.0847	2.3	0.91	524.3	11.4	524.3	10.2	525.0	22.4	524.3	11.4	0%
17CCRT1-29-98	151	1708349	1.1	17.2095	1.1	0.6821	2.4	0.0852	2.1	0.88	526.9	10.6	528.0	9.8	533.8	24.8	526.9	10.6	0%
17CCRT1-29-101	438	96857	1.1	16.9432	1.2	0.7016	2.7	0.0862	2.4	0.89	533.3	12.2	539.7	11.2	567.9	27.1	533.3	12.2	1%
17CCRT1-29-161	356	195433	7.4	16.9395	1.1	0.7207	2.9	0.0886	2.7	0.93	547.1	14.2	551.1	12.4	568.4	23.3	547.1	14.2	1%
17CCRT1-29-36	109	19651	1.8	16.9906	1.1	0.7259	2.1	0.0895	1.8	0.84	552.5	9.4	554.1	9.0	561.8	24.8	552.5	9.4	0%
17CCRT1-29-83	535	127030	4.0	15.9773	1.4	0.7789	3.5	0.0903	3.2	0.92	557.3	17.2	584.8	15.6	694.3	28.8	557.3	17.2	5%
17CCRT1-29-158	310	119933	0.7	16.7875	1.1	0.7536	2.3	0.0918	2.0	0.88	566.2	11.0	570.3	10.1	587.9	23.9	566.2	11.0	1%
17CCRT1-29-44	712	448187	9.8	16.8772	1.1	0.7524	2.4	0.0921	2.2	0.89	568.2	11.8	569.6	10.6	576.3	24.0	568.2	11.8	0%
17CCRT1-29-51	72	39280	1.0	16.2808	1.5	0.8114	3.1	0.0959	2.7	0.87	590.0	15.3	603.2	14.2	654.1	32.7	590.0	15.3	2%
17CCRT1-29-22	298	360741	1.4	16.3552	1.1	0.8317	2.8	0.0987	2.6	0.92	606.8	14.8	614.6	12.8	644.3	22.7	606.8	14.8	1%
17CCRT1-29-55	1378	175392	14.2	16.2258	1.2	0.8508	2.6	0.1002	2.4	0.90	615.4	13.9	625.1	12.3	661.3	24.9	615.4	13.9	2%
17CCRT1-29-180	428	106913	2.6	16.4913	1.2	0.8585	2.8	0.1027	2.6	0.91	630.4	15.5	629.3	13.3	626.4	25.1	630.4	15.5	0%
17CCRT1-29-46	419	3715710	4.1	15.4543	0.8	0.9489	2.7	0.1064	2.6	0.95	651.8	16.0	677.5	13.4	764.8	17.2	651.8	16.0	4%
17CCRT1-29-144	269	91914	1.0	13.6134	1.0	1.6189	1.9	0.1599	1.7	0.87	956.3	15.0	977.6	12.2	1026.6	19.5	1026.6	19.5	2%
17CCRT1-29-169	195	1537466	1.0	12.1545	1.0	2.4100	2.4	0.2125	2.1	0.90	1242.3	24.0	1245.6	16.9	1252.1	19.8	1252.1	19.8	0%
17CCRT1-29-3	79	1174435	2.4	8.9228	1.0	5.0156	2.8	0.3247	2.7	0.94	1812.7	42.4	1822.0	24.1	1833.3	17.3	1833.3	17.3	1%
17CCRT1-29-2	445	595085	1.2	7.1090	1.1	7.8407	2.6	0.4044	2.4	0.91	2189.4	44.1	2212.9	23.4	2235.4	18.4	2235.4	18.4	1%
17CCRT1-29-93	144	213536	0.8	5.6606	1.2	11.2404	2.6	0.4617	2.2	0.88	2446.9	45.7	2543.3	23.8	2621.7	20.5	2621.7	20.5	4%
17CCRT1-29-200	240	170607	1.8	5.3368	1.2	12.9670	2.8	0.5021	2.6	0.91	2622.9	55.7	2677.3	26.7	2719.3	19.2	2719.3	19.2	2%
Sample RT28DZ8 (Río Turbio Formation - upper)																			
RT28DZ8-104	27	374	2.1	23.8335	4.7	0.0300	4.9	0.0052	1.7	0.34	33.4	0.6	30.0	1.5	-229.0	117.2	33.4	0.6	NA
RT28DZ8-103	48	670	2.3	21.5681	2.9	0.0332	3.1	0.0052	0.9	0.31	33.4	0.3	33.1	1.0	16.6	70.3	33.4	0.3	NA
RT28DZ8-97	18	264	2.6	25.4211	8.7	0.0282	9.3	0.0052	3.2	0.35	33.4	1.1	28.2	2.6	-394.3	227.6	33.4	1.1	NA
RT28DZ8-100	40	652	2.2	20.8772	3.2	0.0350	4.7	0.0053	3.4	0.73	34.1	1.2	34.9	1.6	94.3	76.1	34.1	1.2	NA
RT28DZ8-95	101	1661	1.7	21.1167	3.1	0.0352	4.7	0.0054	3.5	0.75	34.6	1.2	35.1	1.6	67.2	74.0	34.6	1.2	NA
RT28DZ8-89	75	1884	1.8	20.8615	3.3	0.0356	3.6	0.0054	1.4	0.40	34.7	0.5	35.6	1.2	96.1	77.5	34.7	0.5	NA
RT28DZ8-93	53	694	2.1	22.7892	4.2	0.0327	4.7	0.0054	2.0	0.43	34.7	0.7	32.7	1.5	-117.4	103.7	34.7	0.7	NA
RT28DZ8-94	56	862	1.6	21.2602	3.5	0.0351	3.6	0.0054	0.8	0.21	34.8	0.3	35.0	1.2	51.1	84.4	34.8	0.3	NA
RT28DZ8-92	88	2210	1.7	20.7248	4.3	0.0360	7.6	0.0054	6.3	0.83	34.8	2.2	36.0	2.7	111.6	100.4	34.8	2.2	NA

RT28DZ8-12	42	667	2.2	21.2078	3.9	0.0353	4.8	0.0054	2.8	0.57	34.9	1.0	35.2	1.7	56.9	93.7	34.9	1.0	NA
RT28DZ8-106	47	1079	2.2	19.5937	4.3	0.0382	4.5	0.0054	1.3	0.29	34.9	0.4	38.1	1.7	242.5	98.5	34.9	0.4	NA
RT28DZ8-11	45	1382	2.2	19.3988	5.2	0.0389	6.1	0.0055	3.1	0.51	35.2	1.1	38.7	2.3	265.5	120.3	35.2	1.1	NA
RT28DZ8-24	65	4701	1.7	18.9874	4.3	0.0397	4.9	0.0055	2.4	0.49	35.2	0.8	39.6	1.9	314.5	97.6	35.2	0.8	NA
RT28DZ8-20	35	801	1.7	19.6467	3.7	0.0385	3.9	0.0055	1.1	0.27	35.3	0.4	38.3	1.5	236.3	86.3	35.3	0.4	NA
RT28DZ8-84	58	1259	1.5	21.5810	4.9	0.0351	5.3	0.0055	1.9	0.37	35.3	0.7	35.0	1.8	15.2	118.2	35.3	0.7	NA
RT28DZ8-82	89	1871	1.7	20.8973	2.7	0.0363	3.1	0.0055	1.5	0.49	35.4	0.5	36.2	1.1	92.0	63.5	35.4	0.5	NA
RT28DZ8-87	41	753	1.5	22.0865	3.4	0.0344	3.7	0.0055	1.3	0.36	35.4	0.5	34.3	1.2	-40.7	83.5	35.4	0.5	NA
RT28DZ8-70	44	695	2.3	21.6604	1.7	0.0352	2.0	0.0055	1.1	0.54	35.5	0.4	35.1	0.7	6.4	41.0	35.5	0.4	NA
RT28DZ8-27	61	1002	2.0	20.9123	4.8	0.0365	5.0	0.0055	1.5	0.29	35.6	0.5	36.4	1.8	90.3	114.5	35.6	0.5	NA
RT28DZ8-26	94	1289	1.6	21.8769	2.0	0.0349	3.1	0.0055	2.3	0.75	35.6	0.8	34.9	1.0	-17.6	48.4	35.6	0.8	NA
RT28DZ8-22	117	2156	1.5	21.3744	2.4	0.0358	2.5	0.0055	0.9	0.34	35.7	0.3	35.7	0.9	38.2	56.4	35.7	0.3	NA
RT28DZ8-77	54	1166	1.3	20.9944	2.9	0.0365	3.7	0.0056	2.4	0.63	35.7	0.8	36.4	1.3	81.0	68.7	35.7	0.8	NA
RT28DZ8-14	50	1178	2.2	20.6718	2.7	0.0371	2.9	0.0056	0.9	0.30	35.7	0.3	37.0	1.0	117.7	64.4	35.7	0.3	NA
RT28DZ8-16	69	1182	1.4	21.7320	5.3	0.0353	5.5	0.0056	1.3	0.24	35.7	0.5	35.2	1.9	-1.6	128.0	35.7	0.5	NA
RT28DZ8-17	95	1313	1.3	21.8967	3.2	0.0351	3.6	0.0056	1.6	0.43	35.8	0.6	35.0	1.2	-19.8	78.5	35.8	0.6	NA
RT28DZ8-28	37	632	2.3	21.8888	2.7	0.0351	3.0	0.0056	1.1	0.37	35.8	0.4	35.0	1.0	-18.9	66.5	35.8	0.4	NA
RT28DZ8-71	80	1340	1.8	21.1674	4.4	0.0364	4.7	0.0056	1.7	0.36	35.9	0.6	36.3	1.7	61.5	103.8	35.9	0.6	NA
RT28DZ8-15	50	1156	1.4	19.8214	4.7	0.0388	4.9	0.0056	1.4	0.29	35.9	0.5	38.7	1.9	215.8	108.9	35.9	0.5	NA
RT28DZ8-34	74	1339	2.1	20.5126	3.7	0.0376	3.8	0.0056	1.0	0.27	35.9	0.4	37.4	1.4	135.8	86.0	35.9	0.4	NA
RT28DZ8-64	52	925	2.1	20.5142	3.6	0.0376	3.6	0.0056	0.6	0.17	36.0	0.2	37.5	1.3	135.6	84.3	36.0	0.2	NA
RT28DZ8-31	81	2666	1.7	20.2303	2.4	0.0382	3.3	0.0056	2.3	0.69	36.0	0.8	38.0	1.2	168.3	55.6	36.0	0.8	NA
RT28DZ8-91	124	3183	1.5	21.0618	2.2	0.0367	2.3	0.0056	0.7	0.32	36.0	0.3	36.6	0.8	73.4	52.1	36.0	0.3	NA
RT28DZ8-23	86	1325	1.6	21.1103	1.4	0.0366	2.4	0.0056	1.9	0.82	36.1	0.7	36.5	0.8	68.0	32.2	36.1	0.7	NA
RT28DZ8-61	88	1606	1.6	21.1273	2.5	0.0368	2.6	0.0056	0.6	0.23	36.2	0.2	36.7	0.9	66.0	59.7	36.2	0.2	NA
RT28DZ8-43	23	694	1.4	21.1860	6.6	0.0367	7.1	0.0056	2.5	0.36	36.2	0.9	36.6	2.6	59.4	158.5	36.2	0.9	NA
RT28DZ8-39	30	801	2.7	19.4374	3.4	0.0400	3.6	0.0056	1.3	0.35	36.2	0.5	39.8	1.4	260.9	77.6	36.2	0.5	NA
RT28DZ8-50	76	1315	1.8	21.2343	2.5	0.0366	2.8	0.0056	1.3	0.47	36.3	0.5	36.5	1.0	54.0	59.7	36.3	0.5	NA
RT28DZ8-44	57	4486	2.1	19.1600	4.1	0.0407	4.7	0.0057	2.3	0.49	36.4	0.8	40.5	1.9	293.8	92.8	36.4	0.8	NA
RT28DZ8-83	98	1432	1.5	21.7808	3.6	0.0358	3.7	0.0057	0.9	0.26	36.4	0.3	35.8	1.3	-7.0	85.7	36.4	0.3	NA
RT28DZ8-88	154	2865	1.4	20.7045	1.6	0.0378	2.1	0.0057	1.4	0.66	36.5	0.5	37.6	0.8	113.9	37.6	36.5	0.5	NA
RT28DZ8-41	46	867	1.9	21.0810	1.9	0.0373	2.2	0.0057	1.1	0.48	36.6	0.4	37.1	0.8	71.2	46.2	36.6	0.4	NA
RT28DZ8-49	92	2630	1.8	20.2659	2.6	0.0388	2.7	0.0057	0.8	0.28	36.7	0.3	38.7	1.0	164.2	60.7	36.7	0.3	NA
RT28DZ8-73	74	1315	2.2	21.5666	2.7	0.0365	3.2	0.0057	1.6	0.52	36.7	0.6	36.4	1.1	16.8	65.1	36.7	0.6	NA
RT28DZ8-76	59	859	1.5	21.4556	4.1	0.0367	4.6	0.0057	2.1	0.45	36.7	0.8	36.6	1.7	29.2	98.3	36.7	0.8	NA
RT28DZ8-13	523	9252	1.1	21.1121	1.1	0.0373	2.1	0.0057	1.8	0.86	36.8	0.7	37.2	0.8	67.7	26.1	36.8	0.7	NA
RT28DZ8-21	85	1592	1.9	20.6825	3.5	0.0381	3.6	0.0057	0.8	0.24	36.8	0.3	38.0	1.3	116.4	82.0	36.8	0.3	NA
RT28DZ8-99	252	4288	1.3	20.3501	2.3	0.0390	2.7	0.0058	1.5	0.56	37.0	0.6	38.9	1.0	154.5	53.1	37.0	0.6	NA
RT28DZ8-85	125	3192	1.3	20.8308	2.6	0.0381	2.7	0.0058	0.7	0.26	37.0	0.3	38.0	1.0	99.6	60.6	37.0	0.3	NA

RT28DZ8-102	188	4769	1.4	20.8444	1.3	0.0381	2.5	0.0058	2.1	0.85	37.1	0.8	38.0	0.9	98.0	31.9	37.1	0.8	NA
RT28DZ8-53	42	1913	1.8	20.2584	3.8	0.0394	4.0	0.0058	1.3	0.31	37.2	0.5	39.2	1.6	165.0	89.4	37.2	0.5	NA
RT28DZ8-38	61	1358	1.9	20.5861	2.6	0.0388	2.9	0.0058	1.1	0.40	37.3	0.4	38.7	1.1	127.5	61.5	37.3	0.4	NA
RT28DZ8-37	58	2472	1.4	20.4164	3.5	0.0393	3.8	0.0058	1.5	0.39	37.4	0.6	39.1	1.5	146.9	81.8	37.4	0.6	NA
RT28DZ8-80	95	1489	1.5	21.3569	2.3	0.0376	2.8	0.0058	1.7	0.59	37.4	0.6	37.4	1.0	40.2	54.6	37.4	0.6	NA
RT28DZ8-51	44	1656	1.7	20.0621	3.9	0.0402	3.9	0.0058	0.5	0.13	37.6	0.2	40.0	1.5	187.8	90.9	37.6	0.2	NA
RT28DZ8-69	196	4957	1.7	20.3552	1.2	0.0396	2.0	0.0059	1.6	0.82	37.6	0.6	39.5	0.8	153.9	27.1	37.6	0.6	NA
RT28DZ8-55	285	5590	1.0	21.0783	1.1	0.0383	1.2	0.0059	0.5	0.46	37.6	0.2	38.1	0.4	71.5	25.4	37.6	0.2	NA
RT28DZ8-33	70	966	1.8	14.6151	27.5	0.0554	27.6	0.0059	1.9	0.07	37.7	0.7	54.7	14.7	881.3	579.8	37.7	0.7	NA
RT28DZ8-62	112	3856	1.7	20.1914	2.9	0.0402	3.0	0.0059	0.5	0.18	37.8	0.2	40.0	1.2	172.8	68.1	37.8	0.2	NA
RT28DZ8-109	104	1697	2.1	20.5760	2.3	0.0397	2.8	0.0059	1.5	0.55	38.0	0.6	39.5	1.1	128.6	54.2	38.0	0.6	NA
RT28DZ8-63	260	5526	1.6	20.9472	1.5	0.0392	2.2	0.0060	1.6	0.74	38.3	0.6	39.1	0.8	86.4	34.8	38.3	0.6	NA
RT28DZ8-46	128	5453	2.0	20.7684	1.5	0.0396	2.7	0.0060	2.3	0.83	38.3	0.9	39.4	1.1	106.7	35.5	38.3	0.9	NA
RT28DZ8-67	116	2840	1.9	20.5715	2.7	0.0400	2.9	0.0060	1.0	0.35	38.3	0.4	39.8	1.1	129.1	63.5	38.3	0.4	NA
RT28DZ8-68	365	9346	0.8	20.8919	1.6	0.0394	1.8	0.0060	0.8	0.44	38.4	0.3	39.3	0.7	92.6	38.6	38.4	0.3	NA
RT28DZ8-74	62	1476	1.4	20.4771	2.7	0.0405	2.8	0.0060	0.7	0.27	38.6	0.3	40.3	1.1	139.9	62.7	38.6	0.3	NA
RT28DZ8-59	189	3522	1.6	21.2722	3.2	0.0391	3.5	0.0060	1.4	0.40	38.8	0.5	38.9	1.3	49.7	76.2	38.8	0.5	NA
RT28DZ8-72	95	848	1.5	11.6963	20.3	0.0761	20.3	0.0065	0.7	0.03	41.5	0.3	74.5	14.6	1326.8	397.5	41.5	0.3	NA
RT28DZ8-101	190	6503	0.6	20.9593	1.2	0.0728	1.5	0.0111	1.0	0.65	71.0	0.7	71.4	1.1	85.0	28.0	71.0	0.7	NA
RT28DZ8-25	166	5508	1.0	20.7293	1.4	0.0758	1.6	0.0114	0.8	0.47	73.1	0.6	74.2	1.2	111.1	34.0	73.1	0.6	NA
RT28DZ8-45	201	22503	0.5	20.3200	1.8	0.0784	2.5	0.0115	1.7	0.67	74.0	1.2	76.6	1.8	158.0	43.3	74.0	1.2	NA
RT28DZ8-81	88	3798	0.7	21.1585	1.6	0.0756	2.0	0.0116	1.2	0.60	74.3	0.9	74.0	1.4	62.5	37.7	74.3	0.9	NA
RT28DZ8-32	70	2279	0.6	21.4440	1.9	0.0749	2.5	0.0116	1.5	0.62	74.6	1.1	73.3	1.7	30.5	46.3	74.6	1.1	NA
RT28DZ8-58	158	9406	0.5	20.7703	2.2	0.0776	2.4	0.0117	1.1	0.44	75.0	0.8	75.9	1.8	106.4	51.8	75.0	0.8	NA
RT28DZ8-35	126	6457	0.8	20.6179	1.7	0.0786	1.9	0.0118	0.8	0.40	75.4	0.6	76.9	1.4	123.8	41.2	75.4	0.6	NA
RT28DZ8-40	326	27996	0.7	20.5186	1.1	0.0792	1.4	0.0118	0.8	0.60	75.5	0.6	77.4	1.1	135.2	26.5	75.5	0.6	NA
RT28DZ8-66	117	5964	0.6	20.7099	1.1	0.0804	1.4	0.0121	0.9	0.64	77.3	0.7	78.5	1.0	113.3	25.0	77.3	0.7	NA
RT28DZ8-48	564	76820	3.1	20.5449	0.6	0.0812	0.7	0.0121	0.5	0.64	77.5	0.4	79.2	0.6	132.1	13.1	77.5	0.4	NA
RT28DZ8-86	131	4827	0.7	20.7770	0.9	0.0804	1.1	0.0121	0.7	0.60	77.6	0.5	78.5	0.8	105.7	20.4	77.6	0.5	NA
RT28DZ8-57	42	5419	0.9	19.3006	3.6	0.0879	3.7	0.0123	0.8	0.21	78.8	0.6	85.5	3.0	277.1	82.7	78.8	0.6	NA
RT28DZ8-108	41	1932	1.2	20.4554	2.4	0.0869	2.6	0.0129	1.0	0.39	82.6	0.8	84.6	2.1	142.4	55.9	82.6	0.8	NA
RT28DZ8-107	59	2917	0.8	20.0184	3.3	0.0900	3.6	0.0131	1.4	0.38	83.7	1.1	87.5	3.0	192.9	77.7	83.7	1.1	NA
RT28DZ8-18	436	17086	2.9	20.3835	0.7	0.0893	1.3	0.0132	1.0	0.82	84.5	0.9	86.8	1.1	150.7	16.8	84.5	0.9	NA
RT28DZ8-75	169	4558	0.9	21.0635	1.2	0.0874	1.6	0.0133	1.0	0.64	85.5	0.9	85.0	1.3	73.2	29.1	85.5	0.9	NA
RT28DZ8-19	72	1883	0.8	21.2215	2.8	0.0872	2.9	0.0134	0.8	0.26	86.0	0.6	84.9	2.4	55.4	66.9	86.0	0.6	NA
RT28DZ8-78	278	9452	1.0	20.8191	1.2	0.0935	1.9	0.0141	1.5	0.79	90.4	1.4	90.8	1.7	100.9	27.6	90.4	1.4	NA
RT28DZ8-52	168	14242	4.1	20.2543	1.8	0.0977	2.1	0.0144	1.0	0.49	91.9	0.9	94.7	1.9	165.5	42.5	91.9	0.9	NA
RT28DZ8-110	148	4688	3.2	20.3879	1.1	0.0973	1.3	0.0144	0.6	0.48	92.0	0.6	94.2	1.1	150.2	26.2	92.0	0.6	NA
RT28DZ8-90	247	6970	1.6	20.3946	1.7	0.0993	1.9	0.0147	0.9	0.48	94.0	0.9	96.2	1.7	149.4	39.1	94.0	0.9	NA

RT28DZ8-65	284	11762	1.9	20.5163	0.9	0.1000	1.2	0.0149	0.8	0.65	95.2	0.7	96.8	1.1	135.4	20.5	95.2	0.7	NA
RT28DZ8-105	60	2856	1.4	20.3014	2.5	0.1023	2.6	0.0151	0.7	0.26	96.4	0.6	98.9	2.5	160.1	58.9	96.4	0.6	NA
RT28DZ8-10	126	1944	1.2	19.7941	1.1	0.1066	3.5	0.0153	3.3	0.95	97.9	3.2	102.8	3.4	219.0	24.6	97.9	3.2	NA
RT28DZ8-98	374	16391	1.2	20.6692	0.7	0.1056	4.1	0.0158	4.0	0.99	101.2	4.0	101.9	3.9	118.0	16.4	101.2	4.0	NA
RT28DZ8-30	56	4374	1.7	20.2925	2.2	0.1083	3.4	0.0159	2.6	0.76	101.9	2.6	104.4	3.4	161.1	52.3	101.9	2.6	NA
RT28DZ8-47	64	12603	0.9	19.6959	1.6	0.1121	2.1	0.0160	1.5	0.69	102.4	1.5	107.9	2.2	230.5	35.8	102.4	1.5	NA
RT28DZ8-3	66	1289	1.9	19.6440	4.2	0.1142	4.5	0.0163	1.7	0.36	104.1	1.7	109.8	4.7	236.6	97.5	104.1	1.7	NA
RT28DZ8-79	374	32686	1.8	20.4792	0.9	0.1098	1.5	0.0163	1.1	0.77	104.3	1.2	105.8	1.5	139.7	21.8	104.3	1.2	NA
RT28DZ8-5	74	2315	1.6	19.0303	4.7	0.1186	4.9	0.0164	1.7	0.34	104.6	1.7	113.8	5.3	309.3	106.0	104.6	1.7	NA
RT28DZ8-1	40	545	2.3	15.2249	10.8	0.1486	10.9	0.0164	1.7	0.15	104.9	1.7	140.7	14.3	796.2	226.7	104.9	1.7	NA
RT28DZ8-6	48	2234	1.6	17.9634	3.5	0.1277	4.8	0.0166	3.3	0.68	106.4	3.5	122.1	5.6	439.2	78.9	106.4	3.5	NA
RT28DZ8-42	57	4948	1.5	20.0974	1.6	0.1169	1.8	0.0170	0.8	0.43	108.9	0.8	112.3	1.9	183.7	37.8	108.9	0.8	NA
RT28DZ8-56	406	24768	1.6	20.6218	0.9	0.1141	1.0	0.0171	0.4	0.42	109.1	0.4	109.7	1.0	123.3	20.7	109.1	0.4	NA
RT28DZ8-7	167	3089	1.3	20.2284	3.0	0.1217	3.1	0.0179	0.7	0.22	114.1	0.8	116.6	3.4	168.5	69.6	114.1	0.8	NA
RT28DZ8-54	52	2802	1.3	20.4806	3.9	0.1550	3.9	0.0230	0.5	0.12	146.8	0.7	146.4	5.3	139.5	91.1	146.8	0.7	NA
RT28DZ8-96	50	3123	2.0	20.3928	1.8	0.1558	2.2	0.0230	1.2	0.55	146.8	1.7	147.0	3.0	149.6	42.5	146.8	1.7	NA
RT28DZ8-36	126	10829	1.6	20.4982	0.6	0.1605	2.1	0.0239	2.0	0.96	152.0	3.0	151.1	2.9	137.5	14.3	152.0	3.0	NA
RT28DZ8-7	243	5601	0.6	20.0847	1.1	0.2360	4.8	0.0344	4.6	0.97	217.9	9.9	215.2	9.2	185.1	25.1	217.9	9.9	NA
RT28DZ8-2	199	7348	0.8	19.9346	0.6	0.2746	2.0	0.0397	2.0	0.96	251.0	4.8	246.4	4.4	202.6	13.3	251.0	4.8	NA
RT28DZ8-4	416	21124	1.0	19.6364	0.8	0.2817	2.5	0.0401	2.3	0.95	253.6	5.8	252.0	5.5	237.5	17.6	253.6	5.8	NA
RT28DZ8-9	41	2925	0.9	19.2544	3.3	0.2910	4.9	0.0406	3.6	0.73	256.8	9.0	259.3	11.2	282.6	76.6	256.8	9.0	NA
RT28DZ8-29	221	50827	1.1	19.0362	0.6	0.3159	0.9	0.0436	0.7	0.73	275.2	1.8	278.7	2.2	308.6	14.4	275.2	1.8	NA
RT28DZ8-60	102	23680	1.3	18.8140	0.9	0.3350	1.1	0.0457	0.6	0.54	288.1	1.6	293.4	2.7	335.3	20.2	288.1	1.6	NA
Sample RT28DZ7 (Río Turbio Formation - upper)																			
RT28DZ7-39B	11	427	2.3	14.7859	4.4	0.0467	7.4	0.0050	5.9	0.80	32.2	1.9	46.4	3.3	857.3	91.4	32.2	1.9	NA
RT28DZ7-65B	25	592	1.4	20.0111	2.7	0.0359	3.9	0.0052	2.8	0.71	33.5	0.9	35.9	1.4	193.7	62.9	33.5	0.9	NA
RT28DZ7-102B	29	451	1.2	21.4238	3.9	0.0336	4.1	0.0052	1.1	0.26	33.5	0.4	33.5	1.3	32.7	94.3	33.5	0.4	NA
RT28DZ7-82B	16	261	1.5	24.2134	4.3	0.0298	5.9	0.0052	4.0	0.69	33.6	1.4	29.8	1.7	-269.1	108.7	33.6	1.4	NA
RT28DZ7-38B	18	615	1.6	18.6315	6.3	0.0388	8.0	0.0052	4.9	0.61	33.7	1.6	38.6	3.0	357.3	142.6	33.7	1.6	NA
RT28DZ7-83B	19	277	2.1	26.6690	7.5	0.0271	7.6	0.0052	1.6	0.21	33.7	0.5	27.2	2.0	-520.7	200.0	33.7	0.5	NA
RT28DZ7-105B	17	330	1.8	19.7401	4.0	0.0371	5.1	0.0053	3.2	0.63	34.1	1.1	37.0	1.9	225.3	91.7	34.1	1.1	NA
RT28DZ7-43B	30	1216	1.4	18.4732	5.1	0.0397	5.3	0.0053	1.6	0.29	34.2	0.5	39.5	2.1	376.5	115.1	34.2	0.5	NA
RT28DZ7-55B	24	590	1.4	19.5349	6.4	0.0376	7.0	0.0053	2.9	0.41	34.2	1.0	37.4	2.6	249.4	148.1	34.2	1.0	NA
RT28DZ7-67B	18	592	1.9	19.0044	8.0	0.0389	8.4	0.0054	2.5	0.30	34.5	0.9	38.8	3.2	312.4	183.3	34.5	0.9	NA
RT28DZ7-91	209	15114	2.4	18.5964	21.6	0.0399	22.5	0.0054	6.2	0.27	34.6	2.1	39.7	8.8	361.6	492.9	34.6	2.1	NA
RT28DZ7-36	145	12687	1.2	15.1746	40.9	0.0490	41.5	0.0054	7.3	0.18	34.7	2.5	48.6	19.7	803.2	892.3	34.7	2.5	NA
RT28DZ7-57B	33	1290	2.1	18.5917	4.8	0.0401	4.9	0.0054	1.3	0.26	34.7	0.4	39.9	1.9	362.1	107.6	34.7	0.4	NA
RT28DZ7-66B	26	933	2.0	18.8277	4.3	0.0396	4.4	0.0054	0.9	0.21	34.8	0.3	39.5	1.7	333.6	98.0	34.8	0.3	NA

RT28DZ7-70	122	9381	2.1	22.8209	52.5	0.0327	53.1	0.0054	8.4	0.16	34.8	2.9	32.7	17.1	-120.8	1382.1	34.8	2.9	NA
RT28DZ7-9	217	3054	0.7	22.5009	47.4	0.0334	48.2	0.0054	8.9	0.19	35.0	3.1	33.3	15.8	-86.1	1223.1	35.0	3.1	NA
RT28DZ7-40B	49	2382	1.8	18.5139	5.7	0.0406	5.9	0.0055	1.6	0.27	35.1	0.6	40.4	2.3	371.6	127.8	35.1	0.6	NA
RT28DZ7-85B	63	1082	2.9	21.2797	4.0	0.0354	4.3	0.0055	1.6	0.37	35.2	0.5	35.4	1.5	48.9	94.9	35.2	0.5	NA
RT28DZ7-89	131	45992	2.4	25.0072	24.5	0.0303	25.2	0.0055	6.1	0.24	35.3	2.1	30.3	7.5	-351.7	639.8	35.3	2.1	NA
RT28DZ7-37	123	8466	1.8	18.1558	33.1	0.0417	34.3	0.0055	8.9	0.26	35.3	3.1	41.5	13.9	415.4	759.0	35.3	3.1	NA
RT28DZ7-25B	124	4319	1.8	20.4446	2.1	0.0371	2.2	0.0055	0.7	0.33	35.3	0.3	37.0	0.8	143.6	48.1	35.3	0.3	NA
RT28DZ7-22B	33	722	2.0	20.2965	4.0	0.0374	4.1	0.0055	0.9	0.22	35.4	0.3	37.3	1.5	160.7	93.0	35.4	0.3	NA
RT28DZ7-28	101	6495	1.7	16.3815	56.6	0.0464	57.0	0.0055	6.5	0.11	35.5	2.3	46.1	25.7	640.8	1327.6	35.5	2.3	NA
RT28DZ7-78B	125	4011	0.8	20.6885	3.2	0.0369	3.3	0.0055	0.9	0.27	35.6	0.3	36.8	1.2	115.8	75.9	35.6	0.3	NA
RT28DZ7-96B	41	646	1.7	21.6224	4.2	0.0353	4.3	0.0055	0.6	0.14	35.6	0.2	35.2	1.5	10.6	101.9	35.6	0.2	NA
RT28DZ7-121	162	3683	2.7	20.5309	2.1	0.0372	2.5	0.0055	1.3	0.54	35.6	0.5	37.1	0.9	133.7	48.8	35.6	0.5	NA
RT28DZ7-119	137	1919	2.0	19.9588	1.7	0.0385	2.3	0.0056	1.5	0.65	35.8	0.5	38.3	0.9	199.8	40.2	35.8	0.5	NA
RT28DZ7-52	191	26532	1.3	25.7489	55.8	0.0299	56.0	0.0056	3.8	0.07	35.9	1.4	29.9	16.5	-427.7	1575.2	35.9	1.4	NA
RT28DZ7-90	168	9046	2.1	30.6143	27.4	0.0252	28.0	0.0056	5.6	0.20	35.9	2.0	25.3	7.0	-904.8	807.6	35.9	2.0	NA
RT28DZ7-49	132	14259	1.6	23.3427	50.4	0.0330	51.0	0.0056	7.6	0.15	36.0	2.7	33.0	16.6	-176.9	1334.9	36.0	2.7	NA
RT28DZ7-71	105	6872	2.2	10.2260	201.7	0.0754	201.9	0.0056	8.8	0.04	36.0	3.2	73.9	144.8	1582.4	463.7	36.0	3.2	NA
RT28DZ7-44B	43	955	1.9	20.6347	6.0	0.0379	6.2	0.0057	1.6	0.26	36.5	0.6	37.8	2.3	121.9	140.5	36.5	0.6	NA
RT28DZ7-45B	174	4388	1.3	20.5145	2.3	0.0384	2.5	0.0057	1.0	0.38	36.8	0.4	38.3	0.9	135.6	54.6	36.8	0.4	NA
RT28DZ7-10-40um	130	16624	1.2	20.1358	60.0	0.0392	60.2	0.0057	4.9	0.08	36.8	1.8	39.0	23.0	179.2	1536.2	36.8	1.8	NA
RT28DZ7-107	181	25150	1.7	23.0470	50.3	0.0343	50.5	0.0057	4.5	0.09	36.9	1.7	34.2	17.0	-145.2	1324.1	36.9	1.7	NA
RT28DZ7-80	98	21440	2.1	18.7628	48.1	0.0423	49.1	0.0058	9.7	0.20	37.0	3.6	42.0	20.2	341.5	1153.5	37.0	3.6	NA
RT28DZ7-68	265	38048	1.4	23.4656	22.8	0.0338	23.2	0.0058	4.3	0.19	37.0	1.6	33.8	7.7	-190.0	577.4	37.0	1.6	NA
RT28DZ7-24	174	19912	1.3	17.8530	76.0	0.0449	76.3	0.0058	7.2	0.09	37.3	2.7	44.6	33.3	452.9	2026.2	37.3	2.7	NA
RT28DZ7-84	108	17498	1.6	24.1710	56.2	0.0332	56.8	0.0058	8.2	0.14	37.4	3.0	33.1	18.5	-264.6	1539.9	37.4	3.0	NA
RT28DZ7-53	111	11665	1.9	29.3318	104.9	0.0274	105.2	0.0058	7.9	0.08	37.5	3.0	27.4	28.5	-782.3	0.0	37.5	3.0	NA
RT28DZ7-74	220	9261	1.2	18.3309	13.0	0.0446	14.9	0.0059	7.3	0.49	38.1	2.8	44.3	6.5	393.9	293.2	38.1	2.8	NA
RT28DZ7-5	211	6971	1.1	26.8731	60.1	0.0304	60.4	0.0059	5.3	0.09	38.1	2.0	30.4	18.1	-541.2	1760.1	38.1	2.0	NA
RT28DZ7-42	96	10728	1.5	16.2242	80.4	0.0507	81.0	0.0060	9.3	0.12	38.3	3.6	50.2	39.7	661.5	2161.9	38.3	3.6	NA
RT28DZ7-18	113	1771	1.7	22.5447	166.1	0.0369	166.3	0.0060	8.3	0.05	38.8	3.2	36.8	60.2	-90.8	0.0	38.8	3.2	NA
RT28DZ7-35	146	11396	1.7	28.0974	64.3	0.0297	64.5	0.0061	5.0	0.08	39.0	2.0	29.8	18.9	-662.3	1958.6	39.0	2.0	NA
RT28DZ7-63	123	8667	1.4	21.8243	54.3	0.0399	54.9	0.0063	8.5	0.15	40.6	3.4	39.7	21.4	-11.8	1408.6	40.6	3.4	NA
RT28DZ7-16	148	3765	0.9	17.1070	35.0	0.0517	35.5	0.0064	5.8	0.16	41.2	2.4	51.2	17.7	546.9	788.2	41.2	2.4	NA
RT28DZ7-117	234	6709	0.7	20.2234	1.3	0.0692	1.4	0.0101	0.5	0.36	65.1	0.3	67.9	0.9	169.1	30.6	65.1	0.3	NA
RT28DZ7-6	99	3501	0.8	23.2594	37.9	0.0677	38.6	0.0114	7.5	0.19	73.2	5.4	66.5	24.9	-168.0	973.6	73.2	5.4	NA
RT28DZ7-34	111	20534	0.7	23.7242	42.4	0.0666	42.6	0.0115	4.5	0.11	73.4	3.3	65.5	27.0	-217.5	1109.0	73.4	3.3	NA
RT28DZ7-26	128	30865	0.6	24.1318	13.4	0.0662	13.9	0.0116	3.7	0.26	74.2	2.7	65.1	8.7	-260.5	340.7	74.2	2.7	NA
RT28DZ7-69	129	23023	0.6	22.5982	25.8	0.0709	26.2	0.0116	4.5	0.17	74.4	3.3	69.5	17.6	-96.7	642.5	74.4	3.3	NA
RT28DZ7-114	166	10713	0.6	20.4594	0.6	0.0784	1.2	0.0116	1.1	0.85	74.5	0.8	76.6	0.9	141.9	15.2	74.5	0.8	NA

RT28DZ7-77	229	51213	0.5	20.4670	9.0	0.0785	9.2	0.0116	1.7	0.19	74.7	1.3	76.7	6.8	141.1	212.4	74.7	1.3	NA
RT28DZ7-48	152	29894	0.6	23.4432	14.3	0.0686	14.7	0.0117	3.2	0.22	74.8	2.4	67.4	9.6	-187.6	359.5	74.8	2.4	NA
RT28DZ7-94	92	15804	0.8	21.2516	26.9	0.0757	27.8	0.0117	6.7	0.24	74.8	5.0	74.1	19.8	52.0	653.4	74.8	5.0	NA
RT28DZ7-21	110	15545	0.7	29.7741	45.9	0.0541	46.1	0.0117	4.0	0.09	74.9	3.0	53.5	24.0	-824.8	1369.7	74.9	3.0	NA
RT28DZ7-56B	109	7917	0.6	20.1861	1.6	0.0803	1.7	0.0118	0.7	0.42	75.3	0.5	78.4	1.3	173.4	36.5	75.3	0.5	NA
RT28DZ7-98	745	90693	0.8	20.2246	3.3	0.0803	3.5	0.0118	1.2	0.34	75.4	0.9	78.4	2.7	169.0	77.3	75.4	0.9	NA
RT28DZ7-111	64	17920	0.9	21.5681	41.8	0.0754	42.7	0.0118	8.7	0.20	75.5	6.5	73.8	30.4	16.6	1044.1	75.5	6.5	NA
RT28DZ7-112	59	4717	0.6	14.5126	80.3	0.1132	80.5	0.0119	4.4	0.06	76.3	3.4	108.8	83.2	895.9	2089.2	76.3	3.4	NA
RT28DZ7-87	63	22171	1.1	18.7875	32.2	0.0879	32.6	0.0120	5.5	0.17	76.7	4.2	85.5	26.8	338.5	746.1	76.7	4.2	NA
RT28DZ7-93	74	11050	0.6	19.4241	21.7	0.0851	22.6	0.0120	6.2	0.27	76.8	4.7	82.9	18.0	262.5	504.6	76.8	4.7	NA
RT28DZ7-108	72	12822	0.9	24.8726	39.5	0.0666	40.3	0.0120	8.0	0.20	76.9	6.1	65.4	25.5	-337.8	1052.5	76.9	6.1	NA
RT28DZ7-72	204	41420	1.0	21.2483	12.3	0.0788	12.5	0.0121	2.5	0.20	77.8	2.0	77.0	9.3	52.4	293.4	77.8	2.0	NA
RT28DZ7-27	156	29336	1.7	20.4158	16.6	0.0847	16.9	0.0125	3.4	0.20	80.4	2.7	82.6	13.4	147.0	390.7	80.4	2.7	NA
RT28DZ7-99	87	23358	0.6	22.7615	38.4	0.0815	38.6	0.0135	3.8	0.10	86.2	3.2	79.6	29.6	-114.4	978.6	86.2	3.2	NA
RT28DZ7-97B	113	4332	0.7	20.6740	1.6	0.0901	2.7	0.0135	2.2	0.82	86.5	1.9	87.6	2.3	117.4	36.7	86.5	1.9	NA
RT28DZ7-62	97	49616	0.6	20.5509	22.9	0.0920	23.4	0.0137	4.5	0.19	87.8	3.9	89.4	20.0	131.5	545.2	87.8	3.9	NA
RT28DZ7-115	26	1560	1.8	19.8205	2.5	0.1053	2.8	0.0151	1.3	0.45	96.8	1.2	101.6	2.7	215.9	57.5	96.8	1.2	NA
RT28DZ7-95B	32	1277	1.7	20.3389	2.1	0.1039	2.2	0.0153	0.7	0.34	98.0	0.7	100.4	2.1	155.8	48.1	98.0	0.7	NA
RT28DZ7-92	35	9782	1.1	23.6761	72.4	0.0893	72.9	0.0153	8.6	0.12	98.2	8.4	86.9	60.8	-212.4	2104.4	98.2	8.4	NA
RT28DZ7-23B	44	3520	1.0	20.3667	1.8	0.1042	2.2	0.0154	1.4	0.61	98.4	1.3	100.6	2.1	152.6	41.4	98.4	1.3	NA
RT28DZ7-46	213	81436	5.0	24.8742	11.4	0.0855	11.6	0.0154	2.2	0.19	98.7	2.1	83.3	9.3	-337.9	293.7	98.7	2.1	NA
RT28DZ7-116	85	3898	1.4	20.2876	1.1	0.1057	1.9	0.0156	1.5	0.80	99.5	1.5	102.0	1.8	161.7	26.7	99.5	1.5	NA
RT28DZ7-76	51	30987	1.3	18.2400	30.2	0.1182	30.8	0.0156	5.8	0.19	100.0	5.7	113.4	33.0	405.0	691.3	100.0	5.7	NA
RT28DZ7-79	68	19974	0.9	21.9052	40.6	0.0988	41.3	0.0157	7.7	0.19	100.4	7.7	95.7	37.8	-20.7	1019.9	100.4	7.7	NA
RT28DZ7-113	85	3455	0.8	20.7154	0.7	0.1049	1.1	0.0158	0.8	0.75	100.8	0.8	101.3	1.0	112.7	16.5	100.8	0.8	NA
RT28DZ7-103	47	7037	1.3	24.0651	55.0	0.0906	55.5	0.0158	7.5	0.14	101.1	7.6	88.0	46.8	-253.5	1496.5	101.1	7.6	NA
RT28DZ7-120	57	2412	1.0	20.5032	2.9	0.1064	3.0	0.0158	0.6	0.20	101.2	0.6	102.6	2.9	136.9	69.3	101.2	0.6	NA
RT28DZ7-47	60	19735	2.1	20.8241	29.7	0.1051	30.3	0.0159	6.0	0.20	101.5	6.0	101.4	29.3	100.3	716.9	101.5	6.0	NA
RT28DZ7-54	65	9709	0.9	23.6118	34.5	0.0927	35.9	0.0159	9.7	0.27	101.6	9.8	90.1	30.9	-205.6	888.5	101.6	9.8	NA
RT28DZ7-101	63	20291	1.7	25.1433	28.3	0.0871	28.6	0.0159	4.2	0.15	101.6	4.2	84.8	23.3	-365.7	744.2	101.6	4.2	NA
RT28DZ7-122	84	17380	0.8	19.6412	0.7	0.1119	1.5	0.0159	1.3	0.87	102.0	1.3	107.7	1.5	236.9	16.9	102.0	1.3	NA
RT28DZ7-73	108	32052	1.3	19.8940	29.6	0.1113	29.8	0.0161	3.9	0.13	102.7	4.0	107.1	30.3	207.3	699.0	102.7	4.0	NA
RT28DZ7-118	131	11002	1.1	20.1071	1.3	0.1101	1.4	0.0161	0.4	0.32	102.7	0.4	106.1	1.4	182.5	29.8	102.7	0.4	NA
RT28DZ7-58	61	13802	1.6	21.5901	64.6	0.1032	64.9	0.0162	7.1	0.11	103.3	7.2	99.7	61.7	14.2	1733.1	103.3	7.2	NA
RT28DZ7-100	101	21173	0.9	19.7553	16.3	0.1128	17.0	0.0162	4.6	0.27	103.3	4.8	108.5	17.5	223.5	379.8	103.3	4.8	NA
RT28DZ7-75	60	10519	1.2	25.6564	24.7	0.0872	25.6	0.0162	6.6	0.26	103.8	6.8	84.9	20.9	-418.3	655.9	103.8	6.8	NA
RT28DZ7-61	92	18010	0.8	21.6708	20.1	0.1036	20.8	0.0163	5.3	0.26	104.1	5.5	100.1	19.8	5.2	488.5	104.1	5.5	NA
RT28DZ7-88B	20	2283	1.3	18.7716	2.3	0.1206	2.7	0.0164	1.4	0.52	105.0	1.5	115.6	3.0	340.4	52.9	105.0	1.5	NA
RT28DZ7-122	61	4833	0.7	19.8937	1.7	0.1160	3.0	0.0167	2.4	0.81	107.0	2.6	111.4	3.1	207.4	39.8	107.0	2.6	NA

RT28DZ7-4	339	14053	1.5	21.3664	14.3	0.1082	14.5	0.0168	2.3	0.16	107.2	2.4	104.3	14.4	39.2	343.8	107.2	2.4	NA
RT28DZ7-60	71	24577	0.8	27.7374	35.4	0.0835	36.0	0.0168	6.2	0.17	107.4	6.6	81.4	28.2	-626.9	994.2	107.4	6.6	NA
RT28DZ7-33	78	31540	2.1	19.2208	25.0	0.1265	25.4	0.0176	4.8	0.19	112.7	5.3	121.0	29.0	286.6	578.9	112.7	5.3	NA
RT28DZ7-110	51	30825	2.2	14.0442	22.9	0.1749	24.4	0.0178	8.3	0.34	113.8	9.4	163.7	36.9	963.3	474.4	113.8	9.4	NA
RT28DZ7-86	299	56285	1.4	20.5201	5.8	0.1299	6.0	0.0193	1.4	0.24	123.4	1.8	124.0	7.0	135.0	136.7	123.4	1.8	NA
RT28DZ7-8	116	4723	1.6	18.7098	20.6	0.1455	21.0	0.0198	4.0	0.19	126.1	4.9	138.0	27.0	347.8	469.8	126.1	4.9	NA
RT28DZ7-59	67	35166	0.9	18.8676	23.6	0.1567	23.9	0.0214	3.7	0.15	136.8	4.9	147.8	32.8	328.8	541.7	136.8	4.9	NA
Sample RT28DZ5 (Río Turbio Formation - upper)																			
RT28DZ5-28	24	1340	2.4	15.6942	7.5	0.0353	8.3	0.0040	3.5	0.42	25.9	0.9	35.2	2.9	732.3	158.9	25.9	0.9	NA
RT28DZ5-94	80	7918	1.3	19.6297	3.6	0.0288	3.6	0.0041	0.5	0.15	26.3	0.1	28.8	1.0	238.3	83.0	26.3	0.1	NA
RT28DZ5-58	604	19457	1.1	20.5173	1.3	0.0277	1.4	0.0041	0.6	0.39	26.5	0.1	27.7	0.4	135.3	31.3	26.5	0.1	NA
RT28DZ5-88	616	39540	0.9	20.9300	1.2	0.0275	1.3	0.0042	0.5	0.41	26.9	0.1	27.6	0.4	88.3	28.2	26.9	0.1	NA
RT28DZ5-4	49	3448	1.5	18.0636	4.1	0.0322	5.3	0.0042	3.4	0.64	27.2	0.9	32.2	1.7	426.8	90.7	27.2	0.9	NA
RT28DZ5-73	20	1998	2.0	17.1206	4.8	0.0446	5.5	0.0055	2.7	0.50	35.6	1.0	44.3	2.4	545.1	104.1	35.6	1.0	NA
RT28DZ5-70	63	24670	1.8	19.3987	2.8	0.0433	2.8	0.0061	0.6	0.22	39.2	0.2	43.1	1.2	265.5	63.4	39.2	0.2	NA
RT28DZ5-48	108	9430	1.3	18.0087	3.4	0.0469	3.6	0.0061	1.2	0.33	39.4	0.5	46.6	1.6	433.6	75.5	39.4	0.5	NA
RT28DZ5-55	65	37779	0.9	19.3125	2.8	0.0808	3.0	0.0113	1.1	0.36	72.6	0.8	78.9	2.3	275.7	63.9	72.6	0.8	NA
RT28DZ5-19	81	25233	0.8	19.8174	1.3	0.0792	1.5	0.0114	0.6	0.41	73.0	0.4	77.4	1.1	216.3	30.9	73.0	0.4	NA
RT28DZ5-46	51	6837	0.8	19.6423	2.8	0.0816	3.1	0.0116	1.5	0.47	74.5	1.1	79.6	2.4	236.8	64.0	74.5	1.1	NA
RT28DZ5-44	368	102014	1.0	20.3873	0.7	0.0791	1.4	0.0117	1.2	0.84	74.9	0.9	77.3	1.0	150.2	17.5	74.9	0.9	NA
RT28DZ5-52	77	10376	1.0	20.1595	3.3	0.0800	3.6	0.0117	1.5	0.42	74.9	1.1	78.1	2.7	176.5	76.2	74.9	1.1	NA
RT28DZ5-84	646	148864	0.6	20.5019	0.5	0.0788	0.8	0.0117	0.7	0.77	75.1	0.5	77.0	0.6	137.1	12.6	75.1	0.5	NA
RT28DZ5-62	79	8445	1.1	19.5535	4.8	0.0828	5.0	0.0117	1.2	0.25	75.2	0.9	80.7	3.9	247.2	111.3	75.2	0.9	NA
RT28DZ5-5	401	94173	0.5	20.3901	0.7	0.0797	0.9	0.0118	0.5	0.58	75.5	0.4	77.9	0.6	149.9	16.6	75.5	0.4	NA
RT28DZ5-22	56	49189	1.1	19.5199	1.9	0.0834	2.2	0.0118	1.2	0.53	75.6	0.9	81.3	1.8	251.2	43.9	75.6	0.9	NA
RT28DZ5-95	116	27233	1.0	20.4138	1.4	0.0798	1.6	0.0118	0.9	0.55	75.7	0.7	78.0	1.2	147.2	31.7	75.7	0.7	NA
RT28DZ5-71	577	216985	0.7	20.7386	0.6	0.0789	1.3	0.0119	1.1	0.87	76.0	0.8	77.1	0.9	110.0	14.8	76.0	0.8	NA
RT28DZ5-1	64	17261	1.3	19.8096	2.3	0.0826	2.6	0.0119	1.2	0.46	76.1	0.9	80.6	2.0	217.2	53.7	76.1	0.9	NA
RT28DZ5-76	93	27842	0.9	20.4173	2.2	0.0804	2.5	0.0119	1.1	0.45	76.3	0.8	78.5	1.9	146.8	51.4	76.3	0.8	NA
RT28DZ5-41	44	4698	1.3	20.1983	2.9	0.0823	3.2	0.0121	1.2	0.39	77.2	0.9	80.3	2.4	172.0	68.2	77.2	0.9	NA
RT28DZ5-50	729	146177	1.1	20.0834	1.0	0.0833	1.6	0.0121	1.2	0.77	77.7	0.9	81.2	1.2	185.3	23.3	77.7	0.9	NA
RT28DZ5-8	47	9698	1.1	19.5806	2.5	0.0860	2.6	0.0122	0.8	0.31	78.2	0.6	83.7	2.1	244.0	57.2	78.2	0.6	NA
RT28DZ5-101	523	132053	0.7	20.1376	0.9	0.0849	1.6	0.0124	1.3	0.81	79.4	1.0	82.7	1.3	179.0	21.8	79.4	1.0	NA
RT28DZ5-99	278	52006	1.2	20.0220	1.0	0.0865	1.5	0.0126	1.2	0.78	80.5	1.0	84.2	1.2	192.5	22.5	80.5	1.0	NA
RT28DZ5-60	384	111998	1.3	20.2129	0.7	0.0857	1.2	0.0126	1.0	0.83	80.5	0.8	83.5	1.0	170.3	15.4	80.5	0.8	NA
RT28DZ5-64	219	65022	1.6	20.0686	1.0	0.0869	1.6	0.0126	1.2	0.79	81.0	1.0	84.6	1.3	187.0	22.2	81.0	1.0	NA
RT28DZ5-3	192	29387	1.2	20.1955	0.9	0.0877	1.2	0.0129	0.9	0.72	82.3	0.7	85.4	1.0	172.3	20.2	82.3	0.7	NA
RT28DZ5-35	483	77408	1.4	20.7683	0.9	0.0871	1.5	0.0131	1.2	0.80	84.1	1.0	84.8	1.2	106.7	21.1	84.1	1.0	NA

RT28DZ5-2	87	21322	1.1	20.1132	2.0	0.0908	2.3	0.0132	1.2	0.50	84.8	1.0	88.2	2.0	181.8	46.8	84.8	1.0	NA
RT28DZ5-83	566	112840	0.9	20.3171	0.6	0.0913	0.9	0.0135	0.7	0.78	86.2	0.6	88.7	0.8	158.3	12.9	86.2	0.6	NA
RT28DZ5-42	139	34700	0.7	19.8803	1.5	0.0934	1.9	0.0135	1.1	0.59	86.2	0.9	90.7	1.6	208.9	35.1	86.2	0.9	NA
RT28DZ5-77	77	21012	0.9	19.8870	2.4	0.0936	2.5	0.0135	0.7	0.26	86.5	0.6	90.9	2.2	208.1	56.4	86.5	0.6	NA
RT28DZ5-11	182	47155	1.5	20.4429	0.8	0.0916	1.2	0.0136	1.0	0.79	87.0	0.8	89.0	1.1	143.8	17.8	87.0	0.8	NA
RT28DZ5-104	159	64669	0.5	20.0633	0.9	0.0935	1.3	0.0136	1.0	0.71	87.1	0.8	90.8	1.2	187.6	21.8	87.1	0.8	NA
RT28DZ5-33	107	28386	1.3	19.9330	1.4	0.1029	1.9	0.0149	1.3	0.67	95.1	1.2	99.4	1.8	202.8	32.0	95.1	1.2	NA
RT28DZ5-89	98	42032	1.6	20.0349	1.4	0.1033	1.6	0.0150	0.8	0.49	96.0	0.8	99.8	1.5	191.0	33.0	96.0	0.8	NA
RT28DZ5-100	203	51657	1.1	20.1074	0.8	0.1030	1.0	0.0150	0.6	0.60	96.1	0.6	99.6	1.0	182.5	18.8	96.1	0.6	NA
RT28DZ5-74	52	30049	1.3	19.3373	3.6	0.1079	4.0	0.0151	1.7	0.42	96.8	1.6	104.1	4.0	272.7	83.2	96.8	1.6	NA
RT28DZ5-43	73	36452	1.5	19.7138	1.4	0.1069	1.8	0.0153	1.1	0.60	97.8	1.0	103.1	1.7	228.4	32.6	97.8	1.0	NA
RT28DZ5-98	47	21116	1.9	19.0759	2.5	0.1113	2.7	0.0154	1.1	0.39	98.5	1.0	107.2	2.7	303.9	56.2	98.5	1.0	NA
RT28DZ5-80	175	52797	1.3	20.1048	1.1	0.1062	1.3	0.0155	0.8	0.60	99.1	0.8	102.5	1.3	182.8	24.5	99.1	0.8	NA
RT28DZ5-54	33	14543	1.4	18.8541	2.1	0.1134	2.4	0.0155	1.2	0.51	99.2	1.2	109.1	2.5	330.4	47.2	99.2	1.2	NA
RT28DZ5-97	51	24303	1.0	19.0837	2.0	0.1122	3.1	0.0155	2.3	0.76	99.3	2.3	108.0	3.2	302.9	46.0	99.3	2.3	NA
RT28DZ5-21	45	14595	1.3	19.8488	2.0	0.1085	2.1	0.0156	0.7	0.34	99.9	0.7	104.6	2.1	212.6	45.7	99.9	0.7	NA
RT28DZ5-40	82	24811	1.5	19.7131	1.0	0.1094	1.2	0.0156	0.6	0.54	100.0	0.6	105.4	1.2	228.5	23.3	100.0	0.6	NA
RT28DZ5-96	46	20120	2.0	19.1026	1.5	0.1130	1.7	0.0157	0.7	0.43	100.2	0.7	108.7	1.8	300.7	35.0	100.2	0.7	NA
RT28DZ5-57	235	72238	1.0	20.3496	0.9	0.1063	1.0	0.0157	0.5	0.52	100.4	0.5	102.6	1.0	154.5	20.7	100.4	0.5	NA
RT28DZ5-18	106	31564	1.2	20.0907	1.0	0.1078	1.2	0.0157	0.6	0.52	100.5	0.6	104.0	1.1	184.4	22.9	100.5	0.6	NA
RT28DZ5-45	62	16755	1.4	19.6930	2.3	0.1106	2.9	0.0158	1.8	0.63	101.0	1.8	106.5	2.9	230.8	52.3	101.0	1.8	NA
RT28DZ5-82	36	42194	2.1	19.0786	1.9	0.1143	2.1	0.0158	0.9	0.44	101.1	0.9	109.9	2.2	303.6	43.5	101.1	0.9	NA
RT28DZ5-63	67	22925	1.8	19.6087	1.8	0.1114	2.4	0.0158	1.6	0.66	101.3	1.6	107.2	2.4	240.7	40.9	101.3	1.6	NA
RT28DZ5-30	74	44241	1.9	19.9243	2.0	0.1100	2.1	0.0159	0.7	0.32	101.6	0.7	106.0	2.1	203.8	46.2	101.6	0.7	NA
RT28DZ5-65	62	35650	0.9	19.4433	1.3	0.1129	2.0	0.0159	1.5	0.75	101.8	1.5	108.6	2.1	260.2	30.2	101.8	1.5	NA
RT28DZ5-49	50	14355	1.6	19.2549	1.3	0.1149	1.9	0.0160	1.5	0.76	102.6	1.5	110.4	2.0	282.6	28.7	102.6	1.5	NA
RT28DZ5-38	39	7144	1.1	19.7704	2.6	0.1120	2.7	0.0161	0.6	0.22	102.7	0.6	107.8	2.8	221.8	60.9	102.7	0.6	NA
RT28DZ5-24	99	34188	1.3	19.8588	1.0	0.1117	1.5	0.0161	1.1	0.72	102.9	1.1	107.5	1.5	211.4	23.9	102.9	1.1	NA
RT28DZ5-103	386	295766	2.6	20.1204	0.6	0.1105	1.1	0.0161	1.0	0.85	103.2	1.0	106.5	1.1	181.0	14.1	103.2	1.0	NA
RT28DZ5-91	55	14019	2.0	19.8782	1.6	0.1120	1.9	0.0161	1.1	0.56	103.2	1.1	107.8	1.9	209.2	36.3	103.2	1.1	NA
RT28DZ5-72	108	36831	1.4	20.2715	1.5	0.1103	1.9	0.0162	1.2	0.60	103.7	1.2	106.2	2.0	163.5	36.0	103.7	1.2	NA
RT28DZ5-16	45	26219	1.3	19.6976	1.3	0.1136	1.7	0.0162	1.1	0.65	103.7	1.1	109.2	1.7	230.3	29.4	103.7	1.1	NA
RT28DZ5-66	30	8547	1.8	18.9911	1.5	0.1179	2.4	0.0162	1.9	0.80	103.8	2.0	113.2	2.6	314.0	33.6	103.8	2.0	NA
RT28DZ5-90	46	24603	1.8	19.7419	1.7	0.1137	2.0	0.0163	1.0	0.50	104.1	1.0	109.3	2.1	225.1	39.9	104.1	1.0	NA
RT28DZ5-10	72	20673	2.0	19.1414	1.8	0.1174	1.8	0.0163	0.4	0.20	104.2	0.4	112.7	2.0	296.0	41.1	104.2	0.4	NA
RT28DZ5-79	56	31458	1.5	19.3961	1.6	0.1168	1.9	0.0164	1.0	0.53	105.1	1.1	112.2	2.0	265.8	37.0	105.1	1.1	NA
RT28DZ5-7	55	23517	1.2	19.6442	2.3	0.1154	2.4	0.0164	0.5	0.23	105.1	0.6	110.9	2.5	236.6	52.9	105.1	0.6	NA
RT28DZ5-92	358	231642	2.2	20.1654	1.0	0.1125	1.1	0.0165	0.6	0.52	105.2	0.6	108.2	1.2	175.8	22.4	105.2	0.6	NA
RT28DZ5-39	115	21895	1.7	20.0724	1.2	0.1132	1.4	0.0165	0.7	0.51	105.4	0.7	108.9	1.4	186.6	27.8	105.4	0.7	NA

RT28DZ5-68	34	13878	1.6	19.8858	2.0	0.1143	2.2	0.0165	0.9	0.40	105.4	0.9	109.9	2.3	208.3	47.1	105.4	0.9	NA
RT28DZ5-26	816	189203	1.0	20.5579	0.6	0.1110	1.6	0.0165	1.5	0.94	105.8	1.6	106.9	1.7	130.7	13.3	105.8	1.6	NA
RT28DZ5-47	87	42656	1.1	19.7774	2.1	0.1156	2.3	0.0166	0.9	0.38	106.0	0.9	111.1	2.4	220.9	48.9	106.0	0.9	NA
RT28DZ5-59	365	91811	1.8	20.2493	0.9	0.1136	1.1	0.0167	0.7	0.61	106.7	0.7	109.3	1.2	166.1	21.2	106.7	0.7	NA
RT28DZ5-29	817	395091	2.0	20.2629	0.6	0.1137	1.2	0.0167	1.0	0.86	106.8	1.1	109.4	1.2	164.5	14.4	106.8	1.1	NA
RT28DZ5-23	278	53923	2.3	20.2789	0.7	0.1137	1.1	0.0167	0.8	0.76	106.9	0.9	109.4	1.2	162.7	17.1	106.9	0.9	NA
RT28DZ5-34	825	195466	1.5	20.3406	0.8	0.1138	1.2	0.0168	1.0	0.79	107.3	1.0	109.4	1.3	155.6	17.8	107.3	1.0	NA
RT28DZ5-53	197	42259	2.4	20.2039	0.8	0.1150	2.2	0.0169	2.0	0.93	107.8	2.2	110.6	2.3	171.3	19.2	107.8	2.2	NA
RT28DZ5-85	67	22857	1.4	19.5324	2.2	0.1220	2.4	0.0173	0.9	0.37	110.4	0.9	116.8	2.6	249.7	50.5	110.4	0.9	NA
RT28DZ5-13	355	62440	1.1	20.3694	0.5	0.1172	0.6	0.0173	0.3	0.47	110.6	0.3	112.5	0.7	152.3	12.8	110.6	0.3	NA
RT28DZ5-27	196	39024	1.9	20.2742	0.9	0.1178	1.0	0.0173	0.6	0.54	110.7	0.6	113.1	1.1	163.2	20.2	110.7	0.6	NA
RT28DZ5-32	232	96933	1.7	20.4038	0.7	0.1187	1.1	0.0176	0.9	0.80	112.3	1.0	113.9	1.2	148.3	15.9	112.3	1.0	NA
RT28DZ5-81	173	56440	1.9	20.3528	1.4	0.1193	1.7	0.0176	1.0	0.58	112.5	1.1	114.4	1.9	154.2	33.1	112.5	1.1	NA
RT28DZ5-31	335	118840	1.6	20.4020	1.0	0.1200	1.1	0.0178	0.5	0.46	113.5	0.6	115.1	1.2	148.5	23.1	113.5	0.6	NA
RT28DZ5-25	1312	389924	0.7	20.3183	0.7	0.1221	1.1	0.0180	0.9	0.76	114.9	1.0	116.9	1.3	158.2	17.3	114.9	1.0	NA
RT28DZ5-61	667	338949	1.5	20.5057	0.9	0.1238	1.1	0.0184	0.7	0.65	117.6	0.9	118.5	1.3	136.6	20.1	117.6	0.9	NA
RT28DZ5-86	122	36503	3.1	20.2276	1.7	0.1256	2.0	0.0184	1.1	0.54	117.7	1.3	120.1	2.3	168.6	39.7	117.7	1.3	NA
RT28DZ5-75	254	77166	1.4	19.8778	0.6	0.1360	0.9	0.0196	0.6	0.70	125.2	0.7	129.5	1.0	209.2	14.1	125.2	0.7	NA
RT28DZ5-37	79	11207	2.0	15.4020	19.1	0.1885	20.4	0.0211	7.2	0.35	134.3	9.5	175.4	32.8	771.9	404.7	134.3	9.5	NA
RT28DZ5-56	369	146217	1.0	20.1881	0.8	0.1556	1.9	0.0228	1.7	0.91	145.2	2.5	146.8	2.6	173.2	18.5	145.2	2.5	NA
RT28DZ5-9	283	156734	1.9	19.7575	0.7	0.1655	0.8	0.0237	0.4	0.55	151.1	0.6	155.5	1.1	223.3	15.4	151.1	0.6	NA
RT28DZ5-93	418	352695	0.9	19.6630	1.1	0.1679	1.3	0.0239	0.6	0.52	152.5	1.0	157.6	1.8	234.4	24.7	152.5	1.0	NA
RT28DZ5-78	329	206039	7.1	19.9302	0.8	0.1664	1.0	0.0241	0.7	0.66	153.2	1.0	156.3	1.5	203.1	17.7	153.2	1.0	NA
RT28DZ5-6	289	68133	1.2	19.9538	0.9	0.1668	1.1	0.0241	0.7	0.65	153.8	1.1	156.7	1.7	200.4	20.0	153.8	1.1	NA
RT28DZ5-14	111	39597	1.7	19.1210	0.8	0.3065	0.9	0.0425	0.4	0.45	268.3	1.1	271.5	2.2	298.5	18.6	268.3	1.1	NA
RT28DZ5-20	841	727367	0.6	19.1377	1.1	0.3112	1.3	0.0432	0.6	0.45	272.6	1.5	275.1	3.0	296.5	25.7	272.6	1.5	NA
RT28DZ5-51	58	47282	1.3	18.7500	2.1	0.3235	2.1	0.0440	0.2	0.11	277.5	0.7	284.6	5.3	343.0	47.7	277.5	0.7	NA
RT28DZ5-67	469	103984	1.9	17.9800	3.2	0.3480	3.8	0.0454	2.2	0.57	286.1	6.2	303.2	10.1	437.1	70.3	286.1	6.2	NA
RT28DZ5-36	112	33121	1.2	16.3767	17.0	0.3872	17.2	0.0460	2.1	0.12	289.9	6.1	332.4	48.7	641.5	368.8	289.9	6.1	NA
RT28DZ5-102	338	334745	0.8	18.7068	0.9	0.3403	1.0	0.0462	0.5	0.47	291.0	1.4	297.4	2.7	348.2	20.5	291.0	1.4	NA
RT28DZ5-17	191	121538	1.5	18.8182	1.0	0.3593	1.2	0.0490	0.7	0.57	308.6	2.1	311.7	3.2	334.8	22.3	308.6	2.1	NA
RT28DZ5-87	130	264112	1.4	17.2756	0.6	0.6032	2.0	0.0756	1.8	0.94	469.7	8.4	479.3	7.5	525.4	14.1	469.7	8.4	2%
RT28DZ5-69	763	885099	4.1	17.8488	1.2	0.5940	2.1	0.0769	1.7	0.81	477.6	7.7	473.4	7.8	453.4	26.6	477.6	7.7	-1%
RT28DZ5-12	366	731647	1.5	17.1361	1.1	0.6930	1.6	0.0861	1.1	0.70	532.6	5.6	534.6	6.5	543.2	24.3	532.6	5.6	0%
Sample RT28DZ6 (Río Guillermo Formation)																			
RT28DZ6-68B	110	8296	0.9	18.8945	2.9	0.0261	3.6	0.0036	2.1	0.58	23.0	0.5	26.1	0.9	325.6	65.9	23.0	0.5	NA
RT28DZ6-103B	31	1564	2.1	17.5169	5.1	0.0282	5.5	0.0036	2.1	0.39	23.0	0.5	28.2	1.5	494.9	112.1	23.0	0.5	NA
RT28DZ6-1B	237	15823	2.1	20.4238	1.6	0.0245	1.9	0.0036	0.9	0.48	23.4	0.2	24.6	0.5	146.1	38.5	23.4	0.2	NA

RT28DZ6-102	246	8620	2.0	12.6153	154.0	0.0398	154.3	0.0036	9.9	0.06	23.5	2.3	39.7	60.1	1178.9	519.5	23.5	2.3	NA
RT28DZ6-91B	155	7333	2.2	20.2182	1.8	0.0250	2.0	0.0037	0.9	0.46	23.5	0.2	25.0	0.5	169.7	41.7	23.5	0.2	NA
RT28DZ6-114B	103	6854	2.4	18.8820	2.3	0.0270	2.5	0.0037	0.8	0.34	23.8	0.2	27.1	0.7	327.1	52.9	23.8	0.2	NA
RT28DZ6-34B	127	6940	2.4	19.3645	2.4	0.0273	2.5	0.0038	0.4	0.16	24.6	0.1	27.3	0.7	269.5	55.8	24.6	0.1	NA
RT28DZ6-93B	98	8096	2.6	19.4761	3.8	0.0285	4.0	0.0040	1.2	0.31	25.9	0.3	28.6	1.1	256.4	86.9	25.9	0.3	NA
RT28DZ6-89B	157	9994	1.4	20.0114	2.0	0.0351	2.1	0.0051	0.8	0.39	32.7	0.3	35.0	0.7	193.7	45.6	32.7	0.3	NA
RT28DZ6-47	118	7126	1.6	10.3448	39.3	0.0747	40.3	0.0056	9.2	0.23	36.0	3.3	73.2	28.5	1560.8	768.0	36.0	3.3	NA
RT28DZ6-48B	68	31360	0.8	19.4419	2.0	0.0794	2.3	0.0112	1.2	0.51	71.8	0.8	77.6	1.7	260.4	45.7	71.8	0.8	NA
RT28DZ6-16B	75	9730	0.9	17.0108	9.4	0.0911	9.9	0.0112	3.2	0.32	72.1	2.3	88.6	8.4	559.2	206.1	72.1	2.3	NA
RT28DZ6-46B	65	22686	1.3	19.5181	2.2	0.0812	2.5	0.0115	1.2	0.49	73.7	0.9	79.3	1.9	251.4	50.2	73.7	0.9	NA
RT28DZ6-116	152	26676	0.7	20.2059	1.3	0.0793	1.4	0.0116	0.5	0.35	74.5	0.4	77.5	1.1	171.1	31.2	74.5	0.4	NA
RT28DZ6-50	133	12027	1.1	22.5607	46.2	0.0717	46.6	0.0117	6.0	0.13	75.2	4.5	70.3	31.7	-92.6	1190.3	75.2	4.5	NA
RT28DZ6-3B	45	16253	1.4	19.3917	1.1	0.0851	1.8	0.0120	1.4	0.80	76.7	1.1	82.9	1.4	266.3	24.7	76.7	1.1	NA
RT28DZ6-11	111	14571	0.9	21.4335	79.1	0.0774	79.4	0.0120	6.4	0.08	77.1	4.9	75.7	58.0	31.7	2310.2	77.1	4.9	NA
RT28DZ6-73	373	34362	0.5	24.2519	17.7	0.0685	18.2	0.0120	4.3	0.23	77.2	3.3	67.2	11.8	-273.1	452.4	77.2	3.3	NA
RT28DZ6-122	79	17725	1.2	19.9408	2.2	0.0834	2.4	0.0121	0.8	0.35	77.2	0.6	81.3	1.9	201.9	51.7	77.2	0.6	NA
RT28DZ6-15	199	11879	1.8	18.8153	13.9	0.0906	14.9	0.0124	5.4	0.36	79.2	4.2	88.0	12.6	335.1	317.0	79.2	4.2	NA
RT28DZ6-12	205	33043	1.7	20.7559	18.5	0.0833	19.2	0.0125	5.4	0.28	80.3	4.3	81.2	15.0	108.1	439.3	80.3	4.3	NA
RT28DZ6-32	238	104730	1.1	19.8207	12.1	0.0884	12.8	0.0127	4.4	0.34	81.4	3.5	86.0	10.6	215.9	280.5	81.4	3.5	NA
RT28DZ6-28	233	28050	1.2	23.6994	28.3	0.0757	28.4	0.0130	2.2	0.08	83.4	1.8	74.1	20.3	-214.9	724.5	83.4	1.8	NA
RT28DZ6-58B	72	12853	0.7	19.7885	1.4	0.0922	2.6	0.0132	2.2	0.85	84.7	1.9	89.5	2.2	219.7	31.6	84.7	1.9	NA
RT28DZ6-8	235	21976	0.5	21.0184	21.5	0.0878	22.0	0.0134	4.6	0.21	85.7	3.9	85.5	18.1	78.3	516.8	85.7	3.9	NA
RT28DZ6-22	94	8574	0.9	26.4387	34.3	0.0701	35.3	0.0134	8.2	0.23	86.0	7.0	68.8	23.4	-497.6	934.7	86.0	7.0	NA
RT28DZ6-31	140	18756	1.0	20.2518	35.1	0.0930	35.4	0.0137	4.2	0.12	87.5	3.6	90.3	30.6	165.8	843.6	87.5	3.6	NA
RT28DZ6-76	76	8372	1.1	18.4136	32.3	0.1039	33.7	0.0139	9.8	0.29	88.9	8.6	100.4	32.3	383.8	742.9	88.9	8.6	NA
RT28DZ6-10	528	150446	0.6	21.4308	6.3	0.0893	6.8	0.0139	2.3	0.34	88.9	2.1	86.9	5.6	31.9	151.9	88.9	2.1	NA
RT28DZ6-81	702	93468	0.5	21.3698	5.7	0.0901	6.1	0.0140	2.3	0.37	89.4	2.0	87.6	5.1	38.8	136.3	89.4	2.0	NA
RT28DZ6-21	246	53890	1.4	18.9189	11.8	0.1029	12.3	0.0141	3.7	0.30	90.4	3.3	99.5	11.7	322.7	268.7	90.4	3.3	NA
RT28DZ6-87	83	12278	1.2	19.9674	60.2	0.0994	60.8	0.0144	8.6	0.14	92.1	7.8	96.2	55.8	198.8	1536.0	92.1	7.8	NA
RT28DZ6-61B	73	23850	1.2	19.6618	1.6	0.1015	2.0	0.0145	1.3	0.63	92.6	1.2	98.1	1.9	234.5	36.0	92.6	1.2	NA
RT28DZ6-18	64	8677	0.8	22.6829	43.2	0.0880	43.8	0.0145	7.6	0.17	92.7	7.0	85.6	36.0	-105.9	1107.6	92.7	7.0	NA
RT28DZ6-60B	81	9946	2.0	19.6743	1.6	0.1035	1.9	0.0148	1.1	0.56	94.5	1.0	100.0	1.8	233.0	36.4	94.5	1.0	NA
RT28DZ6-120	641	123843	2.3	20.2246	5.0	0.1015	5.7	0.0149	2.7	0.47	95.3	2.5	98.2	5.3	169.0	117.6	95.3	2.5	NA
RT28DZ6-27	353	54327	1.2	21.0009	12.9	0.0987	13.5	0.0150	3.7	0.28	96.2	3.6	95.6	12.3	80.3	308.0	96.2	3.6	NA
RT28DZ6-66B	65	17115	1.4	19.6851	1.9	0.1054	2.3	0.0151	1.3	0.55	96.3	1.2	101.8	2.3	231.7	45.0	96.3	1.2	NA
RT28DZ6-37	187	44462	1.3	25.4348	22.4	0.0818	22.6	0.0151	3.3	0.14	96.5	3.1	79.8	17.4	-395.7	589.2	96.5	3.1	NA
RT28DZ6-44	113	22929	1.8	19.2531	17.8	0.1081	19.7	0.0151	8.5	0.43	96.6	8.1	104.2	19.5	282.8	409.0	96.6	8.1	NA
RT28DZ6-112B	21	4897	1.6	18.5440	2.0	0.1125	2.3	0.0151	1.2	0.50	96.8	1.1	108.2	2.4	367.9	45.3	96.8	1.1	NA
RT28DZ6-4	133	13240	1.1	21.2830	28.0	0.0985	28.2	0.0152	3.5	0.12	97.3	3.4	95.4	25.7	48.5	680.4	97.3	3.4	NA

RT28DZ6-14	79	20752	1.3	18.5818	41.5	0.1130	41.9	0.0152	6.2	0.15	97.4	6.0	108.7	43.2	363.3	974.4	97.4	6.0	NA
RT28DZ6-35	256	67667	1.6	21.6780	19.8	0.0973	20.1	0.0153	3.1	0.16	97.9	3.0	94.3	18.1	4.4	481.3	97.9	3.0	NA
RT28DZ6-17	50	16388	1.2	14.4141	44.3	0.1468	45.2	0.0154	9.4	0.21	98.2	9.1	139.1	58.9	909.9	958.7	98.2	9.1	NA
RT28DZ6-38	273	38687	2.5	22.1459	13.4	0.0962	13.8	0.0155	3.4	0.24	98.8	3.3	93.3	12.3	-47.3	327.7	98.8	3.3	NA
RT28DZ6-40	118	11836	1.2	19.6164	24.1	0.1087	24.4	0.0155	3.9	0.16	99.0	3.9	104.8	24.3	239.8	562.0	99.0	3.9	NA
RT28DZ6-77	97	24035	1.9	15.8134	29.8	0.1350	30.1	0.0155	4.2	0.14	99.0	4.1	128.5	36.4	716.2	646.7	99.0	4.1	NA
RT28DZ6-118	63	4570	1.3	23.5655	141.8	0.0908	142.0	0.0155	7.0	0.05	99.2	6.9	88.2	120.5	-200.6	1628.3	99.2	6.9	NA
RT28DZ6-65	116	13295	1.3	18.6870	11.0	0.1145	12.8	0.0155	6.5	0.51	99.3	6.4	110.1	13.3	350.6	249.7	99.3	6.4	NA
RT28DZ6-100B	97	48823	1.4	19.8808	1.8	0.1077	2.0	0.0155	0.7	0.35	99.4	0.7	103.9	1.9	208.9	42.7	99.4	0.7	NA
RT28DZ6-115B	35	10429	1.8	19.0897	3.2	0.1124	3.6	0.0156	1.6	0.44	99.5	1.6	108.1	3.7	302.2	73.2	99.5	1.6	NA
RT28DZ6-111B	53	14779	1.2	19.6385	2.4	0.1093	2.7	0.0156	1.1	0.43	99.6	1.1	105.3	2.7	237.2	55.2	99.6	1.1	NA
RT28DZ6-99	77	14548	1.3	8.5919	465.8	0.2503	465.8	0.0156	7.0	0.01	99.8	6.9	226.8	1702.2	1901.5	1256.8	99.8	6.9	NA
RT28DZ6-74	130	16648	1.7	21.6747	25.6	0.0997	26.0	0.0157	4.5	0.17	100.3	4.5	96.5	23.9	4.7	624.3	100.3	4.5	NA
RT28DZ6-19	68	10487	1.7	12.0013	127.2	0.1807	127.4	0.0157	7.5	0.06	100.6	7.4	168.6	200.6	1276.8	290.4	100.6	7.4	NA
RT28DZ6-97	277	36570	1.8	23.8562	17.6	0.0915	17.7	0.0158	2.0	0.12	101.2	2.0	88.9	15.1	-231.4	446.1	101.2	2.0	NA
RT28DZ6-105	93	22385	1.3	18.5253	38.3	0.1179	39.2	0.0158	8.5	0.22	101.3	8.5	113.2	42.0	370.2	891.7	101.3	8.5	NA
RT28DZ6-75	107	12985	1.2	19.5675	40.8	0.1118	41.1	0.0159	5.3	0.13	101.5	5.4	107.6	42.0	245.6	976.1	101.5	5.4	NA
RT28DZ6-63	80	3978	1.0	21.7914	43.2	0.1010	43.5	0.0160	5.2	0.12	102.1	5.3	97.7	40.5	-8.1	1087.2	102.1	5.3	NA
RT28DZ6-84	75	13811	1.8	16.6529	59.4	0.1330	59.5	0.0161	2.8	0.05	102.7	2.9	126.8	71.0	605.3	1414.7	102.7	2.9	NA
RT28DZ6-78	101	24715	1.8	21.0123	47.2	0.1054	47.4	0.0161	4.2	0.09	102.7	4.3	101.8	45.9	79.0	1182.2	102.7	4.3	NA
RT28DZ6-7	75	11716	0.9	44.9697	78.4	0.0494	78.9	0.0161	8.4	0.11	103.0	8.6	48.9	37.7	NA	NA	103.0	8.6	NA
RT28DZ6-20	112	43361	1.5	28.9074	72.4	0.0771	72.6	0.0162	5.6	0.08	103.4	5.8	75.4	52.8	-741.3	2325.3	103.4	5.8	NA
RT28DZ6-72	111	10967	1.7	18.0197	34.2	0.1238	34.4	0.0162	3.7	0.11	103.5	3.8	118.5	38.5	432.2	783.9	103.5	3.8	NA
RT28DZ6-90	70	13384	1.1	27.6467	46.5	0.0808	47.1	0.0162	7.3	0.16	103.6	7.5	78.9	35.7	-618.0	1330.3	103.6	7.5	NA
RT28DZ6-57	109	19315	1.4	21.2064	47.2	0.1072	48.1	0.0165	9.2	0.19	105.4	9.6	103.4	47.3	57.1	1185.6	105.4	9.6	NA
RT28DZ6-67	104	9416	1.4	26.8247	39.1	0.0853	40.1	0.0166	8.6	0.21	106.1	9.0	83.1	32.0	-536.3	1084.5	106.1	9.0	NA
RT28DZ6-85	76	10931	1.5	14.9453	114.7	0.1539	115.1	0.0167	8.7	0.08	106.7	9.2	145.3	157.1	835.0	522.0	106.7	9.2	NA
RT28DZ6-79	162	30202	2.4	22.7260	23.0	0.1014	23.4	0.0167	4.3	0.19	106.8	4.6	98.1	21.9	-110.5	572.0	106.8	4.6	NA
RT28DZ6-23	63	11904	1.2	17.8008	104.1	0.1299	104.3	0.0168	7.2	0.07	107.2	7.7	124.0	122.3	459.4	715.5	107.2	7.7	NA
RT28DZ6-56	76	11306	1.1	12.3740	181.4	0.1870	181.6	0.0168	8.6	0.05	107.3	9.1	174.0	298.9	1216.9	647.7	107.3	9.1	NA
RT28DZ6-116	173	20683	2.5	23.1100	21.6	0.1001	21.8	0.0168	2.5	0.11	107.3	2.6	96.9	20.1	-152.0	542.6	107.3	2.6	NA
RT28DZ6-36	432	104569	0.7	19.4636	7.3	0.1191	7.5	0.0168	1.5	0.20	107.5	1.6	114.3	8.1	257.8	168.3	107.5	1.6	NA
RT28DZ6-82	110	19681	2.7	35.4376	51.9	0.0665	52.3	0.0171	6.5	0.12	109.2	7.0	65.3	33.1	NA	NA	109.2	7.0	NA
RT28DZ6-69	120	14884	1.0	21.4127	23.1	0.1144	23.2	0.0178	2.8	0.12	113.5	3.2	110.0	24.2	34.0	558.7	113.5	3.2	NA
RT28DZ6-49	275	46898	1.2	22.0375	13.7	0.1158	13.9	0.0185	1.8	0.13	118.2	2.1	111.3	14.6	-35.3	334.5	118.2	2.1	NA
RT28DZ6-43	235	39071	1.4	19.8584	10.6	0.1299	10.8	0.0187	2.1	0.20	119.5	2.5	124.0	12.6	211.5	246.3	119.5	2.5	NA
RT28DZ6-101	429	71586	0.6	20.9826	7.5	0.1235	7.9	0.0188	2.3	0.29	120.1	2.8	118.3	8.8	82.3	179.2	120.1	2.8	NA
RT28DZ6-52	120	20016	2.0	21.4510	26.4	0.1218	26.5	0.0190	2.6	0.10	121.0	3.1	116.7	29.2	29.7	642.2	121.0	3.1	NA
RT28DZ6-92	1079	181951	1.5	20.4482	2.7	0.1285	3.1	0.0191	1.5	0.48	121.7	1.8	122.7	3.6	143.2	64.0	121.7	1.8	NA

RT28DZ6-94	97	20078	1.4	18.8818	15.8	0.1462	16.4	0.0200	4.5	0.27	127.8	5.7	138.6	21.2	327.1	359.7	127.8	5.7	NA
RT28DZ6-45	441	134456	2.7	19.7218	6.4	0.1630	6.6	0.0233	1.5	0.24	148.6	2.3	153.3	9.4	227.5	147.7	148.6	2.3	NA
RT28DZ6-98	101	9128	1.6	18.2388	27.1	0.1833	27.6	0.0242	4.8	0.17	154.4	7.3	170.9	43.4	405.2	618.0	154.4	7.3	NA
RT28DZ6-42	307	64212	1.2	19.1571	5.9	0.3140	6.0	0.0436	1.4	0.23	275.3	3.7	277.3	14.7	294.2	134.4	275.3	3.7	NA
RT28DZ6-110	102	41163	1.1	20.2328	17.1	0.3029	17.4	0.0444	3.0	0.17	280.3	8.2	268.6	41.0	168.0	402.4	280.3	8.2	NA
RT28DZ6-26	143	47244	1.2	19.0805	9.5	0.3241	9.7	0.0448	1.8	0.19	282.8	5.1	285.0	24.2	303.3	218.0	282.8	5.1	NA
RT28DZ6-83	86	43072	1.1	20.1895	14.4	0.3301	14.7	0.0483	2.6	0.18	304.3	7.7	289.7	36.9	173.0	338.0	304.3	7.7	NA
RT28DZ6-107	291	36981	1.7	16.2872	3.4	0.7030	4.9	0.0830	3.5	0.72	514.2	17.5	540.6	20.6	653.2	73.2	514.2	17.5	5%
RT28DZ6-117	289	278518	1.8	16.6643	1.9	0.8283	2.1	0.1001	1.0	0.46	615.0	5.8	612.7	9.8	603.9	40.7	615.0	5.8	0%
RT28DZ6-95	237	308653	1.6	13.5154	1.1	1.7226	1.3	0.1689	0.6	0.45	1005.8	5.2	1017.0	8.1	1041.2	22.7	1041.2	22.7	1%
RT28DZ6-25	81	129087	1.1	13.4289	2.4	1.6864	4.1	0.1643	3.3	0.81	980.4	29.9	1003.4	25.9	1054.2	48.0	1054.2	48.0	2%
RT28DZ6-88	42	81685	1.0	8.9918	1.8	4.8807	2.3	0.3183	1.5	0.64	1781.4	23.2	1798.9	19.7	1819.3	32.7	1819.3	32.7	1%
Sample JCF09-237B (Río Guillermo Formation)																			
JCF09-237B-Spot 77	38	2944	1.4	18.1039	12.8	0.0245	13.4	0.0032	4.0	0.30	20.7	0.8	24.5	3.2	421.8	286.3	20.7	0.8	NA
JCF09-237B-Spot 152	197	4831	0.9	21.2208	5.9	0.0213	6.5	0.0033	2.6	0.40	21.1	0.5	21.5	1.4	55.5	141.3	21.1	0.5	NA
JCF09-237B-Spot 108	99	3004	1.3	19.6976	8.4	0.0230	9.1	0.0033	3.6	0.39	21.2	0.8	23.1	2.1	230.3	194.4	21.2	0.8	NA
JCF09-237B-Spot 159	67	2915	1.2	20.8746	10.3	0.0218	10.6	0.0033	2.6	0.25	21.3	0.6	21.9	2.3	94.6	243.4	21.3	0.6	NA
JCF09-237B-Spot 83	172	42230	1.0	19.5318	6.5	0.0233	7.0	0.0033	2.7	0.39	21.3	0.6	23.4	1.6	249.8	149.4	21.3	0.6	NA
JCF09-237B-Spot 59	192	10908	1.2	19.7298	5.4	0.0234	6.0	0.0033	2.5	0.42	21.6	0.5	23.5	1.4	226.5	125.5	21.6	0.5	NA
JCF09-237B-Spot 24	145	2541	1.2	24.6791	5.5	0.0188	6.0	0.0034	2.4	0.40	21.7	0.5	18.9	1.1	317.7	142.3	21.7	0.5	NA
JCF09-237B-Spot 18	140	9333	1.3	20.1931	7.1	0.0231	7.6	0.0034	2.7	0.36	21.8	0.6	23.2	1.7	172.6	166.2	21.8	0.6	NA
JCF09-237B-Spot 154	283	14976	1.5	22.9225	4.5	0.0204	5.1	0.0034	2.3	0.45	21.8	0.5	20.5	1.0	131.8	112.3	21.8	0.5	NA
JCF09-237B-Spot 107	83	44177	1.2	20.6751	6.7	0.0226	7.5	0.0034	3.3	0.44	21.8	0.7	22.7	1.7	117.3	158.6	21.8	0.7	NA
JCF09-237B-Spot 22	57	1654	2.0	23.9953	9.7	0.0195	10.2	0.0034	3.2	0.31	21.9	0.7	19.6	2.0	246.1	246.5	21.9	0.7	NA
JCF09-237B-Spot 48	82	13523	1.3	21.8003	7.3	0.0215	8.0	0.0034	3.1	0.38	21.9	0.7	21.6	1.7	9.1	177.4	21.9	0.7	NA
JCF09-237B-Spot 149	362	20091	1.0	20.6421	5.3	0.0227	5.9	0.0034	2.8	0.46	21.9	0.6	22.8	1.3	121.1	123.8	21.9	0.6	NA
JCF09-237B-Spot 23	75	9625	1.4	19.1207	8.9	0.0246	9.9	0.0034	4.2	0.42	22.0	0.9	24.7	2.4	298.5	203.9	22.0	0.9	NA
JCF09-237B-Spot 114	83	20891	1.1	18.0451	7.5	0.0262	8.2	0.0034	3.1	0.38	22.1	0.7	26.3	2.1	429.1	168.5	22.1	0.7	NA
JCF09-237B-Spot 156	47	2776	1.5	20.1415	11.1	0.0236	11.6	0.0034	3.3	0.28	22.2	0.7	23.7	2.7	178.6	259.8	22.2	0.7	NA
JCF09-237B-Spot 13	112	25328	0.9	22.1986	6.0	0.0216	6.4	0.0035	2.2	0.34	22.3	0.5	21.7	1.4	53.0	145.5	22.3	0.5	NA
JCF09-237B-Spot 165	135	9478	1.4	20.7711	6.1	0.0231	6.6	0.0035	2.4	0.37	22.3	0.5	23.1	1.5	106.3	144.2	22.3	0.5	NA
JCF09-237B-Spot 166	107	26313	1.6	20.0494	6.3	0.0239	7.2	0.0035	3.5	0.48	22.4	0.8	24.0	1.7	189.2	145.8	22.4	0.8	NA
JCF09-237B-Spot 71	47	3851	1.2	20.5871	9.4	0.0233	10.2	0.0035	3.9	0.38	22.4	0.9	23.4	2.3	127.3	221.4	22.4	0.9	NA
JCF09-237B-Spot 85	145	30059	2.1	21.4662	6.4	0.0224	6.8	0.0035	2.1	0.32	22.4	0.5	22.5	1.5	28.0	153.9	22.4	0.5	NA
JCF09-237B-Spot 132	43	2174	0.9	21.8968	12.2	0.0220	12.7	0.0035	3.8	0.30	22.5	0.8	22.1	2.8	19.8	295.2	22.5	0.8	NA
JCF09-237B-Spot 90	38	2024	1.7	14.2825	15.2	0.0337	15.6	0.0035	3.6	0.23	22.5	0.8	33.7	5.2	928.8	313.3	22.5	0.8	NA
JCF09-237B-Spot 74	75	3648	1.2	19.7076	10.7	0.0245	11.1	0.0035	3.0	0.27	22.5	0.7	24.5	2.7	229.1	246.7	22.5	0.7	NA
JCF09-237B-Spot 56	108	4050	2.2	21.2762	7.4	0.0227	7.9	0.0035	2.8	0.36	22.5	0.6	22.8	1.8	49.3	176.0	22.5	0.6	NA

JCF09-237B-Spot 33	178	5878	1.8	22.7810	6.0	0.0212	6.5	0.0035	2.4	0.37	22.5	0.5	21.3	1.4	116.5	148.3	22.5	0.5	NA
JCF09-237B-Spot 57	80	17129	1.4	21.1996	8.1	0.0228	8.7	0.0035	3.3	0.38	22.5	0.7	22.9	2.0	57.9	192.8	22.5	0.7	NA
JCF09-237B-Spot 103	54	224497	1.3	12.5898	13.9	0.0384	14.4	0.0035	3.9	0.27	22.6	0.9	38.2	5.4	1182.9	275.6	22.6	0.9	NA
JCF09-237B-Spot 123	40	2654	2.5	24.0545	10.0	0.0201	10.9	0.0035	4.1	0.38	22.6	0.9	20.2	2.2	252.4	254.7	22.6	0.9	NA
JCF09-237B-Spot 141	206	6007	1.2	23.1177	5.7	0.0210	6.3	0.0035	2.6	0.41	22.7	0.6	21.1	1.3	152.8	142.3	22.7	0.6	NA
JCF09-237B-Spot 66	288	16674	1.5	20.7433	5.1	0.0235	5.5	0.0035	2.2	0.40	22.7	0.5	23.6	1.3	109.5	119.6	22.7	0.5	NA
JCF09-237B-Spot 34	181	4916	1.5	21.2325	5.4	0.0230	6.2	0.0035	3.0	0.49	22.8	0.7	23.1	1.4	54.2	128.3	22.8	0.7	NA
JCF09-237B-Spot 124	52	12529	1.9	25.2628	6.7	0.0193	7.9	0.0035	4.2	0.53	22.8	1.0	19.4	1.5	378.0	174.9	22.8	1.0	NA
JCF09-237B-Spot 95	174	17191	1.5	20.6308	5.8	0.0237	6.1	0.0036	1.9	0.31	22.9	0.4	23.8	1.4	122.3	136.6	22.9	0.4	NA
JCF09-237B-Spot 117	244	11713	2.8	22.6879	4.1	0.0216	4.7	0.0036	2.4	0.51	22.9	0.6	21.7	1.0	106.4	100.3	22.9	0.6	NA
JCF09-237B-Spot 16	110	4028	1.2	13.8386	9.0	0.0355	9.5	0.0036	3.2	0.33	22.9	0.7	35.4	3.3	993.3	182.4	22.9	0.7	NA
JCF09-237B-Spot 52	127	10134	1.6	20.3874	6.0	0.0241	6.4	0.0036	2.1	0.33	23.0	0.5	24.2	1.5	150.2	141.3	23.0	0.5	NA
JCF09-237B-Spot 168	108	89907	1.2	22.2568	6.2	0.0222	6.6	0.0036	2.3	0.35	23.0	0.5	22.2	1.5	59.4	150.9	23.0	0.5	NA
JCF09-237B-Spot 35	166	9622	2.2	20.9759	5.7	0.0235	5.9	0.0036	1.5	0.25	23.0	0.3	23.6	1.4	83.1	135.8	23.0	0.3	NA
JCF09-237B-Spot 15	233	8005	1.2	18.6209	5.5	0.0265	5.8	0.0036	2.1	0.36	23.1	0.5	26.6	1.5	358.6	123.1	23.1	0.5	NA
JCF09-237B-Spot 158	244	13788	1.3	10.4564	3.8	0.0473	4.4	0.0036	2.4	0.53	23.1	0.5	46.9	2.0	1540.6	70.6	23.1	0.5	NA
JCF09-237B-Spot 120	276	8075	3.2	22.3512	4.9	0.0222	5.4	0.0036	2.3	0.42	23.2	0.5	22.3	1.2	69.8	120.4	23.2	0.5	NA
JCF09-237B-Spot 65	157	14818	1.8	20.8331	6.3	0.0238	6.9	0.0036	2.9	0.42	23.2	0.7	23.9	1.6	99.3	148.7	23.2	0.7	NA
JCF09-237B-Spot 140	167	20361	1.6	20.4872	6.2	0.0243	6.6	0.0036	2.1	0.31	23.2	0.5	24.3	1.6	138.7	146.5	23.2	0.5	NA
JCF09-237B-Spot 86	84	8503	2.5	21.2644	6.3	0.0234	7.0	0.0036	3.0	0.44	23.2	0.7	23.5	1.6	50.6	150.1	23.2	0.7	NA
JCF09-237B-Spot 160	58	6426	1.8	14.4758	9.1	0.0344	9.7	0.0036	3.3	0.34	23.2	0.8	34.3	3.3	901.1	188.5	23.2	0.8	NA
JCF09-237B-Spot 21	154	46795	1.2	20.6472	6.6	0.0241	7.0	0.0036	2.3	0.32	23.3	0.5	24.2	1.7	120.5	156.3	23.3	0.5	NA
JCF09-237B-Spot 55	165	33726	1.6	19.1818	6.2	0.0260	6.6	0.0036	2.4	0.36	23.3	0.5	26.1	1.7	291.2	141.2	23.3	0.5	NA
JCF09-237B-Spot 127	167	113136	1.6	20.9422	5.6	0.0238	6.1	0.0036	2.6	0.42	23.3	0.6	23.9	1.4	86.9	131.8	23.3	0.6	NA
JCF09-237B-Spot 98	37	1168	1.4	28.5491	9.7	0.0176	10.5	0.0036	3.9	0.37	23.4	0.9	17.7	1.8	706.4	271.3	23.4	0.9	NA
JCF09-237B-Spot 27	91	3691	1.3	15.7722	7.1	0.0321	7.7	0.0037	2.9	0.38	23.6	0.7	32.1	2.4	721.7	151.8	23.6	0.7	NA
JCF09-237B-Spot 170	31	13839	1.4	12.5813	16.6	0.0404	17.0	0.0037	3.6	0.21	23.7	0.9	40.2	6.7	1184.2	330.7	23.7	0.9	NA
JCF09-237B-Spot 51	79	4479	1.5	21.8356	6.5	0.0233	7.6	0.0037	3.8	0.51	23.8	0.9	23.4	1.7	13.0	157.3	23.8	0.9	NA
JCF09-237B-Spot 87	33	2733	2.1	14.8987	14.9	0.0342	15.3	0.0037	3.8	0.24	23.8	0.9	34.1	5.2	841.5	311.2	23.8	0.9	NA
JCF09-237B-Spot 148	149	8624	1.7	20.2891	4.7	0.0253	5.9	0.0037	3.7	0.62	23.9	0.9	25.3	1.5	161.5	108.9	23.9	0.9	NA
JCF09-237B-Spot 115	110	49278	2.1	20.5091	7.4	0.0251	8.0	0.0037	3.0	0.37	24.1	0.7	25.2	2.0	136.2	175.0	24.1	0.7	NA
JCF09-237B-Spot 144	134	6977	1.6	18.7465	6.9	0.0275	7.6	0.0037	3.2	0.42	24.1	0.8	27.6	2.1	343.4	156.4	24.1	0.8	NA
JCF09-237B-Spot 100	425	14461	2.0	21.4055	3.6	0.0241	4.1	0.0037	2.1	0.51	24.1	0.5	24.2	1.0	34.8	85.1	24.1	0.5	NA
JCF09-237B-Spot 91	237	21424	3.3	22.4899	4.2	0.0230	4.5	0.0038	1.7	0.38	24.2	0.4	23.1	1.0	84.9	102.7	24.2	0.4	NA
JCF09-237B-Spot 50	34	14902	1.5	20.1476	9.2	0.0260	9.8	0.0038	3.3	0.34	24.4	0.8	26.0	2.5	177.8	215.6	24.4	0.8	NA
JCF09-237B-Spot 173	42	1324	1.5	25.9468	9.0	0.0202	9.6	0.0038	3.3	0.34	24.4	0.8	20.3	1.9	447.9	238.6	24.4	0.8	NA
JCF09-237B-Spot 121	42	9006	2.3	13.9031	15.8	0.0378	16.1	0.0038	3.3	0.21	24.5	0.8	37.7	6.0	983.8	323.5	24.5	0.8	NA
JCF09-237B-Spot 84	33	1249	1.6	12.5235	16.6	0.0421	17.1	0.0038	4.1	0.24	24.6	1.0	41.8	7.0	1193.3	329.7	24.6	1.0	NA
JCF09-237B-Spot 94	123	8611	2.1	23.3327	5.7	0.0227	6.6	0.0038	3.3	0.50	24.7	0.8	22.8	1.5	175.8	143.2	24.7	0.8	NA

JCF09-237B-Spot 19	27	1021	1.5	14.9930	17.6	0.0357	18.0	0.0039	4.0	0.22	25.0	1.0	35.6	6.3	828.4	368.8	25.0	1.0	NA
JCF09-237B-Spot 26	24	3793	1.8	4.6386	20.0	0.1231	20.6	0.0041	4.7	0.23	26.6	1.3	117.9	22.9	2948.0	326.9	26.6	1.3	NA
JCF09-237B-Spot 171	74	3452	2.4	10.8604	12.8	0.0526	13.2	0.0041	3.3	0.25	26.7	0.9	52.1	6.7	1469.0	244.1	26.7	0.9	NA
JCF09-237B-Spot 20	19	5098	2.1	8.3518	26.5	0.0704	27.0	0.0043	5.3	0.20	27.4	1.5	69.0	18.0	1952.2	482.5	27.4	1.5	NA
JCF09-237B-Spot 72	37	1913	1.7	24.1651	8.6	0.0243	9.3	0.0043	3.7	0.40	27.4	1.0	24.4	2.2	264.0	217.4	27.4	1.0	NA
JCF09-237B-Spot 29	33	1418	1.3	29.1042	7.9	0.0230	9.1	0.0048	4.5	0.50	31.2	1.4	23.0	2.1	760.3	222.2	31.2	1.4	NA
JCF09-237B-Spot 47	164	35104	1.7	19.8078	6.9	0.0338	7.4	0.0049	2.5	0.34	31.2	0.8	33.7	2.4	217.4	160.6	31.2	0.8	NA
JCF09-237B-Spot 76	118	6256	1.2	21.5362	6.7	0.0315	8.0	0.0049	4.4	0.54	31.6	1.4	31.5	2.5	20.2	162.2	31.6	1.4	NA
JCF09-237B-Spot 88	34	2394	1.9	22.5314	8.5	0.0333	9.7	0.0054	4.7	0.48	35.0	1.6	33.3	3.2	89.4	208.9	35.0	1.6	NA
JCF09-237B-Spot 41	80	2121	1.0	2.8612	2.0	0.2634	3.4	0.0055	2.7	0.80	35.1	0.9	237.4	7.1	3704.8	31.0	35.1	0.9	NA
JCF09-237B-Spot 161	108	2428	1.9	2.6489	0.6	0.3279	3.0	0.0063	3.0	0.98	40.5	1.2	287.9	7.6	3821.9	8.6	40.5	1.2	NA
JCF09-237B-Spot 122	578	18795	2.0	12.9551	12.0	0.0676	12.3	0.0064	2.4	0.19	40.8	1.0	66.4	7.9	1126.1	240.6	40.8	1.0	NA
JCF09-237B-Spot 134	798	65178	4.3	21.0361	2.2	0.0750	3.7	0.0114	2.9	0.80	73.3	2.1	73.4	2.6	76.3	52.3	73.3	2.1	NA
JCF09-237B-Spot 119	403	32849	1.1	21.1695	2.9	0.0777	3.7	0.0119	2.3	0.62	76.5	1.8	76.0	2.7	61.3	68.9	76.5	1.8	NA
JCF09-237B-Spot 28	232	33392	0.8	22.1707	2.6	0.0795	3.3	0.0128	2.1	0.62	81.8	1.7	77.6	2.5	50.0	63.8	81.8	1.7	NA
JCF09-237B-Spot 131	130	143691	1.9	20.7170	3.4	0.0925	4.1	0.0139	2.3	0.55	88.9	2.0	89.8	3.5	112.5	81.3	88.9	2.0	NA
JCF09-237B-Spot 172	161	44055	8.4	20.8771	3.5	0.0965	3.8	0.0146	1.4	0.37	93.5	1.3	93.5	3.4	94.3	83.2	93.5	1.3	NA
JCF09-237B-Spot 12	305	69273	1.9	21.1068	2.9	0.0967	3.5	0.0148	1.9	0.55	94.7	1.8	93.7	3.1	68.3	69.2	94.7	1.8	NA
JCF09-237B-Spot 137	186	22484	2.8	21.0631	3.0	0.0971	3.7	0.0148	2.1	0.58	94.9	2.0	94.1	3.3	73.2	72.1	94.9	2.0	NA
JCF09-237B-Spot 63	132	82208	2.4	20.6318	3.2	0.0992	3.9	0.0148	2.3	0.57	95.0	2.1	96.0	3.6	122.2	76.4	95.0	2.1	NA
JCF09-237B-Spot 40	340	28722	9.0	21.2729	2.3	0.0963	2.8	0.0149	1.7	0.60	95.1	1.6	93.4	2.5	49.7	54.1	95.1	1.6	NA
JCF09-237B-Spot 1	494	65766	7.9	21.0263	2.6	0.0990	3.6	0.0151	2.5	0.68	96.6	2.4	95.9	3.3	77.4	62.3	96.6	2.4	NA
JCF09-237B-Spot 58	101	9010	5.3	22.0015	3.3	0.0963	3.9	0.0154	2.2	0.56	98.3	2.1	93.3	3.5	31.4	79.3	98.3	2.1	NA
JCF09-237B-Spot 110	157	95097	2.2	20.7310	3.2	0.1029	3.6	0.0155	1.8	0.49	99.0	1.8	99.4	3.4	110.9	74.6	99.0	1.8	NA
JCF09-237B-Spot 46	1530	36960	6.1	18.4217	2.1	0.1163	6.9	0.0155	6.5	0.95	99.4	6.4	111.7	7.3	382.8	47.4	99.4	6.4	NA
JCF09-237B-Spot 96	425	45605	5.2	20.8544	2.5	0.1053	4.5	0.0159	3.8	0.84	101.8	3.8	101.6	4.4	96.9	59.0	101.8	3.8	NA
JCF09-237B-Spot 97	52	20006	1.3	20.6334	5.3	0.1066	6.0	0.0159	2.7	0.45	102.0	2.7	102.8	5.8	122.0	125.9	102.0	2.7	NA
JCF09-237B-Spot 136	95	16301	5.4	14.6940	7.6	0.1523	8.0	0.0162	2.5	0.31	103.8	2.6	144.0	10.8	870.2	158.1	103.8	2.6	NA
JCF09-237B-Spot 45	95	42054	3.8	20.5339	4.7	0.1090	5.2	0.0162	2.1	0.41	103.8	2.2	105.1	5.2	133.4	111.4	103.8	2.2	NA
JCF09-237B-Spot 151	126	12944	1.2	21.2990	3.8	0.1055	4.6	0.0163	2.6	0.56	104.2	2.7	101.8	4.5	46.7	91.5	104.2	2.7	NA
JCF09-237B-Spot 162	44	38260	2.0	19.3938	5.3	0.1162	6.0	0.0163	2.9	0.48	104.5	3.0	111.6	6.4	266.1	120.8	104.5	3.0	NA
JCF09-237B-Spot 113	269	39689	1.8	20.5469	2.8	0.1103	3.3	0.0164	1.8	0.54	105.1	1.8	106.3	3.3	131.9	65.2	105.1	1.8	NA
JCF09-237B-Spot 14	135	9172	0.9	7.6242	5.5	0.2974	6.5	0.0164	3.4	0.53	105.2	3.6	264.4	15.1	2113.6	97.0	105.2	3.6	NA
JCF09-237B-Spot 43	76	99522	2.7	20.6538	3.9	0.1204	4.5	0.0180	2.1	0.48	115.2	2.4	115.4	4.9	119.7	92.9	115.2	2.4	NA
JCF09-237B-Spot 112	84	18974	0.8	16.8511	5.5	0.1498	6.3	0.0183	3.0	0.47	116.9	3.5	141.7	8.3	579.7	120.6	116.9	3.5	NA
JCF09-237B-Spot 80	166	89223	1.5	20.3152	2.3	0.1248	2.8	0.0184	1.6	0.57	117.5	1.9	119.5	3.2	158.5	54.0	117.5	1.9	NA
JCF09-237B-Spot 99	56	38552	1.9	20.1066	4.3	0.1301	4.9	0.0190	2.4	0.49	121.2	2.9	124.2	5.8	182.6	100.0	121.2	2.9	NA
JCF09-237B-Spot 143	3257	206825	0.0	20.2643	1.1	0.1344	2.5	0.0198	2.2	0.89	126.1	2.8	128.1	3.0	164.4	25.7	126.1	2.8	NA
JCF09-237B-Spot 60	112	44846	2.3	19.2427	3.0	0.1641	3.6	0.0229	1.9	0.55	146.0	2.8	154.3	5.1	284.0	68.2	146.0	2.8	NA

JCF09-237B-Spot 75	208	41263	1.7	20.3626	3.0	0.1562	3.5	0.0231	1.9	0.53	147.0	2.7	147.4	4.8	153.1	69.9	147.0	2.7	NA
JCF09-237B-Spot 150	292	304118	2.2	20.3023	2.0	0.1590	3.2	0.0234	2.5	0.78	149.2	3.7	149.8	4.5	160.0	47.5	149.2	3.7	NA
JCF09-237B-Spot 89	82	43154	0.9	19.9889	3.4	0.1655	4.2	0.0240	2.5	0.59	152.9	3.7	155.5	6.0	196.3	78.3	152.9	3.7	NA
JCF09-237B-Spot 93	1050	37047	2.4	16.6791	2.7	0.1990	3.6	0.0241	2.3	0.65	153.3	3.6	184.2	6.0	601.9	58.8	153.3	3.6	NA
JCF09-237B-Spot 53	94	35940	1.6	18.5586	2.9	0.1808	3.4	0.0243	1.6	0.49	155.0	2.5	168.8	5.2	366.2	66.4	155.0	2.5	NA
JCF09-237B-Spot 109	94	34647	2.1	20.3222	3.8	0.1688	4.3	0.0249	2.1	0.48	158.4	3.2	158.4	6.3	157.7	88.6	158.4	3.2	NA
JCF09-237B-Spot 155	77	40436	2.0	19.5342	3.6	0.1771	4.5	0.0251	2.7	0.61	159.7	4.3	165.6	6.9	249.5	82.0	159.7	4.3	NA
JCF09-237B-Spot 7	68	2129553	3.7	14.4660	2.2	1.4002	3.9	0.1469	3.3	0.83	883.6	27.1	889.0	23.3	902.5	45.0	883.6	27.1	2%
JCF09-237B-Spot 92	219	1753392	8.8	11.5450	6.3	2.3911	7.9	0.2002	4.8	0.60	1176.4	51.1	1239.9	56.5	1352.0	121.6	1352.0	121.6	13%